Biochemical Analysis and

In Vivo Role of Dna2 Nuclease-Helicase

DISSERTATION
ZUR
ERLANGUNG DER NATURWISSENSCHAFTLICHEN DOKTORWÜRDE
(Dr. sc. nat.)
VORGELEGT DER
MATHEMATISCH-NATURWISSENSCHAFTLICHEN FAKULTÄT
DER
UNIVERSITÄT ZÜRICH
VON

MARYNA LEVIKOVA

AUS
DEUTSCHLAND

PROMOTIONSKOMITEE:

PROF. DR. PETR CEJKA (VORSITZ UND LEITUNG DER DISSERTATION)

PROF. DR. MASSIMO LOPES

PROF. DR. RALF SEIDEL

ZÜRICH, 2015

~ TO MY PARENTS ~

TABLE OF CONTENTS

ZUSAMMENFASSUNG

Genomische Instabilität ist ein Merkmal von fast allen Krebsarten und ist die Voraussetzung für das Erlangen weiterer Krebskennzeichen. In erblichen bedingten Krebstypen entsteht genomische Instabilität aufgrund von Mutationen in Genen, die an der DNS Reparatur beteiligt sind. Dies unterscheidet sich von den sporadischen Krebsarten, bei welchen der Onkogen-induzierte Replikationsstress als Hauptursache für genomische Intsabilität gehandelt wird. Daher sind fehlerfreie DNS Replikation und Reparatur ausschlaggebend für die Erhaltung der Integrität des Genoms und somit auch für die Krebsvorbeugung, sowie für die korrekte Übermittlung genetischer Informationen an nachkommende Generationen.

Dna2 ist ein essentielles Enzym, das in der Evolution zwischen Hefe und Mensch konserviert ist. Es ist auf mehreren Ebenen in die Aufrechterhaltung der genomischen Stabilität involviert. Dna2 erfüllt mehrere Funktionen in der DNS Replikation und während erhöhtem Replikationsstress. Zusätzlich ist Dna2 zusammen mit Sgs1 (in Hefe; Bloom oder Werner Proteine im Menschen) in die Reparatur der genotoxischen DNS Doppelstrang-Brüche eingebunden, genauer gesagt in die Resektion der DNS Enden, welche den verbindlichen Schritt für die Reparatur durch mehrheitlich fehlerfreien Weg der homologen Rekombination darstellt. Außerdem wurde Dna2 sowohl als Teil der telomerischen und mitochondrialen DNS Aufrechterhaltungssysteme beschrieben, als auch ist es bekannt, dass Dna2 für die Aktivierung des Checkpoints für DNS Schäden in Hefe verantwortlich ist.

Während meiner Doktorarbeit habe ich die Funktionen von Dna2 in der Hefe *Saccharomyces cerevisiae* untersucht und dabei hauptsächlich mit aufgereinigten Proteinen gearbeitet. Zunächst haben wir das Dna2 Protein in Hefe exprimiert und aufgereinigt. Wir konnten zeigen, dass das Enzym zusätzlich zur Nuklease-Aktivität auch eine starke Helikase-Aktivität besitzt. Dann begannen wir die Regulation der beiden Aktivitäten innerhalb des Dna2 Proteins zu analysieren. Wir zeigen mithilfe von *in vitro* und *in vivo* Methoden, dass Hefe Dna2 durch eine post-translationale Modifikaton, die als Sumoylierung bezeichnet wid, reguliert wird. Sumoylierung des

N-Terminus des Dna2 Proteins verminderte selektiv die Nuklease-Aktivität auf der biochemischen Ebene und veränderte damit die Balance zwischen Nuklease und Helikase innerhalb von Dna2. Zudem fanden wir *in vivo* eine verstärkte Sumoylierung von Dna2 in der späten S-Phase/frühen G2-Phase des Zellzyklus. Weiterhin ist Modifikation von Dna2 durch SUMO an der Regulation des Proteins infolge der Behandlung mit alkylierenden Substanzen beteiligt.

Als Nächstes haben wir uns mit der essentiellen Funktion von Dna2 während der Replikation des DNS Folgestrangs beschäftigt. Dabei verarbeitet Dna2 zusammen mit der Flap Endonuklease I (Fen1) lange Einzelstrang-DNS Strukturen ('flaps'), die während der Synthese der DNS-Einzelfragmente (Okazaki-Fragmente) entstehen. Die nukleolytische Abspaltung dieser 'flaps' ist notwendig für das Entfernen der möglicherweise genverändernden RNS/DNS Primer, die für die ursprüngliche Synthese der Okazaki-Fragmente benötigt wurden, und erlaubt die Ligation benachbarter Fragmente. Während kurze DNS 'flaps' von Fen1 abgespalten werden, benötigen lange DNS 'flap' Strukturen, die von dem Replikationsprotein A (RPA) gebunden werden, eine sequenzielle Verarbeitung durch sowohl Dna2, als auch Fen1 Enzyme. Mittels *in vitro* Rekonstitutions-Experimente konnten wir zeigen, dass Dna2 allein zu der Verarbeitung der langen DNS 'flaps' fähig ist und die Produkte anschließend durch DNS Ligase I ligiert werden können. Zudem war Dna2 sehr effizient als alleinige Nuklease während der Verarbeitung der Okazaki-Fragmente in Zusammenarbeit mit der DNS Replikation, ohne dass die nukleolytische Aktivität von Fen1 benötigt wurde. Aufgrund dieser Erkenntnisse glauben wir, dass Fen1 die meisten DNS 'flaps' in der S-Phase des Zellzyklus, in der Fen1 hauptsächlich exprimiert wird, verarbeiten kann, während Dna2 für die Abspaltung der 'flaps' zu späteren Zeitpunkten der Replikation, oder auch möglicherweise während der post-replikativen DNS Reparatur, verantwortlich ist.

Desweiteren haben wir die Rolle der Motoraktivität von Dna2 im Zusammenhang mit der Resektion der DNS Enden, die die homologe Rekombination einleitet, untersucht. Unter Gebrauch biochemischer Methoden konnten wir aufdecken, dass die Motoraktivität von Dna2 auf langen Einzelstrang-DNS Passagen vor Allem in Anwesenheit von RPA als Einzelstrang-DNS Translokase agiert und effizienten DNS

Abbau stark stimuliert; ein Effekt, den wir auch beobachteten als Dna2 zusammen mit Sgs1 gehandelt hat. Daher schlagen wir vor, dass die Motoraktivität von Dna2 während der DNS Resektion nicht als DNS Helikase, sondern als Einzelstrang-DNS Translokase funktioniert, und somit erlaubt sie Dna2 mit Sgs1 mitzuhalten und schnellen DNS Abbau zu fördern.

Vielmehr zeigen wir in einem kollaborativen Projekt, dass Dna2 auch in das Verarbeiten der DNS Replikationsgabeln, die sich nach dem Replikationsstress umgedreht haben, involvolviert ist. Außerdem liefern wir weiteren Beweis für das Mitwirken des menschlichen DNA2 Proteins bei der Langstrecken-Resektion zusammen mit Bloom und Werner Proteinen. Zusätzlich konnten wir während einer anderen Kollaboration aufzeigen, dass die Helikase-Aktivität von Dna2 für die zelluläre Antwort auf den Replikationsstress und für die Vervollständigung der Replikation benötigt wird. Zuletzt haben unsere Kollaborateure eine Einzelmolekül-Analyse von der Assoziation des RPA Proteins zu Gabel-DNS Substraten durchgeführt, die über die mechanistische Rolle von RPA während der DNS Replikation Aufschluss gegeben hat.

SUMMARY

Genome instability is a characteristic of almost all human cancers and is a prerequisite for acquisition of further hallmarks of cancer. While in hereditary cancers it arises due to mutations in DNA repair genes, in sporadic cancers it appears that oncogene-induced replication stress is the main cause for genomic instability. Hence, faithful DNA replication and repair are crucial to preserve genome integrity, thus contributing to cancer prevention, and to properly transmit genetic information across generations.

Dna2 is an essential enzyme that is conserved from yeast to humans and is involved in the maintenance of genome stability at multiple levels. It plays a role in unperturbed DNA replication as well as under conditions of replication stress. In addition, Dna2 functions together with Sgs1 (in yeast; Bloom or Werner in humans) in the repair of genotoxic double-strand DNA breaks, specifically in DNA end resection, which is the commitment step to mostly error-free homologous recombination pathway. Furthermore, Dna2 was described to be part of telomeric and mitochondrial DNA maintenance systems, and to mediate checkpoint activation in yeast.

During my PhD I was investigating the functions of Dna2 in *Saccaromyces cerevisiae* and was mainly working with purified yeast proteins. First, we expressed and purified yeast Dna2 and were able to show that it possesses not only a nuclease, but also a vigorous helicase activity. Then we set out to analyze the regulation of the two activities within the Dna2 protein. Using *in vitro* and *in vivo* approaches we show that yeast Dna2 is regulated by a post-translational modification termed sumoylation. On the biochemical level, sumoylation of the N-terminus of Dna2 selectively attenuated its nuclease activity, thus changing the balance between the helicase and the nuclease within the protein. *In vivo*, we show that sumoylation of Dna2 is increased in the late S/G2 phases of the cell cycle and appears to be involved in regulation of Dna2 upon treatment with alkylating agents.

Next, we addressed the essential function of Dna2 in lagging strand DNA replication, where it acts together with Fen1 (Flap endonuclease I) in the processing of long DNA flap structures arising during the maturation of Okazaki fragments. The nucleolytic cleavage of these flaps is required for removal of the potentially mutagenic RNA/DNA primer initially used for the synthesis of the Okazaki fragment and allows ligation of the neighboring fragments. While short flaps are processed by Fen1, long flaps that are bound by replication protein A (RPA) need sequential cleavage by both Dna2 and Fen1 enzymes. Using *in vitro* reconstitution assays, we show that Dna2 is capable of processing the long flaps to products that can be subsequently ligated by DNA ligase I and that Dna2 is highly efficient as a sole nuclease in Okazaki fragment maturation in concert with replication, without the requirement of a second nucleolytic activity of Fen1. We suggest that Fen1 processes most of the flaps in S phase, where it is mainly expressed, and Dna2 is responsible for the cleavage of DNA flaps at later replication time points or possibly also during post-replicative repair processes.

Furthermore, we examined the role of Dna2 motor activity in the context of DNA end resection, which initiates homologous recombination. Employing biochemical approaches we show that on long stretches of ssDNA the motor activity of Dna2 acts as a ssDNA translocase, especially in presence of RPA, and highly stimulates efficient DNA degradation, an effect that we also see when it acts together with Sgs1. We propose that in resection the motor activity of Dna2 functions as a ssDNA translocase, rather than a helicase, and is thus allowing Dna2 to keep up with Sgs1 and promoting efficient DNA degradation.

Moreover, in collaborative projects we were able to show that Dna2 is also involved in the processing of replication forks that reversed upon replication stress and provide further evidence that human DNA2 cooperates with BLM and WRN to promote long-range resection. Additionally, another collaboration yielded proof that the helicase activity of Dna2 is required for the response to replication stress and for the completion of replication. Lastly, single-molecule analysis of RPA association to forked DNA substrates done by our collaborators sheds light on its mechanistic role during DNA replication.

1. INTRODUCTION

1.1 Genome instability as a hallmark of cancer

Cancer is a very complex disease and is according to the WHO the second leading cause of death in Europe. In 2000, Douglas Hanahan and Robert Weinberg suggested six main capabilities that are acquired during multistep tumor development: sustaining proliferative signaling, evading growth suppressors, activating invasion and metastasis, enabling replicative immortality, inducing angiogenesis, and resisting cell death (Figure 1, left part, and (1)). Eleven years later the same authors added deregulating cellular energetics and avoiding immune destruction to the emerging hallmarks, as well as two enabling characteristics: tumor-promoting inflammation, and genome instability and mutation (Figure 1, right part, and (2)).

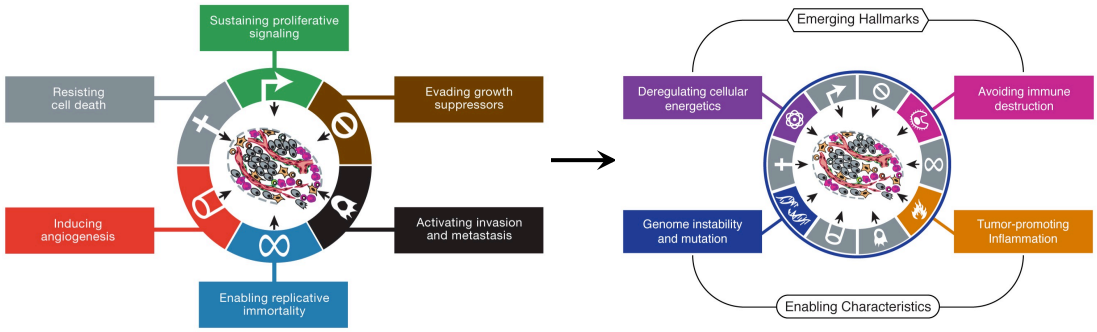

Figure 1. The hallmarks of cancer. Left: original six hallmark capabilities proposed by D. Hanahan and R. A. Weinberg in 2000. Right: four additional hallmarks were suggested by the same authors in 2011, among them genome instability as an enabling characteristic driving tumor progression. Modified from (2).

Genome instability is the main reason for the acquisition of multiple hallmarks described above. Cancers carry a variety of mutations and genetic alterations that drive tumor progression, e.g. mutations inactivating tumor suppressors (2). The genome maintenance systems of our cells are usually very effective in repairing DNA defects that arise from endogenous and exogenous sources, like inaccurate DNA replication and reactive oxygen species (endogenous), or ionizing radiation, UV light and genotoxic chemicals used in chemotherapy (exogenous) (3,4). Each cell in the human body is subjected to 10^4-10^6 DNA lesions per day which are removed by the

highly conserved DNA repair systems, specialized for the particular DNA damage (Figure 2 and (5,6)).

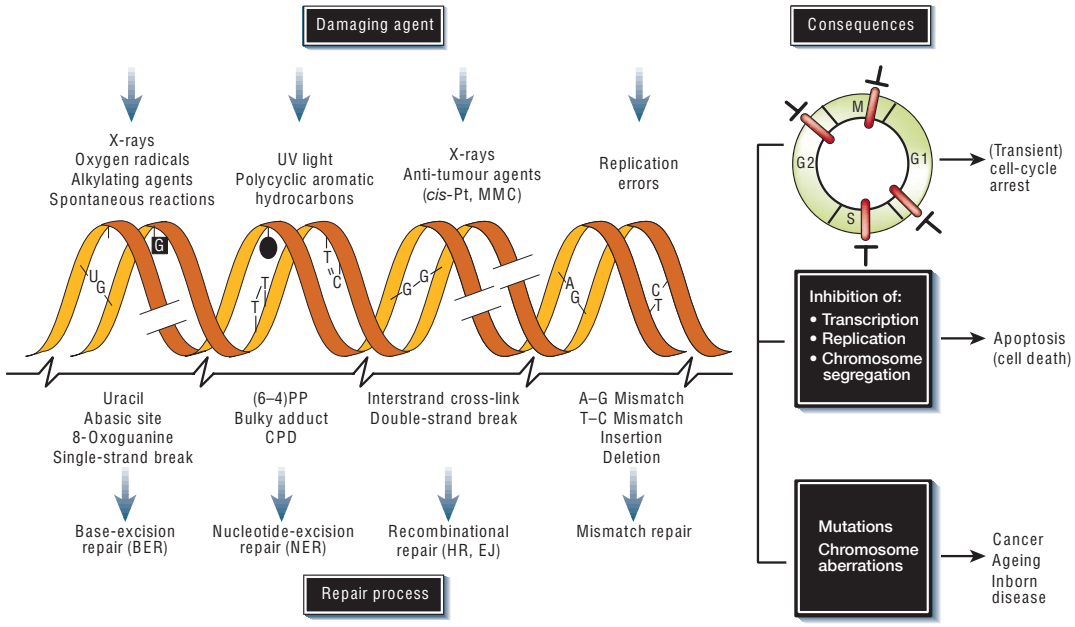

Figure 2. The variety of DNA damage, repair mechanisms and consequences. Various DNA damaging agents lead to different DNA lesions that are removed by the corresponding DNA repair mechanism. Consequences of DNA damage is cell-cycle arrest, changes in DNA metabolism and mutations (long-term). Abbreviations: *cis*-Pt, cisplatin; MMC, mitomycin C; (6-4)PP, 6-4 photoproduct; CPD, cyclobutane pyrimidine dimer; BER, base-excision repair; NER, nucleotide-excision repair; HR, homologous recombination; EJ, end joining. Modified from (5).

Small chemical alterations of DNA like oxidative lesions are removed via incision of the damaged base by base excision repair (BER), while helix-distorting lesions that interfere with transcription and replication are targeted by nucleotide excision repair (NER) that removes a short oligonucleotide sequence containing the injury (7,8). Mismatch repair (MMR) pathway is responsible for correction of insertions, deletions and mismatched base pairs incorporated during DNA replication (9). DNA double-strand breaks (DSBs) belong to the most toxic DNA lesions and are repaired either by homologous recombination (HR) in S and G2 phases of the cell cycle, or by non-homologous end joining (NHEJ) predominantly in G1 (10). In addition, lesions that block DNA replication fork progression can also be bypassed by translesion synthesis (TLS) polymerases without being repaired (11). Fanconi anemia (FA) pathway together with proteins from HR, NER and TLS pathways is responsible for the removal of interstrand crosslinks (ICLs), bridging two opposite DNA strands (12).

Despite the existence of such a plethora of sophisticated DNA repair systems, genome instability is present in all stages of cancer (13). In hereditary cancers the presence of the genomic instability was clearly linked to the mutations in DNA repair genes, also called caretaker genes, that further drive tumorigenesis (mutator hypothesis, (14)). However, for sporadic cancers the molecular mechanism responsible for genome instability is not yet clear but there are two main models existing that could explain it. One model is supporting the mutator hypothesis, although the mutation frequency in caretaker genes in sporadic tumors is rather low and seems to increase only in late cancer development or even during therapy (13). The second one suggests oncogene-induced DNA replication stress as the main reason for genome instability (15). It is supported by high-throughput sequencing studies showing that in sporadic cancers only very few genes are mutated with high frequency, coding either for growth signaling proteins (oncogenes or anti-oncogenes) or for DNA checkpoint proteins like the tumor suppressor protein p53. Those mutations might be the initiating event in cancer development, further leading to DNA damage and replication stress, genome instability, followed by p53 inactivation and the establishment of the other hallmarks (13). Therefore, DNA repair processes as well as DNA replication have to be precisely regulated to prevent cancer development.

1.2 Dna2

1.2.1 Domain structure and activities

Dna2 is an essential protein that was found to be required for DNA replication *in vivo* (16-18). The *S. cerevisiae* Dna2 has a size of 172 kDa and contains an unstructured N-terminal regulatory domain, a RecB family nuclease domain and a superfamily I helicase domain (Figure 3). Four cysteine residues (519, 768, 771, 777) within the nuclease domain coordinate an iron-sulfur cluster that most likely plays a structural role and thus affects the stability of the protein (19,20). Dna2 is evolutionarily

conserved from yeast to human, although the conservation is usually limited to the nuclease and helicase domains, while the N-terminus remains variable (21-23).

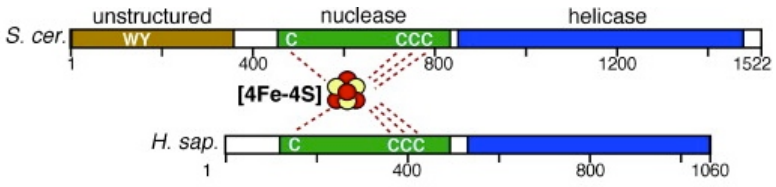

Figure 3. Domain structure of *S. cerevisiae* and human Dna2 proteins. Both proteins contain a nuclease and a helicase domain, yeast protein additionally possesses a regulatory N-terminal domain. [4Fe-4S], iron-sulfur cluster. Modified from (24).

S. cerevisiae Dna2 possesses both nuclease and helicase activities that require a free ssDNA end for loading (16,25-28). The nuclease activity has a 5' to 3' polarity in presence of replication protein A (RPA) and is essential (27-29). In contrast, the ATP-dependent helicase activity, that has the same polarity as the nuclease, was described to be weak and helicase-dead mutants were shown to be viable but exhibited growth defects and sensitivity to methyl methanesulfonate (MMS) and ionizing radiation (IR) (16,17,30,31). The human protein was found to have a nuclease activity as well, while the presence of a helicase activity has been questioned (32-34).

The N-terminal domain (NTD) of yeast Dna2 was shown to be dispensable for the nuclease and helicase activities of the protein, but it was required for normal growth as deletion of the first 405 amino acids rendered yeast cells temperature-sensitive (35). This can be explained by three functions of the NTD that have been found so far. First, the NTD was shown to mediate Dna2 binding to DNA flaps containing secondary structures and Fen1 (flap endonuclease 1, also Rad27) overexpression rescued the temperature-sensitivity of *dna2delta405N* mutants (35,36). Second, the NTD of Dna2 was found to mediate checkpoint activation through Trp128 and Tyr130 residues (37). Interestingly, two overlapping bipartite NLS (nuclear localization signals) exist within the first 48 amino acids of yeast Dna2 protein (38), and there is a third NLS within the C-terminus, which alone is sufficient for nuclear transport as *dna2delta405N* cells are viable (35). Third, NTD was shown to be involved in RPA binding by Dna2 (39).

Human DNA2 does not possess an unstructured N-terminal domain, although the exact translation start is not clear and longer variants (e.g. 1146 amino acids) containing an N-terminal tail might exist (32,40). The human protein does not have any NLS but is still important for nuclear functions despite also being localized to the mitochondria (40,41).

1.2.2 Dna2 and replication: Okazaki fragment maturation

DNA replication is an essential event in living cells and the main mechanism to maintain genome integrity. It occurs in the S phase of the cell cycle before each cell division. The fidelity of replication is safeguarded by many regulatory mechanisms ensuring that all the chromosomes are replicated on time and in an error-free manner before subsequent distribution to the daughter cells (42). Checkpoints within the cell cycle control the cell cycle progression and intervene in case of DNA damage or perturbations of DNA synthesis (43). Replication is initiated from specific sites called origins (ARS, autonomously replicating sequences in budding yeast), by the pre-replicative complex composed of ORC (origin-recognition complex), MCM2-7 (minichromosome maintenance proteins) helicase complex, Cdc6 and Cdt1. The activation of replication requires CDK (cyclin-dependent kinase) and DDK (Dbf4-dependent kinase) activity as well as further proteins; among them are Cdc45, Mcm10 and the essential DNA replication complex GINS (44). Upon unwinding of the dsDNA at the origin by the MCM helicase both strands are primed by the polymerase (pol) α-primase (Stillman 2008). Importantly, unwinding of the DNA results in topological stress due to supercoiling that is then resolved either by transiently breaking one DNA strand and passing the other strand through the break (type I topoisomerases), or by breaking both complementary strands and passing a dsDNA segment (type II topoisomerases) (45). While the leading strand DNA is synthesized continuously by pol ε, the lagging strand DNA is replicated discontinuously in short fragments called Okazaki fragments due to 5' to 3' polarity of eukaryotic DNA polymerases. The lagging strand DNA replication starts with the action of the error-prone pol α that synthesizes a ∼30 nucleotides-long RNA-DNA primer (Figure 4). Proliferating cell nuclear antigen (PCNA) is then recruited by replication factor C

(RFC) and mediates the polymerase switch to pol δ, which further extends the synthesized DNA fragment until it reaches the 5' end of the downstream Okazaki fragment (~200 nucleotides; (46,47)). The RNA-DNA primer is then displaced leading to the formation of 5' flap structures that have to be cleaved before ligation by DNA ligase I can occur. This process is very important for genomic integrity as it ensures the removal of RNA (if not yet removed by RNase HI, (48-50)) and DNA synthesized by the error-prone pol α (51,52). Short 5' flaps displaced by pol δ are removed by the nucleolytic activity of flap endonuclease 1 (Fen1). However, if flaps become long enough to bind RPA, Fen1 is not able anymore to process them (53,54). Current model of long flap processing assumes a sequential action of Dna2 and Fen1 (Figure 4). First, RPA-covered flaps become substrate for Dna2 that shortens them up to 5-8 nucleotides. Only after this initial processing Fen1 can cleave the remaining flap structure that does not support stable RPA binding anymore (25,53-55).

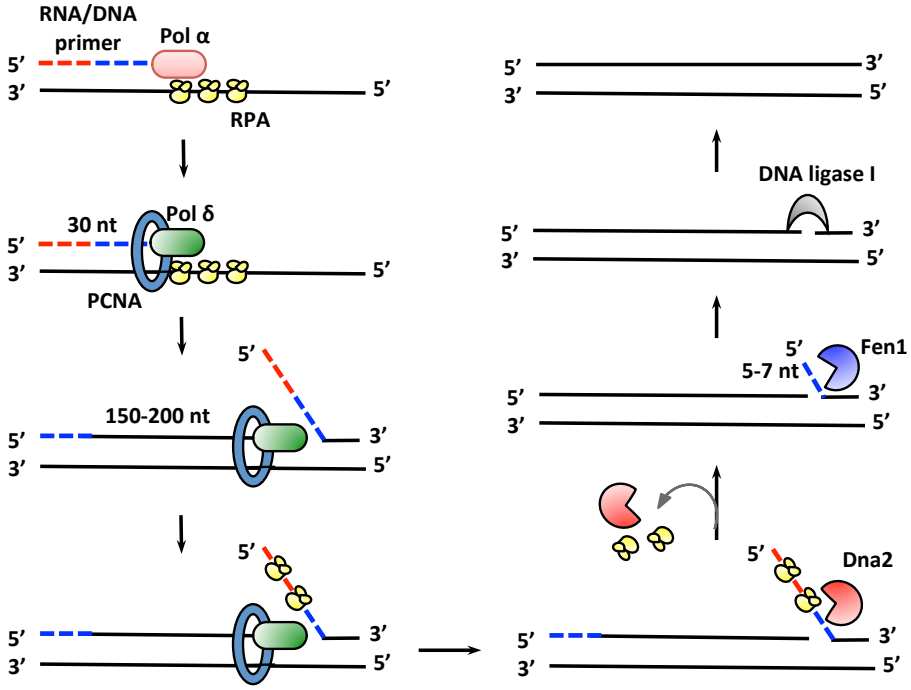

Figure 4. Okazaki fragment processing by sequential action of Dna2 and Fen1. The initial RNA/DNA primer is synthesized by the error-prone polymerase α (pol α) followed by a PCNA-mediated polymerase switch to polymerase δ (pol δ), which performs the synthesis of 150-200 nucleotides. Pol δ displaces the 5' end of the downstream primer leading to the formation of a flap structure that can bind RPA. The flap DNA remaining after Dna2-catalyzed cleavage varies between 5-8 nucleotides in length, so that stable association of RPA is not supported and Fen1 can process the flap structure to a ligatable substrate for DNA ligase I.

However, *dna2Δ* mutation is lethal, while *rad27Δ* cells are viable (16,56,57), which contradicts the notion of Dna2 acting upstream of Fen1.

Further genetic studies showed that mutations promoting the generation of long flaps such as increased strand displacement by exonuclease-deficient pol δ are very sensitive to Dna2 dysfunction. In contrast, limited displacement synthesis resulting in shorter flaps, e.g. by deletion of either Pif1 helicase or POL32 subunit of pol δ, or by the overexpression of Fen1, can suppress lethality of *dna2Δ* (58-61).

Despite being considered as the most important and essential physiological function of Dna2, Dna2-mediated Okazaki fragment processing was never shown *in vivo*. Moreover, there is no *in vitro* data so far about the role of human DNA2 in lagging strand replication. *In vivo*, human DNA2 was found to have a role in replication, but likely independently of Okazaki fragment processing (62).

1.2.3 Dna2 and replication fork reversal

DNA replication fork reversal is now recognized as a global and evolutionary conserved response to replication stress caused by a variety of means, from exogenously induced DNA lesions to endogenous replication perturbations arising from DNA regions that are difficult to replicate (63-65).

First proposed in 1976 (66), fork reversal is defined as a remodeling of a replication fork into a four-way junction by unwinding the nascent DNA strands followed by annealing of parental strands as well as the newly synthesized daughter strands that then form the regressed arm (Figure 5). A number of proteins are involved in the replication fork remodeling process. The fork reversal was shown to be dependent on the recombinase Rad51 as well as on the F-box DNA helicase protein 1 (FBH1) (65,67). The restart of the forks is then driven by the DNA helicase RECQ1, which is in its turn inhibited by PARP1-mediated ADP ribosylation (68). However, forks reversed in response to nucleotide depletion or oncogene-induced replication stress can also be processed nucleolytically by MUS81 and SLX4 nucleases possibly resulting in fork breakage and genome instability (69,70). Interestingly, cells suffering from oncogene-induced replication stress showed MUS81-dependent DSBs upon WRN-depletion (71).

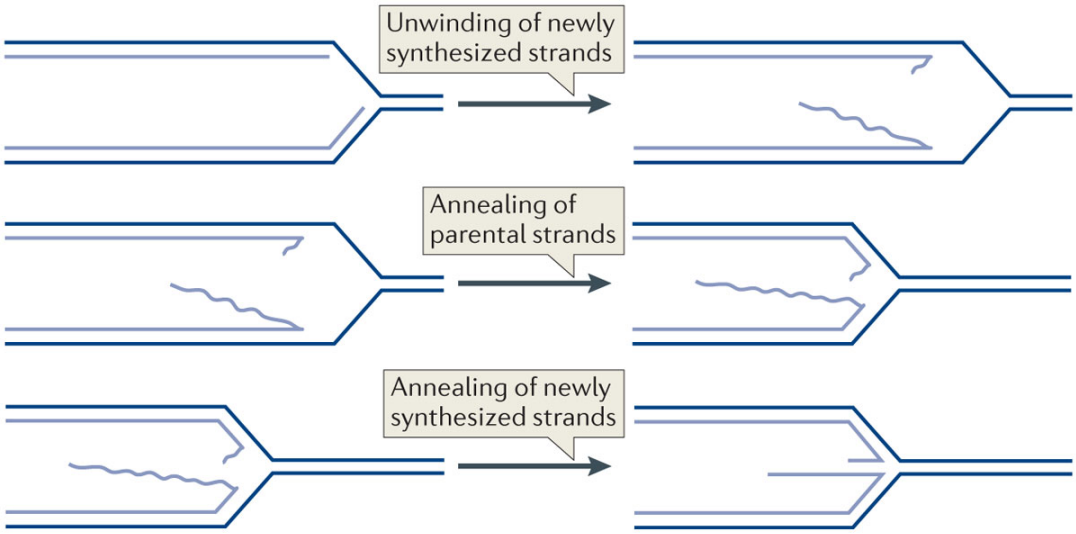

Figure 5: The process of replication fork reversal. First, newly synthesized strands are unwound (top panel), followed by reannealing of parental (middle panel) and nascent strands (bottom panel). Modified from (64).

A recent study in fission yeast suggests that also Dna2 is involved in the fork remodeling process, namely by stabilizing stalled forks upon induction of the intra-S phase checkpoint by hydroxyurea (HU) or MMS (72). Checkpoint-mediated phosphorylation of Dna2 was necessary to promote its association with stalled DNA replication forks (72). Surprisingly, in human cells, depletion of DNA2 resulted in cell cycle arrest in S/G2 phases accompanied by internuclear chromatin bridges and this phenotype was not rescued by FEN1 overexpression (41,62). This finding suggests that the Okazaki-fragment processing independent role of human DNA2 in unperturbed replication might be during the fork remodeling that is also occurring under unperturbed conditions (63,65,73).

While replication fork reversal is regarded to be beneficial upon DNA damage, as it protects the fork and gives more time for repair of the lesions, in some cases it can also promote disease development by e.g. leading to expansion of DNA repeats in neurodegenerative syndroms (63,74); or by contributing to genomic instability in cancers in case the reversed forks are subjected to unscheduled cleavage (70). Thus, studying the mechanisms of replication fork remodeling is crucial for understanding its physiological and pathological roles, and possibly for finding applications for cancer therapy.

1.2.4 Role of Dna2 in double-strand break repair

DSB repair is composed of four different pathways: homologous recombination (HR), single-strand annealing (SSA), non-homologous end-joining (NHEJ) and alternative NHEJ (alt-NHEJ or also microhomology-mediated NHEJ, MMEJ) (Figure 6). NHEJ (also called classical or canonical NHEJ) occurs during all phases of the cell cycle and is initiated by binding of Ku70-Ku80 to broken DNA ends, followed by DNA-PKCs induced end processing by Artemis and finally ligation by DNA ligase IV (75). NHEJ is error-prone, so e.g. B cells make use of it for generating antibody diversity during V(D)J recombination (76).

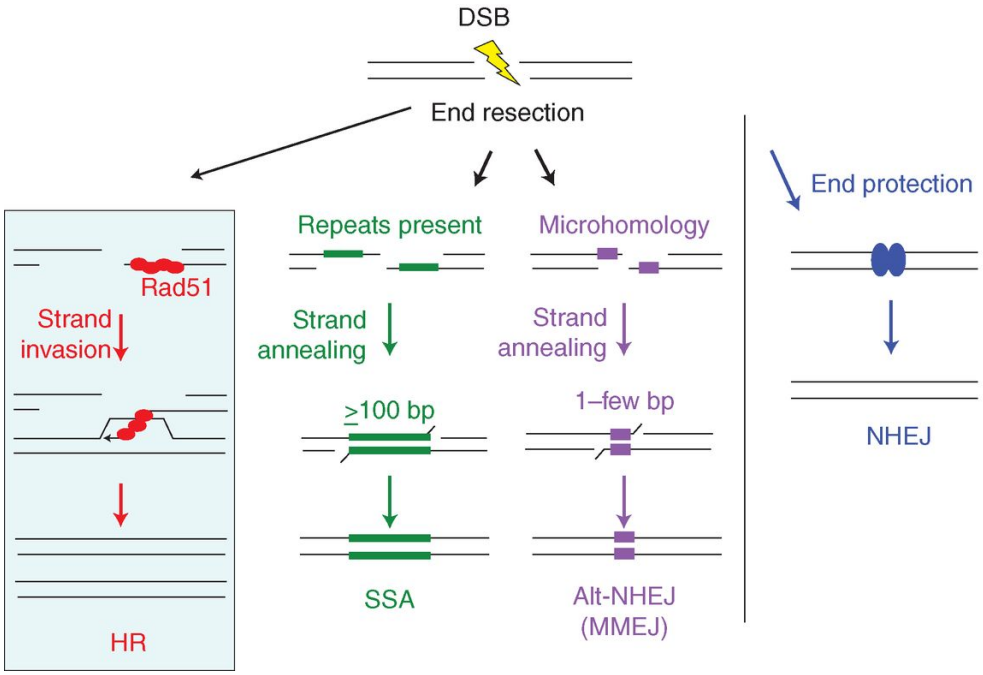

Figure 6: Pathways of double-strand break repair. Abbreviations: HR, homologous recombination; SSA, single-strand annealing; NHEJ, non-homologous end joining; alt-NHEJ, alternative-NHEJ; microhomology-mediated NHEJ (MMEJ). Modified from (77).

The other three DSB repair pathways require resection of the broken ends prior repair. Alt-NHEJ needs only minimal end processing to uncover microhomologies (5-25 bp) between the two strands allowing annealing (78). SSA is characterized by annealing of longer tandemly repeated DNA sequences flanking broken DNA ends and is mediated by Rad52 that reanneals RPA-covered ssDNA. Both pathways lead to deletions and are therefore error-prone (77-79).

HR is mainly active in S and G2 phases of the cell cycle as it needs the sister chromatid as a template and is the mostly error-free pathway for the repair or tolerance of DNA damage (80,81). The DNA lesions repaired by HR can be DSBs induced by exogenous and endogenous sources (e.g. ionizing radiation or reactive oxygen species), as well as programmed DSBs during meiosis (82). In addition, HR is involved in repair of ICLs and DNA gaps, as well as in recovery of stalled or broken replication forks (79). The latter is associated with post-replication repair (PRR) also termed DNA damage tolerance (DDT), processes that allow cells to survive replication-blocking lesions. Two main pathways have evolved in DDT, both governed by Rad6 family proteins and distinct modifications of PCNA: one is error-prone and involves TLS polymerases, while the second pathway is error-free and assumes transient template switch to the undamaged strand presumably by fork regression (already discussed above) and/or post-replicative gap repair by HR (64,79,83,84).

Mechanistically, HR is a very complex process and can result in both crossovers and non-crossovers (Figure 7). Resection leads to the formation of 3' ssDNA tails that are covered by RPA. Various recombination mediators (e.g. Rad51 paralogs, Rad52 in yeast or BRCA2 in humans) allow Rad51 filament formation on the ssDNA; the filament then performs homology search through DNA-strand invasion, thus generating a displacement loop (D-loop) structure. The D-loop formation is the branching point for the three HR sub-pathways: break-induced replication (BIR), synthesis-dependent strand annealing (SDSA) and double Holliday junction (dHJ) pathway. BIR occurs in the absence of a second DNA end and leads to a half-crossover often associated with the loss-of-heterozygocity. SDSA produces exclusively non-crossovers and requires the presence of the second DNA end that is then annealed to the newly synthesized strand after D-loop disruption. The dHJ pathway is responsible for the generation of crossovers in meiotic recombination, while in vegetative cells mainly non-crossovers are produced (79).

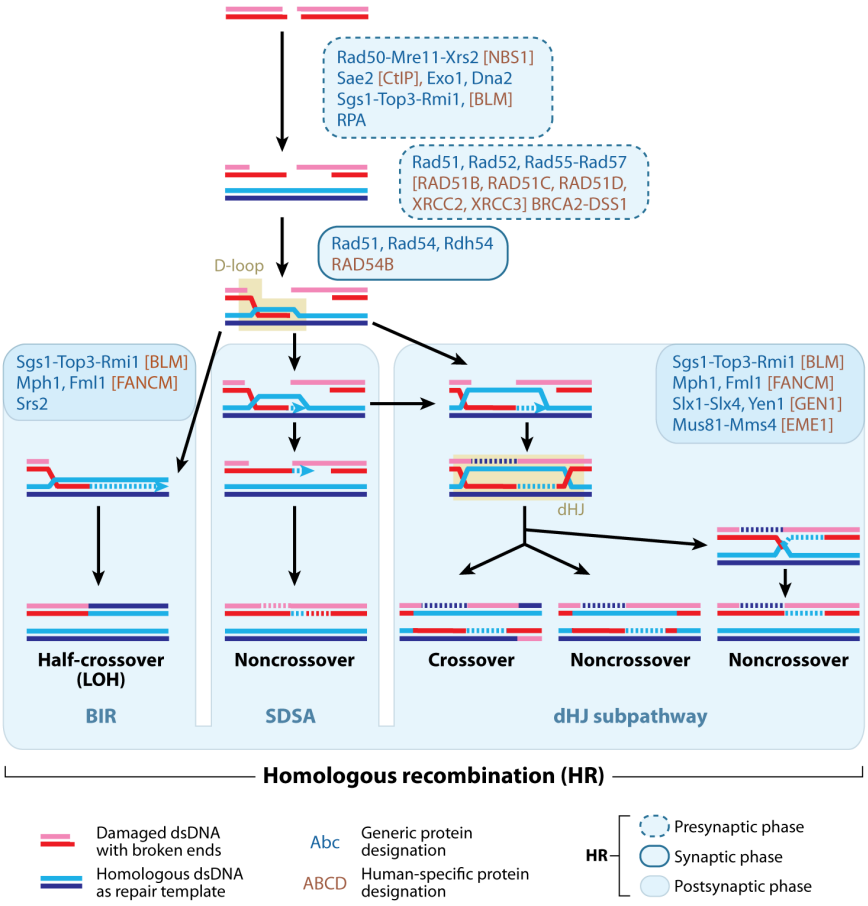

Figure 7. Mechanisms of homologous recombination. Abbreviations: BIR, break-induced replication; dHJ, double Holliday junction; LOH, loss of heterozygosity; SDSA, synthesis-dependent strand annealing. Modified from (79).

Dissolution and resolution are the two mechanisms of dHJ processing. In the dissolution pathway Sgs-Top3-Rmi1 (STR) complex in yeast (BLM-TopoIIIα-RMI1-RMI2, BTR, in humans) drives the convergent branch migration of dHJ resulting in a hemicatenane structure; Top3 action is required during branch migration and for the dissociation of the hemicatenane (85-87).

The resolution of a dHJ junction can be performed by three different structure-specific nucleases: Mus81-Mms4, Slx1-Slx4 and Yen1 (in humans: MUS81-EME1, SLX1-SLX4 and GEN1). While Mus81-Mms4 and Slx1-Slx4 cleave the dHJ asymmetrically, Yen1 was found to introduce symmetrical nicks across the junction. The resolution pathway yields crossover as well as non-crossover products (87).

DNA end resection is the commitment step for alt-NHEJ, SSA and HR (Figure 6). The term is defined as nucleolytic degradation of 5'-terminated DNA strands that results in 3' ssDNA tails required for recombination. Resection is initiated by the binding of the Mre11-Rad50-Xrs2 complex (MRX; MRE11-RAD50-NBS1, MRN, in humans) that possesses a 3' to 5' exonuclease activity, which is the opposite polarity than needed for HR (Figure 8). Only recently it was shown that in the vicinity of a protein block at the dsDNA end budding yeast Sae2 (human CtIP) stimulates the endonuclease activity within the Mre11 to incise the 5' terminated dsDNA strand (88). Then the strand can be degraded by MRX in 3'-5 direction, while the long-range resection with 5' to 3' polarity is performed either by Exo1 (human EXO1) or by the STR (human BTR) complex in conjunction with RPA and Dna2 (Figure 8, (89,90)).

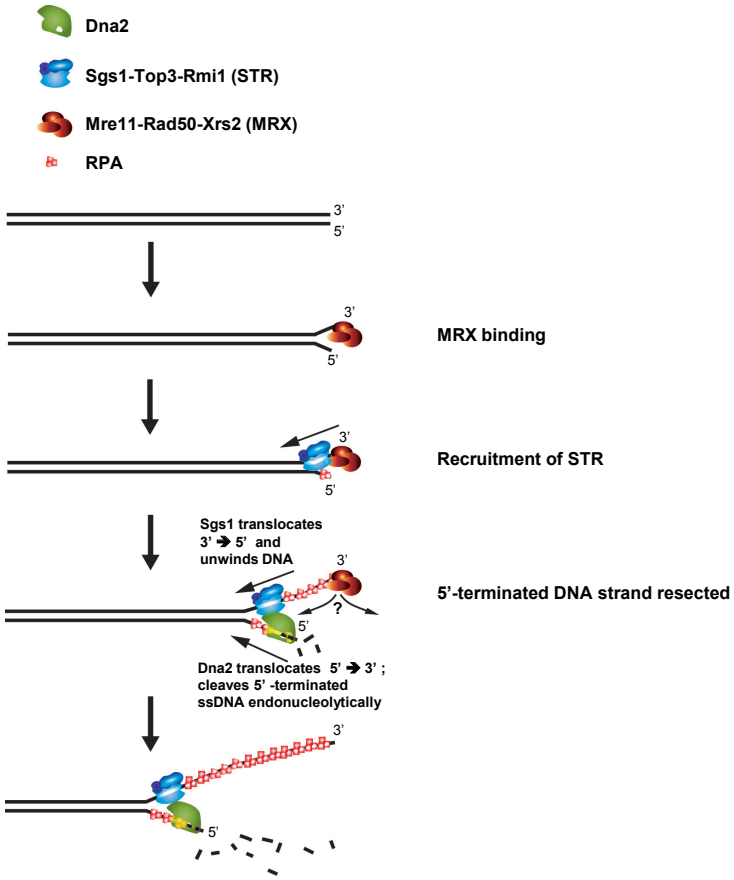

Figure 8. Model for resection of DNA double-strand breaks by Mre11-Rad50-Xrs2, Sgs1-Top3-Rmi1, Dna2 and RPA. Modified from (28).

Sgs1 as well as BLM are members of the RecQ family of helicases that possess an ATP-dependent 3'-5 translocase activity (91). In resection, Sgs1 unwinds the DNA while Dna2 degrades the 5' terminated strand. This reaction is fully dependent on

RPA and requires Top3-Rmi1 *in vivo* (28,92,93). The nuclease activity of Dna2 is essential for DNA end resection, while the helicase was shown to be dispensable (28,93). The long-range resection can generate 2-4 kb of ssDNA with a speed of 4 kb per hour in budding yeast, ensuring efficiency and fidelity of HR (94). Additionally, hDNA2 was shown to function with FANCD2 (Fanconi anemia complementation group D2) in ICL repair. Depletion of DNA2 led to increase sensitivity to ICL agents and reduced HR frequency (95).

1.2.5 Dna2 as checkpoint activator

The cellular response to DNA damage and replication stress, which is part of the cell cycle checkpoint response, is triggered by two protein kinases of the phosphatidylinositol 3-kinase-related protein kinase (PIKK) family: Mec1 (homolog of human ATR) that is activated by the presence of RPA-coated ssDNA, and Tel1 (human ATM) that recognizes DSBs. Activation of the checkpoint results in the stabilization of stalled replication forks, increased repair and dNTP synthesis, inhibition of late origin firing and changes in gene expression allowing the cell to overcome DNA damage; or in case of severe damage it initiates apoptosis in higher eukaryotes (96). Tel1 (ATM) is recruited to DSBs via its interaction with MRX (MRN) and phosphorylates histone H2AX as well as Rad53 (human Chk2) in some cases, leading to the activation of further downstream mediator and effector proteins, and cell cycle arrest. UV light and oxidative damage that are repaired by BER and NER, respectively, activate Mec1 due to ssDNA gaps appearing in course of the repair (96). Moreover, DSBs that become subject of resection are serving as Mec1 activator upon exposure of the 3' terminated ssDNA tails (97). Mec1 is associated with Ddc2 (human ATRIP) and acts only as a heterodimer (98). Although Mec1-Ddc2 is recruited to ssDNA via the interaction with RPA70 subunit, it still needs further interactions with sensor proteins to stimulate its kinase activity (99,100). Three of these Mec1-activator proteins were found in *S. cerevisiae* (Figure 9). Their activity is dependent on the cell cycle and show partial redundancy for checkpoint activation (24). The first activator is the 9-1-1 checkpoint clamp (yeast Ddc1-Rad17-Mec3; human RAD9-

RAD1-HUS1) that is the sole activator of Mec1 in G1 in *S. cerevisiae.* The stimulatory function is carried out by the Ddc1 protein (101).

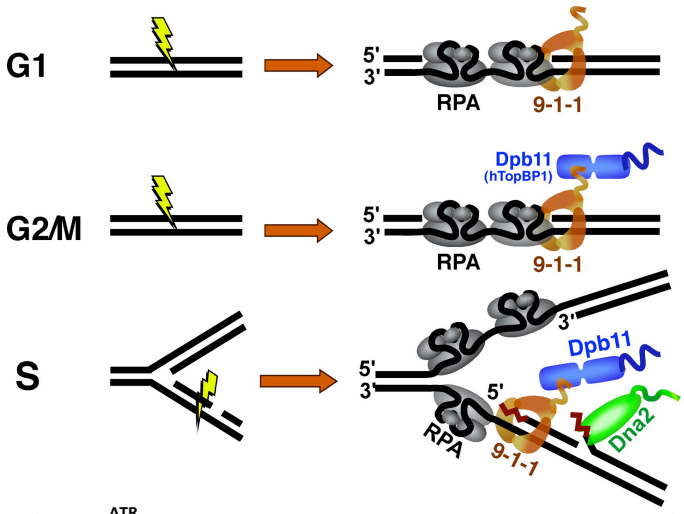

Figure 9. Activation of Mec1^{ATR} during the cell cycle. While in G1 9-1-1 protein (RAD9-RAD1-HUS1 in humans; Ddc1-Rad17-Mec3 in *S. cerevisiae*) is the sole activator of Mec1, in G2 Dpb11 can carry out this function as well. However, in S phase Dna2 can serve as a Mec1 activator in a third redundant pathway, upon replication stalling induced by hydroxyurea. Modified from (24).

In G2 phase, however, the 9-1-1 protein is additionally responsible for the recruitment of the second activator, Dpb11 (human TOPBP1), and both proteins are required for full G2 checkpoint signaling (102). In metazoans Dpb11 (TOPBP1) is the sole activator of Mec1 (ATR), although 9-1-1 is still required for Dpb11 recruitment (103). The S-phase checkpoint is quite complex and demonstrates a high level of redundancy. In budding yeast, in addition to the activation by Ddc1 and Dpb11, Mec1 can also be activated by Dna2 in S-phase, requiring its two aromatic residues within the N-terminal domain – Trp128 and Tyr130 (37). To abrogate Mec1 activation in S-phase all three of these proteins have to be inactivated. However, to completely abolish the S-phase checkpoint also Tel1 has to be inactivated and these checkpoint-deficient cells are very sick, grow slowly and fail to complete DNA replication even in the absence of DNA damaging agents (37). These findings underline the importance of the checkpoint function even in unperturbed DNA replication.

1.2.6 Additional tasks for Dna2: telomere and mitochondrial DNA maintenance

Chromosomal ends or telomeres resemble in many ways a DSB. However, it is pivotal for the cells that the DSB repair pathways do not initiate on a telomere, as this would result in fusion or loss of the telomeres, which actually can be seen in most cancers and largely contributes to the genome instability (104). Telomeres consist of long non-protein coding repeats synthesized by the telomerase, a telomere-specific reverse transcriptase. At the end of the telomere there is a 3' ssDNA overhang (50-300 nucleotides) that pairs with the repeats in the dsDNA, thus generating a protective t-loop in human cells (105). This structure together with the mammalian telomere-specific shelterin complex protects the telomere end from DNA repair enzymes and DNA damage signaling (104). In budding yeast, the 3' tail that is also called G-tail at the end of the telomere is much shorter (12-15 nucleotides) and serves as the binding platform for the CST capping complex (Cdc3-Stn1-Ten1). Furthermore, dsDNA repeats are bound by Rif1/2 and Rap1 proteins that together with CST protect telomeres from repair and checkpoint activation (106). Surprisingly, many DNA repair proteins are found at the telomeres: e.g. Ku70-Ku80 that contributes to capping, or Sgs1 and Sae2 that are responsible for C-strand resection after replication to generate the 3' G-tails (107,108). Also Dna2 was shown to localize to telomeres during G1 and late S/G2 phases (109). In mammals, DNA2 was found at telomeres as well and deletion of DNA2 in mouse cells led to telomere replication defects, fragile telomeres and sister telomere associations. Furthermore, heterozygous DNA2 knockout mice developed aneuplody-associated cancers with dysfunctional telomeres (110). Telomeric repeats are G-rich and were shown to fold in G-quadruplex (G4) structures that might block replication (111,112). Both human and yeast Dna2 were described to unwind/cleave the G4 structures which might be one of the functions of Dna2 at telomeres and would explain the phenotype of DNA2 knockout mice (110,113).

The finding that *dna2Δ* cells containing a *pif1-m2* variant (necessary for their viability), which still localized to mitochondria and showed full function, failed to

grow on glycerol media suggested a mitochondrial function for Dna2 as well (58). Also human DNA2 was reported to be mainly found in mitochondria where it colocalized with the helicase Twinkle (40,41). Moreover, human DNA2 interacted and stimulated pol γ and is thought to participate together with FEN1 in long-patch base excision repair of oxidative lesions in mtDNA (40). Finally, patients suffering from progressive myopathy were found to carry DNA2 mutations inferring that this protein is not only important for nuclear but also for mitochondrial DNA maintenance (114).

1.2.7 Dna2 as a potential therapeutic target

Cancer research of more than three decades allowed developing a steadily growing number of cancer therapies that target one of the hallmarks of cancer (Figure 10).

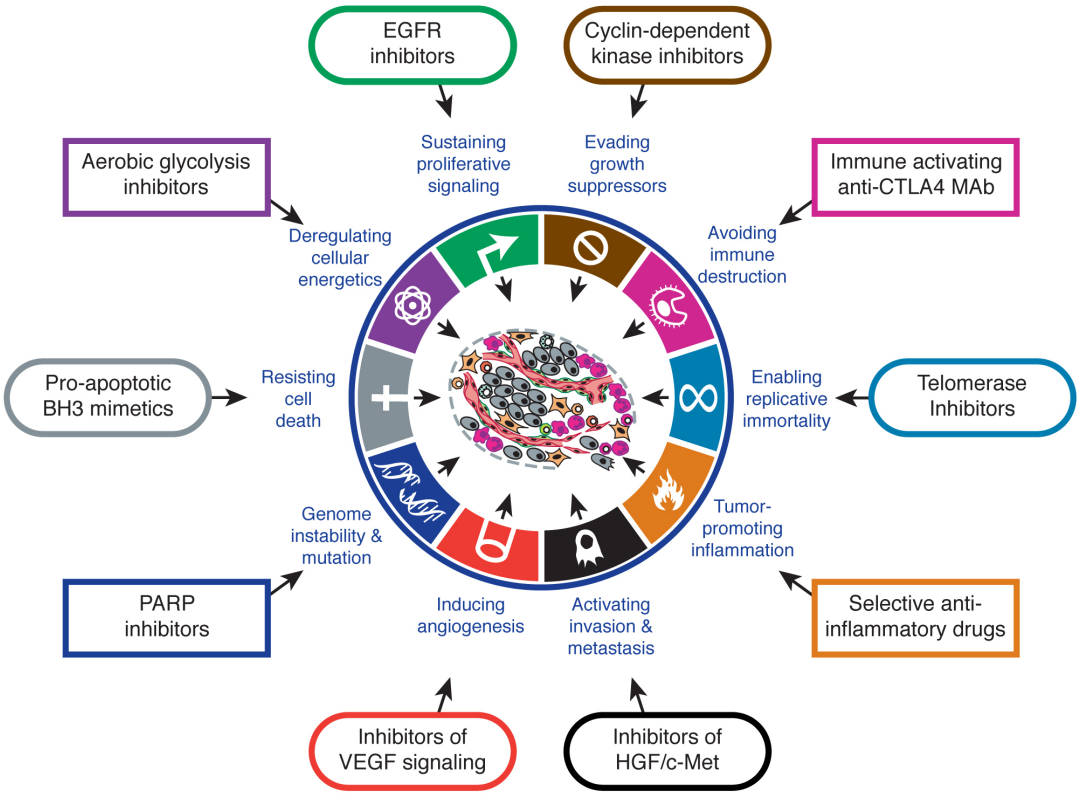

Figure 10. Therapeutic targeting of the hallmarks of cancer. Schematics showing compounds interfering with the single acquired capabilities required for tumor growth and progression. Modified from (2).

Also, the targeting of genome instability became an attractive therapy. So far, only the inhibitors of PARP1 enzyme made it to the clinics as a so-called personalized

medicine for treatment of BRCA1/BRCA2 deficient tumors (115). Their efficacy is based on the concept of synthetic lethality: PARP1 inhibitors selectively kill cells that are HR deficient due to BRCA1/BRCA2 mutation (116). It is obvious that more therapies are required that target the hallmark of genome instability.

There is a growing amount of evidence that DNA2 is involved in cancer development and progression, although the exact contribution is far from being clear. DNA2 was found to be overexpressed in a variety of human cancers and the expression correlated with the disease outcome, suggesting a tumor-promoting role for DNA2 (117). Conversely, a recent study uncovered activity-impairing mutations of DNA2 in estrogen-dependent cancers, although depletion of DNA2 inhibited xenograft growth in mice (118). The authors suggested that impairment of DNA2 activity might trigger cancer development, while an elevated DNA2 activity is possibly important for cancer progression and allows the tumor to cope with replication stress, thus providing a growth advantage to the cancer cells (118). This hypothesis is further supported by the phenotype of DNA2 knockout mice that develop aneuplody-associated cancers (110). Taken together, these findings suggest that cancer patients might benefit from therapies targeting DNA2: tumors with high DNA2 levels might thus loose their proliferative capacity, while cancers with mutated DNA2 form could be treated with additional inhibitors of DNA repair/replication proteins to induce synthetic lethality (118).

Despite the tremendous progress in targeted cancer therapies, chemo- and radiotherapy are still very often used as treatments for many types of tumors. Both therapies are based on the induction of a large amount of DNA damage in cancer cells, thus leading to cell death (119). Caffeine was shown to sensitize cancer cells to radio- and chemotherapy (120,121). On the molecular level, caffeine was suggested to inhibit p53, ATM and ATR proteins (122). However, caffeine-induced radiosensitivity was additionally proposed to result from HR-inhibition (123). A very recent study by the group of James Haber provided a possible explanation how caffeine affects HR: they show that caffeine treatment leads to proteosomal degradation of both Sae2 and Dna2 in budding yeast, thus compromising DNA end

resection pathway (124). This underlines the potential of DNA2 not only in a targeted cancer therapy, but also in classical chemo- and/or radiotherapy.

2. RESULTS

2.1 Summary of results

My PhD project started with the expression and purification of *S. cerevisiae* Dna2 protein followed by biochemical characterization of its helicase activity. Dna2 is an iron-sulfur cluster protein and is thus very sensitive to oxidation and long dialysis procedures. Therefore, we shortened and optimized the protein purification protocol, and obtained a highly active Dna2 protein preparation. We were able to show that our Dna2 preparation exhibits a vigorous but cryptic helicase activity, in contrast to previous reports from other groups, and that the helicase activity of Dna2 is masked by its nuclease (Levikova *et al*., PNAS 2013; see 2.2.1).

Next, we wanted to investigate how both helicase and nuclease activities are regulated within the Dna2 protein. We found out that Dna2 is modified by sumoylation *in vitro* and *in vivo.* Sumoylation of Dna2 attenuated the nuclease activity of Dna2 without affecting its helicase. Moreover, sumoylation levels of Dna2 varied during the cell cycle being highest in late S/G2 phases. Dna2 protein levels differed as well depending on the cell cycle stage and also decreased upon treatments with MMS and bleomycin, representing an additional level of regulation of Dna2 (Levikova *et al*., manuscript in preparation, see 2.2.2).

Dna2 was shown to function together with Fen1 in Okazaki fragment processing during lagging strand DNA replication. Having a preparation of *S. cerevisiae* Dna2 protein that displayed a higher and also somewhat different activity, we set out to revisit its exact role in Okazaki fragment maturation. Previous studies postulated a model stating that Dna2 shortens long DNA flaps arising during lagging strand DNA synthesis up to 5-8 nt, thus requiring a second nuclease activity of Fen1, before adjacent Okazaki fragments can be ligated. We demonstrated that Dna2 is able to cleave DNA flaps at or near their base, and is very efficient in Okazaki fragment maturation without Fen1, which is supported by genetic data. We suggest a Fen1-independent role for Dna2 in lagging strand DNA synthesis, probably in late replication for processing of DNA flaps that escaped Fen1 cleavage (Levikova and Cejka, NAR 2015, in press, see 2.2.3)

Further, we analyzed the potent helicase activity within the wild type Dna2 protein in more detail with regard to its role in DNA end resection. We demonstrated that the motor activity of Dna2 can act as a ssDNA translocase, rather than a helicase, to stimulate fast and efficient ssDNA degradation particularly in the presence of RPA. We propose that in DNA end resection, where Dna2 acts with Sgs1 to degrade 5'-terminated DNA strands, the translocase activity of Dna2 helps it to keep up with the lead helicase Sgs1 and to rapidly cleave the unwound 5'-terminated DNA strand (Levikova and Cejka, manuscript in preparation, see 2.2.4).

In collaboration with the laboratory of Prof. Alessandro Vindigni (St Louis University School of Medicine, MO, USA) we set out to define the role of Dna2 in the processing and restart of reversed DNA replication forks. We showed by employing biochemical and cell biological methods that human DNA2 cooperates with WRN (and yeast Dna2 with Sgs1) to process replication forks upon replication stress-induced reversal, thus driving their restart (Thangavel *et al*., JCB 2015, see 2.3.1).

In another collaborative project with the laboratory of Prof. Ulrich Rass (FMI Basel, Switzerland) we elucidated the role of Dna2 helicase in completion of DNA replication and its interplay with the Holliday-junction resolvase Yen1 in budding yeast. We provided biochemical data with the helicase-dead Dna2 variant (Ölmezer *et al*., under revision in Nat. Com., see 2.3.2)

In a further collaboration with the laboratory of PD Dr. Pavel Janscak (University of Zurich, Switzerland) we expressed and purified human DNA2 protein that is similarly difficult to purify as its yeast homolog. We showed that human DNA2 cooperates with WRN and BLM helicases in long-range DNA end resection (Sturzenegger *et al*., JBC 2014, see 2.3.3).

RPA was shown to specifically interact with Dna2 and stimulate its activity. The detailed properties of yeast and human RPA were analyzed in single molecule experiments performed in the laboratory of Prof. Ralf Seidel (University of Leipzig, Germany). We provided the purified proteins for this study (Kemmerich *et al*., manuscript in preparation, see 2.2.4).

2.2 Primary results

2.2.1 Nuclease activity of *Saccharomyces cerevisiae* Dna2 inhibits its potent helicase activity

Maryna Levikova, Daniel Klaue, Ralf Seidel and Petr Cejka.

Article published in PNAS, 2013.

I designed the research together with R.S. and P.C. and performed most of the experiments with the help of P.C. The single molecule experiments in Figure 3 and Supplementary Figure S6 were carried out by D.K. All authors analyzed the data and I wrote the manuscript together with R.S and P.C.

Nuclease activity of *Saccharomyces cerevisiae* Dna2 inhibits its potent DNA helicase activity

Maryna Levikova[a], Daniel Klaue[b], Ralf Seidel[b,c], and Petr Cejka[a,1]

[a]Institute of Molecular Cancer Research, University of Zurich, 8057 Zurich, Switzerland; [b]Biotechnology Center, Technische Universität Dresden, 01307 Dresden, Germany; and [c]Institute for Molecular Cell Biology, University of Münster, 48149 Münster, Germany

Edited* by Stephen C. Kowalczykowski, University of California, Davis, CA, and approved April 23, 2013 (received for review January 8, 2013)

Dna2 is a nuclease-helicase involved in several key pathways of eukaryotic DNA metabolism. The potent nuclease activity of *Saccharomyces cerevisiae* Dna2 was reported to be required for all its in vivo functions tested to date. In contrast, its helicase activity was shown to be weak, and its inactivation affected only a subset of Dna2 functions. We describe here a complex interplay of the two enzymatic activities. We show that the nuclease of Dna2 inhibits its helicase by cleaving 5′ flaps that are required by the helicase domain for loading onto its substrate. Mutational inactivation of Dna2 nuclease unleashes unexpectedly vigorous DNA unwinding activity, comparable with that of the most potent eukaryotic helicases. Thus, the ssDNA-specific nuclease activity of Dna2 limits and controls the enzyme's capacity to unwind dsDNA. We postulate that regulation of this interplay could modulate the biochemical properties of Dna2 and thus license it to carry out its distinct cellular functions.

DNA nuclease | replication protein-A | Sgs1

The Dna2 enzyme functions at the crossroads of key DNA metabolic processes. It was initially identified in screens for *Saccharomyces cerevisiae* mutants deficient in DNA replication (1, 2), and its importance was underscored by the finding that *dna2Δ* mutants are not viable (3). When the *DNA2* gene was cloned, it was shown to be conserved in evolution from yeast to humans and found to contain conserved nuclease and helicase motifs (4). Further work identified a number of genetic and physical interactions of Dna2 with factors required for the synthesis and maturation of the lagging strand during DNA replication, including Rad27 [homolog of human Flap endonuclease 1, FEN1 (5)]. Overexpression of Rad27 rescued growth defects of some *dna2* point mutants, and, conversely, overexpression of Dna2 suppressed *rad27Δ* defects (5). Subsequent work established that Dna2 functions together with Rad27 in the removal of single-stranded (ss) flaps generated at the 5′ termini of Okazaki fragments by polymerase δ-catalyzed strand displacement. Although Rad27 seems to have a more general role in flap processing, Dna2 is required to cleave only a subset of longer flaps bound by Replication Protein A (RPA), which stimulates its nuclease activity while inhibiting cleavage by Rad27. In this process, Dna2 and Rad27 were proposed to function in a sequential manner, with Dna2 loading first onto the flap termini and shortening them with its 5′–3′ nuclease. Rad27 was then proposed to further cleave the shortened flaps at the ss/dsDNA junctions, creating thus ligatable substrates for Cdc9 (DNA ligase 1), which completes Okazaki fragment maturation (6–8). The role of Dna2 in Okazaki fragment processing is now generally accepted although it still remains somewhat puzzling why *dna2Δ* cells are inviable whereas *rad27Δ* mutants are not.

More recently, it has been shown that Dna2 has an independent and conserved function in dsDNA break repair (9). Specifically, Dna2 belongs to one of the pathways that resect 5′ ends of dsDNA breaks to initiate homologous recombination. This process leads to the formation of long 3′ overhangs, which become coated by the strand exchange protein Rad51, and which also prime DNA synthesis during the downstream steps in homologous recombination. Genetic and later biochemical work established that Dna2 functions together with the vigorous Sgs1 helicase (Bloom in human cells) downstream of the Mre11-Rad50-Xrs2 (MRX) complex (9–14). MRX first recognizes dsDNA breaks and is likely involved in their initial processing, and subsequently helps recruit Sgs1 and Dna2. Sgs1 helicase then unwinds the DNA from the break and the ssDNA is coated by RPA, which stimulates the 5′–3′ nuclease activity of Dna2. The specific degradation of the 5′ end of the unwound DNA ensures the correct polarity of resection, which is required for homologous recombination (12, 13). However, the roles of Dna2 are not limited to Okazaki fragment and dsDNA break processing. Dna2 was also shown to function in telomere maintenance (15), aging (16), long-patch base excision repair (17), and prevention of reversal of stalled replication forks (18). The expression of human DNA2 was increased in human cancers and negatively correlated with disease outcome, indicating that DNA2 function is relevant for human health (19). However, the role of Dna2/DNA2 in these latter processes remains poorly defined.

The potent nuclease activity of Dna2 seems to be critical for all of its functions, including replication and recombination. Point mutants lacking the nuclease activity are inviable as a *dna2Δ* strain (20). The nuclease activity of Dna2 is ssDNA-specific, and shows both 5′–3′ and 3′–5′ polarities. Because RPA stimulates the 5′–3′ nuclease and inhibits the 3′–5′ activity, it is likely that only the 5′–3′ directionality is important in vivo (12, 13). It has been shown that the Dna2 nuclease can load only on a free ssDNA tail, and that it subsequently cleaves DNA endonucleolytically into short oligonucleotides (21, 22).

Much less is known about the function of the helicase activity of Dna2. To date, very weak 5′–3′ unwinding capacity has been demonstrated for the yeast enzyme (4, 7, 23). Interestingly, similarly to the Dna2 nuclease, also the helicase domain requires a free DNA end (22). In contrast, no unwinding activity could be detected in the *Xenopus laevis* Dna2. Whether human DNA2 possesses helicase activity remains controversial (24–27). Yeast point mutants lacking helicase activity show impaired growth but

Significance

The integrity of DNA must be preserved to pass genetic information onto the next generation and to prevent genomic instability. One of the key enzymes involved in DNA metabolism is the nuclease-helicase Dna2, which is required for both DNA replication and the repair of broken DNA. Our work revealed that Dna2 from *Saccharomyces cerevisiae* possesses a potent but cryptic helicase capacity, which is controlled by the nuclease activity of the same polypeptide. Regulating the interplay between both enzymatic activities might explain how Dna2 can take on its distinct cellular roles.

Author contributions: M.L., R.S., and P.C. designed research; M.L., D.K., and P.C. performed research; M.L., D.K., R.S., and P.C. analyzed data; and M.L., R.S., and P.C. wrote the paper.

The authors declare no conflict of interest.

*This Direct Submission article had a prearranged editor.

[1]To whom correspondence should be addressed. E-mail: cejka@imcr.uzh.ch.

This article contains supporting information online at www.pnas.org/lookup/suppl/doi:10.1073/pnas.1300390110/-/DCSupplemental.

are viable under most conditions (23). Overexpression of Rad27 partially rescues *dna2* helicase-deficient mutants, suggesting that the helicase activity might play a supportive but nonessential role in DNA replication (28). The helicase-deficient mutants show a dramatic sensitivity to the DNA alkylating drug methylmethanesulfonate (MMS), pointing to an as-yet uncharacterized role of Dna2 helicase in the repair of DNA damage (29). In contrast, Dna2 helicase activity had no detectable effect on DNA end resection (9). Due to the limited unwinding capacity of Dna2 observed in vitro, the motor was proposed to function as an ssDNA translocase to aid positioning of the nuclease domain on ssDNA and to remove secondary structures from ssDNA, rather than as a DNA helicase to unwind dsDNA (23).

In this work, we expressed *S. cerevisiae* Dna2 and its variants and optimized the purification of these polypeptides. We now show that Dna2 is a potent but cryptic DNA helicase. It functionally interacts with RPA, which enables it to unwind tens of kilobases of dsDNA. Surprisingly, the nuclease of wild-type Dna2 interferes with this remarkable helicase capacity by cleaving ssDNA tails that the helicase requires for loading onto DNA to initiate unwinding. The interplay between the two main biochemical activities of Dna2 might fine-tune its behavior to suit its distinct cellular roles.

Results

Expression and Purification of Wild-Type Dna2 and Nuclease- and Helicase-Dead Variants. *S. cerevisiae* Dna2 is a large protein (172 kDa) consisting of 1,522 amino acids (Fig. 1*A*). We noticed previously that recombinant Dna2 was rather unstable, rapidly losing activity during extended dialysis procedures used in earlier preparation protocols (12). Furthermore, it was sensitive to the omission of reducing agents, possibly due to the presence of an oxidation-prone iron–sulfur cluster (30, 31). Modification of the purification procedure allowed us to obtain Dna2 with a high specific nuclease activity (12). In this work, we further optimized and shortened the purification process (*Materials and Methods*) and obtained nearly homogenous wild-type Dna2 and nuclease-dead Dna2 E675A, as well as helicase-dead Dna2 K1080E variants (Fig. 1 *A* and *B* and Fig. S1 *A* and *B*).

Dna2 Possesses a Vigorous DNA Helicase Activity. The ssDNA-specific nuclease activity of Dna2 was proposed to obscure the detection of its limited unwinding property (22). Therefore, the nuclease-dead Dna2 variants were used to characterize its helicase activity. One of these mutants is Dna2 E675A, which had been designed based on the homology between *Escherichia coli* RecB and *S. cerevisiae* Dna2 nuclease sites (20). Indeed, mutation of the conserved glutamate at position 675 to alanine largely inactivated the nuclease activity of Dna2, and Dna2 E675A has been shown to exhibit a weak helicase activity (22, 23). Here, having used the optimized preparation procedure, we set out to examine the helicase activity of this variant. Dna2 E675A could readily unwind a synthetic Y-structure oligonucleotide-based substrate containing 31 base pairs of dsDNA (Fig. 1*C*). To our great surprise, the helicase was active at subnanomolar concentrations (Fig. 1*C*). Previously, ~20 nM enzyme was needed to unwind a similar length of dsDNA (22, 23), indicating that our preparation possesses >20-fold higher specific DNA unwinding activity. In agreement with previous data (23), supplementing the reaction with *S. cerevisiae* replication protein A (RPA) did not further stimulate its unwinding capacity whereas *E. coli* Single Strand DNA Binding protein (SSB) strongly inhibited DNA unwinding (Fig. 1 *C* and *D*). We show that a 5′-tailed DNA is a preferred structure for Dna2 E675A unwinding, with ~0.05 nM Dna2 E675A required to unwind 50% of the DNA substrate, which was used at 1 nM concentration (Fig. 1*E* and Fig. S2). The unwinding of the 5′-tailed DNA substrate was therefore clearly catalytic, with one enzyme molecule being capable of unwinding at least ~10 DNA substrate molecules during the time course of the reaction. The vigorous activity stands in contrast with previous studies

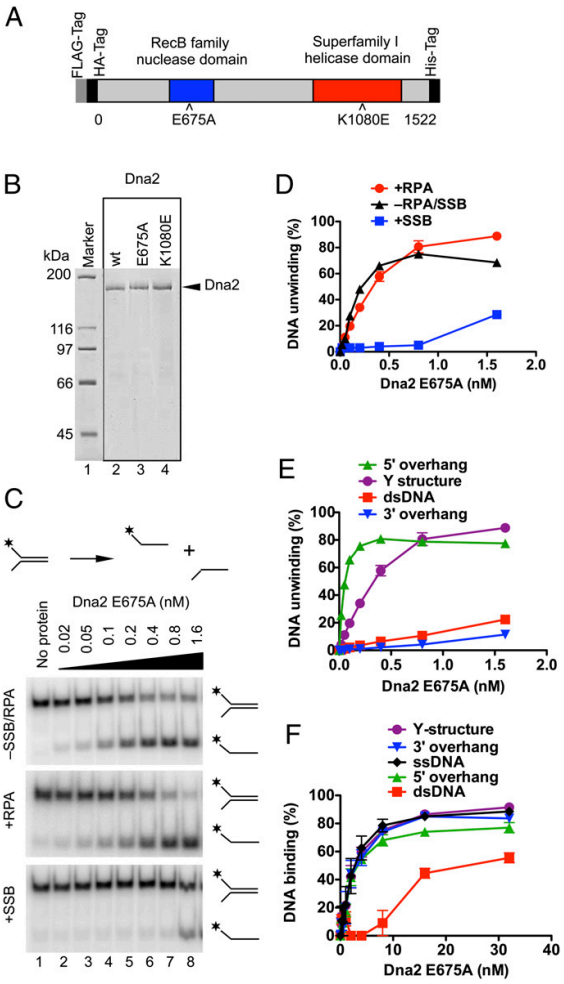

Fig. 1. The nuclease-inactive Dna2 E675A variant possesses a vigorous DNA helicase activity. (*A*) A schematic representation of the recombinant Dna2 protein used in this study. The polypeptide contains an N-terminal FLAG and HA tags, and a C-terminal 6xHis tag. Positions of mutations inactivating the nuclease activity (E675A) or helicase activity (K1080E) are indicated. (*B*) Purified Dna2 wild-type (wt), E675A, and K1080E variant proteins (550 ng each) used in this study were stained with Coomassie blue. (*C*) Representative polyacrylamide gels (10%) showing the DNA helicase activity of Dna2 E675A on a ^{32}P-labeled Y-structure DNA substrate (1 nM). The length of both ssDNA arms was 19 nt. As indicated, the reactions were supplemented with either *S. cerevisiae* RPA or *E. coli* SSB (both 22 nM). *, position of the ^{32}P label. (*D*) Quantitation of the helicase assays such as shown in C. Error bars, SE, $n = 3$. (*E*) Quantitation of the helicase assays such as shown in Fig. S2. Error bars, SE, $n = 3$. (*F*) Quantitation of electrophoretic mobility shift assays showing the binding of Dna2 E675A to various ^{32}P-labeled DNA substrates (1 nM). Error bars, SE, $n = 3$.

where ~15- to 100-fold excess enzyme over DNA substrate was required to detect DNA unwinding (22, 23). We further show that ~0.3 nM Dna2 E675A was required to unwind 50% of the Y-structure DNA substrate; thus, the presence of an additional 3′ ssDNA arm (Y-structure vs. 5′ overhang) inhibited DNA unwinding ~sixfold (Fig. 1*E* and Fig. S2). As anticipated for a 5′–3′ DNA helicase, the unwinding of 3′-tailed or fully dsDNA substrates was inefficient (Fig. 1*E* and Fig. S2). The difference between the specific DNA

unwinding activity presented here and in earlier reports (22, 23) is likely due to the optimized enzyme preparation procedure used in this work (*Materials and Methods* and *Discussion*).

Next, we used electrophoretic mobility shift assays to assess the binding of Dna2 E675A to DNA. We saw that Dna2 E675A binds rather indiscriminately (K_d ~5 nM) to structures that contain ssDNA. A 5′ ssDNA overhang was bound equally well as a 3′ ssDNA overhang, despite the fact that the former structure is an excellent substrate for the Dna2 E675A helicase whereas the latter is not (Fig. 1*F* and Fig. S3*A*). Similar results were obtained in the presence of competitor DNA in the electrophoretic mobility shift assays (Fig. S3*B*). These results show that Dna2 E675A is a vigorous DNA helicase with high affinity for DNA.

RPA Stimulates Dna2 E675A to Unwind Long Stretches of DNA. Dna2 nuclease-deficient variants were previously shown to be only capable of unwinding short, oligonucleotide-based DNA structures. The fraction of unwound substrate decreased dramatically with the length of the duplex DNA; the unwinding of a 91-bp duplex was ~15-fold less efficient than the unwinding of a 30-bp duplex (23). Is has been proposed that Dna2 is a weak and nonprocessive DNA helicase (23). We have decided to analyze unwinding of long-length DNA with our preparation of Dna2 E675A. Surprisingly, the enzyme could readily unwind plasmid-based 2.7-kbp dsDNA containing a 3-nt-long 5′ ssDNA tail (Fig. 2*A*). Half of the DNA substrate was unwound by only 200 pM Dna2 E675A, a concentration similar to that required for the unwinding of oligonucleotide-based DNA substrates (Fig. 1 *C* and *E*). However, unlike in the case of the oligonucleotide-based substrates, the unwinding of the 2.7-kbp dsDNA was absolutely dependent on RPA, as no DNA unwinding was observed when RPA was omitted (Fig. 2*A*, lane 12). *E. coli* SSB could not replace RPA (Fig. 2*A*, lane 13), indicating that species-specific interaction between yeast Dna2 and yeast RPA plays an essential role in promoting long-length DNA unwinding by the Dna2 helicase.

Sgs1 is the most vigorous DNA helicase characterized to date in eukaryotes (32). Given that it functions in DNA end resection together with Dna2 (9, 12, 13), we set out to compare the unwinding capacities of Sgs1 and Dna2 E675A. Sgs1 helicase can initiate DNA unwinding of blunt-ended, 3′− or 5′-tailed DNA with similar efficiency (32). To compare the relative activities of both enzymes, we selected 5′-tailed DNA, which is required for unwinding by Dna2 E675A. Remarkably, we show that Sgs1 was only slightly (~30%) better in unwinding of the 2.7-kbp-long dsDNA than Dna2 E675A (Fig. 2 *A* and *B*), and similar results were obtained in kinetic experiments (Fig. 2*C* and Fig. S4). We thus conclude that Dna2 E675A is almost as vigorous a DNA helicase as Sgs1.

To further characterize the unwinding capacity of Dna2 E675A, we tested its ability to unwind long stretches of dsDNA. We have digested bacteriophage λ DNA with HindIII and ^{32}P-labeled the restriction fragments. This procedure created linear DNA molecules of up to 23 kbp in length with 3-nt-long 5′ overhangs. Dna2 E675A could efficiently unwind DNA fragments of all lengths and produced a pattern of ssDNA molecules that comigrated with the heat-denatured substrate (Fig. 2 *D* and *E*). The reaction was remarkably efficient; 1.2 nM Dna2 E675A unwound ~50% of the DNA substrate, which was present at a concentration corresponding to 2.4 nM DNA ends. Furthermore, the 23-kbp fragment was unwound only ~twofold less efficiently than the 2.0-kbp fragment, showing that the length of duplex DNA only marginally affects the unwinding efficiency in the presence of *S. cerevisiae* RPA. Unlike *E. coli* SSB, human RPA could substitute cognate *S. cerevisiae* RPA, and, as expected, the reaction was completely dependent on ATP (Fig. S5). We conclude that S. *cerevisiae* Dna2 E675A is a very vigorous DNA helicase, capable of unwinding tens of kilobases of dsDNA in length in a reaction dependent on RPA and ATP.

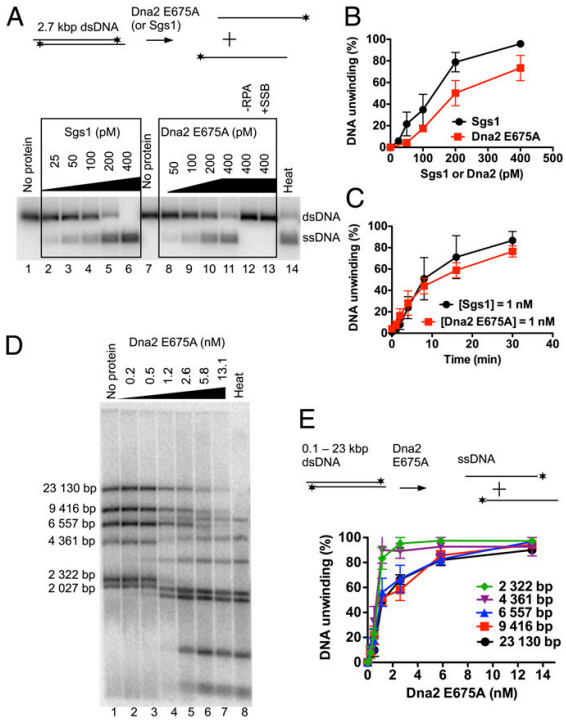

Fig. 2. Dna2 E675A can unwind long lengths of dsDNA in the presence of RPA. (*A*) Representative agarose gels (0.8%) showing the helicase activity of Dna2 E675A or Sgs1 on a ^{32}P-labeled 2.7-kbp-long dsDNA substrate with a 3-nt 5′ ssDNA overhang (1 nM). The reactions were supplemented with *S. cerevisiae* RPA (0.4 μM) except lane 12 (RPA omitted) and lane 13 (RPA replaced with *E. coli* SSB). Heat, heat-denatured DNA substrate; *, position of the ^{32}P label. (*B*) Quantitation of the helicase assays as in *A*. Error bars, SE, n = 3. (*C*) Kinetics of DNA unwinding of 5′-tailed 2.7-kbp-long dsDNA (1 nM) by either Dna2 E675A (1 nM) or Sgs1 (1 nM) in the presence of RPA (0.4 μM). Error bars, SE, n = 3. (*D*) λ phage DNA was digested with HindIII to produce dsDNA fragments ranging from 125 bp to 23 kbp in length, and ^{32}P-labeled with Klenow fragment of DNA polymerase I. The resulting DNA fragments had 5′ ssDNA tails of 3 nt in length at their ends. Various concentrations of Dna2 E675A were incubated with the restricted DNA (2.4 nM of DNA ends) in the presence of RPA (1.08 μM). Heat, heat-denatured substrate. The panel shows a representative agarose gel (1%). (*E*) Quantitation of the helicase assays such as shown in *D*. Error bars, SE, n = 3.

Single Molecule Experiments Reveal High DNA Unwinding Processivity of Dna2 E675A. To gain insight into the processivity and the rate of DNA unwinding by Dna2 E675A, we carried out single-molecule magnetic tweezers experiments (Fig. 3 *A* and *B*). As substrate we used a 6.6-kbp-long dsDNA fragment that contained 0.6-kbp dsDNA tails with multiple digoxigenin or biotin modifications at either end to allow its binding to the surface of an anti-digoxigenin–coated fluidic cell and to streptavidin-coated magnetic beads. The construct contained a 40-nt 5′-terminated ssDNA flap to allow the loading of Dna2. A pair of magnets above the fluidic cell was used to stretch single bead-tethered DNA constructs, and video microscopy was used to read out the DNA end-to-end distance in real time (33).

When adding Dna2 E675A in the presence of RPA and ATP, rapid DNA unwinding was observed that resulted in an apparent increase in the DNA length (Fig. 3 *B* and *C*). This increase is due to the larger extension of RPA-coated ssDNA in comparison with dsDNA (34, 35). No significant DNA lengthening (>100 bp)

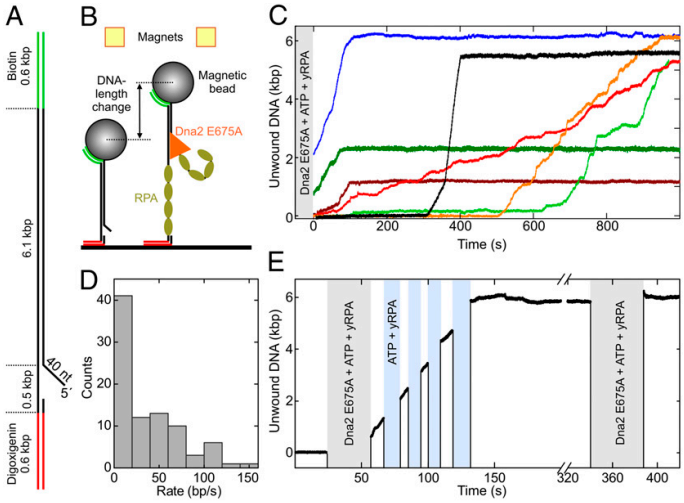

Fig. 3. Single molecule experiments reveal highly processive DNA unwinding by Dna2 E675A. (*A*) Sketch of the DNA construct and (*B*) the magnetic tweezers assay. (*C*) Representative DNA unwinding events by Dna2 E675A ($F = 25 \pm 2$ pN, SD). DNA lengthening was observed only after addition of the enzyme, RPA, and ATP in the reaction buffer (gray box). (*D*) Histogram of rates for unwinding 500 bp of DNA ($F = 25 \pm 2$ pN, SD). Unwinding trajectories ($n = 14$) were split into successive 500-bp segments, and the mean unwinding rate was determined from the slope of a linear fit to each segment. The mean unwinding rate was 38 ± 4 bp·s^{-1} (SE). (*E*) Removal of free Dna2 E675A from solution during a DNA unwinding reaction. The reaction was initiated by adding the enzyme in the presence of RPA and ATP (left gray box). After several hundred unwound bps, ~50 μl of ATP and RPA in reaction buffer were flushed through the fluidic cell (cell volume 30 μl) (blue boxes). The procedure was repeated four times during one unwinding event.

was observed in the absence of either RPA, ATP, or the 5′-terminated flap (but in presence of Dna2), in agreement with our previous data showing that RPA, ATP, and a 5′ ssDNA tail were required for the unwinding of long lengths of DNA by the Dna2 helicase. As expected, no DNA lengthening was found when RPA was added in the absence of the helicase at the applied forces. The observed DNA lengthening is thus due to DNA unwinding by Dna2 E675A.

Unwinding rates were found to be highly variable (Fig. 3 *C* and *D*) as found also for other DNA translocases (36). Although some events displayed a rather constant unwinding rate of up to 120 bp·s^{-1} over distances of several kbp, also much slower events (down to 15 bp·s^{-1}) were observed with similar frequency. The average unwinding rate over 500 bp of DNA was found to be 38 ± 4 bp·s^{-1} (SE) at a force of 25 pN (Fig. 3*D*). Slow events often displayed multiple unwinding rate changes or stalls, with periods of fast DNA unwinding in between. However, rate changes and stalls were characteristic of fast unwinding events as well (Fig. S6*A*). Because we measured DNA unwinding under an external tension, we also investigated how the unwinding process is influenced by different forces. Because the unwinding rates were variable from molecule to molecule, we applied different forces during a single unwinding run of a molecule (Fig. S6*B*). The unwinding rate was found to decrease ~fivefold when lowering the force from 30 to 10 pN. Nonetheless DNA unwinding of several kbp was found also at the lower forces.

An average unwinding distance of 4.2 ± 0.5 kbp (SE, $n = 25$) was obtained (Fig. 3*C*). Activity was terminated after unwinding several kbp or the complete 6.1-kbp DNA substrate ($F = 25$ pN). Partially also the loss of the magnetic bead was observed. DNA unwinding activity commenced after highly variable lag times ranging from 0 to 800 s with a mean of 85 ± 31 s (SE, $n = 25$) (Fig. 3*C*). Variable lag times and the abrupt termination of helicase reactions before unwinding of the full-length substrate, suggested that, in most cases, the reaction was catalyzed by a single Dna2 E675A complex. Thus, Dna2 E675A could be a processive DNA helicase. To investigate processivity in further detail, we repeatedly flushed out Dna2 E675A (by adding buffer containing ATP and RPA only) just after an unwinding event had been initiated. Each flush corresponded to ~1.7 flow cell volumes. DNA unwinding was not affected by removing free Dna2 E675A from the solution either during or after the flush (Fig. 3*E*). Adding Dna2 E675A back in after the unwinding stopped did not initiate further unwinding. Our results strongly suggest that a single enzyme complex drives the observed long-range DNA unwinding. In summary, these measurements show that Dna2 E675A is a highly processive helicase capable of unwinding kbp-sized DNA fragments in a single run.

Dna2 E675A Possesses Vigorous DNA-Dependent Atpase Activity That Is Stimulated by RPA. The unexpected DNA helicase activity of Dna2 E675A prompted us to characterize its capacity to hydrolyze ATP. To this point, we used a spectrophotometric assay, which measures ATPase activity based on a reaction coupled to the oxidation of NADH (37, 38). To obtain kinetic parameters for ATP hydrolysis, we first varied ATP concentration in the presence of Y-structure DNA as a cofactor (Fig. S7). The curve showing the dependence of the ATPase activity on ATP concentration was hyperbolic, and a fit to the Michaelis–Menten equation yielded $V_{max} = 21 \pm 2$ μM·min^{-1} and $K_m = 130 \pm 24$ μM. The ATPase was stimulated by RPA, with $V_{max} = 24 \pm 2$ μM·min^{-1} and $K_m = 56 \pm 10$ μM (Fig. S7). Next, we used poly(dT) as cofactor, which is ssDNA devoid of secondary structure, and varied its concentration (Fig. 4*A*). The fit to the data yielded $V_{max} = 9.6 \pm 1$ μM·min^{-1} and $K_m = 164 \pm 44$ nM. Supplementing the reactions with RPA promoted the rate of ATP hydrolysis and resulted in $V_{max} = 22 \pm 2$ μM·min^{-1} and $K_m = 181 \pm 33$ nM.

Next, we compared the ATPase activity in the presence of various DNA cofactors. The greatest ATPase activity was observed in the presence of 5′-tailed DNA (Fig. 4*B*). The apparent k_{cat}, which is the apparent ATP turnover number, was ~85 s^{-1}, which is comparable with the k_{cat} of Sgs1 ~82 s^{-1} on the same DNA structure (32). Nearly as effective was the Y-structure dsDNA, with k_{cat} ~79 s^{-1}. Other DNA substrates were substantially

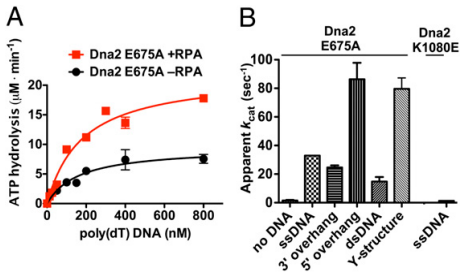

Fig. 4. Dna2 E675A shows DNA-dependent ATPase activity that is stimulated by RPA. (*A*) Rate of ATP hydrolysis and its dependence on the DNA concentration. The reactions contained Dna2 E675A (4 nM), ATP (1 mM), RPA where indicated (150 nM), and the indicated concentrations of poly(dT). (*B*) Apparent ATP turnover number and its dependence on various DNA structures (1 μM nucleotides). The reactions contained Dna2 E675A (3 nM) and ATP (1 mM). Error bars, SE, $n = 2$.

less effective; ssDNA stimulated about 2.6-fold less than 5′-tailed DNA, and 3′-tailed DNA and dsDNA stimulated 3.5- or 6.1-fold less efficiently, respectively (Fig. 4*B*). The capacity of the DNA structures to promote ATP hydrolysis by Dna2 E675A corresponded to the unwinding preference. The 5′-tailed and Y-structure DNA substrates were the preferred substrates for DNA unwinding by Dna2 E675A (Fig. 1*E*), and they were also the most efficient in stimulating its ATPase activity (Fig. 4*B*). Almost no ATPase activity was observed in the absence of DNA, showing that the ATPase activity of Dna2 E675A is DNA-dependent (Fig. 4*B*). As expected, the ATPase-deficient Dna2 K1080E variant showed no ATPase activity (Fig. 4*B*). In summary, these parameters establish that Dna2 E675A is a strong ATPase that has a high affinity for both ATP and DNA.

Nuclease Activity Within Dna2 Limits Its Unwinding Capacity. Having established that Dna2 E675A variant lacking the nuclease activity is a vigorous DNA helicase, we next wanted to study the interplay of the nuclease with the helicase within the wild-type protein. The nuclease of Dna2 is ssDNA-specific but may act on dsDNA upon spontaneous denaturation/melting of dsDNA ends (39). We show in Fig. 5*A* that, whereas 1 nM Dna2 E675A was sufficient to completely unwind a 2.7-kbp dsDNA substrate (lane 2), the same concentration of wild-type Dna2 had no detectable activity (lane 3). When we used 10- to 50-fold higher wild-type Dna2 concentration (10 and 50 nM), only limited DNA degradation was observed, as indicated by the release of the radioactive label (Fig. 5*A*, lanes 4 and 5), or mobility shift of unlabeled DNA stained with ethidium bromide (Fig. 5*B*). DNA degradation by wild-type Dna2 was largely restricted to the vicinity of the DNA ends (compare panels *A* and *B* in Fig. 5). Thus, wild-type Dna2 apparently lacked the vigorous helicase activity observed in the nuclease-dead E675A variant. This observation suggests either that the helicase/ATPase domain of the wild-type protein is compromised, or that the nuclease of Dna2 inhibits its own helicase activity. To differentiate between these two possibilities, we compared the initial rates of ATP hydrolysis between the wild-type and the nuclease-dead Dna2 E675A proteins. We show that both polypeptides display similar levels of ATPase activity (Fig. 5*C*), indicating that the ATPase/helicase domain in the wild-type protein is active and therefore likely properly folded. This result suggested that the nuclease of wild-type Dna2 limits the engagement of its helicase. We next set out to study this phenomenon in more detail.

Because the nuclease activity of Dna2 preferentially degrades 5′ ssDNA overhangs, and these overhangs are required for DNA unwinding by the Dna2 E675A variant (Fig. 1*E*), we asked whether the nuclease of wild-type Dna2 might cleave the 5′ ssDNA tails before they can be accessed by the helicase. This activity could explain the apparent lack of DNA unwinding activity of wild-type Dna2. To this point, we set out to compare enzyme concentrations required for the unwinding and/or the nucleolytic degradation of oligonucleotide-based DNA substrates. Specifically, we compared the nuclease activity of Dna2 wild type and Dna2 K1080E with the helicase activity of Dna2 E675A. All these enzyme variants were prepared using an identical procedure, and we noted that independent preparations of the same enzyme variant led to consistent levels of specific activity (*Materials and Methods*). We observed that, first, the nuclease activities of both wild-type and helicase-dead K1080E enzymes were indistinguishable based on substrate utilization (Fig. 5*D*). The lack of the helicase activity therefore did not affect the initial 5′ end cleavage by Dna2. Second, the nuclease activity was ∼sixfold more frequent than the helicase activity based on substrate utilization: although 50 pM wild-type and helicase-dead K1080E Dna2 cleaved ∼50% of the 5′ tails within 30 min, as much as 300 pM of nuclease-dead Dna2 E675A was required to unwind 50% of the DNA substrate during the same time period (Fig. 5*D*). These results show that the wild-type protein

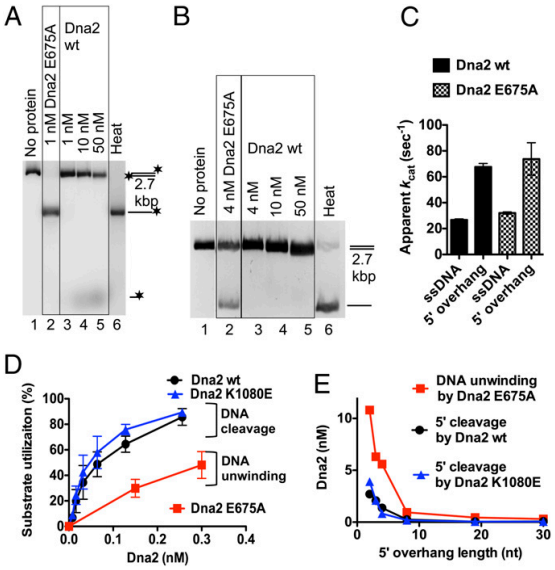

Fig. 5. The nuclease activity of Dna2 interferes with its helicase activity. (*A*) A representative experiment comparing the activities of wild-type Dna2 and nuclease-dead E675A variant on 5′-tailed 2.7-kbp dsDNA substrate ^{32}P-labeled at the 3′ end (1 nM). Reactions were incubated in the presence of *S. cerevisiae* RPA (0.4 μM). *, position of the ^{32}P label. Heat, heat-denatured substrate. (*B*) A representative experiment comparing the activities of wild-type Dna2 and nuclease-dead E675A variant on 5′-tailed 2.7-kbp dsDNA substrate (3.8 nM). Reactions were incubated for 30 min in the presence of *S. cerevisiae* RPA (1.68 μM). A 1% agarose gel was stained with ethidium bromide. Heat, heat-denatured substrate. (*C*) Comparison of apparent ATP turnover numbers of Dna2 wild-type and Dna2 E675A variant. The reactions contained the indicated DNA structures (1 μM nucleotides), Dna2 wild type or E675A (3 nM) and ATP (1 mM). Error bars, SE, $n = 2$. (*D*) Comparison of nuclease and/or helicase activities of Dna2 wild-type, K1080E, and E675A variants, respectively, based on substrate utilization. All assays contained RPA (22.5 nM). Error bars, SE, $n = 2$. (*E*) Dependence of Dna2 activities on the length of the 5′ ssDNA overhang. Dna2 concentrations required for 50% of maximal DNA cleavage (by Dna2 wild type or Dna2 K1080E) or 50% of maximal DNA unwinding (by Dna2 E675A) were plotted against the length of the 5′ ssDNA overhang. The data were obtained by analysis of the results such as from Fig. S8.

is more likely to degrade a 5′ ssDNA tail, rather than to use it to initiate DNA unwinding.

We next wondered whether varying the length of the 5′ ssDNA tail might differentially affect the nuclease or the helicase activities of Dna2. To this point, we analyzed wild-type Dna2, E675A, and K1080E variants on duplex DNA substrates containing 5′ ssDNA tails of 0- to 30-nt in length. Both nuclease and helicase activities preferred longer ssDNA tails (Fig. S8 *A*–*C*). However, irrespectively of the length of the ssDNA tail, ∼four- to sixfold higher enzyme concentration was required for DNA unwinding by Dna2 E675A than for the nucleolytic cleavage by either wild type or Dna2 K1080E (Fig. 5*E*). The nuclease activity was thus clearly dominant in the wild-type protein. In summary, our data show that the nuclease of Dna2 limits its unwinding capacity.

Nuclease Activity of Wild-Type Dna2 Interferes with Its Stable Binding to DNA. Nuclease-dead Dna2 E675A efficiently binds 5′-tailed DNA (K_d ∼5 nM) and binds dsDNA with ∼eightfold lower efficiency (K_d ∼40 nM, Fig. 6 *A* and *C*; see also Fig. 1*F*). In contrast, wild-type Dna2 rapidly cleaves the 5′ tail and binds the resulting structure with affinity comparable with dsDNA (K_d ∼40 nM, Fig. 6 *B* and *C*), showing that the nuclease activity interferes with DNA binding. We have also used ssDNA blocked with biotin-bound streptavidin on both ends as a substrate for electrophoretic mobility shift assays. Blocked ends are known to inhibit both the ssDNA-specific nuclease as well as the helicase activity of Dna2 (21, 22). Using this uncleavable DNA, we show that both wild-type Dna2 and the E675A variant bound this structure with similar affinity (K_d ∼8 nM), indicating that wild-type Dna2 is capable of strong DNA binding (Fig. 6 *D*–*F*). Finally, we observed that, whereas the rate of ATP hydrolysis by Dna2 E675A was relatively constant in the presence of 5′-tailed DNA as a cofactor, it rapidly decreased in case of wild-type Dna2 (Fig. 6*G*). In agreement with the data presented in Fig. 6 *A*–*C*, we believe that the nuclease activity of the wild-type protein rapidly degrades the ssDNA tail during the course of the reaction, producing duplex or nearly duplex DNA structures that no longer stimulate its ATPase activity (Fig. 6*H*).

Taken together, these data explain why the nuclease activity of Dna2 strongly inhibits its unwinding capacity. We show that the nuclease degrades 5′ ssDNA tails, which in turn inhibits DNA binding and thus the unwinding capacity of Dna2. Previously, it was believed that the nuclease of Dna2 obscures the detection of the products of its limited unwinding activity (22). The data presented here suggest a different scenario, in which the nuclease

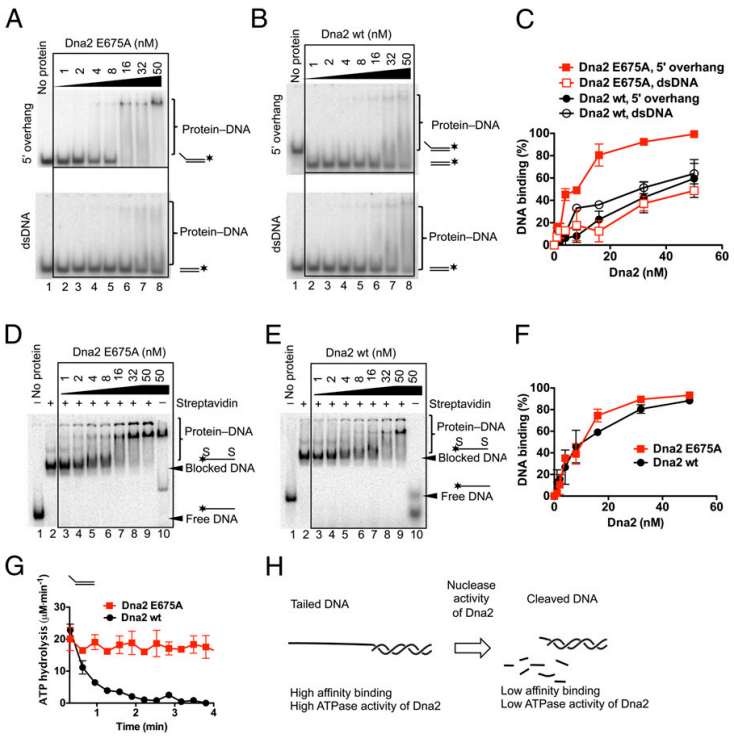

Fig. 6. The nuclease activity of Dna2 inhibits its binding to DNA. (*A*) Electrophoretic mobility shift assays were performed with a range of Dna2 E675A concentrations and ^{32}P-labeled 30-nt-long 5′-tailed DNA or fully dsDNA (both 1 nM). The panel shows representative 6% polyacrylamide gels. *, position of the ^{32}P label. (*B*) Electrophoretic mobility shift assay as in *A*, but with wild-type Dna2. (*C*) Quantitation of DNA binding assays such as from *A* and *B*. Error bars, SE, n = 2. (*D*) Electrophoretic mobility shift assays were performed with a range of Dna2 E675A concentrations and ^{32}P-labeled 70-nt-long ssDNA substrate (1 nM). The DNA substrate contained biotin near both of its ends, which was bound to streptavidin where indicated. Shown is a representative 6% polyacrylamide gel. *, position of the ^{32}P label; S, position of biotin-bound streptavidin. (*E*) Electrophoretic mobility shift assay as in *D*, but with wild-type Dna2. (*F*) Quantitation of the assays such as from *D* and *E*. Error bars, SE, n = 2. (*G*) Kinetics of ATP hydrolysis by wild-type Dna2 and Dna2 E675A (both 4 nM). The reactions contained 30-nt-long 5′ overhang substrate (1 μM nucleotides). Error bars, SE, n = 2. (*H*) Model explaining the kinetics of ATP hydrolysis by wild-type Dna2 on a 5′-tailed substrate. Initially, the overhang substrate stimulates the ATPase activity of wild-type Dna2. The nuclease activity then degrades the ssDNA tail, which results in a substrate that no longer efficiently stimulates the ATPase activity.

activity prevents the helicase activity from engaging its respective substrate.

Helicase Activity of Wild-Type Dna2 Promotes Its Capacity to Degrade dsDNA. Up to this point, we demonstrated that the nuclease of wild-type Dna2 inhibits its unwinding capacity. By cleaving ssDNA tails that serve as entry points for the helicase, the nuclease impedes DNA binding and thus the initiation of dsDNA unwinding. In subsequent experiments, we set out to find conditions to detect the unwinding capacity of the wild-type enzyme.

Using 5′-tailed dsDNA substrate ^{32}P-labeled at the ssDNA tail, the activity of wild-type Dna2 was indistinguishable from that of the helicase-dead K1080E variant. The helicase activity did not stimulate cleavage of the 5′-terminated ssDNA tail, and we could detect no DNA unwinding intermediates (Fig. S9 *A* and *B*). Similarly to experiments presented in Fig. 5 *D* and *E*, the helicase activity thus had no apparent effect on the behavior of Dna2. We reasoned that Dna2 binds and translocates on the tailed oligonucleotide, which gets then preferentially cleaved, and this cleavage may limit the detection of DNA unwinding intermediates. We next labeled the bottom oligonucleotide that does not contain the overhang (see diagram at the top of Fig. 7*A*), and analyzed the activity of wild-type, helicase-dead K1080E, and nuclease-dead Dna2 E675A variants. The nuclease of both wild type and K1080E degraded the 5′-terminated DNA overhang, resulting in species that comigrated with the tail-less dsDNA marker (Fig. 7 *A* and *B*). Importantly, we could also clearly detect ssDNA in reactions with wild-type Dna2 (Fig. 7*A*, lanes 3–6). In contrast, ssDNA was nearly undetectable in reactions with the helicase-dead K1080E variant; the minimal amount of ssDNA we observed was likely the result of the nuclease acting on the top strand upon spontaneous thermal melting of the DNA substrate in the presence of RPA (Fig. 7*B*). The ssDNA was apparent at wild-type Dna2 concentrations as low as 16–32 pM (Fig. 7*A*), which was also the minimal protein concentration required to detect DNA unwinding by the nuclease-dead Dna2 E675A variant (Fig. 7*C*). These results, together with the ATPase assays (Fig. 5*C*), indicate that wild-type Dna2 likely possesses the same level of helicase activity as the nuclease dead Dna2 E675A variant.

The experiments in Fig. 7 *A* and *B* also showed that the helicase activity of Dna2 promotes degradation of dsDNA. The degradation of DNA by the helicase-deficient Dna2 K1080E variant was mostly limited to the 5′-terminated ssDNA overhang, as the species comigrating with tail-less DNA was the dominant product across a wide range of enzyme concentrations (Fig. 7*B*). In contrast, wild-type Dna2 could more efficiently enter and degrade dsDNA as well, as witnessed by the appearance of small-molecular-weight DNA species, denoted as degraded DNA (Fig. 7*A*).

To further investigate the role of the Dna2 helicase in degradation of dsDNA, we carried out additional experiments with a 5′-tailed substrate that was 3′-labeled at the dsDNA end (see diagram at the top of Fig. 8*A*). As above, the helicase activity of wild-type Dna2 promoted degradation of dsDNA (Fig. 8 *A* and *B*). We show that dsDNA degradation requires the presence of the 5′-terminated ssDNA tail, as tail-less dsDNA was not cleaved at similar enzyme concentrations (Fig. S10*A*). Furthermore, the dsDNA degradation was dependent on RPA, as no significant 3′ end cleavage product was observed in the absence of RPA, with both wild-type Dna2 or the helicase-dead K1080E variant (Fig. S10*B*). RPA therefore stimulates the degradation of dsDNA by both wild-type and helicase-dead Dna2 K1080E, probably by melting the dsDNA ends. The dsDNA degradative capacity is then further enhanced by the helicase activity of Dna2 (Fig. 8 *A* and *B*).

Finally, we investigated the degradation of plasmid-sized tailed DNA on agarose gels stained with ethidium bromide. Limited degradation of DNA near its ends resulted in change of mobility (Fig. 8*C*). In the absence of ATP, a condition favored by the Dna2 nuclease (4), both wild-type and helicase-dead Dna2 K1080E variant degraded DNA to a similar extent. Upon supplementing the reaction with ATP, which lowered the free magnesium concentration required by the nuclease and activated the helicase, DNA degradation by the wild-type enzyme was promoted whereas DNA degradation by the K1080E variant was inhibited. Thus, in the presence of ATP, the helicase of Dna2 clearly promotes degradation of dsDNA. The extent of DNA degradation is, however, limited in comparison with the extent of DNA unwound by the equivalent concentration of the nuclease-dead Dna2 E675A mutant (Fig. 5 *A* and *B*).

In summary, our data reveal an unusual interplay of the nuclease and helicase activities of Dna2. The nuclease activity strongly reduces the ability of Dna2 to unwind DNA. However, the inhibition of the DNA unwinding capacity is not total, and we show that the helicase activity may promote nucleolytic degradation of dsDNA. The ssDNA-specific nuclease activity thus controls the unwinding capacity and the ability of the enzyme to process and degrade dsDNA. We propose that modulation of the interplay between the nuclease and helicase activities in vivo might represent a regulatory mechanism for Dna2 to fine-tune its behavior to carry out specific cellular functions. Conditions that promote the nuclease activity would result in Dna2 degradation limited to ssDNA tails whereas inhibition of the nuclease activity would allow the enzyme to process also dsDNA (Fig. 9 and *Discussion*).

Discussion

The Dna2 nuclease-helicase functions in multiple fundamental cellular processes ranging from lagging-strand DNA synthesis,

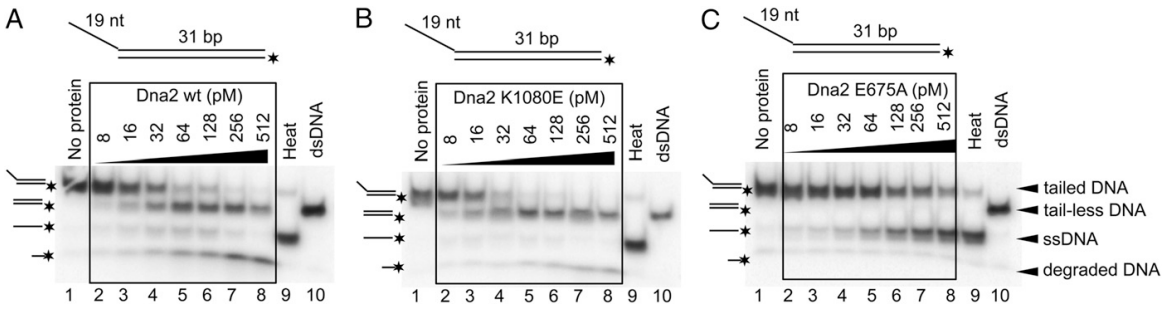

Fig. 7. Wild-type Dna2 possesses DNA helicase activity. (*A*) Processing of 5′-tailed DNA by wild-type Dna2. The bottom oligonucleotide was ^{32}P-labeled at the 5′ end. The reactions contained RPA (22.5 nM). Heat, heat-denatured DNA substrate. *, position of the ^{32}P label. The panel shows a representative 10% polyacrylamide gel. (*B*) Experiment as in panel *A*, but with helicase-dead Dna2 K1080E variant. (*C*) Experiment as in panel *A*, but with nuclease-dead Dna2 E675A variant.

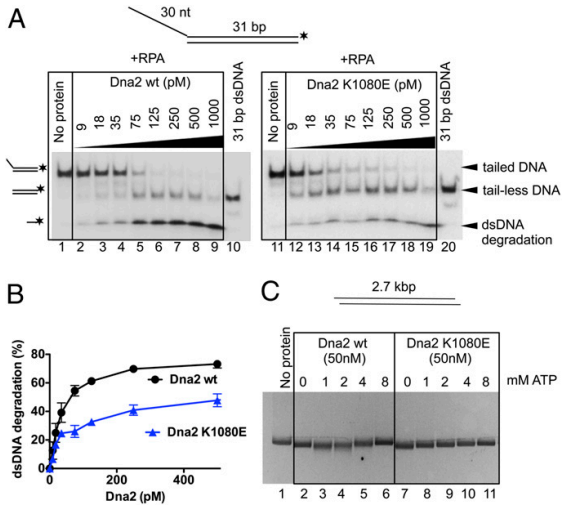

Fig. 8. The helicase activity of wild-type Dna2 moderately promotes its capacity to degrade dsDNA. (*A*) A representative polyacrylamide gel (10%) showing the activity of wild-type Dna2 and K1080E variant on 3′-labeled 5′-ssDNA tailed substrate (1 nM). *, position of the ^{32}P label. All reactions contained RPA (22.5 nM). (*B*) Quantitation of data such as from panel *A*. Error bars, SE, $n = 2$. (*C*). Degradation of 2.7-kbp dsDNA with 4-nt-long 5′ ssDNA overhangs by wild-type Dna2 and helicase dead Dna2 K1080E variant in the presence of various ATP concentrations, as indicated. The reactions contained 3.8 nM DNA and were supplemented with RPA (1.68 μM). The reaction products were separated on 1% agarose gel and stained with ethidium bromide. Panel shows a representative experiment.

replication fork stability, and dsDNA break repair, to the repair of damaged DNA (6, 18, 29, 39). Recombinant Dna2 possesses a potent nuclease activity that appears to be essential for all Dna2 functions, but the 5′–3′ DNA helicase activity of the enzyme was described as weak. The observed limited unwinding capacity led to the speculation that the motor function of Dna2 might act as an ssDNA translocase that removes secondary structures from ssDNA rather than to unwind dsDNA (23). We noticed that recombinant Dna2 was very unstable and sensitive to the omission of reducing agents during purification. Because Dna2 was recently shown to contain an iron–sulfur cluster (30, 31), we speculated that it might be prone to inactivation by oxidation. Indeed, our current purification protocol yielded a highly active enzyme with strong nuclease and helicase activities.

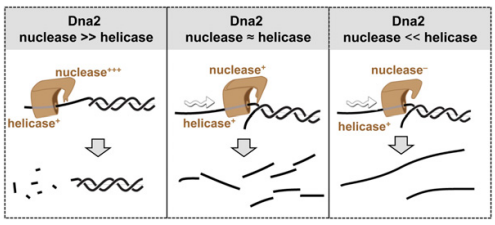

Fig. 9. Model of the interplay of helicase and nuclease activities of Dna2. In the presence of vigorous nuclease activity, the helicase capacity is inhibited and the DNA degradation is limited to ssDNA (*Left*). Moderate inhibition of the nuclease activity might allow the enzyme to degrade dsDNA (*Center*). Complete inactivation of nuclease activity, such as in nuclease-dead Dna2 E675A variant, turns the enzyme into a vigorous DNA helicase (*Right*). See text for details.

Unexpectedly, biochemical characterization of the wild-type, nuclease-dead, and helicase-dead enzyme variants generated in the course of this study revealed that Dna2 possesses a vigorous but cryptic helicase activity. Mutational inactivation of the Dna2 nuclease unleashes this helicase activity. Nuclease-dead Dna2 E675A variant is capable of catalytic unwinding of oligonucleotide-based DNA substrates at subnanomolar enzyme concentrations (Fig. 1). Furthermore, it shows functional interaction with RPA, which allows it to unwind tens of kilobases of dsDNA in length at low nanomolar enzyme concentrations (Fig. 2). The helicase and ATPase activities of Dna2 E675A compare favorably with the RecQ family Sgs1 helicase (Figs. 2 and 4), which is possibly the most vigorous eukaryotic helicase characterized to date (32). Single molecule experiments revealed that DNA unwinding by Dna2 E675A is highly processive (Fig. 3).

The Dna2 nuclease inhibits this vigorous unwinding capacity; although the ATPase activity of wild-type Dna2 is comparable with that of the nuclease-dead Dna2 E675A variant, the former protein is inefficient in dsDNA unwinding (Fig. 5). The Dna2 helicase requires a free 5′ terminus to load onto to initiate DNA unwinding. We show that the nuclease activity of wild-type Dna2 is more likely to degrade such structures rather than use them for DNA unwinding (Figs. 5 and 6). Dna2 thus represents a remarkable example of an enzyme in which one biochemical property (nuclease) negatively regulates the other (helicase) by competing for the same substrate (5′-tailed DNA).

The nuclease-mediated inhibition of the unwinding capacity was not total, and we were able to observe a fraction of unwound DNA in reactions with wild-type Dna2 as well (Fig. 7). As a result, the helicase activity of wild-type Dna2 promoted the degradation of dsDNA to a limited extent (Figs. 7 and 8). We therefore speculate that modulation of the nuclease activity might regulate the global activity of Dna2. In this scenario, moderate inhibition of the nuclease activity might promote dsDNA unwinding and, consequently, also degradation of dsDNA. Conversely, stimulation of the nuclease would inhibit the helicase, which would restrict the nucleolytic activity of the enzyme to ssDNA (Fig. 9). The regulatory mechanism proposed here might therefore restrict the unwinding capacity only to situations when it is required. It is of interest that overexpression of nuclease-dead Dna2 proteins had a dominant negative effect in *dna2-1* mutants with impaired both helicase and nuclease functions of Dna2 under certain growth conditions (20). Similarly, overexpression of nuclease-dead human DNA2 was more detrimental than overexpression of both nuclease and helicase-dead construct (40). This result, together with our data showing that the nuclease activity limits the helicase function, implies that hyperactive and unregulated Dna2 helicase is toxic, and highlights the importance of restricting the helicase activity of Dna2 in vivo.

How could the activity of Dna2 be regulated in vivo? Obvious candidates for potential regulators are interactors and/or posttranslational modifications. During DNA replication, Dna2 forms a complex with Rad27 whereas, during dsDNA break repair, it interacts with Sgs1 (5, 12). It is thus possible that these two proteins affect the balance between the helicase and nuclease activities. Furthermore, the activity of human DNA2 was found to be stimulated by acetylation (41). The effect of acetylation on the relative activities of the helicase and nuclease functions is unknown. Similarly, Dna2 is also phosphorylated in vivo, which regulates its recruitment to DNA and controls its function on stalled replication forks (18, 42). It will be of interest to investigate how these modifications affect the biochemical behavior of Dna2. The Dna2 polypeptide contains a large (~405-amino acid) N-terminal domain, which mediates the interaction with RPA, but which was also found to interact with a region of Dna2 located between the helicase and nuclease domains (43). Based on this intramolecular interaction, it has been proposed that the N-terminal domain might have a regulatory role, in that its

position might affect the biochemical activities of Dna2 (43). Finally, it is also possible that the interplay between the nuclease and helicase activities of Dna2 might be controlled via the redox states of its iron–sulfur cluster (30, 31).

Dna2 physically and functionally interacts with the Sgs1 helicase in DNA end resection to initiate homologous recombination (12). The Sgs1–Dna2 heterodimer is functionally similar to the resection machinery of *E. coli*, the RecBCD factor. Both complexes possess two helicases and a single nuclease activity, and both must load on free DNA ends, yet degrade DNA endonucleolytically (12). Similarly, the Sgs1–Dna2 complex could be a bipolar helicase, with each subunit translocating on opposite strands but in the same overall direction (12). The unwinding capacity of the heterodimer cannot be inhibited by 5′ cleavage, as Sgs1 is likely the lead helicase that translocates with a 3′ to 5′ polarity. A vigorous motor activity of Dna2 would be important here, as only rapidly moving Dna2 could "keep up" with the Sgs1 helicase. We also point out that the motor activity of Dna2 was reported dispensable for DNA end resection in an earlier study (9). In complementation experiments, the expression of wild-type and Dna2 variants was driven from a plasmid in the latter work, and higher than physiological Dna2 levels may have masked the involvement of the Dna2 helicase. Nevertheless, the role of the Dna2 helicase in DNA end resection remains unclear and deserves further attention.

In RecBCD, both RecB and RecD motors precede the RecB nuclease domain to feed ssDNA into the RecB nuclease site in a highly coordinated manner (44). The RecC subunit, however, contains a defunct nuclease domain, which is interestingly situated ahead of the RecD motor (44–46). Our biochemical data presented here might imply that the Dna2 nuclease is similarly placed ahead of the Dna2 helicase although detailed structural analysis will be required to test this hypothesis. In *Bacillus subtilis*, the processing of dsDNA ends is catalyzed by the AddAB complex, which in contrast contains one helicase motor and two nuclease domains (47). The AddB subunit is however clearly related to Dna2, and both proteins contain an iron–sulfur cluster (30, 31). Data presented here together with previous work (12, 47, 48) demonstrate that the interplay of helicase and nuclease activities regulates dsDNA end processing in eukaryotes as well.

Materials and Methods

DNA Substrates. The oligonucleotides used for the preparation of the Y-structure, dsDNA, ssDNA, 19-nt 5′-tailed and 19-nt 3′-tailed ssDNA substrates have been described previously (32). The oligonucleotide used to prepare the 30-nt 5′-tailed ssDNA substrate was PC 92, GGTACTCAAGTGACGTCATAGACGATTACATTGCTAGGACATGCTGTCTAGAGACTATCGC. The oligonucletides were ^{32}P-labeled either at the 5′terminus with [γ-^{32}P]ATP and T4 polynucletide kinase (New England Biolabs), or at the 3′ end with [α-^{32}P] cordycepin-5′-triphosphate and terminal transferase (New England Biolabs) according to the manufacturer's instructions. Unincorporated nucleotides were removed using MicroSpin G25 columns (GE Healthcare). pUC19 dsDNA and bacteriophage λ dsDNA were digested with HindIII and purified by phenol-chloroform extraction and ethanol precipitation. The linearized dsDNA was then 3′-labeled with [α-^{32}P]dATP and Klenow fragment of DNA polymerase I (New England Biolabs). Unincorporated nucleotides were removed using MicroSpin G25 columns (GE Healthcare). Streptavidin-blocked oligonucleotide was prepared by incubating streptavidin (15 nM) with the DNA substrate in reaction buffer for 15 min before addition of other recombinant proteins and initiation of the reaction.

Recombinant Proteins. Sgs1 and RPA proteins were expressed and purified as described (32, 49). SSB was a gift from S. Kowalczykowski (University of California, Davis) and human RPA from Stephanie Bregenhorn (University of Zurich). Wild-type Dna2 as well as Dna2 E675A and K1080E variants were expressed from a modified pGAL:DNA2 (20) vector that contained amino (N)-terminal Flag and HA tags and a C-terminal His_6 tag, in the *S. cerevisiae* strain WDH668 (50). Yeast cells (4L) were grown to approximately OD ~0.6 in a standard synthetic medium, lacking uracil, and supplemented with glycerol (3% vol/vol) and lactic acid (2% vol/vol) as carbon sources. Expression of Dna2 was induced with galactose, the cells were lysed, and Dna2 was bound to Ni^{2+}-NTA agarose (Qiagen) as described previously (12). Dna2 was eluted with 250 mM imidazole. The fractions containing proteins were pooled, diluted 1:8 with de-gassed dilution buffer (25 mM Tris·HCl (pH 7.5), 150 mM NaCl, 10% (vol/vol) glycerol, 0.5 mM β-mercaptoethanol, 10 $\mu g \cdot ml^{-1}$ leupeptin, 1 mM phenylmethylsulphonyl fluoride and protease-inhibitor mixture (Sigma, P8340, diluted 1:1,000)) and incubated batch-wise with M2 anti-FLAG affinity resin (0.5 mL; Sigma) for 45 min. The resin was then washed with degassed wash buffer (25 mM Tris·HCl (pH 7.5), 150 mM NaCl, 10% (vol/vol) glycerol, 1 mM β-mercaptoethanol), and Dna2 was eluted with wash buffer supplemented with 4xFLAG Peptide (200 $\mu g \cdot ml^{-1}$; Sigma). Fractions containing protein were pooled, and small aliquots were frozen in liquid nitrogen and stored at −80 °C. The final protein concentration was estimated by densitometry by comparison with dilution series of broad range protein marker (BioRad) on 10% (wt/vol) polyacrylamide gel stained with Coomassie blue. The protein yields were ~150–250 μg and concentration ~100–400 nM for Dna2 wild-type, K1080E, and E675A variants. The specific activities of independent enzyme preparations varied by about ±15% with respect to a mean value.

Helicase and Nuclease Assays. The experiments were performed in a 15-μl volume in 25 mM Tris-acetate (pH 7.5), 2 mM magnesium acetate, 1 mM ATP, 1 mM DTT, 0.1 mg/mL BSA (New England Biolabs), 1 mM phosphoenolpyruvate, 16 U/mL pyruvate kinase, DNA substrate, and recombinant proteins, as indicated. Unless indicated otherwise, the reactions were incubated for 30 min at 30 °C and carried out and analyzed as described previously (32). We noted that recombinant Dna2 was unusually sensitive to protein dilution, and supplementing the reactions with BSA was often required to observe enzymatic activity.

Magnetic Tweezers Assay. The DNA construct was prepared by digesting plasmid pNLrep with BamHI, BsrGI, and Nt.BbvCI, filling part of the the gap created by the nicking enzyme with an DNA oligomer (oliomer sequence: 5′-TTTTTTTTTTTTTTTTTTTTTTTTTTTTTTTTTTTTTTTTCAGCTAGCCTCAGCCTACAATCACC) and ligating the biotin (BsrGI digested) and digoxigenin-modified (BamHI digested) tails as described (53, 52). Magnetic tweezers experiments were carried out as described before (33). Helicase experiments were done at room temperature using the same buffer as the bulk helicase assays (but lacking the ATP recycling system) using 1 nM Dna2 E675A and 22 nM RPA. RPA itself at this concentration was found to slowly unwind dsDNA (4 $bp \cdot s^{-1}$) by polymerizing on ssDNA at forces of 35 pN. Experiments were therefore always performed at lower forces where this behavior was not observed. To convert DNA length changes during unwinding at a given force into a corresponding number of unwound bp, force-extension measurements on the bare DNA construct and on the unwound RPA-coated construct were used.

ATPase and Electrophoretic Mobility Shift Assays. These experiments were performed as described previously (32, 37, 38).

ACKNOWLEDGMENTS. We thank Stephen Kowalczykowski (University of California, Davis) for help during the initial phase of this project and for the recombinant SSB protein. We thank Judith Campbell (California Institute of Technology) for the Dna2 expression construct and Stephanie Bregenhorn (University of Zurich) for human RPA. We acknowledge Pavel Janscak, Elda Cannavo, Lepakshi, Josef Jiricny (all from University of Zurich), Cosimo Pinto (ETH Zurich), and Mark Dillingham (University of Bristol) for discussions and helpful comments on the manuscript. This work was supported by Swiss National Science Foundation Professorship PP00P3 133636.

1. Kuo C, Nuang H, Campbell JL (1983) Isolation of yeast DNA replication mutants in permeabilized cells. *Proc Natl Acad Sci USA* 80(21):6465–6469.
2. Budd ME, Campbell JL (1995) A yeast gene required for DNA replication encodes a protein with homology to DNA helicases. *Proc Natl Acad Sci USA* 92(17):7642–7646.
3. Budd ME, Choe WC, Campbell JL (1995) DNA2 encodes a DNA helicase essential for replication of eukaryotic chromosomes. *J Biol Chem* 270(45):26766–26769.
4. Bae SH, et al. (1998) Dna2 of Saccharomyces cerevisiae possesses a single-stranded DNA-specific endonuclease activity that is able to act on double-stranded DNA in the presence of ATP. *J Biol Chem* 273(41):26880–26890.
5. Budd ME, Campbell JL (1997) A yeast replicative helicase, Dna2 helicase, interacts with yeast FEN-1 nuclease in carrying out its essential function. *Mol Cell Biol* 17(4): 2136–2142.
6. Bae SH, Bae KH, Kim JA, Seo YS (2001) RPA governs endonuclease switching during processing of Okazaki fragments in eukaryotes. *Nature* 412(6845): 456–461.
7. Bae SH, Seo YS (2000) Characterization of the enzymatic properties of the yeast dna2 Helicase/endonuclease suggests a new model for Okazaki fragment processing. *J Biol Chem* 275(48):38022–38031.

8. Kao HI, Veeraraghavan J, Polaczek P, Campbell JL, Bambara RA (2004) On the roles of Saccharomyces cerevisiae Dna2p and Flap endonuclease 1 in Okazaki fragment processing. *J Biol Chem* 279(15):15014–15024.
9. Zhu Z, Chung WH, Shim EY, Lee SE, Ira G (2008) Sgs1 helicase and two nucleases Dna2 and Exo1 resect DNA double-strand break ends. *Cell* 134(6):981–994.
10. Mimitou EP, Symington LS (2008) Sae2, Exo1 and Sgs1 collaborate in DNA double-strand break processing. *Nature* 455(7214):770–774.
11. Gravel S, Chapman JR, Magill C, Jackson SP (2008) DNA helicases Sgs1 and BLM promote DNA double-strand break resection. *Genes Dev* 22(20):2767–2772.
12. Cejka P, et al. (2010) DNA end resection by Dna2-Sgs1-RPA and its stimulation by Top3-Rmi1 and Mre11-Rad50-Xrs2. *Nature* 467(7311):112–116.
13. Niu H, et al. (2010) Mechanism of the ATP-dependent DNA end-resection machinery from *Saccharomyces cerevisiae*. *Nature* 467(7311):108–111.
14. Nimonkar AV, et al. (2011) BLM-DNA2-RPA-MRN and EXO1-BLM-RPA-MRN constitute two DNA end resection machineries for human DNA break repair. *Genes Dev* 25(4): 350–362.
15. Choe W, Budd M, Imamura O, Hoopes L, Campbell JL (2002) Dynamic localization of an Okazaki fragment processing protein suggests a novel role in telomere replication. *Mol Cell Biol* 22(12):4202–4217.
16. Lesur I, Campbell JL (2004) The transcriptome of prematurely aging yeast cells is similar to that of telomerase-deficient cells. *Mol Biol Cell* 15(3):1297–1312.
17. Zheng L, et al. (2008) Human DNA2 is a mitochondrial nuclease/helicase for efficient processing of DNA replication and repair intermediates. *Mol Cell* 32(3):325–336.
18. Hu J, et al. (2012) The intra-S phase checkpoint targets Dna2 to prevent stalled replication forks from reversing. *Cell* 149(6):1221–1232.
19. Peng G, et al. (2012) Human nuclease/helicase DNA2 alleviates replication stress by promoting DNA end resection. *Cancer Res* 72(11):2802–2813.
20. Budd ME, Choe Wc, Campbell JL (2000) The nuclease activity of the yeast DNA2 protein, which is related to the RecB-like nucleases, is essential in vivo. *J Biol Chem* 275(22):16518–16529.
21. Kao HI, Campbell JL, Bambara RA (2004) Dna2p helicase/nuclease is a tracking protein, like FEN1, for flap cleavage during Okazaki fragment maturation. *J Biol Chem* 279(49):50840–50849.
22. Balakrishnan L, Polaczek P, Pokharel S, Campbell JL, Bambara RA (2010) Dna2 exhibits a unique strand end-dependent helicase function. *J Biol Chem* 285(50):38861–38868.
23. Bae SH, et al. (2002) Coupling of DNA helicase and endonuclease activities of yeast Dna2 facilitates Okazaki fragment processing. *J Biol Chem* 277(29):26632–26641.
24. Kim JH, et al. (2006) Isolation of human Dna2 endonuclease and characterization of its enzymatic properties. *Nucleic Acids Res* 34(6):1854–1864.
25. Masuda-Sasa T, Polaczek P, Campbell JL (2006) Single strand annealing and ATP-independent strand exchange activities of yeast and human DNA2: Possible role in Okazaki fragment maturation. *J Biol Chem* 281(50):38555–38564.
26. Liu Q, Choe W, Campbell JL (2000) Identification of the Xenopus laevis homolog of Saccharomyces cerevisiae DNA2 and its role in DNA replication. *J Biol Chem* 275(3): 1615–1624.
27. Masuda-Sasa T, Imamura O, Campbell JL (2006) Biochemical analysis of human Dna2. *Nucleic Acids Res* 34(6):1865–1875.
28. Budd ME, Campbell JL (2000) The pattern of sensitivity of yeast dna2 mutants to DNA damaging agents suggests a role in DSB and postreplication repair pathways. *Mutat Res* 459(3):173–186.
29. Formosa T, Nittis T (1999) Dna2 mutants reveal interactions with Dna polymerase alpha and Ctf4, a Pol alpha accessory factor, and show that full Dna2 helicase activity is not essential for growth. *Genetics* 151(4):1459–1470.
30. Yeeles JT, Cammack R, Dillingham MS (2009) An iron-sulfur cluster is essential for the binding of broken DNA by AddAB-type helicase-nucleases. *J Biol Chem* 284(12): 7746–7755.
31. Pokharel S, Campbell JL (2012) Cross talk between the nuclease and helicase activities of Dna2: Role of an essential iron-sulfur cluster domain. *Nucleic Acids Res* 40(16): 7821–7830.
32. Cejka P, Kowalczykowski SC (2010) The full-length *Saccharomyces cerevisiae* Sgs1 protein is a vigorous DNA helicase that preferentially unwinds holliday junctions. *J Biol Chem* 285(11):8290–8301.
33. Klaue D, Seidel R (2009) Torsional stiffness of single superparamagnetic microspheres in an external magnetic field. *Phys Rev Lett* 102(2):028302.
34. De Vlaminck I, et al. (2010) Torsional regulation of hRPA-induced unwinding of double-stranded DNA. *Nucleic Acids Res* 38(12):4133–4142.
35. Dessinges MN, Lionnet T, Xi XG, Bensimon D, Croquette V (2004) Single-molecule assay reveals strand switching and enhanced processivity of UvrD. *Proc Natl Acad Sci USA* 101(17):6439–6444.
36. Fuller DN, Raymer DM, Kottadiel VI, Rao VB, Smith DE (2007) Single phage T4 DNA packaging motors exhibit large force generation, high velocity, and dynamic variability. *Proc Natl Acad Sci USA* 104(43):16868–16873.
37. Kreuzer KN, Jongeneel CV (1983) Escherichia coli phage T4 topoisomerase. *Methods Enzymol* 100:144–160.
38. Kowalczykowski SC, Krupp RA (1987) Effects of Escherichia coli SSB protein on the single-stranded DNA-dependent ATPase activity of Escherichia coli RecA protein: Evidence that SSB protein facilitates the binding of RecA protein to regions of secondary structure within single-stranded DNA. *J Mol Biol* 193(1):97–113.
39. Kang YH, Lee CH, Seo YS (2010) Dna2 on the road to Okazaki fragment processing and genome stability in eukaryotes. *Crit Rev Biochem Mol Biol* 45(2):71–96.
40. Duxin JP, et al. (2012) Okazaki fragment processing-independent role for human Dna2 enzyme during DNA replication. *J Biol Chem* 287(26):21980–21991.
41. Balakrishnan L, Stewart J, Polaczek P, Campbell JL, Bambara RA (2010) Acetylation of Dna2 endonuclease/helicase and flap endonuclease 1 by p300 promotes DNA stability by creating long flap intermediates. *J Biol Chem* 285(7):4398–4404.
42. Chen X, et al. (2011) Cell cycle regulation of DNA double-strand break end resection by Cdk1-dependent Dna2 phosphorylation. *Nat Struct Mol Biol* 18(9):1015–1019.
43. Bae SH, et al. (2001) Tripartite structure of Saccharomyces cerevisiae Dna2 helicase/endonuclease. *Nucleic Acids Res* 29(14):3069–3079.
44. Dillingham MS, Kowalczykowski SC (2008) RecBCD enzyme and the repair of double-stranded DNA breaks. *Microbiol Mol Biol Rev* 72(4):642–671.
45. Rigden DJ (2005) An inactivated nuclease-like domain in RecC with novel function: Implications for evolution. *BMC Struct Biol* 5:9.
46. Singleton MR, Dillingham MS, Gaudier M, Kowalczykowski SC, Wigley DB (2004) Crystal structure of RecBCD enzyme reveals a machine for processing DNA breaks. *Nature* 432(7014):187–193.
47. Yeeles JT, Gwynn EJ, Webb MR, Dillingham MS (2011) The AddAB helicase-nuclease catalyses rapid and processive DNA unwinding using a single Superfamily 1A motor domain. *Nucleic Acids Res* 39(6):2271–2285.
48. Saikrishnan K, et al. (2012) Insights into Chi recognition from the structure of an AddAB-type helicase-nuclease complex. *EMBO J* 31(6):1568–1578.
49. Kantake N, Sugiyama T, Kolodner RD, Kowalczykowski SC (2003) The recombination-deficient mutant RPA (rfa1-t11) is displaced slowly from single-stranded DNA by Rad51 protein. *J Biol Chem* 278(26):23410–23417.
50. Solinger JA, Lutz G, Sugiyama T, Kowalczykowski SC, Heyer WD (2001) Rad54 protein stimulates heteroduplex DNA formation in the synaptic phase of DNA strand exchange via specific interactions with the presynaptic Rad51 nucleoprotein filament. *J Mol Biol* 307(5):1207–1221.
51. Luzzietti N, Knappe S, Richter I, Seidel R (2012) Nicking enzyme-based internal labeling of DNA at multiple loci. *Nat Protoc* 7(4):643–653.
52. Luzzietti N, et al. (2011) Efficient preparation of internally modified single-molecule constructs using nicking enzymes. *Nucleic Acids Res* 39(3):e15.

Supporting Information

Levikova et al. 10.1073/pnas.1300390110

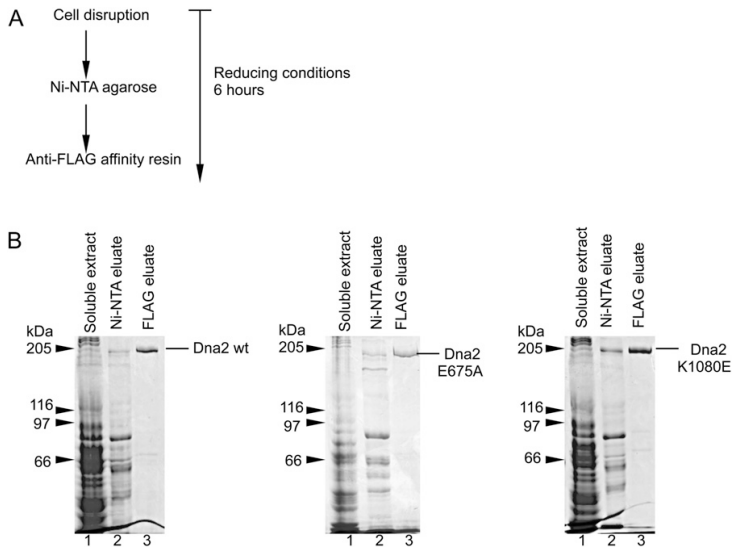

Fig. S1. (*A*) A schematic representation of the nuclease-helicase Dna2 purification process. See *Materials and Methods* for details. (*B*) Purification of wild-type Dna2 and its variants. Panels show representative 10% SDS/PAGE gels stained with Coomassie Brilliant Blue.

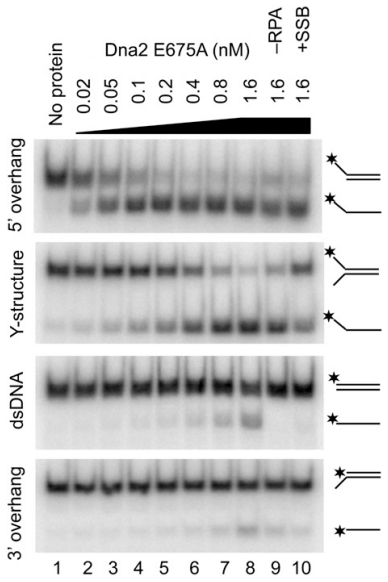

Fig. S2. Representative polyacrylamide gels (10%) showing DNA helicase activity of Dna2 E675A on various ^{32}P-labeled DNA substrates (1 nM), as indicated. The length of the ssDNA tails was 19 nt. Reactions were supplemented with *Saccharomyces cerevisiae* replication protein A [RPA, 22 nM, except lane 9 (RPA omitted) and lane 10 (RPA replaced with *Esherichia coli* single-strand DNA binding protein). The second image (Y-structure) is identical to the top image from Fig. 1*C*.

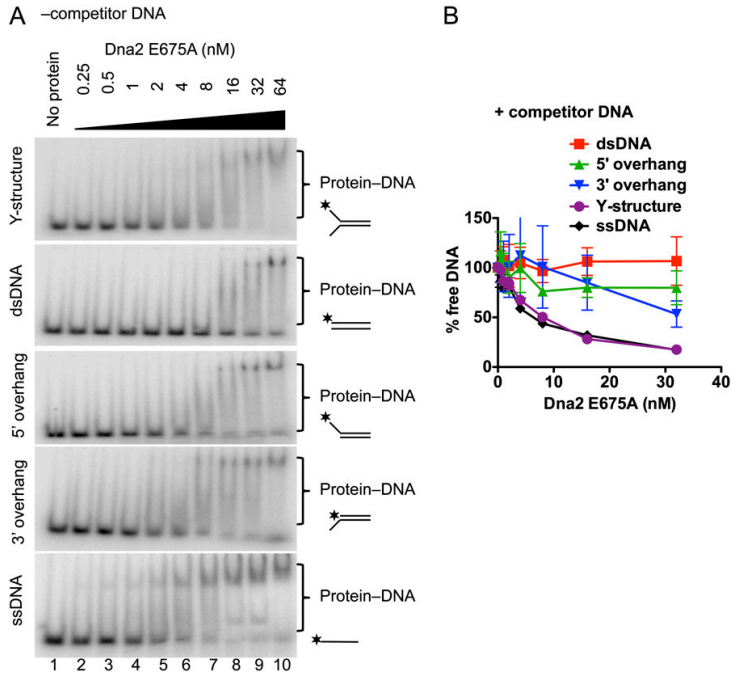

Fig. S3. (*A*) Electrophoretic mobility shift assays were performed with a range of Dna2 E675A concentrations with various DNA substrates (1 nM), as indicated. Shown are representative 6% polyacrylamide gels. *, position of the ^{32}P label. (*B*) Quantitation of electrophoretic mobility shift assays carried out in the presence of a dsDNA competitor (50 ng pUC19 dsDNA). The reactions were performed with a range of Dna2 E675A concentrations with various DNA substrates (1 nM), as indicated, and analyzed on 6% polyacrylamide gels. *, position of the ^{32}P label. Data represent the average of at least two independent experiments. Error bars, SE.

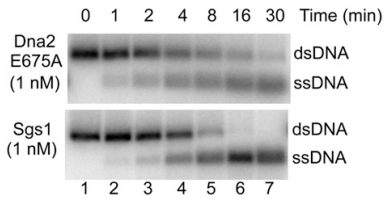

Fig. S4. A representative experiment showing the kinetics of unwinding of 5′-tailed 2.7-kbp-long dsDNA (1 nM) by either Dna2 E675A (1 nM) or Sgs1 (1 nM) in the presence of RPA (0.4 μM).

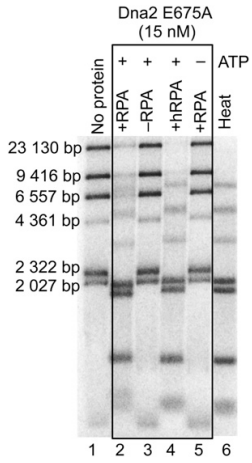

Fig. S5. Unwinding of long lengths of dsDNA by Dna2 E675A. λ phage DNA was digested with HindIII to produce dsDNA fragments ranging from 125 bp to 23 kbp in length, and ^{32}P-labeled with Klenow fragment of DNA polymerase I. The resulting DNA fragments had 5′ ssDNA tails of 3 nt in length at their ends. The 15 nM Dna2 E675A was incubated with the restricted DNA (2.4 nM of DNA ends) in the absence or presence of yeast RPA (1.08 μM) or human RPA (hRNA) (1.08 μM), where indicated. ATP was omitted from the reaction in lane 5. Heat, heat-denatured substrate. Sizes of dsDNA substrates are indicated on the left. The panel shows a representative agarose gel (1%).

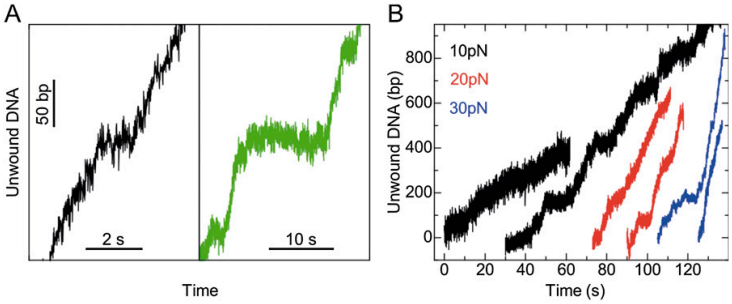

Fig. S6. Single molecule analysis of DNA unwinding by Dna2 E675A. (*A*) Magnified views of stalling events in the black and light green trajectories from Fig. 3*C*. (*B*) DNA unwinding by Dna2 E675A at various forces, as indicated by the legend. Two different DNA molecules (left and right traces at the given color) are shown. For each molecule, different forces were applied during a single unwinding run to ensure that the same helicase molecule was studied. Mean unwinding rates were 6 ± 2, 11 ± 4, and 30 ± 9 bp·s^{-1} (SE) at 10, 20, and 30 pN of applied force, respectively.

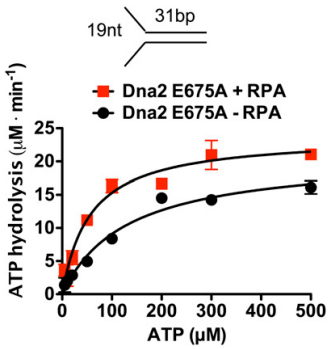

Fig. S7. Rate of ATP hydrolysis and its dependence on ATP concentration. The reactions contained Dna2 E675A (3 nM), Y-structure DNA substrate (1 μM nucleotides), RPA where indicated (22.5 nM), and varying concentrations of ATP. The kinetic parameters for ATP hydrolysis were obtained by fitting the data into a Michaelis–Menten equation.

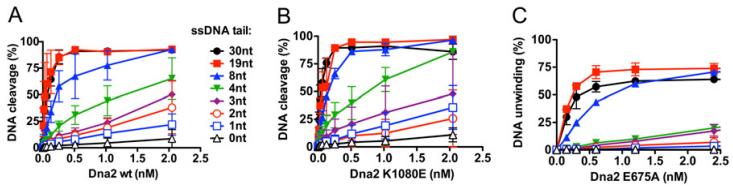

Fig. S8. Comparison of nuclease and/or helicase activities of Dna2 wild-type, K1080E, and E675A variants. (*A*) Quantitation of DNA cleavage by wild-type Dna2. ^{32}P-labeled DNA substrates with 5′ ssDNA tails of different lengths, as indicated, were used in reactions supplemented with RPA (22.5 nM) and subsequently analyzed on 10% polyacrylamide gels. The data represent the average of at least two independent experiments. Error bars, SE. (*B*) Quantitation of DNA cleavage by Dna2 K1080E variant. Reactions were carried out and analyzed as in *A*. The data represent the average of at least two independent experiments. Error bars, SE. See panel *A* for legend. *(C)* Quantitation of DNA unwinding by Dna2 E675A. Reactions were carried out and analyzed as in *A*. The data represent the average of at least two independent experiments. Error bars, SE. See panel *A* for legend.

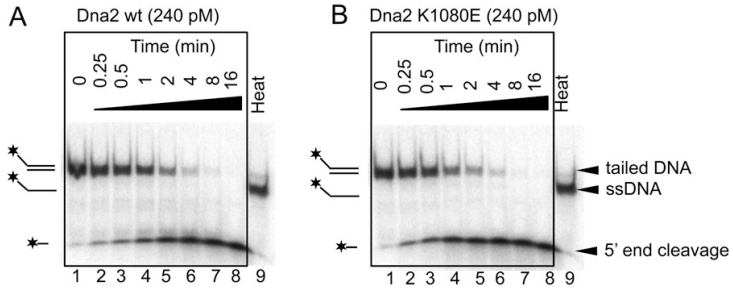

Fig. S9. Processing of 5′-tailed DNA by wild-type and helicase-dead Dna2 K1080E variant. (*A*) DNA degradation by wild-type Dna2. The 5′-labeled 5′ ssDNA tailed DNA substrate (1 nM) was used in a kinetic assay with 240 pM Dna2 in the presence of RPA (22.5 nM). Heat, heat-denatured DNA substrate. *, position of the ^{32}P label. The panel shows a representative 10% polyacrylamide gel. (*B*) Same assay as in *A*, but with Dna2 K1080E variant.

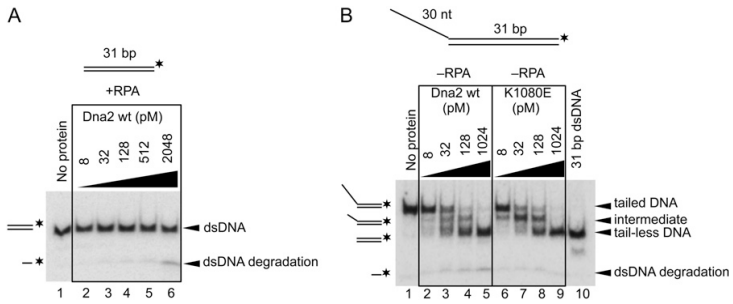

Fig. S10. Degradation of dsDNA by wild-type Dna2 requires 5′ overhang and RPA. (*A*) A representative polyacrylamide gel (10%) showing the activity of wild-type Dna2 on tail-less dsDNA substrate (1 nM). *, position of the ^{32}P label. All reactions contained RPA (9.6 nM). (*B*) A representative polyacrylamide gel (10%) showing the activity of wild-type and K1080E Dna2 on tailed dsDNA substrate (1 nM) in the absence of RPA. *, position of the ^{32}P label.

2.2.2 *Saccharamyces cerevisiae* Dna2 is regulated by sumoylation

Maryna Levikova, Veronika Altmannova, Lumir Krejci and Petr Cejka.

Manuscript.

I designed the research together with L.K. and P.C. and performed the experiments with the help of V.A. I analyzed the data together with L.K. and P.C. and wrote the manuscript.

Saccharomyces cerevisiae Dna2 is regulated by sumoylation

Maryna Levikova[a], Veronika Altmannova[b], Lumir Krejci[b,c,d] and Petr Cejka[a]

[a] Institute of Molecular Cancer Research, University of Zurich, Winterthurerstrasse 190, 8057 Zurich, Switzerland

[b] Department of Biology, Masaryk University, Brno 62500, Czech Republic

[c] National Center for Biomolecular Research, Masaryk University, Brno 62500, Czech Republic

[d] International Clinical Research Center, St. Anne's University Hospital, Brno 62500, Czech Republic

Key words: DNA helicase / DNA nuclease / Dna2 / Sumoylation / Cell cycle

Address correspondence to: Petr Cejka, Institute of Molecular Cancer Research, University of Zurich, Winterthurerstrasse 190, Zurich, 8057. Phone: +41-44-635-4786; E-mail: cejka@imcr.uzh.ch

Abstract

Dna2 is an essential nuclease-helicase and a key player in several DNA metabolic pathways including DNA replication and repair. To execute all its functions Dna2 has to be precisely regulated at multiple levels. Here we show that sumoylation is one of the mechanisms controlling *S. cerevisiae* Dna2 activity and stability. We report that Dna2 is sumoylated *in vitro* and *in vivo*, and sumoylation as well as protein levels of Dna2 are cell cycle dependent. We map the sites of sumoylation to the N-terminal regulatory domain. Further, we demonstrate that sumoylation of Dna2 impairs its nuclease but not its helicase activity. Taken together, these findings strongly suggest that Dna2 sumoylation regulates its activity *in vivo*.

Introduction

Posttranslational modifications (PTMs) modulate protein properties and regulate their functions. Covalent attachment of small ubiquitin-like modifier (SUMO) proteins to target substrates is an established PTM with an emerging role in DNA damage response (DDR) (1-5). SUMO is a 76 amino acid containing protein that is attached to the lysine of the target substrate via its C-terminal glycine residue by enzymatic reactions carried out by E1, E2 and E3 ligases, similarly to the ubiquitin system. While vertebrate cells posses three SUMO proteins (SUMO1, and almost identical SUMO2 and SUMO3), budding yeast contain only a single SUMO protein named Smt3 (2,6).

Sumoylation can have a variety of effects on the target protein. As it targets the lysines of its substrate it may compete with other PTMs like acetylation and ubiquitination (7,8). For IκBα and Rad52 it was shown that sumoylation prevents proteosomal degradation of these proteins by blocking ubiquitination (7,9). Next, sumoylation can inhibit protein-protein interactions, as it was shown for yeast proliferating cell nuclear antigen (PCNA) and PCNA-interacting protein-box (PIP-box) factor Eco1 (10). Finally, sumoylation can also promote protein-protein interactions (3). The stimulatory effect is based on the property of the SUMO proteins to bind to SUMO-interacting motifs, SIMs (11). Remarkably, the SUMO-SIM interaction can be not only intermolecular (called SUMO glue), but also intramolecular, as most of the proteins targeted by sumoylation also bear SIMs (3,4,12). A well-studied example for intramolecular SUMO-SIM interaction is the thymine DNA glycosylase (TDG) that functions in the base excision pathway. Sumoylation of TDG results in a conformational change of the enzyme involving its N-terminal domain (13).

Many proteins acting in DNA metabolism are regulated by sumoylation, although typically only a minor fraction of a protein is modified (4). Proteins involved in the homologous recombination (HR) pathway and DNA damage checkpoint were shown to be subjects of a collective sumoylation wave triggered by DNA end resection upon DNA damage (12,14). Also human flap endonuclease 1 (FEN1), a protein that is involved in lagging strand replication as well as in several DNA repair pathways, was

shown to be regulated by sumoylation. Specifically, sumoylation of FEN1 led to its degradation via the ubiquitin-proteasome system after the completion of the S-phase (15).

Dna2 is an essential nuclease-helicase involved in several key processes of DNA metabolism, including DNA replication, homologous recombination and checkpoint activation (16-21). The nuclease activity was shown to be vigorous and essential for the replication function of Dna2 (22-24). Recently, Dna2 was additionally found to be a strong helicase, although the helicase activity is masked by its nuclease (25).

Here we report that *S. cerevisiae* Dna2 is sumoylated *in vitro* and *in vivo*. Sumoylation attenuates the nuclease activity of Dna2, while the helicase activity is not affected. *In vivo*, sumoylation appears to be protective against MMS- and bleomycin-induced decrease in Dna2 protein levels. Furthermore, sumoylation as well as protein levels of Dna2 are regulated in a cell-cycle dependent manner, suggesting that Dna2 presence and activity is tightly regulated during DNA replication and cell division.

Results

S. cerevisiae Dna2 is sumoylated *in vitro* and *in vivo*

To test whether Dna2 as many other proteins involved in DNA metabolism is sumoylated (4), we first performed an *in vitro* sumoylation assay with recombinant proteins from *S. cerevisiae* (Fig. 1A). Indeed, when Smt3 was included in the sumoylation reaction, wild type Dna2 as well as Dna2 variants migrated higher in the silver-stained gel than the mock-treated proteins (Fig. 1A). This led us to a conclusion that yeast Dna2 can be sumoylated *in vitro.* Next, we set out to test whether the sumoylation of *S. cerevisiae* Dna2 is also occurring *in vivo* (Fig. 1B, C). To detect modified Dna2 we overexpressed His-tagged Smt3 and performed Ni-NTA affinity pulldowns of His-Smt3-protein conjugates under denaturing conditions, as described previously (26). We were able to detect slower migrating Dna2-myc-form in the pulldown samples, while this band was missing when the pulldown was performed with cells transformed with the empty parental vector control (Figure 1B, compare lanes 7 and 11),

or when Dna2 was not endogenously myc-tagged (Fig. 1B, compare lanes 7 and 9). We suggest that this Dna2 variant represents a sumoylated form of Dna2. Interestingly, upon treatment of cells with MMS, an alkylating agent, the sumoylation level of Dna2 decreased by ≈60% (Fig. 1B, compare lanes 7 and 8, Fig. 1C). We also observed an overall decrease of Dna2 protein in the cell extracts upon treatment with MMS (Fig. 1B, compare lanes 1 and 2, or 5 and 6). Same effect was visible when cells were treated with bleomycin (radiomimetic drug) and etoposide (topoisomerase II inhibitor) (Supplementary Fig. 1, compare lanes 1, 3 and 4). However, topoisomerase inhibition did not lead to decrease in Dna2 sumoylation (Supplementary Fig. 1, lane 9), while MMS and bleomycin treatments seemed to have two effects: the amount of Dna2-myc-Smt3 species was somewhat reduced, while at the same time presumably unmodified Dna2-myc (lower band) disappeared completely (Supplementary Fig. 1, lanes 7 and 8). Proteasomal degradation of Dna2 upon genotoxic treatments was just recently reported for yeast cells treated with caffeine, independently of its checkpoint inhibition effect (27). Our data infer that budding yeast Dna2 is modified by sumoylation and the sumoylated form appears to be partially resistant to MMS and bleomycin-induced decrease in Dna2 protein levels.

Cell-cycle dependent regulation of Dna2 sumoylation

Cell cycle is a highly regulated process involving a large amount of various proteins that are fine-tuned by PTMs. Sumoylation of human FEN1, a nuclease involved in Okazaki fragment processing, was shown to peak in late S and precedes its ubiquitin-mediated proteasomal degradation (15). In yeast, Dna2 was also implied to function together with Fen1 in the processing of flaps arising during lagging strand DNA synthesis (16,28). We set out to test whether Dna2, similarly to Fen1, is regulated during cell cycle progression. For this purpose we synchronized the *S. cerevisiae* cells in the G1 phase by addition of α-factor and monitored Dna2 protein as well as sumoylation levels after the release in S phase (Fig. 2A, B). Surprisingly, the amounts of Dna2 were low in G1 and S phases, while they substantially increased in late S and G2/M phases (Fig. 2B, left part). This variation of Dna2 protein levels contrasts to that described for FEN1, as FEN1 levels were highest in G1 and S and largely decreased in G2/M (15). When checking Dna2 sumoylation, we observed the highest levels in late

S/G2 phase (Fig. 2B, lane 9). Unlike it was shown for FEN1 (15), Dna2 protein levels did not decrease after its modification by SUMO (Fig. 2B, lane 4, G2/M), inferring that sumoylation of Dna2 does not likely promote its degradation. Additionally, cells treated with MMS displayed an accumulation in S-phase (Fig. 2C), suggesting that the MMS-induced decrease in sumoylation in Figure 1C might be attributable to cell cycle arrest. Taken together, these findings demonstrate that Dna2 is regulated during the cell cycle not only at protein level, but also likely by post-translational modifications such as sumoylation.

***In vitro* sumoylation of Dna2 impairs its nuclease activity**

Next, we decided to evaluate the impact of sumoylation on the biochemical activities of *S. cerevisiae* Dna2. Specifically, we wanted to test whether sumoylation affects the balance between the nuclease and helicase activities within the Dna2 enzyme, thus changing the conditions compared to unmodified protein where the nuclease masks the helicase (25). In Figure 3 we analyzed the nuclease and helicase activities of *in vitro* sumoylated Dna2 in comparison to mock-treated proteins on a 5'-tailed substrate. Sumoylated wild type Dna2 was ≈3-fold less efficient in substrate cleavage than its non-sumoylated counterpart (Fig. 3A, B). The length distribution of DNA fragments produced by modified compared to unmodified Dna2 was not changed, when we tested for ssDNA degradation (Supplementary Fig. 2A, B), suggesting that sumoylated Dna2 was still able to efficiently translocate on ssDNA. This is further supported by the fact that ATPase activity, which powers the ssDNA translocase, of sumoylated Dna2 wt did not differ from that of the mock-treated protein and excludes the possibility that the *in vitro* sumoylation reaction compromises the whole protein (Supplementary Fig. 2C). Moreover, helicase-dead Dna2 K1080E variant displayed the same decrease in DNA cleavage activity upon sumoylation as the wild type protein (Fig. 3C, D). However, nuclease-dead Dna2 E675A did not show any defect in DNA unwinding upon sumoylation (Fig. 3E, F). This is in agreement with the results indicating that ssDNA translocase and ATPase activities of wild type Dna2 were not affected by sumoylation. Also, in an assay using a 5' tailed substrate where the bottom oligonucleotide is radioactively labeled at the 5' end, which can be used to see unwinding by Dna2 wt as described in (25), no difference in accumulation of

tailed DNA (means unwound substrate detected by the presence of bottom oligonucleotide) was observed between sumoylated and unmodified Dna2 wt (Supplementary Fig. 2D). Collectively, this data show that sumoylation of Dna2 selectively attenuates its nuclease activity without impairing the helicase, thus changing the balance of the two key biochemical activities within Dna2.

Sumoylation of Dna2 6KA is abolished *in vitro*

Eventually, the question remained which lysines within the Dna2 protein are modified by sumoylation. To address this issue we performed mass spectrometry analysis of *in vitro* sumoylated Dna2 that determined six potential lysine residues (Fig. 4A). All of these lysines are part of the unstructured N-terminal domain of Dna2 that was shown to mediate the checkpoint activation, to promote binding to secondary structure DNA, as well as to be involved in the interaction with RPA (19,29-31). First, we purified Dna2 variants lacking the N-terminal 405 amino acids and tested them in an *in vitro* sumoylation assay (Figure 4B, C). The sumoylation of Dna2 Δ405N variants was largely abrogated compared to the full-length protein (Fig. 4C, compare lanes 3, 5 and 8 to lane 11). Next, we substituted all the six lysines to alanines within the Dna2 enzyme (Dna2 6KA), purified the protein and tested again whether it can be sumoylated *in vitro* (Fig. 4D, E). As anticipated, the sumoylation of Dna2 6KA was highly inefficient in comparison to the wild type protein (Fig. 4E, compare lanes 4 and 6). Thus, the six lysine residues identified by mass spectrometry are most likely to be modified by SUMO protein *in vitro*.

Discussion

Dna2 is an essential protein that is carrying out a multitude of functions in DNA metabolic pathways (21). It is obvious that Dna2 has to be carefully regulated to be able to exert all its tasks. Cdk1-dependent phosphorylation of Dna2 at Thr4, Ser17 and Ser237 residues was already shown to stimulate its recruitment to double-strand breaks, to stimulate resection and subsequent checkpoint activation (30). Here we demonstrate that Dna2 is also regulated by sumoylation. We show that Dna2 is

sumoylated *in vitro* and *in vivo* (Fig. 1). Sumoylation of Dna2 appears to be protective from MMS and bleomycin-induced decrease in Dna2 protein levels (Supplementary Fig. 1), suggesting an involvement in regulation of homologous recombination. A recent study inferred that Dna2 is subjected to proteasomal degradation upon caffeine treatment, independently of checkpoint inhibition (27). Our data would now suggest that sumoylated Dna2 is degradation-resistant. Next, we reveal that protein and sumoylation levels of Dna2 also vary during the cell cycle exactly in the way opposite to what was described for human FEN1 (Fig. 2 and (15)). Having in mind that Dna2 and Fen1 were shown to process long DNA flaps during Okazaki fragment maturation (16,28) and Dna2 is essential for replication (17), it is tempting to speculate that Dna2 is more required in late S phase to process DNA flaps that escaped from Fen1 cleavage. Alternatively, Dna2 could be also recruited to DNA flaps arising during post-replicative repair. This is further supported by data that suggested a role for *S. cerevisiae* Dna2 in late S phase, as *dna2Δ* cells arrested in G2/M (32). Furthermore, also human cells depleted from DNA2 arrest in late S/G2, while *fen1Δ* yeast cells accumulate already in S, again supporting the notion of Fen1 and Dna2 acting in different time frames (33,34). Additionally, our recent work demonstrated that Dna2 is able to process long DNA flaps without the need of Fen1, thus explaining high Dna2 protein levels in late S/G2, when Fen1 is most likely already sequestered by the proteasome ((48)-Levikova and Cejka, NAR 2015, in press; (15)). It is possible, that sumoylation affects Fen1 and Dna2 in two distinct manners: for Fen1, it mediates its degradation in late S (15), while modification of Dna2 leads to protein stabilization possibly by shielding it from ubiquitin-mediated proteasomal degradation, so that Dna2 can finalize the processing of DNA flaps and complete DNA replication. Intriguingly, human EXO1 was just recently shown to be targeted by SUMO and subsequently degraded by ubiquitin-dependent proteasome, similarly to FEN1 (15,35). Given the fact that Exo1 functions in a DNA resection pathway that is redundant to that involving Sgs1-Top3-Rmi1 and Dna2 (36), differential effects of sumoylation on Exo1 and Dna2 might influence the DNA resection pathway choice.

Moreover, we showed that sumoylation impairs the nuclease activity of Dna2 without affecting its helicase (Fig. 3), suggesting that sumoylation of Dna2 might occur in

cases when its helicase activity is required, possibly after MMS treatment. In accord, it was shown that helicase-dead *dna2* mutants are sensitive to MMS (24). Furthermore, we were able to identify six lysine residues of Dna2 that all locate to its N-terminal domain. Substitution of those lysines to alanines abolished Dna2 sumoylation *in vitro* (Fig. 4). By using the *in silico* SIM prediction tool (37,38) we obtained four possible SIMs within Dna2: at the amino acid positions 470-474, 638-642, 671-675, 1183-1187. Interestingly, the first three SIMs cluster in the nuclease domain of Dna2. This led us to the hypothesis that sumoylated N-terminus of Dna2 might bind to the SIMs within the nuclease domain intramolecularly, similarly to non-covalent contacts within sumoylated TDG shown previously (13,39,40), thus attenuating the nuclease activity of Dna2 as observed in our assays.

Taken together, our results suggest that Dna2 is regulated by sumoylation in multiple ways: sumoylated Dna2 appears to be resistant to proteasomal degradation induced by genotoxic treatments and exhibits impaired nuclease activity; moreover, sumoylation levels of Dna2 vary throughout the cell cycle being highest in late S/G2 when Dna2 is most likely executing its essential replication function.

Materials and Methods

Recombinant proteins

Wild type Dna2 as well Dna2 E675A and Dna2 K1080E variants were expressed from a modified pGAL:DNA2 vector (23). Dna2 Δ405N proteins (wt, E675A and K1080E) as well as Dna2 6KA were expressed from a pYes2 vector. All Dna2 proteins were purified as described previously (25). RPA protein was expressed and purified as described (41).

Expression and purification of *S. cerevisiae* SUMO machinery proteins, including GST-Aos1/Uba1, His-Ubc9, His-Flag-Smt3, His-Siz1 (1-465) and His-Siz2 was described previously (42,43). His-Flag-Smt3-KR (all lysines substituted by arginines) was purified the same way as wild type Smt3.

In vitro sumoylation assays and mass spectrometry analysis

In vitro sumoylation assays were performed as described previously (44). Proteins were then separated by SDS-PAGE and stained by silver staining. The mass spectrometry analysis of sumoylated Dna2 was carried out by Dorothea Anrather and Gustav Ammerer in Max. F. Perutz Laboratories, Vienna, Austria.

DNA substrates

The oligonucleotides X12-3 and X12-4SC were used for the preparation of the 19 nt-5'-tailed ssDNA substrate, and 292 and X12-4SC for 30 nt-5'-tailed ssDNA substrate, as described previously (25,45). The oligonucleotides used for nuclease and helicase assays were ^{32}P-labeled at the 5' terminus with [gamma-^{32}P] ATP and T4 polynucleotide kinase (New England Biolabs) according to manufacturer instructions. Unincorporated nucleotides were removed using MicroSpin G25 columns (GE Healthcare) before annealing of the substrates. The randomly labeled 2200 nt-long substrate was prepared by amplification of the yeast DNA Ligase I gene by PCR from yeast genomic DNA using the following primers: forward: 5' ACGCATTAGCTAGCGGATCCCTGGAAGTTCTGTTCCAGGGGCCCATGCGCAGATTACTGACCGGTTG 3'; reverse: 5' ACGCATTACTCGAGATTTTGCATGTGGGATTGGT 3'. In addition to the standard dNTP concentration in the PCR reaction (200 nM each), [alpha-^{32}P] dATP (60nM) was added. The PCR reaction was purified using Chroma Spin TE-400 columns (Clontech).

Nuclease, helicase and ATPase assays

The experiments were performed in a 15-µl volume in 25 mM Tris-acetate (pH 7.5), 2 mM magnesium acetate, 1 mM ATP, 1 mM dithiothreitol, 0.1 mg/ml BSA (New England Biolabs), 1 mM phosphoenolpyruvate, 16 U/ml pyruvate kinase, 1 nM DNA substrate, 16.8 nM RPA for 5'-tailed oligonucleotide-based substrates, 350 nM RPA for 2200 nt-long substrate, and Dna2 variants, as indicated. The reactions with oligonucleotide-based substrates were incubated for 30 min at 30 °C, and carried out and analyzed as described previously (45). Reactions with the 2200 nt-long substrate were incubated at 30°C and aliquots were taken at indicated time points. Reactions were stopped by adding equal volume of the formamide dye (95% (v/v) formamide,

20 mM EDTA, 0.01% bromophenol blue), samples were heated at 95°C for 4 min and separated on 20 % denaturing polyacrylamide gels (ratio acrylamide:bisacrylamide 19:1, Biorad). After fixing in a solution containing 40% methanol, 10% acetic acid and 5% glycerol for 30 min, the gels were dried on DE81 chromatography paper (Whatman), and exposed to storage phosphor screens (GE Healthcare). The screens were scanned by Typhoon phosphor imager (GE Healthcare). ATPase assays were performed as described previously (45,46).

Yeast strains and plasmids

All experiments were performed using *S. cerevisiae* FF18733 strain (MATa his7-2 leu2-3,112 lys1-1 trp1-289 ura3-52, F. Fabre). Dna2 gene was C-terminally tagged with 9-MYC tag using pYM18 plasmid, as described previously (47). Plasmids used for His-Smt3 pulldown experiments were YEp181-CUP1-His-SMT3 and the parental vector YEplac181.

Detection of Smt3-Dna2 conjugates

Yeast strains were grown exponentially until OD_{600}=1 in minimal medium, lysed under denaturing conditions, proteins were precipitated and Ni-NTA affinity chromatography was performed as described previously (26). Sumoylation of Dna2 was analyzed by western blotting using the following antibodies: anti-c-Myc-tag mAb (A00704, GenScript), anti-Smt3 (ab14405, Abcam), anti-His-tag mAb (A00186, GenScript). Genotoxic treatments were conducted always for 1.5 h before harvesting using the following drug amounts (final concentration): MMS 0.03% (Sigma-Aldrich), Bleomycin 5 µg/mL (Merck Millipore), Etoposide 295 µg/mL (Sigma-Aldrich).

Cell synchronization and flow cytometry

Cells were grown until OD_{600}=0.3-0.4 and synchronized by addition of α-factor (4 µg/mL, Primmbiotech) in YPD medium for 2 h. Cells were released into S-phase by treatment with Pronase (20 mg/mL, Sigma-Aldrich). Samples were taken for flow cytometry and Ni-NTA pulldowns at indicated time points. For flow cytometry, cells were fixed in 70% ethanol and 250 mM Tris-HCl pH 7.5 at 4°C for at least overnight, treated with RNase A (1 mg/mL, Roche) at 37°C overnight, washed, and resuspended

in 50 mM Tris-HCl pH 7.5, 200 mM NaCl and 80 mM $MgCl_2$ containing propidium iodide (50 µg/mL, Sigma-Aldrich). After brief sonication in 50 mM Tris-HCl pH 7.5 the DNA content was measured using CyAn ADP 9 flow cytometer (Beckman Coulter) operated with Summit software and the data was analyzed with FlowJo software (TreeStar).

Acknowledgements

This work has been supported by Swiss National Science Foundation Professorship PP00P3 133636 for P.C., and the Czech Science Foundation (GACR 13- 26629S and 207/12/2323) and the European Regional Development Fund (Project FNUSA-ICRC) (No. CZ.1.05/1.1.00/02.0123) for L.K. We thank Dorothea Anrather and Gustav Ammerer (Max. F. Perutz Laboratories, Vienna, Austria) for mass spectrometry analysis. We would like to thank Judith Campbell (Caltech, USA) for the Dna2 expression construct, Helle Ulrich (Mainz, Germany) for YEp181-CUP1-His-SMT3 and YEplac181 plasmids, and Primo Schär (Basel, Switzerland) for pYM18 plasmid.

Author contribution: P.C., M.L. and L.K. conceived the general idea of the study, all authors planned experiments, M.L. and V.A. carried out the experiments, and M.L. wrote the manuscript.

Conflict of interest

The authors declare no conflict of interest.

References:

1. Flotho, A. and Melchior, F. (2013) Sumoylation: a regulatory protein modification in health and disease. *Annu Rev Biochem*, **82**, 357-385.
2. Jackson, S.P. and Durocher, D. (2013) Regulation of DNA damage responses by ubiquitin and SUMO. *Mol Cell*, **49**, 795-807.
3. Jentsch, S. and Psakhye, I. (2013) Control of nuclear activities by substrate-selective and protein-group SUMOylation. *Annu Rev Genet*, **47**, 167-186.
4. Sarangi, P. and Zhao, X. (2015) SUMO-mediated regulation of DNA damage repair and responses. *Trends Biochem Sci*, **40**, 233-242.
5. Ulrich, H.D. (2014) Two-way communications between ubiquitin-like modifiers and DNA. *Nat Struct Mol Biol*, **21**, 317-324.
6. Bergink, S. and Jentsch, S. (2009) Principles of ubiquitin and SUMO modifications in DNA repair. *Nature*, **458**, 461-467.
7. Sacher, M., Pfander, B., Hoege, C. and Jentsch, S. (2006) Control of Rad52 recombination activity by double-strand break-induced SUMO modification. *Nat Cell Biol*, **8**, 1284-1290.
8. Shalizi, A., Gaudilliere, B., Yuan, Z., Stegmuller, J., Shirogane, T., Ge, Q., Tan, Y., Schulman, B., Harper, J.W. and Bonni, A. (2006) A calcium-regulated MEF2 sumoylation switch controls postsynaptic differentiation. *Science*, **311**, 1012-1017.
9. Desterro, J.M., Rodriguez, M.S. and Hay, R.T. (1998) SUMO-1 modification of IkappaBalpha inhibits NF-kappaB activation. *Mol Cell*, **2**, 233-239.
10. Moldovan, G.L., Pfander, B. and Jentsch, S. (2006) PCNA controls establishment of sister chromatid cohesion during S phase. *Mol Cell*, **23**, 723-732.
11. Kerscher, O. (2007) SUMO junction-what's your function? New insights through SUMO-interacting motifs. *EMBO Rep*, **8**, 550-555.
12. Psakhye, I. and Jentsch, S. (2012) Protein group modification and synergy in the SUMO pathway as exemplified in DNA repair. *Cell*, **151**, 807-820.
13. Steinacher, R. and Schar, P. (2005) Functionality of human thymine DNA glycosylase requires SUMO-regulated changes in protein conformation. *Curr Biol*, **15**, 616-623.
14. Cremona, C.A., Sarangi, P. and Zhao, X. (2012) Sumoylation and the DNA damage response. *Biomolecules*, **2**, 376-388.
15. Guo, Z., Kanjanapangka, J., Liu, N., Liu, S., Liu, C., Wu, Z., Wang, Y., Loh, T., Kowolik, C., Jamsen, J. *et al.* (2012) Sequential posttranslational modifications program FEN1 degradation during cell-cycle progression. *Mol Cell*, **47**, 444-456.
16. Bae, S.H., Bae, K.H., Kim, J.A. and Seo, Y.S. (2001) RPA governs endonuclease switching during processing of Okazaki fragments in eukaryotes. *Nature*, **412**, 456-461.
17. Budd, M.E., Choe, W.C. and Campbell, J.L. (1995) DNA2 encodes a DNA helicase essential for replication of eukaryotic chromosomes. *J Biol Chem*, **270**, 26766-26769.
18. Cejka, P., Cannavo, E., Polaczek, P., Masuda-Sasa, T., Pokharel, S., Campbell, J.L. and Kowalczykowski, S.C. (2010) DNA end resection by Dna2-Sgs1-RPA

and its stimulation by Top3-Rmi1 and Mre11-Rad50-Xrs2. *Nature*, **467**, 112-116.

19. Kumar, S. and Burgers, P.M. (2013) Lagging strand maturation factor Dna2 is a component of the replication checkpoint initiation machinery. *Genes Dev*, **27**, 313-321.
20. Thangavel, S., Berti, M., Levikova, M., Pinto, C., Gomathinayagam, S., Vujanovic, M., Zellweger, R., Moore, H., Lee, E.H., Hendrickson, E.A. *et al.* (2015) DNA2 drives processing and restart of reversed replication forks in human cells. *J Cell Biol*, **208**, 545-562.
21. Wanrooij, P.H. and Burgers, P.M. (2015) Yet another job for Dna2: Checkpoint activation. *DNA Repair (Amst)*.
22. Bae, S.H., Choi, E., Lee, K.H., Park, J.S., Lee, S.H. and Seo, Y.S. (1998) Dna2 of Saccharomyces cerevisiae possesses a single-stranded DNA-specific endonuclease activity that is able to act on double-stranded DNA in the presence of ATP. *J Biol Chem*, **273**, 26880-26890.
23. Budd, M.E., Choe, W. and Campbell, J.L. (2000) The nuclease activity of the yeast DNA2 protein, which is related to the RecB-like nucleases, is essential in vivo. *J Biol Chem*, **275**, 16518-16529.
24. Formosa, T. and Nittis, T. (1999) Dna2 mutants reveal interactions with Dna polymerase alpha and Ctf4, a Pol alpha accessory factor, and show that full Dna2 helicase activity is not essential for growth. *Genetics*, **151**, 1459-1470.
25. Levikova, M., Klaue, D., Seidel, R. and Cejka, P. (2013) Nuclease activity of Saccharomyces cerevisiae Dna2 inhibits its potent DNA helicase activity. *Proc Natl Acad Sci U S A*, **110**, E1992-2001.
26. Davies, A.A. and Ulrich, H.D. (2012) Detection of PCNA modifications in Saccharomyces cerevisiae. *Methods Mol Biol*, **920**, 543-567.
27. Tsabar, M., Eapen, V.V., Mason, J.M., Memisoglu, G., Waterman, D.P., Long, M.J., Bishop, D.K. and Haber, J.E. (2015) Caffeine impairs resection during DNA break repair by reducing the levels of nucleases Sae2 and Dna2. *Nucleic Acids Res*.
28. Ayyagari, R., Gomes, X.V., Gordenin, D.A. and Burgers, P.M. (2003) Okazaki fragment maturation in yeast. I. Distribution of functions between FEN1 AND DNA2. *J Biol Chem*, **278**, 1618-1625.
29. Bae, K.H., Kim, H.S., Bae, S.H., Kang, H.Y., Brill, S. and Seo, Y.S. (2003) Bimodal interaction between replication-protein A and Dna2 is critical for Dna2 function both in vivo and in vitro. *Nucleic Acids Res*, **31**, 3006-3015.
30. Chen, X., Niu, H., Chung, W.H., Zhu, Z., Papusha, A., Shim, E.Y., Lee, S.E., Sung, P. and Ira, G. (2011) Cell cycle regulation of DNA double-strand break end resection by Cdk1-dependent Dna2 phosphorylation. *Nat Struct Mol Biol*, **18**, 1015-1019.
31. Lee, C.H., Lee, M., Kang, H.J., Kim, D.H., Kang, Y.H., Bae, S.H. and Seo, Y.S. (2013) The N-terminal 45-kDa domain of Dna2 endonuclease/helicase targets the enzyme to secondary structure DNA. *J Biol Chem*, **288**, 9468-9481.
32. Fiorentino, D.F. and Crabtree, G.R. (1997) Characterization of Saccharomyces cerevisiae dna2 mutants suggests a role for the helicase late in S phase. *Mol Biol Cell*, **8**, 2519-2537.

33. Duxin, J.P., Dao, B., Martinsson, P., Rajala, N., Guittat, L., Campbell, J.L., Spelbrink, J.N. and Stewart, S.A. (2009) Human Dna2 is a nuclear and mitochondrial DNA maintenance protein. *Mol Cell Biol*, **29**, 4274-4282.
34. Vallen, E.A. and Cross, F.R. (1995) Mutations in RAD27 define a potential link between G1 cyclins and DNA replication. *Mol Cell Biol*, **15**, 4291-4302.
35. Bologna, S., Altmannova, V., Valtorta, E., Koenig, C., Liberali, P., Gentili, C., Anrather, D., Ammerer, G., Pelkmans, L., Krejci, L. *et al.* (2015) Sumoylation regulates EXO1 stability and processing of DNA damage. *Cell Cycle*, 0.
36. Symington, L.S. (2014) End resection at double-strand breaks: mechanism and regulation. *Cold Spring Harb Perspect Biol*, **6**.
37. Ren, J., Gao, X.J., Jin, C.J., Zhu, M., Wang, X.W., Shaw, A., Wen, L.P., Yao, X.B. and Xue, Y. (2009) Systematic study of protein sumoylation: Development of a site-specific predictor of SUMOsp 2.0. *Proteomics*, **9**, 3409-3412.
38. Zhao, Q., Xie, Y., Zheng, Y., Jiang, S., Liu, W., Mu, W., Liu, Z., Zhao, Y., Xue, Y. and Ren, J. (2014) GPS-SUMO: a tool for the prediction of sumoylation sites and SUMO-interaction motifs. *Nucleic Acids Res*, **42**, W325-330.
39. Baba, D., Maita, N., Jee, J.G., Uchimura, Y., Saitoh, H., Sugasawa, K., Hanaoka, F., Tochio, H., Hiroaki, H. and Shirakawa, M. (2005) Crystal structure of thymine DNA glycosylase conjugated to SUMO-1. *Nature*, **435**, 979-982.
40. Mohan, R.D., Rao, A., Gagliardi, J. and Tini, M. (2007) SUMO-1-dependent allosteric regulation of thymine DNA glycosylase alters subnuclear localization and CBP/p300 recruitment. *Mol Cell Biol*, **27**, 229-243.
41. Kantake, N., Sugiyama, T., Kolodner, R.D. and Kowalczykowski, S.C. (2003) The recombination-deficient mutant RPA (rfa1-t11) is displaced slowly from single-stranded DNA by Rad51 protein. *J Biol Chem*, **278**, 23410-23417.
42. Altmannova, V., Eckert-Boulet, N., Arneric, M., Kolesar, P., Chaloupkova, R., Damborsky, J., Sung, P., Zhao, X., Lisby, M. and Krejci, L. (2010) Rad52 SUMOylation affects the efficiency of the DNA repair. *Nucleic Acids Res*, **38**, 4708-4721.
43. Takahashi, Y., Toh, E.A. and Kikuchi, Y. (2003) Comparative analysis of yeast PIAS-type SUMO ligases in vivo and in vitro. *J Biochem*, **133**, 415-422.
44. Sarangi, P., Bartosova, Z., Altmannova, V., Holland, C., Chavdarova, M., Lee, S.E., Krejci, L. and Zhao, X. (2014) Sumoylation of the Rad1 nuclease promotes DNA repair and regulates its DNA association. *Nucleic Acids Res*, **42**, 6393-6404.
45. Cejka, P. and Kowalczykowski, S.C. (2010) The full-length Saccharomyces cerevisiae Sgs1 protein is a vigorous DNA helicase that preferentially unwinds holliday junctions. *J Biol Chem*, **285**, 8290-8301.
46. Kowalczykowski, S.C. and Krupp, R.A. (1987) Effects of Escherichia coli SSB protein on the single-stranded DNA-dependent ATPase activity of Escherichia coli RecA protein. Evidence that SSB protein facilitates the binding of RecA protein to regions of secondary structure within single-stranded DNA. *J Mol Biol*, **193**, 97-113.
47. Janke, C., Magiera, M.M., Rathfelder, N., Taxis, C., Reber, S., Maekawa, H., Moreno-Borchart, A., Doenges, G., Schwob, E., Schiebel, E. *et al.* (2004) A versatile toolbox for PCR-based tagging of yeast genes: new fluorescent

proteins, more markers and promoter substitution cassettes. *Yeast*, **21**, 947-962.

48 Levikova, M., and Cejka, P. (2015) The *S. cerevisiae* Dna2 can function as a sole nuclease in the processing of Okazaki fragments in DNA replication. *Nucleic Acids Res, in press*.

Figure Legends

Figure 1: Dna2 is sumoylated *in vitro* and *in vivo*. (**A**) Silver-stained gel showing *in vitro* sumoylated (+) and mock-treated (−) Dna2 proteins. Sumoylated Dna2 migrates higher in the gel and is indicated on the right. Dna2 K1080E - helicase-dead, Dna2 E675A - nuclease-dead variant. (**B**) Ni-NTA pulldown of His-Smt3 protein conjugates from *S. cerevisiae* cells containing epitopically myc-tagged Dna2 and were transformed with His-Smt3 plasmid or an empty vector. Input and pulldown samples were analyzed by western blotting using anti-myc, anti-Smt3 and anti-His antibodies. Cells were treated with 0.03% MMS, where indicated. Representative western blot is shown. (**C**) Quantitation of Dna2 sumoylation levels such in (**B**). *Relative intensity: intensity of Dna2-Smt3 band normalized to Dna2-myc input; untreated sample was set as 100%. Averages shown, n=3; s.e.m.

Figure 2: Protein levels as well as sumoylation of Dna2 are regulated during the cell cycle. (**A**) *S. cerevisiae* cells containing epitopically myc-tagged Dna2 and His-Smt3 plasmid were synchronized in G1 by the α-factor and released into S phase. Cell cycle progression was monitored by flow cytometry (1N and 2N DNA content indicated). (**B**) Sumoylation of Dna2 was monitored by Ni-NTA pulldown of His-Smt3 protein conjugates in course of the cell cycle. Input and pulldown samples were analyzed by western blotting using anti-myc, and anti-His antibodies. Representative western blot from three independent experiments is shown. Dna2 levels are markedly decreased in G1 and S, while sumoylation of Dna2 is highest in late S/G2 and decreases in G2/M. (**C**). Cell cycle profile of *S. cerevisiae* cells containing epitopically myc-tagged Dna2 that were treated with 0.03% MMS, analyzed by flow cytometry (1N and 2N DNA content indicated). MMS treatment leads to cell cycle arrest in S-phase.

Figure 3: Sumoylation of Dna2 attenuates its nuclease but not its helicase activity. (**A**) Representative native PAA gel showing the degradation of 5' tailed substrate by sumoylated and mock-treated Dna2 wt. The top oligonucleotide was ^{32}P labeled at the 5' end. The reactions contained RPA (22 nM) and various Dna2 concentrations, as indicated. *, position of ^{32}P label. (**B**) Quantitation of the experiments such as in (**A**). Averages shown, n=2; error bars s.e.m. (**C**) Experiment as in (**A**), but with helicase-dead Dna2 K1080E. (**D**) Quantitation of the experiments such as in (**C**). Averages shown, n=2; error bars s.e.m. (**E**) Representative native PAA gel showing the unwinding of 5' tailed substrate by sumoylated and mock-treated nuclease-dead Dna2 E675A. The top oligonucleotide was ^{32}P labeled at the 5' end. The reactions contained RPA (22 nM) and various Dna2 concentrations, as indicated. *, position of ^{32}P label. Heat, heat-denatured substrate. (**F**) Quantitation of the experiments such as in (**E**). Averages shown, n=2; error bars s.e.m.

Figure 4: Dna2 6KA mutant is weakly sumoylated *in vitro*. (**A**) Schematic representation of the domain structure of the Dna2 protein. Lysine residues that were determined by mass spectrometry of *in vitro* sumoylated protein are depicted in red. (**B**) Coomassie stained gel showing purified Dna2 wt, E675A and K1080E proteins, all lacking the N-terminal 405 amino acids, from *S. cerevisiae*. (**C**) Silver-stained gel showing *in vitro* sumoylated (+) and mock-treated (−) Δ405N and full-length Dna2 proteins. Sumoylated Dna2 migrates higher in the gel. Dna2 Δ405N proteins are sumoylated much less than the full-length Dna2. (**D**) Coomassie stained gel showing purified Dna2 6KA (K21A, K33A, K60A, K93A, K103A, K247A) from *S. cerevisiae*. (**E**) Silver-stained gel showing *in vitro* sumoylated (+) and mock-treated (−) wt Dna2 and 6KA proteins. Sumoylated Dna2 migrates higher in the gel and is indicated on the right. Dna2 6KA is sumoylated only weakly.

Figure 1

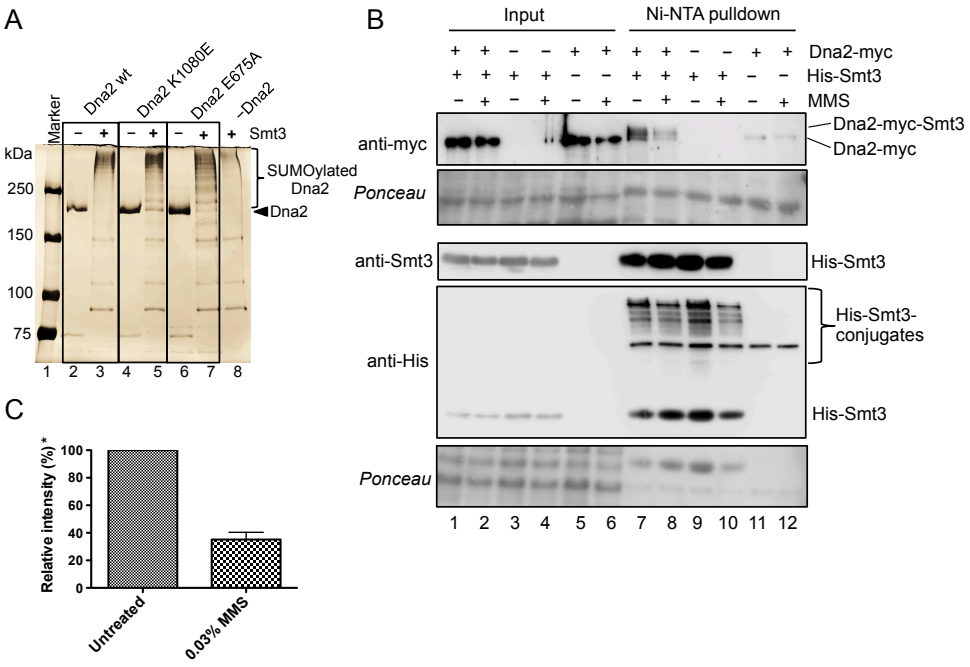

Figure 1: Dna2 is sumoylated *in vitro* and *in vivo.*
(**A**) Silver-stained gel showing *in vitro* sumoylated (+) and mock-treated (−) Dna2 proteins. Sumoylated Dna2 migrates higher in the gel and is indicated on the right. Dna2 K1080E - helicase-dead, Dna2 E675A - nuclease-dead variant. (**B**) Ni-NTA pulldown of His-Smt3 protein conjugates from *S. cerevisiae* cells containing epitopically myc-tagged Dna2 and were transformed with His-Smt3 plasmid or an empty vector. Input and pulldown samples were analyzed by western blotting using anti-myc, anti-Smt3 and anti-His antibodies. Cells were treated with 0.03% MMS, where indicated. Representative Western blot is shown. (**C**) Quantitation of Dna2 sumoylation levels such in (**B**). *Relative intensity: intensity of Dna2-Smt3 band normalized to Dna2-myc input; untreated sample was set as 100%. Averages shown, n=3; s.e.m.

Figure 2

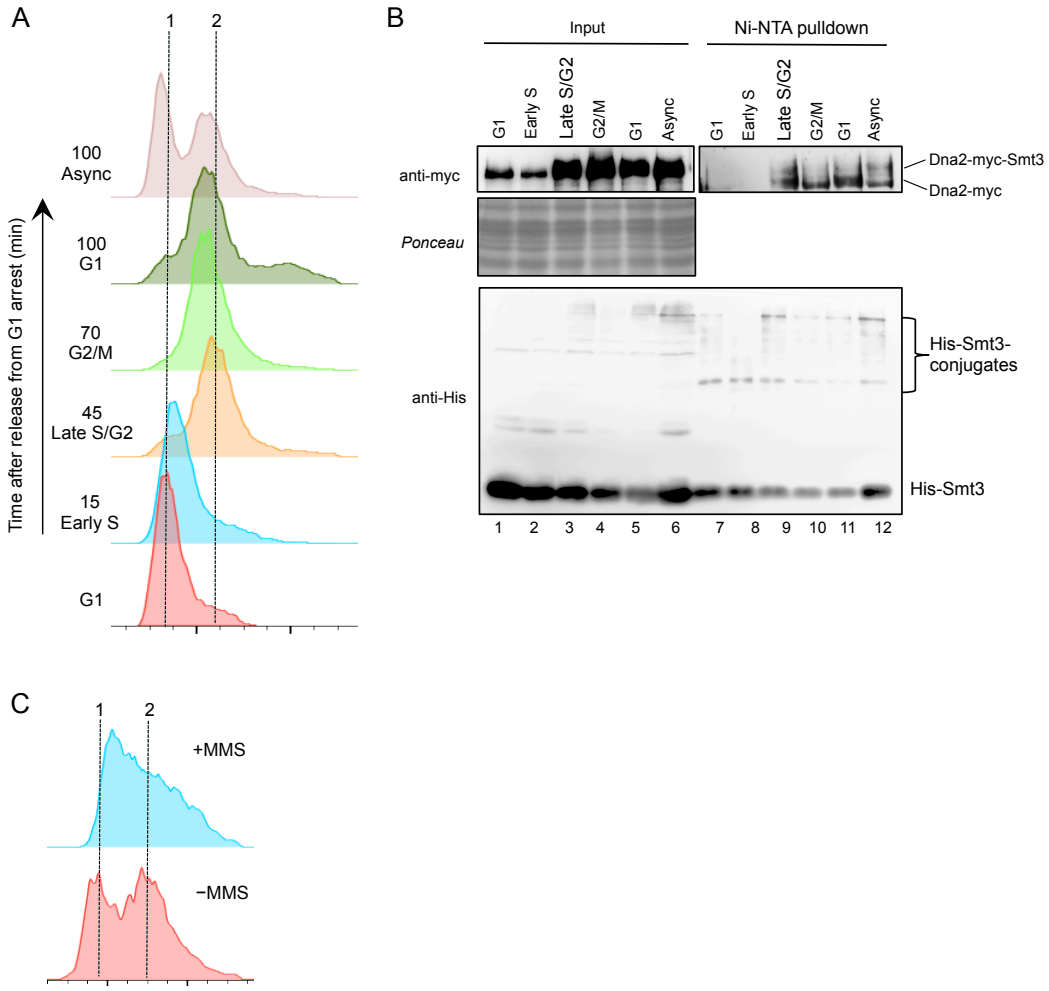

Figure 2: Protein levels as well as sumoylation of Dna2 are regulated during the cell cycle.
(**A**) *S. cerevisiae* cells containing epitopically myc-tagged Dna2 and His-Smt3 plasmid were synchronized in G1 by the α-factor and released into S phase. Cell cycle progression was monitored by flow cytometry (1N and 2N DNA content indicated). (**B**) Sumoylation of Dna2 was monitored by Ni-NTA pulldown of His-Smt3 protein conjugates in course of the cell cycle. Input and pulldown samples were analyzed by western blotting using anti-myc, and anti-His antibodies. Representative western blot from three independent experiments is shown. Dna2 levels are markedly decreased in G1 and S, while sumoylation of Dna2 is highest in late S/G2 and decreases in G2/M. (**C**). Cell cycle profile of *S. cerevisiae* cells containing epitopically myc-tagged Dna2 that were treated with 0.03% MMS, analyzed by flow cytometry (1N and 2N DNA content indicated). MMS treatment leads to cell cycle arrest in S-phase.

Figure 3

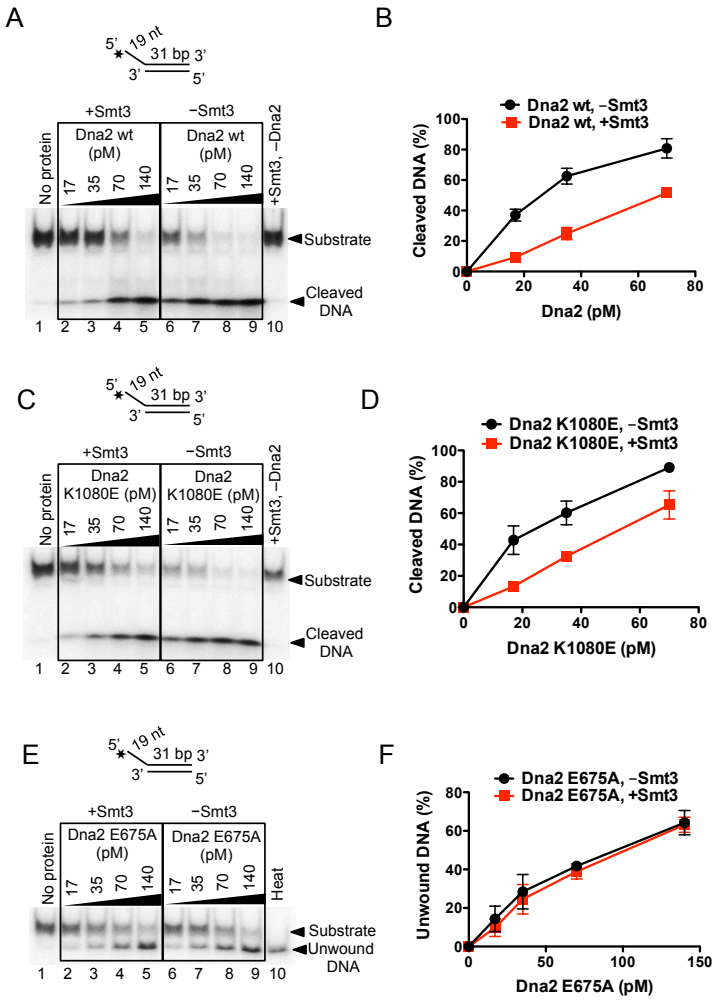

Figure 3: Sumoylation of Dna2 attenuates its nuclease but not its helicase activity
(**A**) Representative native PAA gel showing the degradation of 5' tailed substrate by sumoylated and mock-treated Dna2 wt. The top oligonucleotide was ^{32}P labeled at the 5' end. The reactions contained RPA (22 nM) and various Dna2 concentrations, as indicated. *, position of ^{32}P label. (**B**) Quantitation of the experiments such as in (**A**). Averages shown, n=2; error bars s.e.m. (**C**) Experiment as in (**A**), but with helicase-dead Dna2 K1080E. (**D**) Quantitation of the experiments such as in (**C**). Averages shown, n=2; error bars s.e.m. (**E**) Representative native PAA gel showing the unwinding of 5' tailed substrate by sumoylated and mock-treated nuclease-dead Dna2 E675A. The top oligonucleotide was ^{32}P labeled at the 5' end. The reactions contained RPA (22 nM) and various Dna2 concentrations, as indicated. *, position of ^{32}P label. Heat, heat-denatured substrate. (**F**) Quantitation of the experiments such as in (**E**). Averages shown, n=2; error bars s.e.m.

Figure 4

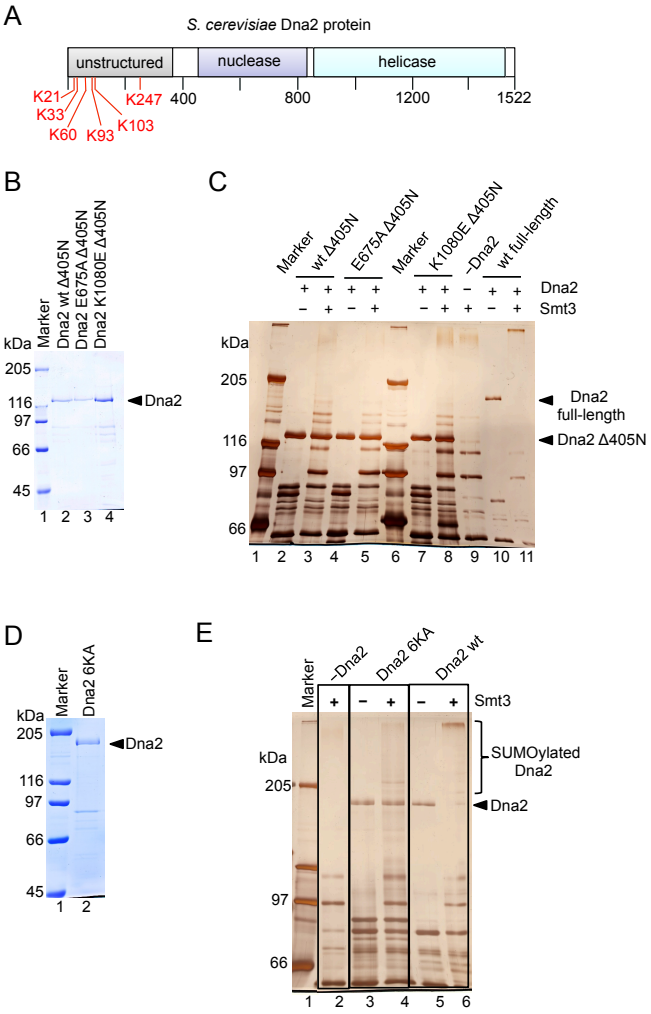

Figure 4: Dna2 6KA mutant is weakly sumoylated *in vitro.*
(**A**) Schematic representation of the domain structure of the Dna2 protein. Lysine residues that were determined by mass spectrometry of *in vitro* sumoylated protein are depicted in red. (**B**) Coomassie stained gel showing purified Dna2 wt, E675A and K1080E proteins, all lacking the N-terminal 405 amino acids, from *S. cerevisiae*. (**C**) Silver-stained gel showing *in vitro* sumoylated (+) and mock-treated (−) Δ405N and full-length Dna2 proteins. Sumoylated Dna2 migrates higher in the gel. Dna2 Δ405N proteins are SUMOylated much less than the full-length Dna2. (**D**) Coomassie stained gel showing purified Dna2 6KA (K21A, K33A, K60A, K93A, K103A, K247A) from *S. cerevisiae*. (**E**) Silver-stained gel showing *in vitro* sumoylated (+) and mock-treated (−) wt Dna2 and 6KA proteins. Sumoylated Dna2 migrates higher in the gel and is indicated on the right. Dna2 6KA is sumoylated only weakly.

Supplementary Figure 1

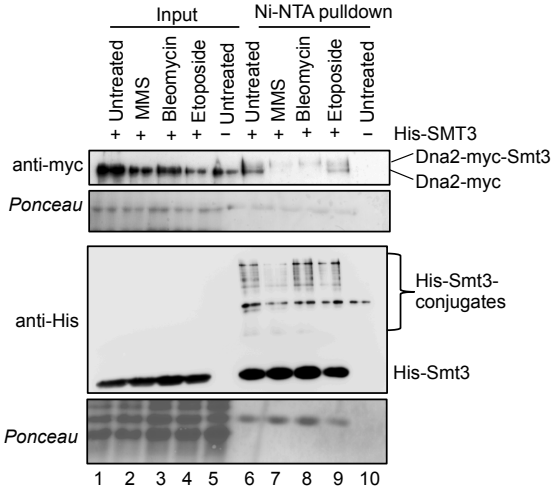

Supplementary Figure 1: Sumoylation of Dna2 is decreased after MMS and Bleomycin treatments *in vivo.* Ni-NTA pulldown of His-Smt3 protein conjugates from *S. cerevisiae* cells containing epitopically myc-tagged Dna2 and were transformed with His-Smt3 plasmid or an empty vector. Input and pulldown samples were analyzed by western blotting using anti-myc and anti-His antibodies. Cells were treated with either 0.03% MMS, or 5 µg/mL Bleomycin, or 295 µg/mL (0.5 mM) Etoposide, where indicated. Representative western blot from three independent experiments is shown.

Supplementary Figure 2

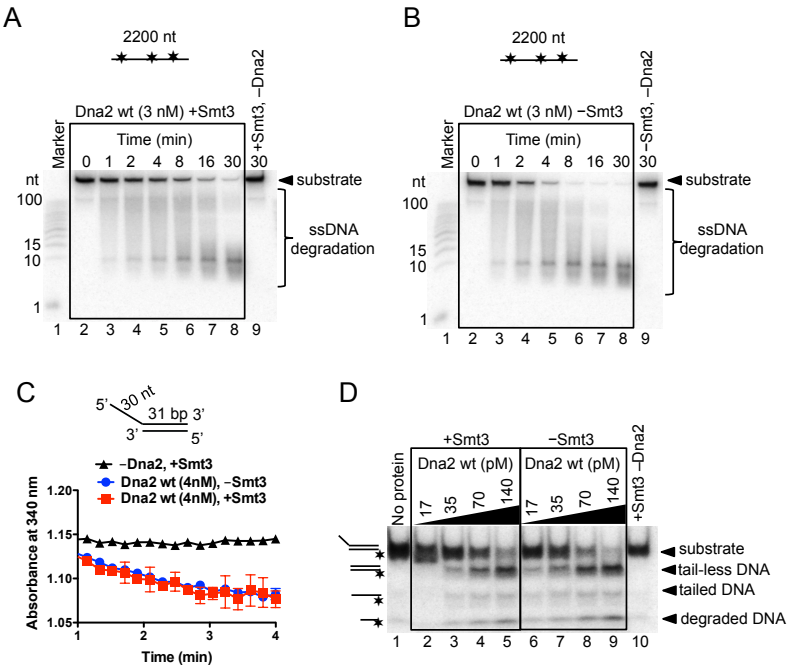

Supplementary Figure 2: *In vitro* sumoylated Dna2 exhibits decreased nuclease activity, while helicase and ATPase remain untouched. (**A**). Representative denaturing 20% PAA gel showing the degradation kinetics of a uniformly labeled 2200 nt-long substrate by sumoylated Dna2 wt. (**B**) Experiment as in (**A**), but with mock-treated Dna2 wt. (**C**) Kinetics of ATP hydrolysis by sumoylated Dna2 wt compared to mock-treated control. The reactions contained 30 nt-long 5' overhang substrate (1 μM in nucleotides). (**D**) Processing of 5' tailed DNA substrate by sumoylated Dna2 wt. The bottom oligonucleotide was ^{32}P labeled at the 5' end. The reactions contained RPA (22.5 nM) and various Dna2 concentrations, as indicated. *, position of ^{32}P label.

2.2.3 The *S. cerevisiae* Dna2 can function as a sole nuclease in the processing of Okazaki fragments in DNA replication

Maryna Levikova and Petr Cejka.

Article in press in Nucleic Acids Research, 2015.

I designed the research together with P.C. and performed the experiments. I analyzed the data and wrote the manuscript together with P.C..

The *S. cerevisiae* Dna2 can function as a sole nuclease in the processing of Okazaki fragments in DNA replication

Maryna Levikova and Petr Cejka*

Institute of Molecular Cancer Research, University of Zurich, Winterthurerstrasse 190, CH-8057 Zurich, Switzerland

* To whom correspondence should be addressed. Tel: +41 44 635 4786; Email: cejka@imcr.uzh.ch

ABSTRACT

During DNA replication, synthesis of the lagging strand occurs in stretches termed Okazaki fragments. Before adjacent fragments are ligated, any flaps resulting from the displacement of the 5' DNA end of the Okazaki fragment must be cleaved. Previously, Dna2 was implicated to function upstream of Fen1 in the processing of long flaps bound by the replication protein A (RPA). Here we show that Dna2 efficiently cleaves long DNA flaps exactly at or directly adjacent to the base. A fraction of the flaps cleaved by Dna2 can be immediately ligated. When coupled with DNA replication, the flap processing activity of Dna2 leads to a nearly complete Okazaki fragment maturation at sub-nanomolar Dna2 concentrations. Our results indicate that a subsequent nucleolytic activity of Fen1 is not required in most cases. In contrast Dna2 is completely incapable to cleave short flaps. We show that also Dna2, like Fen1, interacts with PCNA. We propose a model where Dna2 alone is responsible for cleaving of RPA-bound long flaps, while Fen1 or Exo1 cleave short flaps. Our results argue that Dna2 can function in a separate, rather than in a Fen1-dependent pathway.

INTRODUCTION

All cells must replicate their DNA before each cell division. While leading strand DNA synthesis occurs continuously in a 5' to 3' direction, the lagging strand is synthesized in short stretches termed Okazaki fragments due to the 5' to 3' polarity of DNA polymerases. First, the DNA polymerase α-primase complex (pol α) synthesizes a ~30-nucleotide RNA-DNA primer. The replication factor C (RFC) then binds the junction between the RNA-DNA primer and the parental DNA strand and initiates the loading of proliferating cell nuclear antigen (PCNA). Recruitment of PCNA mediates a switch from pol α to pol δ, which extends the newly synthesized DNA strand to up to ~200 nucleotides (nt) (1,2). RNAse H1 is primarily responsible for the removal of RNA from DNA (3-6). PCNA binds pol δ (7,8) and enhances its processivity (9), and also serves as a binding platform for further replicative factors including flap endonuclease 1 (Fen1 or Rad27) and DNA ligase I (Lig1 or Cdc9) (8,10-14). After pol δ reaches the 5' end of the downstream Okazaki fragment it may continue DNA synthesis leading to the displacement of the RNA-DNA primer. This creates 5'-terminated flaps of various lengths that must be cleaved before ligation by Lig1 can occur. This process is also important for the maintenance of genome stability as it contributes to the removal of RNA as well as DNA from the initial primer synthesized by error-prone pol α (15,16).

Dna2 is an essential protein that was found to be necessary for DNA replication *in vivo* (17-19). While it is not necessary for bulk DNA synthesis (20), newly replicated DNA in *dna2-1* cells contained low molecular weight fragments, showing that Dna2 is required for sealing nicks in newly replicated DNA, reminiscent of cells lacking Lig1 (18,21). Dna2 has both DNA nuclease and helicase activities (22-25). While a loss of its nuclease activity is lethal, helicase-deficient mutants are viable under some growth conditions (19,24). This suggested that specifically the nuclease activity of Dna2 is essential for DNA replication. The Pif1 helicase was shown to stimulate the displacement activity of pol δ, leading thus to long flap formation and providing requirement for Dna2 (26-28). In accord, *pif1Δ* mutation rescues the lethality of *dna2Δ* cells (29). Additional deletion of *pol32* (pol δ subunit responsible for DNA strand displacement activity) further suppresses the growth defects of *pif1Δ dna2Δ* cells

(29,30). At the same time, the lethality of *dna2Δ* cells can be also rescued by a mutation of *rad9*, leading to inactivation of DNA damage checkpoint (31). Nevertheless, these data collectively suggest that Dna2 *in vivo* is required for the processing of long flaps in *S. cerevisiae* DNA replication.

Short flaps are primarily processed by the flap endonuclease 1 (Fen1). Fen1 is a component of the Okazaki fragment maturation complex composed of pol δ, PCNA and Lig1 (7,8,10-14,32). It has been demonstrated that Fen1 becomes incapable of cleaving flaps that are long enough to bind RPA. Thus, RPA mediates the nuclease switch between Fen1 and Dna2 (33). While inhibiting DNA cleavage by Fen1 (26,33), RPA promotes the nuclease of Dna2 (22,33,34). However, recombinant Dna2 was shown to only shorten long flaps to ~5-8 nt, even when used at very high concentrations. DNA cleavage at these positions did not support ligation and therefore a second nuclease activity was needed (22,33,35). As Dna2 was found to be part of a complex with Fen1 *in vivo* (36), it was proposed that Fen1 must act downstream of Dna2 (32,33,35). Indeed, a combination of recombinant Dna2 and Fen1 allowed Okazaki fragment processing *in vitro*, leading to a two-step Okazaki fragment processing model (33). In contrast to *dna2Δ* cells, *rad27Δ* mutants are viable, albeit grow slowly and display elevated recombination and mutation rates (37,38). The viability of *rad27Δ* cells seems to contradict the model where Fen1 acts downstream of Dna2 (32,33,35). To this point, Fen1 activity was proposed to be redundant with that of the exonuclease 1 (Exo1) (33). Indeed, overexpression of Exo1 could suppress some of the phenotypic defects of *rad27Δ* cells and *exo1Δ rad27Δ* mutant is lethal (39). However, there is no evidence to date suggesting that Dna2 physically interacts with Exo1, nor that Exo1 acts downstream of Dna2. On the contrary, Dna2 and Exo1 nucleases function in strictly separate pathways during DNA end resection (40). Furthermore, the direct interaction between Dna2 and Fen1 could not be confirmed in a later study (41). Also, overexpression of Dna2 suppressed the growth defects associated with deletion of *rad27*, while overexpression of Fen1 suppressed the lethality of *dna2Δ* cells (36). Also this supports the notion that Dna2 and Fen1 can function in separate pathways. Despite that, available *in vitro* data with recombinant Dna2 were in contrast with such an explanation.

Here we show that Dna2 cleaves DNA flaps near their base, and is thus able to support complete Okazaki fragment maturation without the requirement of Fen1 during DNA replication *in vitro*. This finding provides a possible explanation of the diverse phenotypes of *dna2Δ* and *rad27Δ* cells. It strongly suggests that Dna2 can function as the sole nuclease in the processing of at least a fraction of long DNA flaps in DNA replication.

MATERIALS AND METHODS

DNA substrates

The oligonucleotides used to prepare the flapped substrates were as follows: "bottom" X12-4NC and "top" Flap 19 X12-4C were annealed with a variety of "top flap" oligonucleotides to prepare flapped substrates of 30 (oligonucleotide 292), 8 (293), and 4 nt in length (294): X12-4NC, 5'-GCGATAGTCTCTAGACAGCATGTCCTAGCAAGCC AGAATTCGGCAGGCTA-3'; Flap 19 X12-4C, 5'-TAGCCTGCCGAATTCTGGC-3'; 292, 5'-GGTACTCAAGTGACGTCATAGACGATTACATTGCTAGGACATGCTGTCTAGAGACTATCGC-3'; 293, 5'-GGATTACATTGCTAGGACATGCTGTCTAGAGACTATCGC-3'; 294, 5'-GACAT TGCTAGGACATGCTGTCTAGAGACTATCGC-3'. For 8 nt double flap substrate, oligonucleotides X12-4NC, Flap 20 X12-4C and 293 were annealed. The sequence of Flap 20 X12-4C is: 5'-TAGCCTGCCGAATTCTGGCA-3'.

The oligonucleotides were ^{32}P-labeled at the 3' end with [alpha-^{32}P] cordycepin-5'-triphosphate and terminal deoxynucleotidyl transferase (New England Biolabs) according to manufacturer instructions. Unincorporated nucleotides were removed using MicroSpin G25 columns (GE Healthcare).

The circular 3.197 kb-long ssDNA used in the replication assays was pGEM-3Zf(-) that was prepared as described previously (42). This DNA was annealed with either pR_T12flap 5'-TTTTTTTTTTTTACCATCTGGCCCCAGTGCTGCAATG-3' (primer with a 12 nt-flap), pR_T30flap 5'-TTTTTTTTTTTTTTTTTTTTTTTTTTTTTTACCATCTGGCCCCAGTGCT GCAATG-3' (primer with a 30 nt-flap), or pR_20 5'-GCGATCTGTCTATTTCGTTC-3' (fully complementary primer without a flap).

Recombinant proteins

RPA protein was prepared as described (43). Wild type Dna2 as well as nuclease-dead E675A, helicase-dead K1080E and the E675A/K1080E double mutant were expressed and purified as described previously (25). We note that care must be taken during cell lysis to prevent a loss of activity. Also, Dna2 is particularly sensitive to oxidation, so reducing agents must be included throughout the procedure. Yeast *LIG1* (*CDC9*) gene was amplified from yeast genomic DNA by PCR using primers Lig1_for 5'- ACGCATTAGCTAGCGGATCCCTGGAAGTTCTGTTCCAGGGGCCCATGCGCAGATTACT GACCGGTTG-3' and Lig1_rev 5'-ACGCATTACTCGAGATTTTGCATGTGGGATTGGT-3'. The PCR product was digested by NheI and XhoI restriction endonucleases (both New England Biolabs) and cloned into corresponding sites in pFB-MBP-Sgs1-his vector (44), creating pFB-MBP-Lig1-his. Lig1 was expressed in insect *Sf9* cells and purified by affinity chromatography as described previously for Sgs1 (44).

Yeast *FEN1* (*RAD27*) was amplified from yeast genomic DNA by PCR using primers Fen1_for: 5'- ACGCATTAGCTAGCGAATTCCTGGAAGTTCTGTTCCAGGGGCCCATGGGTAT TAAAGGTTTGAATGC-3' and Fen1_rev: 5'- ACGCATTACTCGAGTCTTCTTCCCTTTGTGAC TT-3'. The PCR product was digested by NheI and XhoI restriction endonucleases (both New England Biolabs) and cloned into corresponding sites in pFB-MBP-Sgs1-his vector (44), creating pFB-MBP-Fen1-his. MBP tag was excised from this vector by digestion with the restriction endonuclease BamHI (New England Biolabs) followed by self-ligation of pFB-Fen1-his. Then, a fragment coding for PP-MBP (PP is PreScission protease cleavage site) was amplified by PCR from the pFB-MBP-Sgs1-his vector (44) using primers XhoI_PP2G_MBP_for 5'- ACGCATTACTCGAGCTGGAAGTTCTGTTCCAGG GGCCCGGTGGTATGAAAATCGAAGAAGGTAA-3' and MBP_XhoI_rev 5'ACGCATTACTCG AGCCCGAGGTTGTTGTTATTGT-3'. The PCR product was digested by XhoI restriction endonuclease (New England Biolabs) and cloned into pFB-Fen1-His directly after Fen1, creating pFB-Fen1-MBP-his. Fen1 was expressed in insect *Sf9* cells. Cells were lysed and MBP-tagged Fen1 was first incubated with amylose resin as described previously for Sgs1 (44). Eluates from amylose resin were applied on Ni-NTA agarose column and extensively washed with wash buffer (50 mM Tris-HCl pH 7.5, 2 mM β-mercaptoethanol, 10% glycerol, 0.5 mM phenylmethylsulfonyl fluoride, 1 M NaCl and 20 mM imidazole), followed by a wash with the same buffer, but containing 0.3

M NaCl and 60 mM imidazole. Protein was eluted with wash buffer containing 0.3 M NaCl and 0.3 M imidazole. MBP and His tags were cleaved by PreScission protease and the eluate was incubated with glutathione and amylose resins. The sample was centrifuged (2000 g, 5 min), and supernatant containing Fen1 was dialyzed into 50 mM Tris-HCl pH 7.5, 5 mM β-mercaptoethanol, 150 mM NaCl, 10% glycerol and frozen in small aliquots.

Yeast three subunit pol δ and pol δ exonuclease-deficient variant (Pol3-D520V, mutation introduced by site-directed mutagenesis) were expressed in the yeast strain WDH668 as described previously (45) and purified according to existing protocols (27). PCNA and RFC were expressed and purified from *E. coli* by minor modifications of previously established procedures (46,47).

Nuclease assays

Nuclease assays were performed in a 15 µl volume in 25 mM Tris-acetate pH 7.5, 10 mM magnesium acetate (unless indicated otherwise), 1 mM ATP, 1 mM dithiothreitol, 0.1 mg/ml bovine serum albumin (BSA, New England Biolabs), 1 mM phosphoenolpyruvate, 80 U/ml pyruvate kinase, 1 nM DNA substrate (in molecules) and recombinant proteins as indicated. Where indicated, RPA was present at 27 nM, which is sufficient to fully cover the entire DNA in the reactions assuming all DNA was single-stranded. Samples were incubated at 30°C for 30 min, reaction was stopped by adding an equal amount of formamide dye (95% (v/v) formamide, 20 mM EDTA, 0.01% bromophenol blue), samples were heated at 95°C for 4 min and separated on 20 % denaturing polyacrylamide gels (ratio acrylamide:bisacrylamide 19:1, Biorad). After fixing in a solution containing 40% methanol, 10% acetic acid and 5% glycerol for 30 min, the gels were dried on DE81 chromatography paper (Whatman), and exposed to storage phosphor screens (GE Healthcare). The screens were scanned by Typhoon phosphor imager (GE Healthcare).

Replication assays

Replication assays with plasmid-based substrates were performed similarly as described previously (32) in a 15 µl volume in 25 mM Tris-acetate pH 7.5, 10 mM magnesium acetate, 125 mM NaCl, 1 mM ATP, 1 mM dithiothreitol, 0.1 mg/ml BSA (New

England Biolabs), 1 mM phosphoenolpyruvate, 80 U/ml pyruvate kinase, 100 µM dNTPs (each) and 6.4 nM (molecules, 100 ng) ssDNA substrate. PCNA (20 nM), RFC (20 nM) and RPA (1 µM, concentration saturating 100% of DNA) were added to the reaction and preincubated for 1 min at 30 °C. Pol δ (5 nM), Dna2 and/or yeast Fen1 (concentrations as indicated in figures or figure legends) and Lig1 (20 nM) were then added and the reactions were incubated, if not indicated otherwise, at 30°C for 60 min. The reactions were stopped by adding 5 µl of 2% stop solution (150 mM EDTA, 2% SDS, 30% glycerol, bromophenol blue) and 1 µl proteinase K (20.3 mg/ml, Roche) for 10 min at 30°C and separated on 1% agarose gels containing GelRed (1:10,000 v/v, Biotinum). Gels were analyzed by an AlphaImager gel imaging system.

Pulldown assays

To test for interactions between Dna2 and RPA or PCNA, 2 µg of recombinant Dna2 was diluted in Tris-buffered saline (TBS, 50 mM Tris-HCl, pH 7.5, 150 mM NaCl), bound to anti-HA resin (25 µl, Pierce) and washed with TBS-T (TBS containing 0.05% Tween 20). Then, recombinant RPA (1.33 µg) or PCNA (0.34 µg) were added and the resin was incubated at 4°C for 1 h. The resin was again washed with TBS-T and proteins were eluted with 0.1 M glycine, pH 2.5, according to manufacturer's instructions. The proteins in the eluate were analyzed by SDS-PAGE stained with silver.

RESULTS

Dna2 cleaves DNA flaps near their base

Previously, we were able to purify recombinant *S. cerevisiae* Dna2 with high levels of DNA helicase and nuclease activities (25,34). Here we tested the behavior of Dna2 and mutant variants (Supplementary Figure S1A) on flapped substrates that mimic structures arising upon displacement synthesis during Okazaki fragment processing (Figure 1A). We first used a substrate with a 30 nt-long 5' ssDNA flap, and examined the exact cleavage position by *S. cerevisiae* Dna2 in the presence of RPA. Cleavage at exactly the base of the flap (position 0) would produce a fragment of 32 nucleotides in length. It is known that Dna2 must load onto the 5' ssDNA end, and translocate along the ssDNA flap before cleavage occurs (23,35). We show that wild type Dna2

protein efficiently cleaved the flap at -1, 0 or +1 positions in most cases (Figure 1B, cleavage at -1 position leaves behind a flap of 1 nt in length, cleavage adjacent to flap base within dsDNA corresponds to +1 position). In contrast, nuclease-dead (E675A) and double-dead (nuclease and helicase-dead, E675A/K1080E) Dna2 variants did not show any activity, demonstrating that the cleavage is inherent to the nuclease of Dna2 and not a product of a contamination (Figure 1B). These results differ from those published previously (33,35), which reported that Dna2 only shortens flaps up to the length of ~5-8 nucleotides in a vast majority of cases. The position of cleavage was unchanged in magnesium concentrations between 2 and 10 mM, indicating that DNA melting near the flap base cannot explain the observed position of cleavage (compare Figure 1B with Supplementary Figure S1C). A comparison of DNA flap cleavage by Dna2 and Fen1 is shown in Supplementary Figure S1D; Fen1 cleaves past the flap just within the dsDNA. Furthermore, Dna2 cleaved the long flap sequentially, with the first cut being ~5-10 nt away from the flap end (Supplementary Figure S1E). This is in agreement with previous observations that Dna2 must load on a free flap end and translocate along DNA before cleavage occurs (35). RPA did not stimulate the overall efficiency of DNA cleavage by Dna2, but promoted cutting at positions near the flap base (Figure 1C-E). Without RPA, Dna2 often cleaved at -1 or 0 positions, while no cleavage at +1 position was observed (Figure 1C, right part). Furthermore, without RPA, a large fraction of the flap was only cleaved ~20 nt away from the flap base (Figure 1C, right part), likely due to secondary structure in the flap that prevents Dna2 translocation along the ssDNA, which is in full agreement with previous data (48). With RPA, Dna2 cleaved majority of the substrate in the vicinity of the flap base (Figure 1C, left part, Figure 1E). We also show that Dna2 was able to cleave an 8 nt-long flap in the same manner as the 30 nt-long flap, but could not cleave a 4 nt-long flap (Supplementary Figure S2A and B), which is instead as expected a good substrate for Fen1 (Supplementary Figure S2C-E). RPA inhibited the cleavage of the 30 nt-long flaps by Fen1, while it had no effect on the processing of the short flaps (Supplementary Figure S2C-G), in agreement with previous data (33,35,49-54). The helicase activity of Dna2 did not significantly affect the position of cleavage (Figure 1F and Supplementary Figure S3A and B). In summary, these data

suggest that Dna2 is able to cleave flaps of at least 8 nt in length at or very near their base.

The product of Dna2 can be directly ligated

The capacity of Dna2 to cut at or near the flap base prompted us to investigate whether a fraction of the cleaved flaps can be ligated by the cognate Lig1. Previously, it was shown not to be the case as Dna2 was leaving a ~5-8 nt flap behind that prevented ligation in a vast majority of cases (33). This gave rise to the two-step model where a second nucleolytic activity was needed (33). We show in Figure 2A-C that ~10-15% of the cleaved flap structures could be directly ligated by Lig1, which corresponded to the flaps cleaved exactly at the base (position "0" in Figure 2B). RPA moderately increased ligation efficiency (Figure 2C, primary data for reactions without RPA not shown), while the helicase of Dna2 had no effect (Figure 2D; Supplementary Figure S3C). Furthermore, ~15-25% of 8 nt-long flap structures cleaved by either wild type or helicase-dead Dna2 were ligated by Lig1 as well (Supplementary Figure S4A-D, primary data for reactions without RPA not shown). In contrast, the nuclease activity of Fen1 resulted in almost undetectable ligation efficiency on 4 nt or longer flaps (~1% product, Supplementary Figure S5A and B). This is most likely due to the fact that Fen1 predominantly cleaves DNA not exactly at the flap base, but just inside dsDNA (+1 position, Supplementary Figure S1D), and this cleavage position does not produce a substrate for Lig1. In accord, Fen1 is known to prefer a substrate containing an additional 1 nt 3' flap (55). Taken together, these data indicate that a fraction of flap structures cleaved by Dna2 exactly at their base (~15-20%) can be directly ligated by Lig1. The nuclease but not the helicase of Dna2 is essential for this process.

Dna2 is highly efficient in flap processing during replication

In replication, the processing of flap structures occurs coupled with DNA synthesis by pol δ (1). It was shown that pol δ can accommodate for inaccurate cleavage (9,32,56,57). Hence, flap cleavage at the +1 position (in dsDNA), can be coupled with 1 nt synthesis by pol δ, which creates a ligatable substrate (9). Likewise, cleavage at -1 position (leaving behind a 1 nt flap) can be accommodated by the proofreading 3' -

5' exonuclease activity of pol δ. By going 1 nt backwards, the exonuclease of pol δ likewise leads to a ligatable substrate (57). We expressed and purified the three-subunit pol δ, PCNA and RFC to test whether Dna2 on its own can mediate efficient flap processing in the context of ongoing DNA replication. Previously, it was shown that Dna2 was required for cleavage of exclusively long flaps (e.g. 30 nt) that are bound by RPA, and efficient maturation was only achieved in conjunction with Fen1 (32,33). We used a plasmid based ssDNA substrate with a primer containing 30 nt-long ssDNA flap (Figure 3A; Figure 3B, lane 2). Pol δ in conjunction with RFC, PCNA, RPA and Lig1 efficiently synthesized DNA (Figure 3B, lane 3, open circular DNA, ocDNA), but no covalently closed supercoiled DNA (scDNA) was detected, showing that the flap structure prevented ligation. As shown in Figure 3B, lanes 4-8, supplementing the reactions further with Dna2 resulted in nearly complete Okazaki fragment maturation already at sub-nanomolar Dna2 concentrations (see also Figure 3C). DNA synthesis was fully dependent on the presence of pol δ, PCNA, RFC and RPA but did not require Lig1, while generation of scDNA required additionally both Dna2 and Lig1 (Figure 3D). The same results were obtained when we used a substrate with a 12 nt-long flap (Supplementary Figure S6A-D). Nuclease- and helicase-dead Dna2 was not able to support the reactions (Figure 3E, Supplementary Figure S6E). When using a substrate without a flap, the maturation was fully independent of Dna2 (Figure 3F), as expected, but still required all other components (Figure 3G). Next, we tested to which extent the Okazaki fragment maturation activity of Dna2 is dependent on the proofreading exonuclease of pol δ. To this point, we substituted wild type pol δ with 3' exo- pol δ variant, Pol3(D520V), in the replication assays (Figure 4A). The generation of scDNA was strongly inhibited in the absence of the pol δ exonuclease (Figure 4B, lane 14 and Figure 4C), showing that the proofreading activity of pol δ is very important for flap processing during DNA replication in conjunction with Dna2, in accord with a previous study (57).

Fen1, in contrast, was unable to process the 30 nt-long flap in the presence of RPA (Supplementary Figure S7A and B), while it very efficiently supported the reactions with a 4 nt-long flapped substrate (Supplementary Figure S7C-E) and to a lesser degree reactions with a 12 nt-long flaps (Supplementary Fig. S7F-H) as expected (58). Furthermore, Fen1 was fully incapable to process the 4 nt-long flaps without the 3'

exonuclease of pol δ (Supplementary Figure S7J-K), most likely due to the increased strand displacement activity that was described for the Pol3-DV mutant (57). Genetic studies showed that *rad27Δ pol3-DV* cells grow very slowly and an additional deletion of *rad51* is lethal (56,57). However, the lethality of the *rad27Δ pol3-DV rad51Δ* triple mutant can be rescued by overexpression of Dna2, suggesting that Dna2 can process these flaps in the absence of Fen1 (57). Our experiments demonstrate that Dna2 in concert with DNA replication is highly efficient in flap processing as a single nuclease, thus suggesting that Dna2 may function in Okazaki fragment maturation as the sole flap processing enzyme.

Dna2 does not function with Fen1 in a concerted manner

Our data so far indicated that the Dna2 nuclease was remarkably capable of promoting flap processing during DNA replication. To test whether Fen1 can further stimulate the ligation efficiency in conjunction with Dna2, we combined the two nucleases together with RPA and Lig1 on the 30 nt-long flap oligonucleotide-based substrate (Figure 5A). As shown in Figure 5B and C, the presence of Fen1 lowered ligation efficiency from ~15% to ~5% in a Fen1 concentration-dependent manner, in accord with the observed cleavage position of Fen1 that precludes ligation (Supplementary Figure 1D).

We next analyzed the activity of Fen1 and Dna2 in replication-coupled assays on plasmid based DNA substrates. As Fen1 was incapable to process the 30 nt flapped substrates (Supplementary Figure S7A and B), we tested whether it could promote the production of covalently closed DNA in concert with Dna2. Using a suboptimal Dna2 concentration (0.13 nM), we show in kinetic assays that an equimolar concentration of Fen1 had no effect on the ligation efficiency (Figure 5D, E and G). When a 10-fold higher Fen1 concentration was used, a moderate stimulation of the reaction was observed (Figure 5F and G). Therefore, Fen1 was able to complete the flap processing downstream of Dna2 in some cases. We showed above that Dna2 cleaves the flap sequentially; thus, we believe that Fen1 could process the flaps that were previously shortened by Dna2. The fact that the stimulation occurred at Fen1 concentrations that exceeded those of Dna2 argues against the notion that both enzymes function in a coordinated manner. However, this assumes that both protein prepara-

tions contain an identical proportion of an active enzyme. To study the effect of Fen1 on flap processing by Dna2 in more detail, we next performed experiments with an even lower Dna2 concentration (32 pM), and titrated Fen1 into the reactions. We observed that Fen1 promoted the formation of covalently closed DNA at concentrations equal or higher than 128 pM (Supplementary Figure S8A-C). However, very similar Fen1 concentrations promoted the 4 nt-long flap processing without Dna2 (Supplementary Figure S7C-E). In case of a concerted reaction, we would expect Fen1 being more efficient in reactions with Dna2 rather then on its own, which was not the case. We conclude that Dna2 is sufficient for Okazaki fragment processing in most cases on its own without Fen1. However, we do not exclude that Fen1 can function downstream of Dna2 in a small number of cases when either Dna2 does not cleave near the base of the flap, or when pol δ displaces the annealed 5' end upon Dna2 cleavage before ligation occurs. In accord, we observed that Fen1 but not Dna2 could promote processing of a substrate without a flap (Supplementary Figure S9A-E). These results collectively argue against the requirement for a cooperation between Dna2 and Fen1 in flap processing and rather suggest that their action is not concerted in most cases.

PCNA has a central function in lagging strand DNA replication as it interacts with RFC, pol δ, Lig1 and Fen1 (7,8,10,11,13,14). PCNA also stimulates Fen1 activity (54). PCNA thus not only promotes DNA synthesis by pol δ as a processivity factor (9), but also serves as a docking platform for factors required for Okazaki fragment maturation (59). We show in Supplementary Figure 10 that Dna2 can also directly interact with PCNA under physiological salt concentrations. In addition, as demonstrated previously (60), we confirm that Dna2 interacts with RPA (Supplementary Figure S10). The observation that Dna2 binds PCNA is in accord with human DNA2, which was found to be in complex with replication component And-1 *in vivo* (61). Thus, our data in conjunction with previous work suggest a model (Figure 6) where Dna2 is primarily responsible for the processing of long DNA flaps coated with RPA. This is facilitated by the direct interaction between Dna2 and RPA, and the capacity of Dna2 to degrade RPA-coated ssDNA more rapidly than naked DNA (10,12,34,35,60,62). Fen1 is primarily responsible for short flaps, and is recruited to those *via* its structure specific DNA-binding capacity (32,35,50). The polymerase and 3'-5' exonuclease of pol δ is

then required in most cases downstream of both Dna2 and Fen1 before adjacent fragments can be sealed by Lig1 (9,57).

DISCUSSION

Synthesis of the lagging DNA strand is discontinuous and occurs in short fragments of ~200 nt in length. In order to complete DNA replication, the adjacent Okazaki fragments must be ligated to achieve integrity of the nascent DNA. Direct ligation is often not possible due the displacement synthesis of the lagging DNA strand pol δ, which leads to flap structures of various lengths (1,2). It has been established that Fen1 cleaves short flaps that are not bound by RPA (33). The strand displacement activity of pol δ, in concert with the Pif1 helicase, can lead to longer flaps that become a substrate for RPA (26). Binding of ssDNA by RPA inhibits the cleavage by Fen1 (33). It has been proposed that the nuclease of Dna2 is specifically involved in the processing of these RPA-bound long flaps (32,33). Importantly, it has been presented that Dna2 only shortens long flaps to ~5-8 nucleotides. In previous preparations of Dna2, only a very small proportion of flaps was cleaved at the base, which was attributed to the dsDNA melting capacity of RPA at low magnesium concentrations, which creates a substrate that Dna2 can cut (63). Therefore, Fen1 was proposed to function downstream of Dna2 (33,35). This hypothesis was however in contrast with the viability of *rad27Δ* but lethality of *dna2Δ* mutants (19,36-38). Previously, we characterized recombinant Dna2 that exhibited vigorous nuclease and helicase activities (25). Here we show that recombinant Dna2 cleaves efficiently DNA directly at or on either side of the flap base (Figure 1). The cleavage of DNA by Dna2 is unchanged in magnesium concentrations up to 10 mM and requires the nuclease but not the helicase activity of Dna2. A fraction of flaps that are cleaved precisely at their base can be directly ligated by Lig1 (Figure 2). When coupled with DNA replication, Dna2 was remarkably effective in flap processing by allowing a nearly complete Okazaki fragment maturation at sub-nanomolar concentrations (Figure 3), supported by the polymerase and 3'-5' exonuclease activities of pol δ (Figure 4) (9,57). This showed that in most cases the activity of Fen1 downstream of Dna2 is not required, arguing against the two-nuclease model. We showed that adding Fen1 to Dna2 reac-

tions only led to an increase in ligation efficiency when Fen1 concentration exceeded that of Dna2, and we failed to obtain evidence for cooperativity between Fen1 and Dna2 (Figure 5). Our results thus demonstrate that Fen1 does not promote the processing of a large fraction of long flaps by Dna2 and suggest that Dna2 can function in Okazaki fragment processing as the sole nuclease. However, we believe that Fen1 can still function downstream of Dna2 in cases when Dna2 cleaves the flap inaccurately or when 5' strand displacement occurs again upon Dna2 cleavage before the fragments are ligated.

Dna2 in multiple organisms was proposed to be part of the replication complex. It has been shown that *Xenopus laevis* Dna2 is forming a complex with Mcm10 (minichromosome maintenance complex component 10) and human Dna2 was found to be in complex with And-1 during G1/S transition (61,64). Here we report that *S. cerevisiae* Dna2 interacts with PCNA (Supplementary Figure S10), similarly to Fen1 (10,12). This, together with previously published data, might suggest that Dna2 and Fen1 travel with the DNA replication machinery as components of the Okazaki fragment maturation complex. Alternatively, Dna2 can be recruited to gapped DNA near unprocessed flaps *via* its interaction with PCNA post-replicatively. This is supported by our observation that the levels of Dna2 are low in early S and increase significantly in late S/G2 phase of the cell cycle (M.L. and P.C., unpublished). This contrasts with the expression profile of human FEN1 that is highly expressed in the G1 and S phases of the cell cycle and gets rapidly degraded in late S/G2 (65). This would suggest that Dna2 functions rather late in DNA replication to cleave flaps that are refractory to Fen1 and/or Exo1. In accord, yeast *dna2* mutants are proficient in bulk DNA synthesis, but arrest in G2/M phase of the cell cycle (21). Similarly, replication fork progression is not affected in human cells upon DNA2 downregulation; these cells also accumulate in late S/G2 (66). In contrast *fen1* cells accumulate in S phase due to a block in DNA replication at non-permissive temperature (67). Collectively, we show that Dna2 can function in flap processing independently of Fen1. These results are in agreement with the lethality of *dna2Δ* mutation (36), viability of *rad27Δ* or *exo1Δ* cells (37-39), as well as the lethality of *rad27Δ exo1Δ* double mutants (39). The flap processing activity of Dna2 described here may also play a role in other processes of DNA metabolism not limited to DNA replication.

SUPPLEMENTARY DATA

Supplementary Data are available at NAR Online.

FUNDING

This work was supported by Swiss National Science Foundation Grant [PP00P3 133636 to P.C.]. Funding for open access charge: University of Zurich.
Conflict of interest statement. None declared.

ACKNOWLEDGEMENTS

We thank Ulrich Hübscher (University of Konstanz, Germany), Elda Cannavo, Lucie Mlejnkova, Cosimo Pinto, Lepakshi Ranjha and Roopesh Anand (all University of Zurich) for discussions and comments on the manuscript. We would like to thank Mariela Artola (University of Zurich) for the help in preparation of the ssDNA plasmid used in replication assays. We would like to acknowledge Louise Prakash (University of Texas Medical Branch) and Patrick Sung (Yale university) for pol δ expression vectors. We thank Robert Bambara (University of Rochester) and Manju Hingorani (Wesleyan University) for PCNA and RFC constructs.

REFERENCES

1. Hubscher, U. and Seo, Y.S. (2001) Replication of the lagging strand: a concert of at least 23 polypeptides. *Mol Cells*, **12**, 149-157.
2. Kang, Y.H., Lee, C.H. and Seo, Y.S. (2010) Dna2 on the road to Okazaki fragment processing and genome stability in eukaryotes. *Crit Rev Biochem Mol Biol*, **45**, 71-96.
3. Huang, L., Kim, Y., Turchi, J.J. and Bambara, R.A. (1994) Structure-specific cleavage of the RNA primer from Okazaki fragments by calf thymus RNase HI. *J Biol Chem*, **269**, 25922-25927.
4. Turchi, J.J., Huang, L., Murante, R.S., Kim, Y. and Bambara, R.A. (1994) Enzymatic completion of mammalian lagging-strand DNA replication. *Proc Natl Acad Sci U S A*, **91**, 9803-9807.
5. Murante, R.S., Rumbaugh, J.A., Barnes, C.J., Norton, J.R. and Bambara, R.A. (1996) Calf RTH-1 nuclease can remove the initiator RNAs of Okazaki fragments by endonuclease activity. *J Biol Chem*, **271**, 25888-25897.
6. Qiu, J., Qian, Y., Frank, P., Wintersberger, U. and Shen, B. (1999) Saccharomyces cerevisiae RNase H(35) functions in RNA primer removal during lagging-strand DNA synthesis, most efficiently in cooperation with Rad27 nuclease. *Mol Cell Biol*, **19**, 8361-8371.
7. Gerik, K.J., Li, X., Pautz, A. and Burgers, P.M. (1998) Characterization of the two small subunits of Saccharomyces cerevisiae DNA polymerase delta. *J Biol Chem*, **273**, 19747-19755.
8. Dovrat, D., Stodola, J.L., Burgers, P.M. and Aharoni, A. (2014) Sequential switching of binding partners on PCNA during in vitro Okazaki fragment maturation. *Proc Natl Acad Sci U S A*, **111**, 14118-14123.
9. Garg, P., Stith, C.M., Sabouri, N., Johansson, E. and Burgers, P.M. (2004) Idling by DNA polymerase delta maintains a ligatable nick during lagging-strand DNA replication. *Genes Dev*, **18**, 2764-2773.
10. Li, X., Li, J., Harrington, J., Lieber, M.R. and Burgers, P.M. (1995) Lagging strand DNA synthesis at the eukaryotic replication fork involves binding and stimulation of FEN-1 by proliferating cell nuclear antigen. *J Biol Chem*, **270**, 22109-22112.
11. Montecucco, A., Rossi, R., Levin, D.S., Gary, R., Park, M.S., Motycka, T.A., Ciarrocchi, G., Villa, A., Biamonti, G. and Tomkinson, A.E. (1998) DNA ligase I is recruited to sites of DNA replication by an interaction with proliferating cell nuclear antigen: identification of a common targeting mechanism for the assembly of replication factories. *Embo J*, **17**, 3786-3795.
12. Gomes, X.V. and Burgers, P.M. (2000) Two modes of FEN1 binding to PCNA regulated by DNA. *Embo J*, **19**, 3811-3821.
13. Levin, D.S., McKenna, A.E., Motycka, T.A., Matsumoto, Y. and Tomkinson, A.E. (2000) Interaction between PCNA and DNA ligase I is critical for joining of Okazaki fragments and long-patch base-excision repair. *Curr Biol*, **10**, 919-922.

14. Tom, S., Henricksen, L.A., Park, M.S. and Bambara, R.A. (2001) DNA ligase I and proliferating cell nuclear antigen form a functional complex. *J Biol Chem*, **276**, 24817-24825.
15. Bambara, R.A., Murante, R.S. and Henricksen, L.A. (1997) Enzymes and reactions at the eukaryotic DNA replication fork. *J Biol Chem*, **272**, 4647-4650.
16. Burgers, P.M. (2009) Polymerase dynamics at the eukaryotic DNA replication fork. *J Biol Chem*, **284**, 4041-4045.
17. Kuo, C., Nuang, H. and Campbell, J.L. (1983) Isolation of yeast DNA replication mutants in permeabilized cells. *Proc Natl Acad Sci U S A*, **80**, 6465-6469.
18. Budd, M.E., Choe, W.C. and Campbell, J.L. (1995) DNA2 encodes a DNA helicase essential for replication of eukaryotic chromosomes. *J Biol Chem*, **270**, 26766-26769.
19. Formosa, T. and Nittis, T. (1999) Dna2 mutants reveal interactions with Dna polymerase alpha and Ctf4, a Pol alpha accessory factor, and show that full Dna2 helicase activity is not essential for growth. *Genetics*, **151**, 1459-1470.
20. Kang, H.Y., Choi, E., Bae, S.H., Lee, K.H., Gim, B.S., Kim, H.D., Park, C., MacNeill, S.A. and Seo, Y.S. (2000) Genetic analyses of Schizosaccharomyces pombe dna2(+) reveal that dna2 plays an essential role in Okazaki fragment metabolism. *Genetics*, **155**, 1055-1067.
21. Fiorentino, D.F. and Crabtree, G.R. (1997) Characterization of Saccharomyces cerevisiae dna2 mutants suggests a role for the helicase late in S phase. *Mol Biol Cell*, **8**, 2519-2537.
22. Bae, S.H., Choi, E., Lee, K.H., Park, J.S., Lee, S.H. and Seo, Y.S. (1998) Dna2 of Saccharomyces cerevisiae possesses a single-stranded DNA-specific endonuclease activity that is able to act on double-stranded DNA in the presence of ATP. *J Biol Chem*, **273**, 26880-26890.
23. Bae, S.H. and Seo, Y.S. (2000) Characterization of the enzymatic properties of the yeast dna2 Helicase/endonuclease suggests a new model for Okazaki fragment processing. *J Biol Chem*, **275**, 38022-38031.
24. Budd, M.E., Choe, W. and Campbell, J.L. (2000) The nuclease activity of the yeast DNA2 protein, which is related to the RecB-like nucleases, is essential in vivo. *J Biol Chem*, **275**, 16518-16529.
25. Levikova, M., Klaue, D., Seidel, R. and Cejka, P. (2013) Nuclease activity of Saccharomyces cerevisiae Dna2 inhibits its potent DNA helicase activity. *Proc Natl Acad Sci U S A*, **110**, E1992-2001.
26. Rossi, M.L., Pike, J.E., Wang, W., Burgers, P.M., Campbell, J.L. and Bambara, R.A. (2008) Pif1 helicase directs eukaryotic Okazaki fragments toward the two-nuclease cleavage pathway for primer removal. *J Biol Chem*, **283**, 27483-27493.
27. Wilson, M.A., Kwon, Y., Xu, Y., Chung, W.H., Chi, P., Niu, H., Mayle, R., Chen, X., Malkova, A., Sung, P. *et al.* (2013) Pif1 helicase and Poldelta promote recombination-coupled DNA synthesis via bubble migration. *Nature*, **502**, 393-396.
28. Pike, J.E., Burgers, P.M., Campbell, J.L. and Bambara, R.A. (2009) Pif1 helicase lengthens some Okazaki fragment flaps necessitating Dna2 nuclease/helicase action in the two-nuclease processing pathway. *J Biol Chem*, **284**, 25170-25180.

29. Budd, M.E., Reis, C.C., Smith, S., Myung, K. and Campbell, J.L. (2006) Evidence suggesting that Pif1 helicase functions in DNA replication with the Dna2 helicase/nuclease and DNA polymerase delta. *Mol Cell Biol*, **26**, 2490-2500.
30. Stith, C.M., Sterling, J., Resnick, M.A., Gordenin, D.A. and Burgers, P.M. (2008) Flexibility of eukaryotic Okazaki fragment maturation through regulated strand displacement synthesis. *J Biol Chem*, **283**, 34129-34140.
31. Budd, M.E., Antoshechkin, I.A., Reis, C., Wold, B.J. and Campbell, J.L. (2011) Inviability of a DNA2 deletion mutant is due to the DNA damage checkpoint. *Cell Cycle*, **10**, 1690-1698.
32. Ayyagari, R., Gomes, X.V., Gordenin, D.A. and Burgers, P.M. (2003) Okazaki fragment maturation in yeast. I. Distribution of functions between FEN1 AND DNA2. *J Biol Chem*, **278**, 1618-1625.
33. Bae, S.H., Bae, K.H., Kim, J.A. and Seo, Y.S. (2001) RPA governs endonuclease switching during processing of Okazaki fragments in eukaryotes. *Nature*, **412**, 456-461.
34. Cejka, P., Cannavo, E., Polaczek, P., Masuda-Sasa, T., Pokharel, S., Campbell, J.L. and Kowalczykowski, S.C. (2010) DNA end resection by Dna2-Sgs1-RPA and its stimulation by Top3-Rmi1 and Mre11-Rad50-Xrs2. *Nature*, **467**, 112-116.
35. Kao, H.I., Campbell, J.L. and Bambara, R.A. (2004) Dna2p helicase/nuclease is a tracking protein, like FEN1, for flap cleavage during Okazaki fragment maturation. *J Biol Chem*, **279**, 50840-50849.
36. Budd, M.E. and Campbell, J.L. (1997) A yeast replicative helicase, Dna2 helicase, interacts with yeast FEN-1 nuclease in carrying out its essential function. *Mol Cell Biol*, **17**, 2136-2142.
37. Gary, R., Park, M.S., Nolan, J.P., Cornelius, H.L., Kozyreva, O.G., Tran, H.T., Lobachev, K.S., Resnick, M.A. and Gordenin, D.A. (1999) A novel role in DNA metabolism for the binding of Fen1/Rad27 to PCNA and implications for genetic risk. *Mol Cell Biol*, **19**, 5373-5382.
38. Symington, L.S. (1998) Homologous recombination is required for the viability of rad27 mutants. *Nucleic Acids Res*, **26**, 5589-5595.
39. Tishkoff, D.X., Boerger, A.L., Bertrand, P., Filosi, N., Gaida, G.M., Kane, M.F. and Kolodner, R.D. (1997) Identification and characterization of Saccharomyces cerevisiae EXO1, a gene encoding an exonuclease that interacts with MSH2. *Proc Natl Acad Sci U S A*, **94**, 7487-7492.
40. Cannavo, E., Cejka, P. and Kowalczykowski, S.C. (2013) Relationship of DNA degradation by Saccharomyces cerevisiae exonuclease 1 and its stimulation by RPA and Mre11-Rad50-Xrs2 to DNA end resection. *Proc Natl Acad Sci U S A*, **110**, E1661-1668.
41. Bae, S.H. and Seo, Y.S. (2000) In vitro evidence that purified yeast Rad27 and Dna2 are not stably associated with each other suggests that an additional protein(s) is required for a complex formation. *J Biochem Mol Biol*, **33**, 155-161.
42. Baerenfaller, K., Fischer, F. and Jiricny, J. (2006) Characterization of the "mismatch repairosome" and its role in the processing of modified nucleosides in vitro. *Methods Enzymol*, **408**, 285-303.

43. Kantake, N., Sugiyama, T., Kolodner, R.D. and Kowalczykowski, S.C. (2003) The recombination-deficient mutant RPA (rfa1-t11) is displaced slowly from single-stranded DNA by Rad51 protein. *J Biol Chem*, **278**, 23410-23417.
44. Cejka, P. and Kowalczykowski, S.C. (2010) The full-length Saccharomyces cerevisiae Sgs1 protein is a vigorous DNA helicase that preferentially unwinds holliday junctions. *J Biol Chem*, **285**, 8290-8301.
45. Johnson, R.E., Prakash, L. and Prakash, S. (2006) Yeast and human translesion DNA synthesis polymerases: expression, purification, and biochemical characterization. *Methods Enzymol*, **408**, 390-407.
46. Biswas, E.E., Chen, P.H. and Biswas, S.B. (1995) Overexpression and rapid purification of biologically active yeast proliferating cell nuclear antigen. *Protein Expr Purif*, **6**, 763-770.
47. Finkelstein, J., Antony, E., Hingorani, M.M. and O'Donnell, M. (2003) Overproduction and analysis of eukaryotic multiprotein complexes in Escherichia coli using a dual-vector strategy. *Anal Biochem*, **319**, 78-87.
48. Bae, S.H., Kim, D.W., Kim, J., Kim, J.H., Kim, D.H., Kim, H.D., Kang, H.Y. and Seo, Y.S. (2002) Coupling of DNA helicase and endonuclease activities of yeast Dna2 facilitates Okazaki fragment processing. *J Biol Chem*, **277**, 26632-26641.
49. Harrington, J.J. and Lieber, M.R. (1994) The characterization of a mammalian DNA structure-specific endonuclease. *Embo J*, **13**, 1235-1246.
50. Murante, R.S., Rust, L. and Bambara, R.A. (1995) Calf 5' to 3' exo/endonuclease must slide from a 5' end of the substrate to perform structure-specific cleavage. *J Biol Chem*, **270**, 30377-30383.
51. Hosfield, D.J., Frank, G., Weng, Y., Tainer, J.A. and Shen, B. (1998) Newly discovered archaebacterial flap endonucleases show a structure-specific mechanism for DNA substrate binding and catalysis resembling human flap endonuclease-1. *J Biol Chem*, **273**, 27154-27161.
52. Bornarth, C.J., Ranalli, T.A., Henricksen, L.A., Wahl, A.F. and Bambara, R.A. (1999) Effect of flap modifications on human FEN1 cleavage. *Biochemistry*, **38**, 13347-13354.
53. Kimura, S., Ueda, T., Hatanaka, M., Takenouchi, M., Hashimoto, J. and Sakaguchi, K. (2000) Plant homologue of flap endonuclease-1: molecular cloning, characterization, and evidence of expression in meristematic tissues. *Plant Mol Biol*, **42**, 415-427.
54. Tom, S., Henricksen, L.A. and Bambara, R.A. (2000) Mechanism whereby proliferating cell nuclear antigen stimulates flap endonuclease 1. *J Biol Chem*, **275**, 10498-10505.
55. Kao, H.I., Henricksen, L.A., Liu, Y. and Bambara, R.A. (2002) Cleavage specificity of Saccharomyces cerevisiae flap endonuclease 1 suggests a double-flap structure as the cellular substrate. *J Biol Chem*, **277**, 14379-14389.
56. Jin, Y.H., Obert, R., Burgers, P.M., Kunkel, T.A., Resnick, M.A. and Gordenin, D.A. (2001) The 3'-->5' exonuclease of DNA polymerase delta can substitute for the 5' flap endonuclease Rad27/Fen1 in processing Okazaki fragments and preventing genome instability. *Proc Natl Acad Sci U S A*, **98**, 5122-5127.
57. Jin, Y.H., Ayyagari, R., Resnick, M.A., Gordenin, D.A. and Burgers, P.M. (2003) Okazaki fragment maturation in yeast. II. Cooperation between the

polymerase and 3'-5'-exonuclease activities of Pol delta in the creation of a ligatable nick. *J Biol Chem*, **278**, 1626-1633.
58. Kao, H.I., Veeraraghavan, J., Polaczek, P., Campbell, J.L. and Bambara, R.A. (2004) On the roles of Saccharomyces cerevisiae Dna2p and Flap endonuclease 1 in Okazaki fragment processing. *J Biol Chem*, **279**, 15014-15024.
59. Moldovan, G.L., Pfander, B. and Jentsch, S. (2007) PCNA, the maestro of the replication fork. *Cell*, **129**, 665-679.
60. Bae, K.H., Kim, H.S., Bae, S.H., Kang, H.Y., Brill, S. and Seo, Y.S. (2003) Bimodal interaction between replication-protein A and Dna2 is critical for Dna2 function both in vivo and in vitro. *Nucleic Acids Res*, **31**, 3006-3015.
61. Duxin, J.P., Moore, H.R., Sidorova, J., Karanja, K., Honaker, Y., Dao, B., Piwnica-Worms, H., Campbell, J.L., Monnat, R.J., Jr. and Stewart, S.A. (2012) Okazaki fragment processing-independent role for human Dna2 enzyme during DNA replication. *J Biol Chem*, **287**, 21980-21991.
62. Bae, S.H., Kim, J.A., Choi, E., Lee, K.H., Kang, H.Y., Kim, H.D., Kim, J.H., Bae, K.H., Cho, Y., Park, C. *et al.* (2001) Tripartite structure of Saccharomyces cerevisiae Dna2 helicase/endonuclease. *Nucleic Acids Res*, **29**, 3069-3079.
63. Stewart, J.A., Miller, A.S., Campbell, J.L. and Bambara, R.A. (2008) Dynamic removal of replication protein A by Dna2 facilitates primer cleavage during Okazaki fragment processing in Saccharomyces cerevisiae. *J Biol Chem*, **283**, 31356-31365.
64. Wawrousek, K.E., Fortini, B.K., Polaczek, P., Chen, L., Liu, Q., Dunphy, W.G. and Campbell, J.L. (2010) Xenopus DNA2 is a helicase/nuclease that is found in complexes with replication proteins And-1/Ctf4 and Mcm10 and DSB response proteins Nbs1 and ATM. *Cell Cycle*, **9**, 1156-1166.
65. Guo, Z., Kanjanapangka, J., Liu, N., Liu, S., Liu, C., Wu, Z., Wang, Y., Loh, T., Kowolik, C., Jamsen, J. *et al.* (2012) Sequential posttranslational modifications program FEN1 degradation during cell-cycle progression. *Mol Cell*, **47**, 444-456.
66. Duxin, J.P., Dao, B., Martinsson, P., Rajala, N., Guittat, L., Campbell, J.L., Spelbrink, J.N. and Stewart, S.A. (2009) Human Dna2 is a nuclear and mitochondrial DNA maintenance protein. *Mol Cell Biol*, **29**, 4274-4282.
67. Vallen, E.A. and Cross, F.R. (1995) Mutations in RAD27 define a potential link between G1 cyclins and DNA replication. *Mol Cell Biol*, **15**, 4291-4302.

FIGURE LEGENDS

Figure 1. Dna2 cleaves DNA near a base of a flap. (**A**) Nuclease assay. (**B**) Wild type (wt), nuclease-dead (E675A) or double-dead (E675A/K1080E, EA/KE) Dna2 variants (all 2 nM) were incubated with a DNA substrate containing a 30 nt-long flap, (*, radioactive label), in the presence of RPA in a buffer containing 2 mM magnesium acetate. The reaction products were separated on 20% polyacrylamide denaturing urea gel. Cleavage at the base of the flap produces a fragment of 32 nt in length (position 0). (**C**) Increasing concentrations of Dna2 were incubated with a substrate containing a 30 nt-long flap as in (**B**), but in 10 mM magnesium acetate buffer, with or without RPA, as indicated. §, substrate cleaved by Dna2 in the absence of RPA. (**D**) Quantification of experiments such as in (**C**). Averages shown, n=2; error bars, s.e.m. (**E**) Quantitation of products cleaved within 5 nt of flap base from (**C**). Averages shown, n=2; error bars, s.e.m. (**F**) Experiment as in (**C**), but with helicase-dead Dna2 K1080E variant in the presence of RPA.

Figure 2. The product of Dna2 can be directly ligated. (**A**) Assay. (**B**) Increasing concentrations of wild type Dna2 were incubated with a substrate containing a 30 nt-long flap with or without Lig1, in the presence of RPA. The reaction products were separated on a 20% polyacrylamide denaturing urea gel. Cleavage at the base of the flap produces a fragment of 32 nt in length. Ligation of the cleaved intermediate results in a final product of 51 nt in length. (**C**) Quantitation of data such as in (**B**), with wild type or mutants of Dna2 (nuclease-dead, E675A; helicase and nuclease-dead, EA/KE). The ^{32}P label was placed either at the 3' terminus of the flapped oligonucleotide or at the 5' terminus of the upstream primer. Averages shown, n=2; error bars, s.e.m. (**D**) Quantitation of experiments such as in (**B**), but with helicase-dead Dna2 K1080E. The ^{32}P label was placed either at the 3' terminus of the flapped oligonucleotide or at the 5' terminus of the upstream primer. Averages shown, n=2; error bars, s.e.m.

Figure 3. Dna2 is highly efficient in flap processing during replication. (**A**) Replication assay. See 'Materials and Methods' for details. (**B**) Dna2 is required for the completion of replication of a substrate containing a 5' ssDNA flap of 30 nt in length. Reactions contained pol δ, PCNA, RFC, RPA, Lig1 and Dna2 as indicated. Positions of substrate ssDNA, open circular intermediate (ocDNA) and closed circular supercoiled final product (scDNA) are indicated. Final product appears in a Dna2 concentration dependent manner. (**C**) Quantitation of data such as in (**B**). Averages shown, n=3; error bars, s.e.m. (**D**) Pol δ, RFC, PCNA and RPA are required for DNA synthesis, Dna2 and Lig1 for the formation of scDNA product. A “complete” reaction contained all components as described in (**B**) without Dna2. Proteins were omitted from the reactions as indicated. (**E**) Nuclease activity of Dna2 is required for flap processing. Nuclease- and helicase-dead Dna2 E675A/K1080E variant was used where indicated. (**F**) Same assay as in (**E**), but using a substrate without a flap. Dna2 was not required for the processing of the flap-less substrate. A “complete” reaction contained all components as described in (**B**) without Dna2. Marker, a sample containing DNA species corresponding to scDNA, linear DNA and ocDNA. (**G**) Replication assay with a flap-less substrate. Protein components were omitted from the reactions where indicated. A “complete” reaction contained all components as described in (**B**) without Dna2.

Figure 4. Effect of pol δ exonuclease activity on Okazaki fragment processing by Dna2 and Fen1. (**A**) Replication assay with a 30 nt-long flapped primer. (**B**) Reactions contained RFC, PCNA, RPA, Lig1 and Dna2, where indicated. Pol δ wild type or the exonuclease-deficient mutant (pol δ exo−) were titrated into the reactions. Positions of substrate ssDNA, open circular intermediate (ocDNA) and closed circular supercoiled final product (scDNA) are indicated. In the presence of pol δ exo−, Dna2 stimulates the completion of replication only to a minor extent. (**C**) Quantitation of data such as in (**B**). Averages shown, n=2; error bars, s.e.m.

Figure 5. Effect of Fen1 on the flap processing by Dna2. (**A**) Assay. (**B**) Increasing concentrations of Fen1 were used to supplement reactions containing RPA, and Dna2 or Lig1 as indicated. The presence of Fen1 led to a decrease of the final ligated reaction

product. (**C**) Quantitation of data such as in (**B**). Averages shown, n=2; error bars, s.e.m. (**D**) Replication assay. (**E**) Kinetic replication reactions contained pol δ, PCNA, RFC, RPA, Lig1 and either 0.13 nM Dna2 (left part), or 0.13 nM Dna2 and 0.13 nM Fen1 (right part). Positions of substrate ssDNA, open circular intermediate (ocDNA) and closed circular supercoiled final product (scDNA) are indicated on the right. Samples were terminated at various time points, as indicated. (**F**) Same assay as in (**E**) but with 0.13 nM Dna2 and 1.3 nM Fen1. (**G**) Quantitation of experiments such as in (**E**) and (**F**) Averages shown, n=3; error bars, s.e.m.

Figure 6. Model of Okazaki fragment processing in eukaryotes. In cases when flaps formed upon the strand displacement activity of pol δ are long enough to bind RPA, Dna2 alone is primarily responsible for their processing in most cases (left). Short flaps are primarily processed by Fen1, Exo1 or possibly other nucleases (middle and right). See text for details.

Figure 1

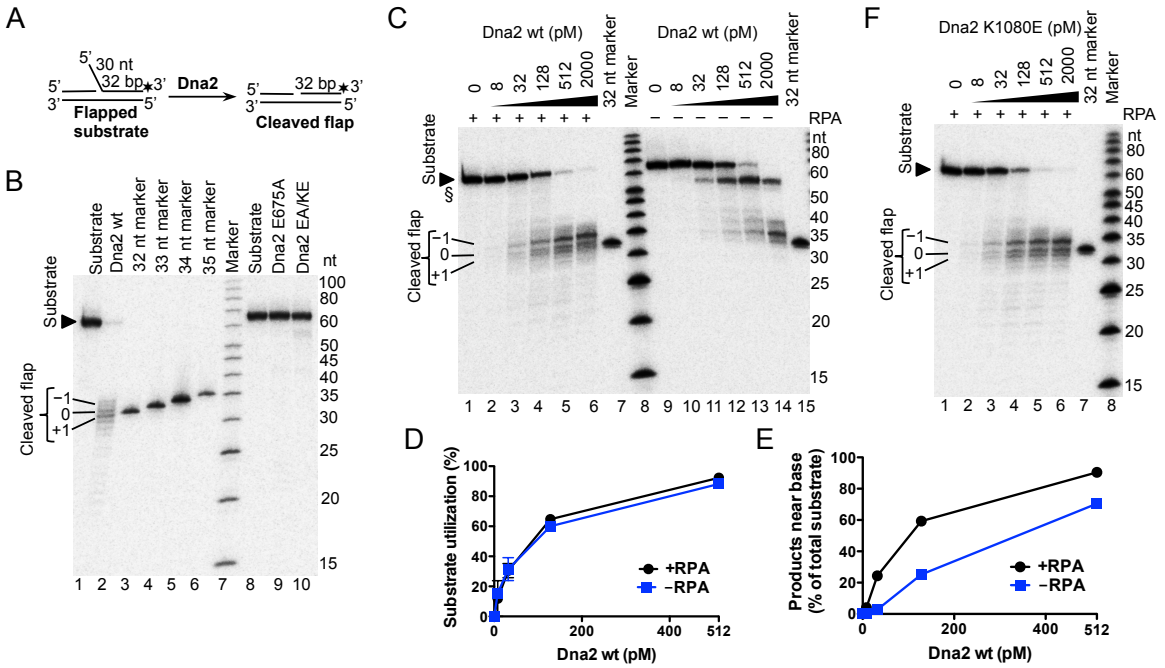
A
5' 30 nt
32 bp
3'
5'
3'
Dna2
Flapped substrate
Cleaved flap
B
Substrate
Dna2 wt
32 nt marker
33 nt marker
34 nt marker
35 nt marker
Marker
Dna2 E675A
Dna2 EA/KE
nt
Cleaved flap
−1
0
+1
1 2 3 4 5 6 7 8 9 10
C
Dna2 wt (pM)
0 8 32 128 512 2000
32 nt marker
Marker
RPA
Substrate
Cleaved flap
1 2 3 4 5 6 7 8 9 10 11 12 13 14 15
D
Substrate utilization (%)
+RPA
−RPA
Dna2 wt (pM)
E
Products near base (% of total substrate)
+RPA
−RPA
Dna2 wt (pM)
F
Dna2 K1080E (pM)
0 8 32 128 512 2000
32 nt marker
Marker
RPA
Substrate
Cleaved flap
1 2 3 4 5 6 7 8

Figure 2

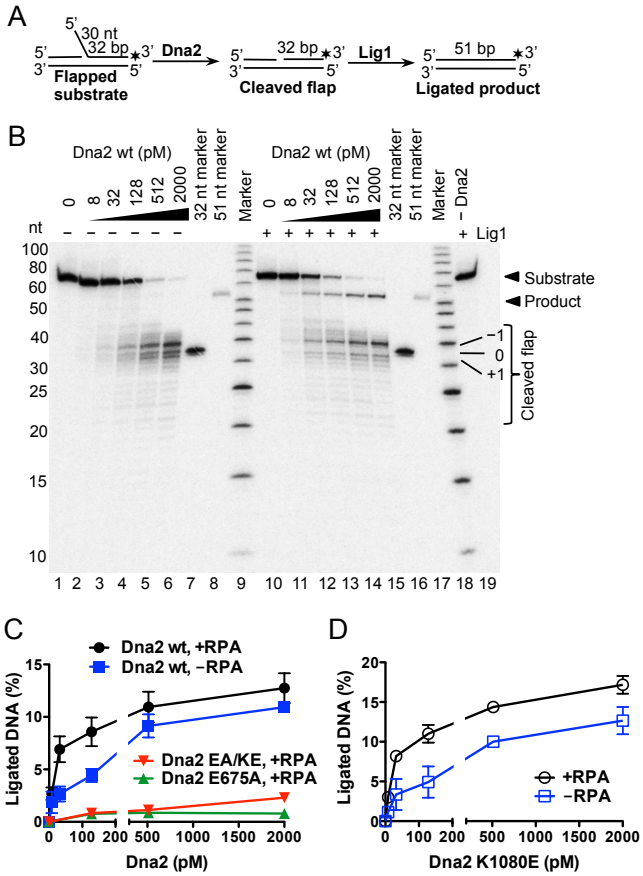
A
5'
30 nt
32 bp
3'
Dna2
5'
3'
Flapped substrate
5'
32 bp
3'
Lig1
Cleaved flap
5'
51 bp
3'
Ligated product
B
Dna2 wt (pM)
0
8
32
128
512
2000
32 nt marker
51 nt marker
Marker
nt
Dna2 wt (pM)
Marker
– Dna2
+ Lig1
Substrate
Product
−1
0
+1
Cleaved flap
100
80
60
50
40
30
25
20
15
10
1 2 3 4 5 6 7 8 9 10 11 12 13 14 15 16 17 18 19
C
Dna2 wt, +RPA
Dna2 wt, −RPA
Dna2 EA/KE, +RPA
Dna2 E675A, +RPA
Ligated DNA (%)
Dna2 (pM)
D
+RPA
−RPA
Ligated DNA (%)
Dna2 K1080E (pM)

Figure 3

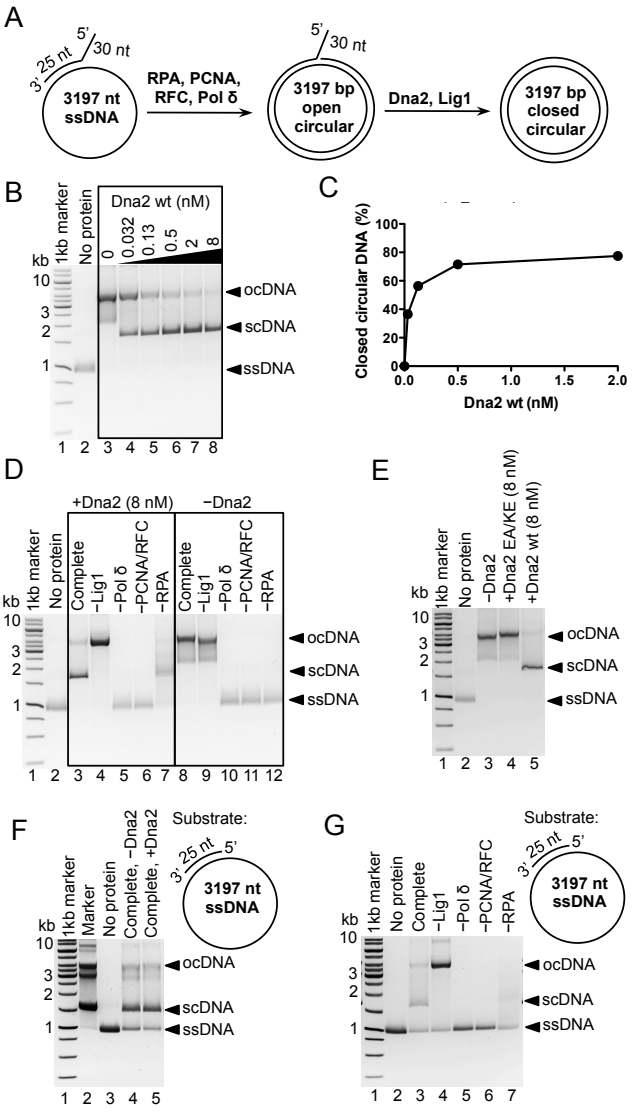
A
3' 25 nt
5'
30 nt
3197 nt ssDNA
RPA, PCNA, RFC, Pol δ
3197 bp open circular
Dna2, Lig1
3197 bp closed circular
B
Dna2 wt (nM)
0
0.032
0.13
0.5
2
8
kb
1kb marker
No protein
10
3
2
1
ocDNA
scDNA
ssDNA
1 2 3 4 5 6 7 8
C
Closed circular DNA (%)
100
80
60
40
20
0
0.0
0.5
1.0
1.5
2.0
Dna2 wt (nM)
D
+Dna2 (8 nM)
−Dna2
1kb marker
No protein
Complete
−Lig1
−Pol δ
−PCNA/RFC
−RPA
ocDNA
scDNA
ssDNA
1 2 3 4 5 6 7 8 9 10 11 12
E
1kb marker
No protein
−Dna2
+Dna2 EA/KE (8 nM)
+Dna2 wt (8 nM)
ocDNA
scDNA
ssDNA
1 2 3 4 5
F
Substrate:
3' 25 nt 5'
3197 nt ssDNA
1kb marker
Marker
No protein
Complete, −Dna2
Complete, +Dna2
ocDNA
scDNA
ssDNA
1 2 3 4 5
G
Substrate:
3' 25 nt 5'
3197 nt ssDNA
1kb marker
No protein
Complete
−Lig1
−Pol δ
−PCNA/RFC
−RPA
ocDNA
scDNA
ssDNA
1 2 3 4 5 6 7

Figure 4

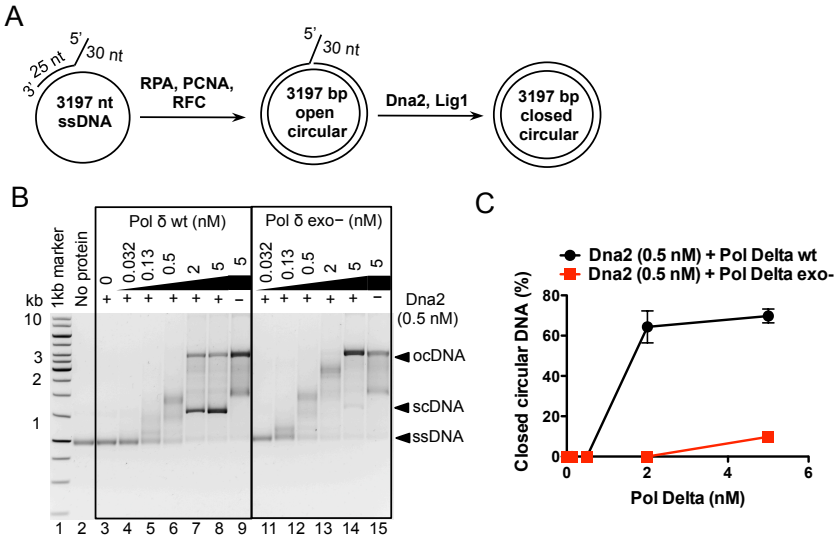
A
3' 25 nt
5' 30 nt
3197 nt ssDNA
RPA, PCNA, RFC
5' 30 nt
3197 bp open circular
Dna2, Lig1
3197 bp closed circular
B
Pol δ wt (nM)
Pol δ exo− (nM)
kb
1kb marker
No protein
0
0.032
0.13
0.5
2
5
5
Dna2 (0.5 nM)
10
3
2
1
ocDNA
scDNA
ssDNA
1 2 3 4 5 6 7 8 9 11 12 13 14 15
C
Dna2 (0.5 nM) + Pol Delta wt
Dna2 (0.5 nM) + Pol Delta exo-
Closed circular DNA (%)
80
60
40
20
0
0
2
4
6
Pol Delta (nM)

Figure 5

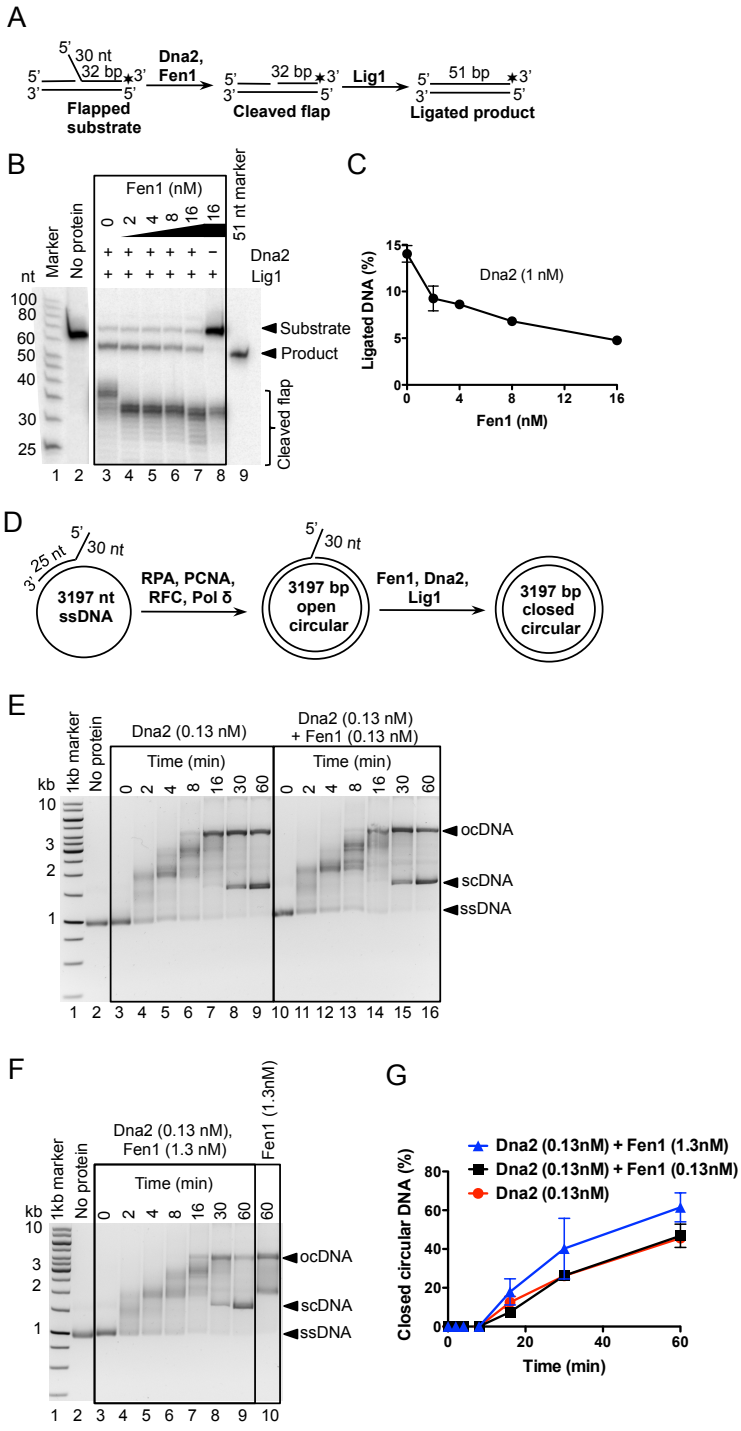
A
5' 30 nt
32 bp
3'
5'
3'
Flapped substrate
Dna2, Fen1
32 bp
Cleaved flap
Lig1
51 bp
Ligated product
B
Fen1 (nM)
0 2 4 8 16 16
51 nt marker
Marker
No protein
Dna2
Lig1
nt
100
80
60
50
40
30
25
Substrate
Product
Cleaved flap
1 2 3 4 5 6 7 8 9
C
Dna2 (1 nM)
Ligated DNA (%)
15
10
5
0
0 4 8 12 16
Fen1 (nM)
D
5' 30 nt
3' 25 nt
3197 nt ssDNA
RPA, PCNA, RFC, Pol δ
3197 bp open circular
Fen1, Dna2, Lig1
3197 bp closed circular
E
Dna2 (0.13 nM)
Dna2 (0.13 nM) + Fen1 (0.13 nM)
Time (min)
0 2 4 8 16 30 60
kb
1kb marker
No protein
10
3
2
1
ocDNA
scDNA
ssDNA
1 2 3 4 5 6 7 8 9 10 11 12 13 14 15 16
F
Dna2 (0.13 nM), Fen1 (1.3 nM)
Fen1 (1.3nM)
Time (min)
0 2 4 8 16 30 60
60
kb
1kb marker
No protein
10
3
2
1
ocDNA
scDNA
ssDNA
1 2 3 4 5 6 7 8 9 10
G
Dna2 (0.13nM) + Fen1 (1.3nM)
Dna2 (0.13nM) + Fen1 (0.13nM)
Dna2 (0.13nM)
Closed circular DNA (%)
80
60
40
20
0
0 20 40 60
Time (min)

Figure 6

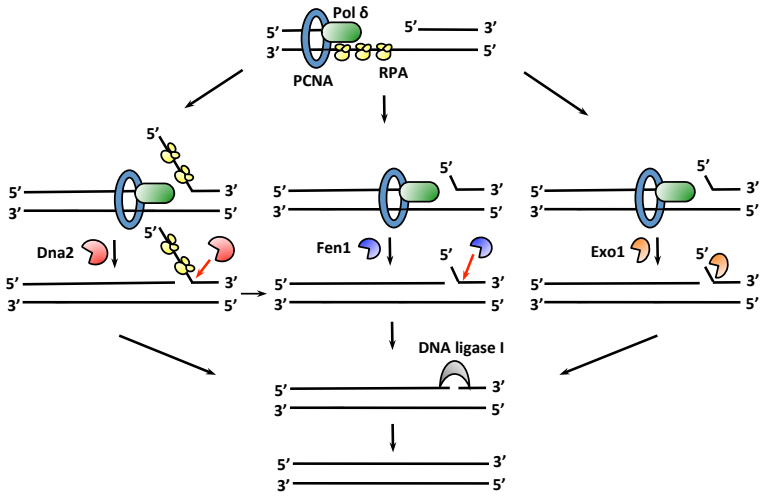

Supplementary Figure 1

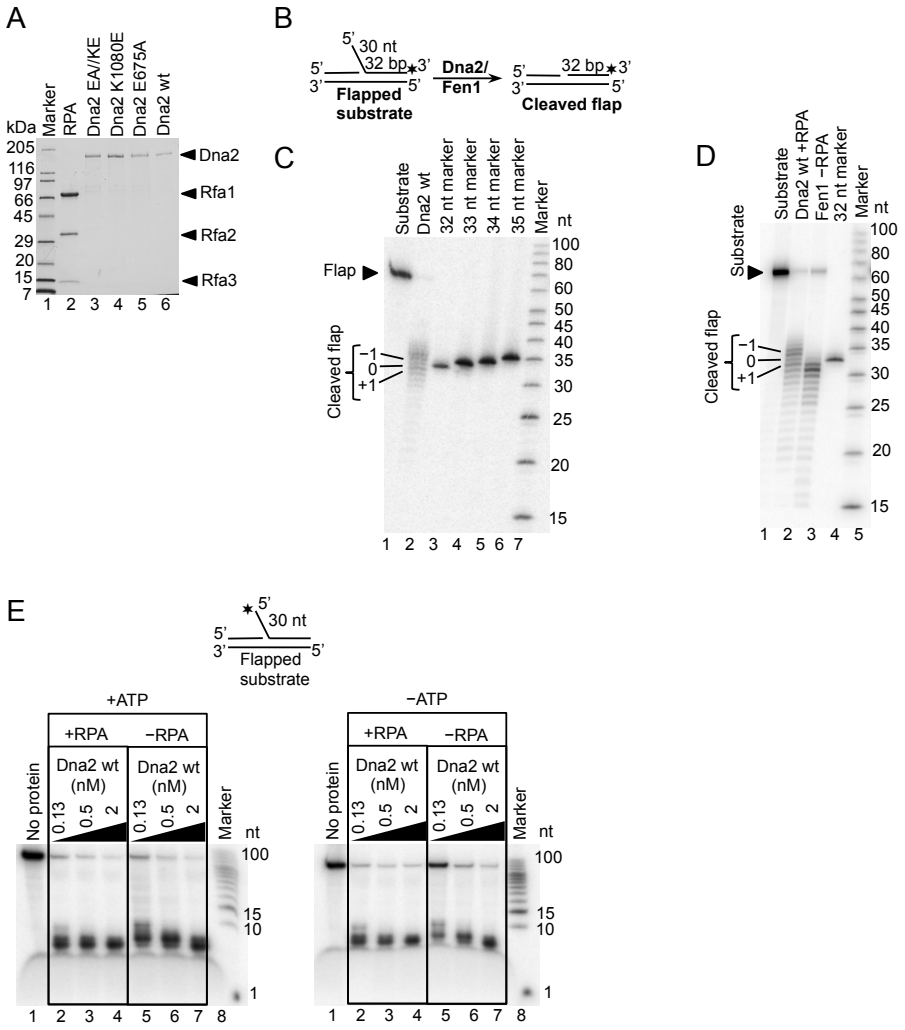

Supplementary Figure 1. Flap cleavage by Dna2 and Fen1. (**A**) Coomassie stained polyacrylamide gel showing purified wild type Dna2 (wt), Dna2 E675A (nuclease-dead variant), Dna2 K1080E (helicase-dead variant), Dna2 E675A/K1080E (EA/KE, helicase- and nuclease-dead variant) and RPA (Rfa1, Rfa2, Rfa3 subunits) used in this study. (**B**) Nuclease assay. (**C**) Experiment as in Figure 1B, but in a buffer containing 10 mM magnesium acetate. (**D**) Experiment as in (**C**) showing a comparison of Dna2 and Fen1 nuclease activities. Lane 2, Dna2 (2 nM), with RPA. Lane 3, Fen1 (8 nM), no RPA. (**E**) Experiment as in (**C**), but with a 30 nt flapped substrate where the ^{32}P label was placed at the 5' terminus of the downstream primer. Various concentrations of wt Dna2 in the absence or presence of RPA and ATP were used, as indicated.

Supplementary Figure 2

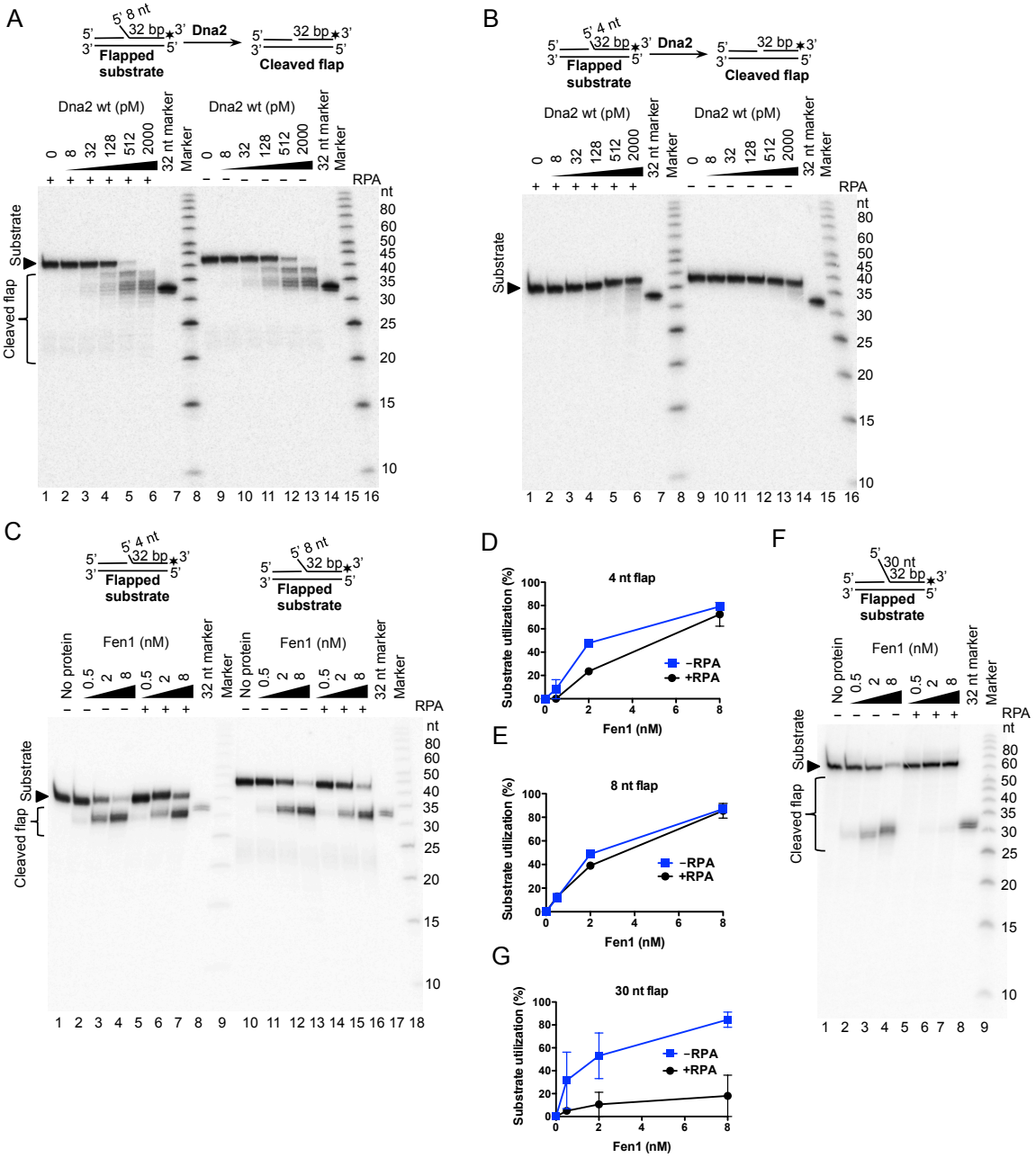

Supplementary Figure 2. Cleavage of various flapped substrates by Dna2 and Fen1. (**A**) Experiment as in Figure 1C, but with a DNA substrate containing an 8 nt-long flap. Dna2 is able to cleave flaps of 8 nt in length. (**B**) Experiment as in Figure 1C, but with a DNA substrate containing a 4 nt-long flap. Dna2 is not able to cleave short flaps of 4 nt in length. (**C**) Various concentrations of Fen1 protein were incubated with a substrate containing either a 4 nt- or 8 nt-long flap, with or without RPA, as indicated. Cleavage at the base of the flap would produce a DNA fragment of 32 nt in length. Fen1 preferentially cleaves DNA beyond the flap base within the dsDNA region. (**D**) Quantitation of 4 nt-long flapped substrate degradation by Fen1 from experiments such as in (**C**). Averages shown, n=2; error bars, s.e.m. (**E**) Quantitation of 8 nt-long flapped substrate degradation by Fen1 from experiments such as in (**C**). Averages shown, n=2; error bars, s.e.m. (**F**) Experiment as in (**C**), but with a 30 nt-long flapped substrate. (**G**) Quantitation of experiments such as in (**F**). Averages shown, n=2; error bars, s.e.m.

Supplementary Figure 3

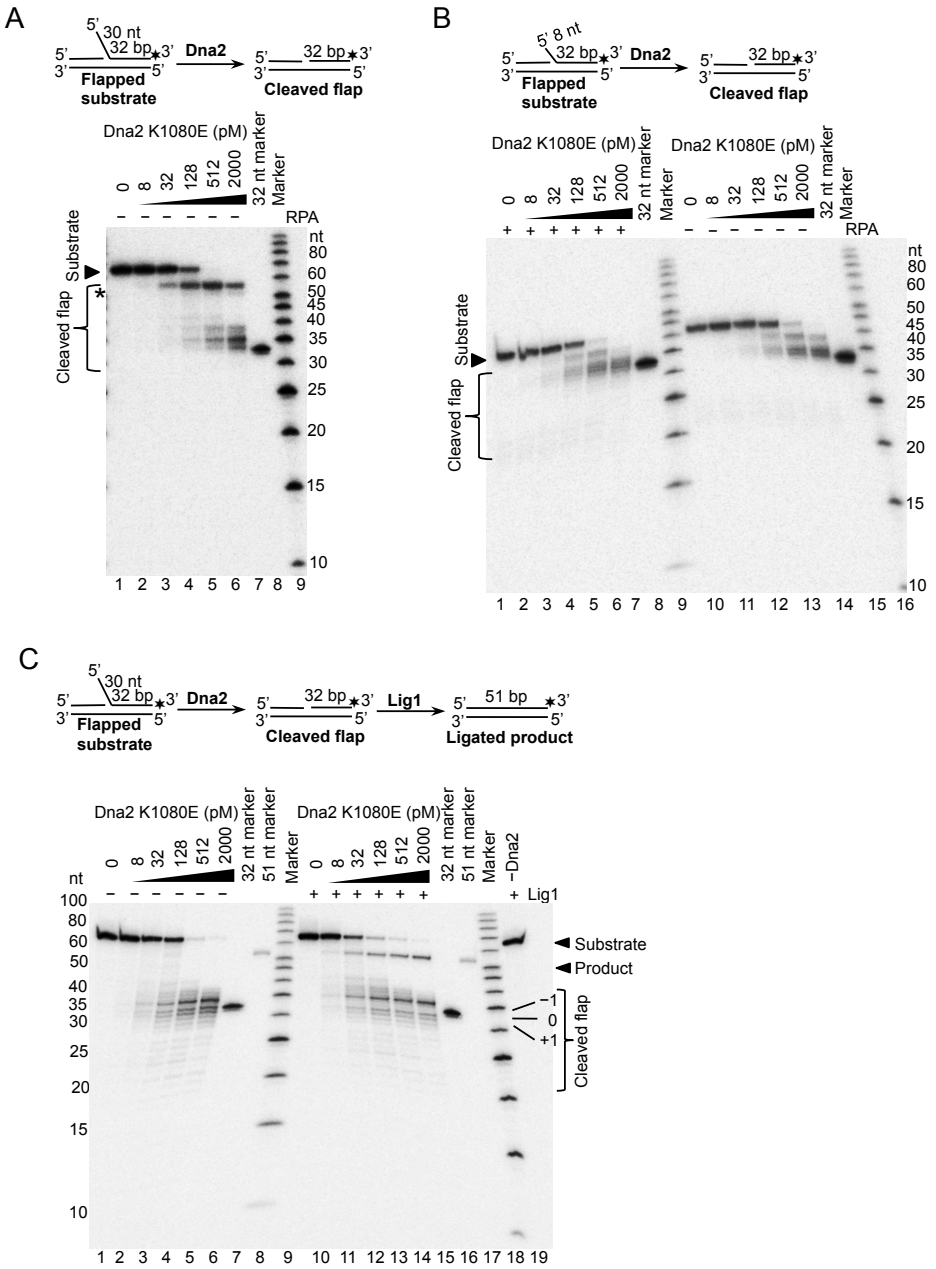

Supplementary Figure 3. Cleavage and ligation of DNA flaps by helicase-dead Dna2**.** (**A**) Experiment as in Figure 1C, but with a helicase-dead Dna2 K1080E variant, without RPA. *, Substrate cleaved by Dna2 in the absence of RPA. The helicase activity of Dna2 does not affect DNA flap cleavage. (**B**) Experiment as in Figure 1C, but with a 8 nt-long DNA flap, and helicase-dead Dna2 K1080E variant. (**C**) Experiment as in Figure 2B, but with helicase-dead Dna2 K1080E.

Supplementary figure 4

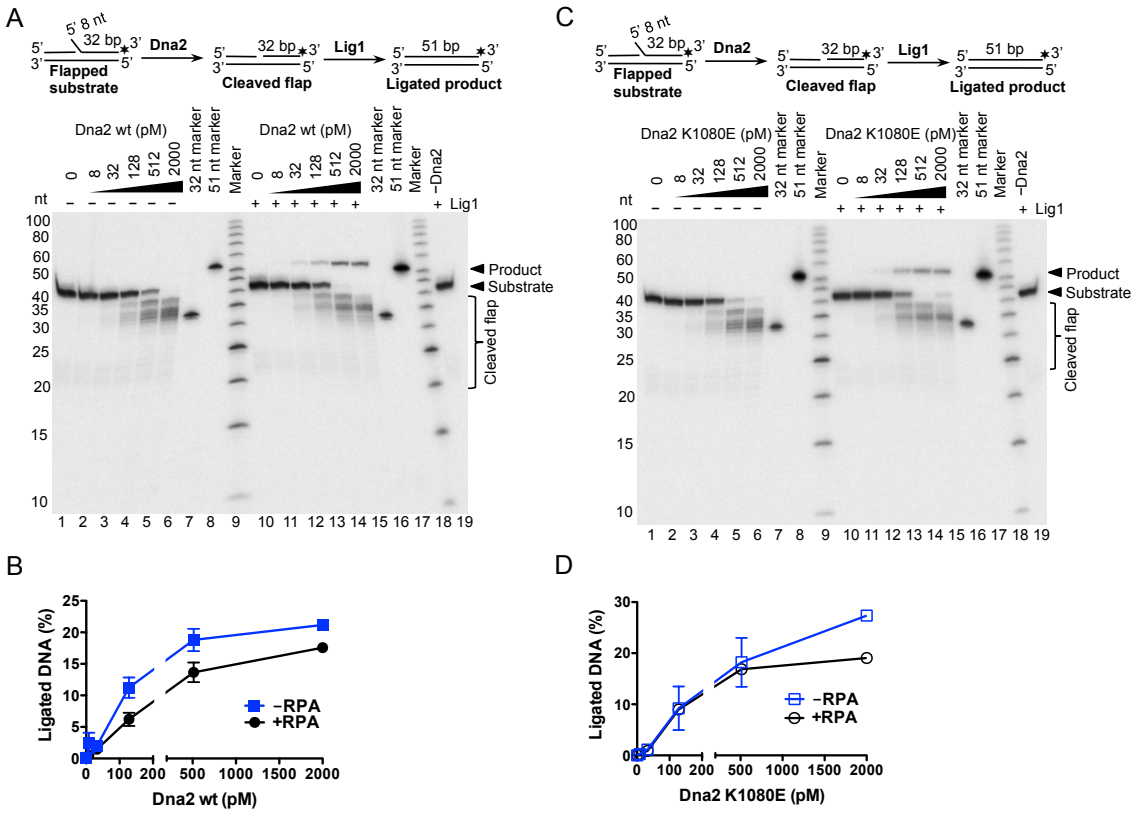

Supplementary Figure 4. Processing of 8 nt-long flaps by Dna2 and Lig1. (**A**) Experiment as in Figure 2B, but with a DNA substrate containing an 8 nt-long flap. (**B**) Quantitation of experiments such as in (**A**). Averages shown, n=2; error bars, s.e.m. (**C**) Experiment as in Figure 2B, but with a DNA substrate containing an 8 nt-long flap, and helicase-dead Dna2 K1080E. (**D**) Quantitation of experiments such as in (**C**). Averages shown, n=2; error bars, s.e.m.

Supplementary figure 5

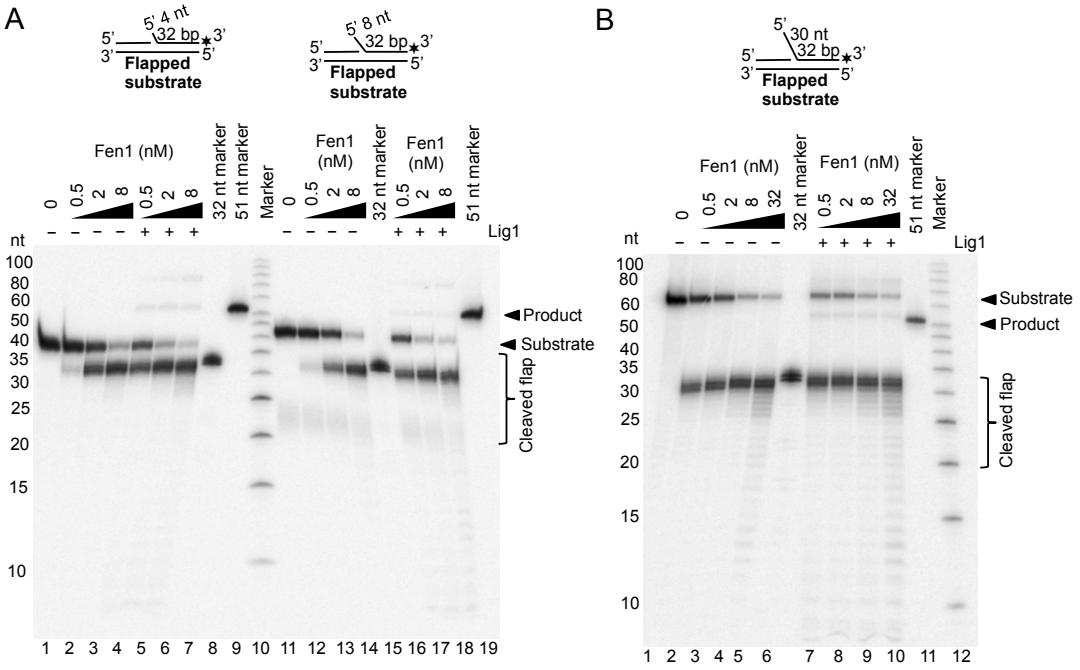

Supplementary Figure 5. Cleavage of flapped substrates by Fen1 does not efficiently produce a substrate for Lig1. (**A**) Increasing concentrations of Fen1 were incubated with a substrate containing either a 4 nt- or 8 nt-long flap with or without Lig1 in the absence of RPA. Cleavage at the base of the flap would produce a fragment of 32 nt in length. Ligation of the cleaved intermediate would result in a final product of 51 nt in length. (**B**) Experiment as in (**A**), but with a 30 nt-long flapped substrate.

Supplementary figure 6

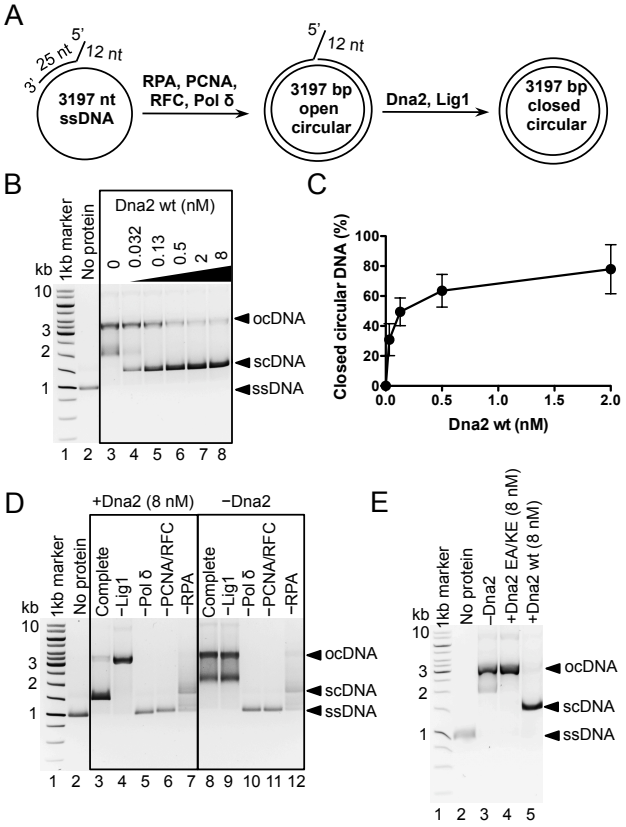

Supplementary Figure 6. Processing of 12 nt-long flaps by Dna2 during DNA replication. (**A**) Replication assay. (**B**) Experiment as in Figure 3B, but with a DNA substrate containing a 12 nt-long flap. (**C**) Quantitation of data such as in (**B**). Averages shown, n=2; error bars, s.e.m. (**D**) Pol δ, RFC, PCNA and RPA are required for DNA synthesis, Dna2 and Lig1 for the formation of scDNA product. A "complete" reaction contained all components as described in (**B**) without Dna2. Proteins were omitted from the reactions as indicated. (**E**) Nuclease activity of Dna2 is required for flap processing during replication. Nuclease- and helicase-dead Dna2 E675A/K1080E variant was used where indicated.

Supplementary figure 7

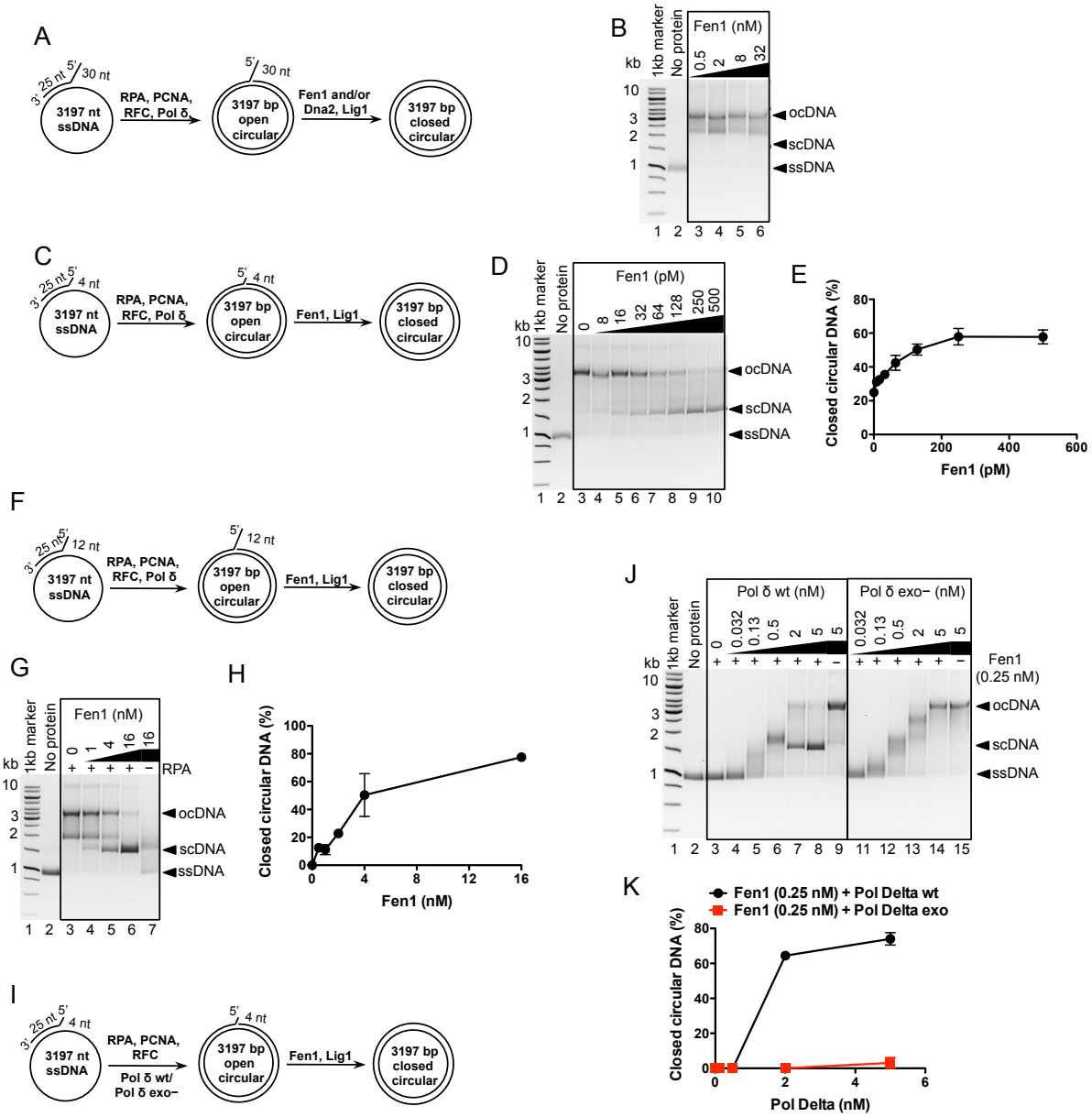

Supplementary Figure 7. Analysis of a flap endonuclease activity of Fen1 during DNA replication. (**A**) Replication assay with a 30 nt-long flapped primer. (**B**) Reactions contained pol δ, PCNA, RFC, RPA, Lig1 and Fen1 as indicated. Positions of substrate ssDNA, open circular intermediate (ocDNA) and closed circular supercoiled final product (scDNA) are indicated. Fen1 is unable to promote completion of replication. (**C**) Replication assay with a 4 nt-long flapped primer. (**D**) Same experiment as in (**B**), but with a 4 nt flapped primer. Final product appears in a Fen1 concentration-dependent manner. (**E**) Quantitation of experiments such as in (**D**). Averages shown, n=2; error bars, s.e.m. (**F**) Replication assay with a 12 nt-long flapped primer. (**G**) Same experiment as in (**B**), but with a 12 nt flapped primer. Final product appears in a Fen1 concentration-dependent manner. (**H**) Quantitation of experiments such as in (**G**). Averages shown, n=2; error bars, s.e.m. (**I**) Replication assay with a 4 nt-long flapped primer. (**J**) Experiment as in Figure 4B, but with a 4 nt flapped primer substrate and Fen1 instead of Dna2. No scDNA product is detectable with pol δ exo− and Fen1. (**K**) Quantitation of data such as in (**J**). Averages shown, n=2; error bars, s.e.m.

Supplementary figure 8

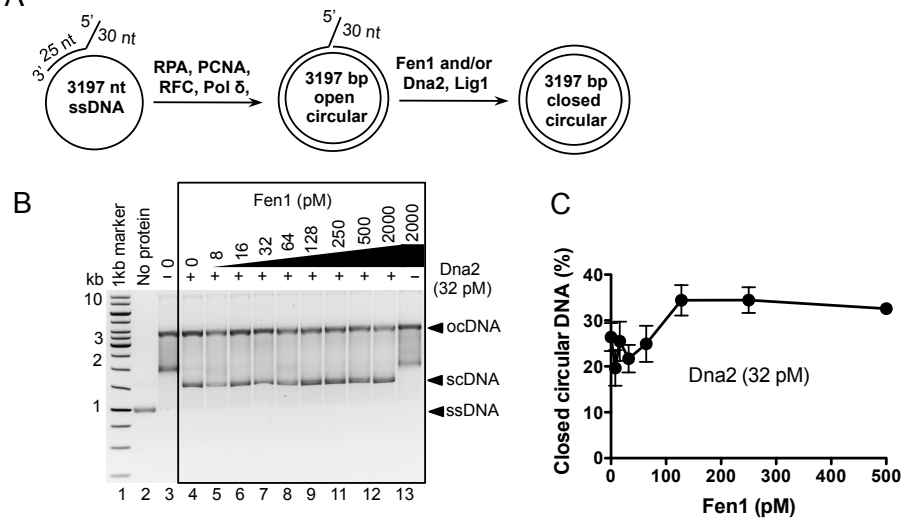

Supplementary Figure 8. Fen1 moderately promotes flap processing activity of Dna2 in some cases. (**A**) Replication assay. (**B**) Replication reactions contained pol δ, PCNA, RFC, RPA, Lig1, Dna2 and Fen1 at indicated concentrations. Positions of substrate ssDNA, open circular intermediate (ocDNA) and expected closed circular supercoiled final product (scDNA) are indicated. Addition of at least 128 nM Fen1 moderately stimulated the appearance of the scDNA product. (**C**) Quantitation of experiments such as in (**B**). Averages shown, n=2; error bars, s.e.m.

Supplementary figure 9

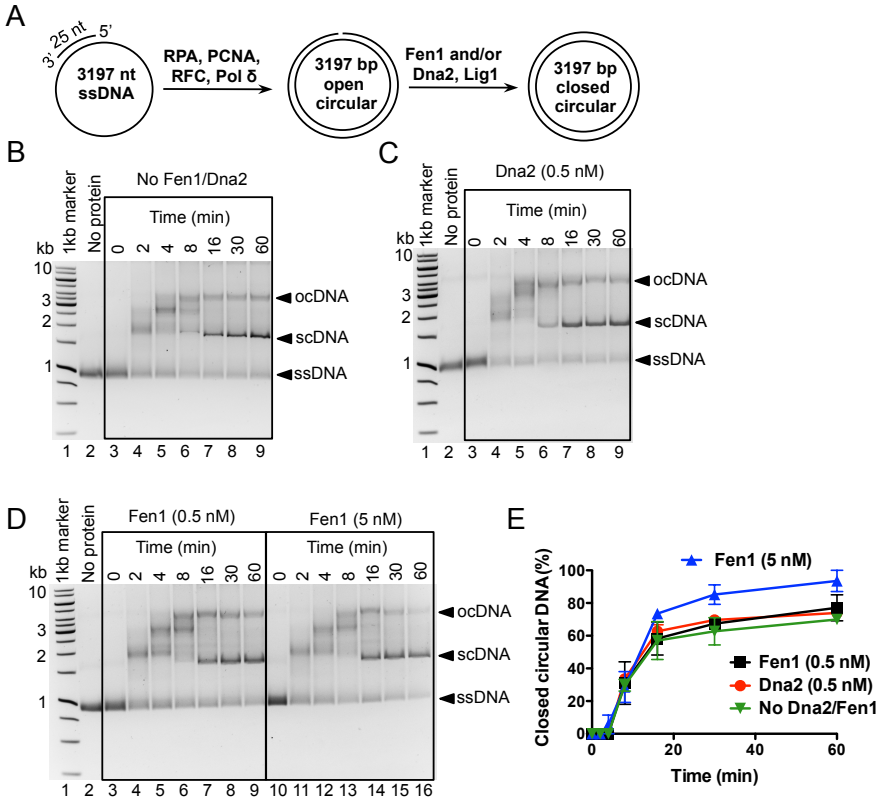

Supplementary Figure 9. Fen1 moderately promotes replication of a substrate containing a primer without a flap. (**A**) Replication assay. (**B**) Kinetic replication reactions contained pol δ, PCNA, RFC, RPA and Lig1. Positions of substrate ssDNA, open circular intermediate (ocDNA) and closed circular supercoiled final product (scDNA) are indicated on the right. Samples were terminated at various time points, as indicated. (**C**) Experiment as in (**B**), but also containing Dna2 (0.5 nM). Addition of Dna2 had not effect on the kinetics of appearance of scDNA product. (**D**) Experiment as in (**B**), but also containing Fen1 (0.5 or 5 nM). Addition of 5 nM Fen1 moderately accelerated the appearance of scDNA product. (**E**) Quantitation of experiments such in (**B**), (**C**) and (**D**). Averages shown, n=2; error bars, s.e.m.

Supplementary figure 10

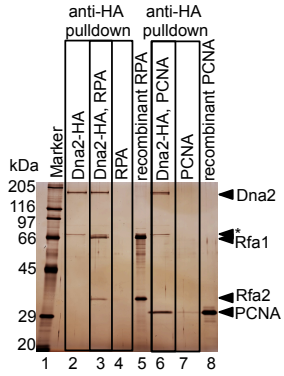

Supplementary Figure 10. Dna2 directly interacts with PCNA. Purified recombinant HA-tagged Dna2 was bound to anti-HA resin, and incubated (lanes 3 and 6) or not (lane 2) with recombinant RPA or PCNA, respectively. RPA and PCNA do not bind to anti-HA resin alone (lanes 4 and 7). Controls, recombinant RPA (80 ng, lane 5) and PCNA (20 ng, lane 8). *, degradation product of Dna2. Rfa1, Rfa2 and Rfa3 are the three subunits of RPA. Shown is a silver-stained polyacrylamide gel representative of three independent experiments.

2.2.4 The helicase activity of *S. cerevisiae* Dna2 acts as a ssDNA translocase and promotes ssDNA degradation

Maryna Levikova and Petr Cejka.

Manuscript.

I designed the research together with P.C. and performed the experiments with the help of P.C. I analyzed the data together with P.C. and wrote the manuscript.

The helicase activity of *S. cerevisiae* Dna2 acts as ssDNA translocase and promotes ssDNA degradation

Maryna Levikova and Petr Cejka

Institute of Molecular Cancer Research, University of Zurich, Winterthurerstrasse 190, 8057 Zurich, Switzerland

Key words: DNA helicase / DNA nuclease / Dna2 / ssDNA translocase / DNA resection

Address correspondence to: Petr Cejka, Institute of Molecular Cancer Research, University of Zurich, Winterthurerstrasse 190, Zurich, 8057. Phone: +41-44-635-4786; E-mail: cejka@imcr.uzh.ch

Abstract

Dna2 is an essential nuclease-helicase involved in multiple processes of DNA metabolism. During the initiation step of homologous recombination, the DNA end resection, Dna2 was shown to function together with Sgs1 to degrade 5'-teminated DNA ends. So far, the helicase activity of Dna2 was reported to be dispensable for all of its functions. We show here that efficient ssDNA degradation by the Dna2 enzyme is stimulated by its motor activity that acts as a ssDNA translocase, rather than a DNA helicase. Furthermore, RPA promotes Dna2-mediated ssDNA degradation at multiple levels. Also, in reconstituted DNA resection assays with Sgs1, Dna2 helicase promotes DNA degradation. Thus, we suggest that the motor activity of Dna2 functions as a ssDNA translocase to enhance the degradative capability of Dna2 by actively translocating on ssDNA resulting from dsDNA unwinding by Sgs1.

Introduction

DNA helicases function in all processes of DNA metabolism that require strand-separation of duplex DNA. The majority of these enzymes unwind nucleic acids with either 3' to 5' or 5' to 3' polarity by coupling ATP hydrolysis to translocation on ssDNA (1). However, it is not yet clear whether dsDNA unwinding by helicases is only a "byproduct" of their translocation on ssDNA, or whether it is an additional process. Furthermore, structurally similar enzymes were described, termed DNA translocases, that employ their ATPase activity only for the motion along DNA without the unwinding reaction (2). Hence, the difference between DNA helicases and ssDNA translocases is not completely clarified.

Dna2 is an essential enzyme that possesses a RecB family nuclease domain and a helicase activity provided by superfamily II helicase domain (3-5). The helicase of Dna2 has a 5' to 3' polarity and is stimulated by replication protein A (RPA), while the nuclease can act in both directions, although in presence of RPA DNA degradation by Dna2 is inhibited in the 3' to 5' direction (6,7), so Dna2 likely degrades DNA 5' to 3' under physiological conditions. However, although the helicase activity of Dna2 was recently shown to be very strong and processive, it is still masked by the nuclease of the wild type protein (7). The nuclease activity of Dna2 is essential, while the helicase mutants (*dna2-2*) are viable, but exhibit growth defects and sensitivity to alkylating agents and ionizing radiation (8,9).

S. cerevisiae Sgs1 contains a superfamily II helicase domain with a 3' to 5' polarity and is a RecQ helicase (10-12). It forms a complex with Top3 and Rmi1 proteins (13,14). Sgs1 was shown to be involved in homologous recombination (HR) pathway at different steps: during initial DNA end resection and later, in the double Holliday junction dissolution pathway (6,15-18). The DNA end resection is carried out by Sgs1-Top3-Rmi1 complex in conjunction with Dna2 and RPA: Sgs1 unwinds the DNA and Dna2 degrades the 5'-terminated strand, thus producing RPA-covered 3' single-stranded overhangs that are required for downstream steps of HR (6,18,19). However, only the nuclease activity of Dna2 was shown to be required for this function *in vivo*, although the study was carried out by ectopically overexpressing Dna2 helicase-

dead variant, thus possibly masking potential effects (18). Interestingly, *sgs1Δ dna2-2* double mutants were more sensitive to ionizing radiation than the single mutants, indicating that Sgs1 activity is required in absence of Dna2 helicase (8). Moreover, a recent study uncovered that Dna2 and Sgs1 cooperate in another DNA repair pathway, namely during restart of reversed DNA replication forks by most likely degrading the reversed arm. Again, the helicase of Dna2 was shown to be dispensable for this activity (20). These findings raised the question why Dna2 evolved such a potent helicase activity, which is comparable to that of Sgs1 (7), without any implications *in vivo*. One possible hypothesis originates from studies of the nuclease-helicase RecBCD complex in bacteria. RecB has a 3' to 5' helicase and a nuclease activity, while the faster RecD translocates on the opposite strand with 5' to 3' polarity, thus coordinating two helicase and one nuclease activity within a functional unit, similar to Sgs1-Dna2. Upon encountering the Chi (crossover hotspot instigator) sequence RecB becomes the lead motor and degrades preferentially only the 5'-terminated strand. The helicase activities within RecBCD are highly coordinated: the RecBCD complex can clearly carry out functions that exceed the sum of its parts (21). So, we decided to test whether there is any similar coordination between Sgs1 and Dna2 activities as well.

Here we report that the motor activity within the wild type Dna2 protein greatly stimulates ssDNA degradation by acting as a ssDNA translocase. The nucleolytic degradation capacity of Dna2 is strongly dependent on the presence of RPA and ATP. In *in vitro* reconstituted resection assays, wild type Dna2 is more efficient than the helicase-dead variant, suggesting that the helicase activity of Dna2 promotes DNA end resection.

Results

Helicase activity of wild type Dna2 promotes efficient ssDNA degradation

Previously, we have shown that our Dna2 preparations exhibit strong nuclease and helicase activities (7). In Figure 1A, we confirm that wild type and helicase-dead Dna2 efficiently degrade a Y-structure substrate, while nuclease-dead Dna2 unwinds

it. In agreement with previous results (7), no helicase activity of wt Dna2 is detectable when using this substrate with 5' labeled top oligonucleotide and we did not observe any difference in DNA cleavage when comparing wt Dna2 and helicase-dead variant (Fig. 1A, left and middle panel). We hypothesized that the helicase activity might become more crucial when using longer ssDNA substrates mimicking the resection situation *in vivo,* when multiple thousands of nucleotides are resected. Next, we explored the degradation of ssDNA fragments of various lengths (between 0.1 and 23 kb) by wt Dna2 compared to helicase-dead Dna2 K1080E variant in a kinetic setup (Fig. 1B). Surprisingly, we observed that wild type Dna2 was multiple folds faster in degradation of all ssDNA fragments than the helicase-dead Dna2 K1080E (Fig. 2B left compared to right part). After 4 minutes almost all fragments were degraded by wt Dna2, while Dna2 K1080E needed 16 minutes (Fig. 1B, compare lanes 5 and 16). Taken together, these results let us conclude that the helicase activity of Dna2 strongly promotes degradation of long stretches of ssDNA.

Dna2 can act as an endonuclease on circular plasmid DNA only in absence of RPA

Next, we wondered whether the fast ssDNA degradation by wild type Dna2 might be achieved through its endonucleolytic activity, as e.g. human DNA2 was shown to cleave telomeric G4 quadruplex structures endonucleolytically (22). We set out to test this by using circular plasmid ssDNA and dsDNA substrates (Figure 2). In presence of RPA no endonuclease activity was observed on circular ssDNA substrate with wild type Dna2 and its variants in both, magnesium- and manganese-containing buffer (Figure 2AB). However, if RPA was omitted from the reactions, wild type and helicase-Dna2 were able to cleave ssDNA endonucleolytically, while nuclease-dead Dna2 E675A was not, showing that the activity was specific for Dna2 (Figure 2AB). Finally, Dna2 was not able to cleave circular dsDNA (Figure 2C). Altogether, these experiments show that Dna2 cannot cleave DNA endonucleolytically in presence of RPA, which the physiological condition in most cases. Thus, the observed efficient ssDNA degradation by Dna2 was not stimulated by its endonucleolytic activity and the enzyme had to initiate the cleavage from the free DNA end, as described previously (23).

ssDNA translocase activity of Dna2 stimulates degradation of long DNA

Next, we investigated what is the length of ssDNA products generated by Dna2. To be able to monitor the length distribution of DNA fragments processed by Dna2 we generated a randomly ^{32}P labeled 2.2 kbp-long substrate by PCR (see Materials and Methods for details). This substrate was heated to yield 2200 nt-long ssDNA, incubated with wt Dna2 and K1080E variant in a kinetic experiment. Products were separated on an agarose gel (Fig. 3A). Wild type Dna2 was again more efficient in DNA degradation than the helicase-dead protein (Fig. 3A, compare 4 min time points). Moreover, we observed an additional band appearing above the degradation product "cloud" produced by Dna2 wt, but not by Dna2 K1080E (Fig. 3A, lanes 3-6), indicating that the product lengths might be different. To better resolve these species the same reactions were separated on denaturing 20% polyacrylamide urea gels (Fig. 3B). The cleavage pattern produced by Dna2 wt contained fragments ranging from 5 to 100 nt in length, appearing as a smear on the gel (Fig. 3B, left panel). In contrast, Dna2 K1080E was less efficient in DNA degradation and yielded fragments only between 5 and 12 nt in length (Fig. 3B and D). Image analysis of fragment distribution revealed that Dna2 wt first produces an 80 nt-long DNA product that is subsequently degraded to 5-12 nt-long pieces (Fig. 3C left panel and Fig. 3E), while ssDNA degradation by Dna2 K1080E only results in fragments of 5-12 nt in length (Fig. 3 right panel and Fig. 3E). These observations suggested that the ATP-dependent Dna2 motor activity acts as a ssDNA translocase to promote efficient ssDNA degradation. This hypothesis is further supported by the fact that in absence of ATP the cleavage pattern produced by wt Dna2 is indistinguishable from that of Dna2 K1080E (Fig. 3F).

RPA strongly promotes fast ssDNA degradation by Dna2

RPA was shown to specifically interact with Dna2 and to stimulate both its nuclease and helicase activities, especially when the enzyme acted on long DNA substrates (6,7,24). To test the contribution of RPA to ssDNA degradation by wild type Dna2 we carried out experiments using the randomly labeled PCR-based ssDNA substrate in the presence and absence of RPA (Fig. 4A-C). Without RPA, the degradation of DNA was slower. Furthermore, both wild type and helicase-dead Dna2 were comparable

in their capacity to degrade ssDNA (Fig. 3A and B). Remarkably, in reactions without RPA (but with ATP) wt Dna2 degraded DNA in a way reminiscent of the Dna2 K1080E variant (Fig. 4A and C). This means that RPA stimulates the ssDNA translocase activity of Dna2, which is in agreement with previously published observations of RPA promoting Dna2 helicase and ATPase activities (7).

Next, as we knew that Dna2 has to start DNA degradation from the free end, we investigated how the size of the initially cleaved ssDNA product is influenced by both RPA and the helicase activity of Dna2. For this purpose we used a 93 nt-long DNA substrate labeled at the 5' end and monitored Dna2-mediated cleavage by separating the products on denaturing urea gels (Fig. 4D-F). Cleavage by wild type Dna2 in presence of RPA led to the appearance of two species: the already known fragment between 5 and 12 nt in length and a smaller amount of longer products showing as a smear, especially at earlier time points (Fig. 4D, left gel; see lanes 2-5 for longer products). However, without RPA the DNA degradation was very inefficient resulting only in a small amount of products between 8 and 100 nt at later time points (Fig. 4D and F, right gels), suggesting that RPA additionally promotes efficient recruitment of Dna2 to the substrate, in agreement with previously published data (24). Finally, when the helicase activity of Dna2 was compromised either by absence of ATP (Fig. 4E) or in a helicase-dead Dna2 variant (Fig. 4F, left part), only 5-12 nt-long fragments showed on the gel, but not the longer products that were visible with the wild type protein, supporting the notion that Dna2 motor function acts as a translocase to promote degradation of ssDNA. These data led us to the model showed in Figure 3G. For fast ssDNA degradation, initiated by cuts that are approximately 80 nt apart from each other, Dna2 requires its ATP-dependent helicase/translocase activity and the presence of RPA. If the motor activity is compromised by mutation or absence of ATP, or RPA is omitted, the DNA cleavage is slow and the cuts are close to each other. RPA might play here two distinct roles: it stimulates Dna2 recruitment to the substrate, but it also promotes efficient translocation of Dna2 on ssDNA and substrate cleavage.

Resection by Sgs1 and Dna2 is stimulated by Dna2 helicase

Dna2 was shown to function together with Sgs1 in the resection of DNA breaks (6,18). To test whether the helicase activity also exhibits its stimulatory effect when Dna2 is coupled to Sgs1 we performed an *in vitro* resection assay with a 2.7 kbp-long substrate (Fig. 5A and B). Wild type Dna2 was ≈2-fold more efficient in DNA resection with Sgs1 than the helicase-dead Dna2 K1080E (Fig. 5A and B). We then wanted to monitor the length of produced DNA products by using the randomly labeled PCR-based substrate as a blunt-ended dsDNA in a kinetic resection experiment (Fig. 5C). Moreover, in this assay we also included other components of the resection machinery: Top3-Rmi1 and Mre11-Rad50-Xrs2 (6,10,14,18). Although no difference in resection speed between reactions containing Dna2 wt and K1080E variant were detected (Fig. 4C), we observed the appearance of larger DNA fragments with Dna2 wild type protein inherent to its translocase activity (Fig. 5C left gel), despite being less pronounced than previously seen in Figure 2B. Those results can be explained by the fact that the substrate is blunt-ended and MRX cannot initiate the resection properly without the stimulation of its endonuclease activity by Sae2 and a protein block at the DNA end, as it was shown previously (25). Nevertheless, collectively these observations imply that the helicase activity of Dna2 also contributes to more efficient resection together with Sgs1.

Discussion

Dna2 is involved in several key processes of DNA metabolism, including DNA repair by homologous recombination and DNA replication (6,20,26,27). So far, primarily the nuclease activity of Dna2 was implicated to be important to carry out these functions ((18,20) and (30)-Levikova and Cejka, NAR 2015, in press). However, in our recent study we were able to show that Dna2 is a very strong helicase and its activity is comparable to that of Sgs1 (7). In Figure 1 we demonstrate that the helicase activity of wild type Dna2 greatly promotes ssDNA degradation. We show then that DNA degradation was not due to the endonucleolase activity of Dna2, confirming that the enzyme needs a free end to engage (Figure 2). Furthermore, we show that efficient

nucleolytic activity of Dna2 is dependent on its ATP-mediated ssDNA translocase activity and the presence of RPA (Fig. 3 and 4). RPA appears to promote ssDNA degradation in two various ways: by enhanced Dna2 recruitment and by stimulating its translocase activity (Fig. 4). Our data indicate that in absence of RPA Dna2 is inefficient in DNA degradation and translocation, as well as that it is capable of endonucleolytic cleavage. A recent study reported a genome-wide DNA replication fork breakage upon RPA exhaustion in ATR-deficient cells (28). Some of the effects described in this study might be thus attributable to altered Dna2 activity in absence of RPA. Our *in vitro* resection assays indicate that Dna2 helicase activity promotes DNA end degradation in conjunction with Sgs1 (Fig. 5). Considering that Dna2 and Sgs1 helicase activities are comparably strong (7), we think that in DNA resection pathway Sgs1 might be the lead helicase, similar to RecB in bacteria, unwinding dsDNA, while the motor activity of Dna2 acts as an efficient ssDNA translocase, rather than a helicase, thus helping to keep up with Sgs1. In contrast to RecBCD, the nuclease activity is associated with Dna2, which is the 5' to 3' translocating enzyme. The notion that Dna2 helicase activity is contributing to efficient DNA end resection is in agreement with genetic experiments with *dna2-2* (helicase-dead) budding yeast strains showing increased sensitivity to alkylating agents and ionizing radiation, treatments that also induce DNA double-strand breaks (8,9). Interestingly, *dna2-2* cells show a slight increase in telomere length (9), which is indicative of more roles for Dna2 helicase activity in DNA metabolism that need to be further investigated.

Materials and Methods

Recombinant proteins

Wild type Dna2 as well Dna2 E675A and Dna2 K1080E variants were expressed from a modified pGAL:DNA2 vector (4) and were purified as described previously (7). Sgs1, Top3-Rmi1 and Mre11-Top3-Rmi1 were expressed and purified as described previously (6,16,25). RPA protein was expressed and purified as described (29).

DNA substrates

The oligonucleotides X12-3 and X12-4NC were used for the preparation of the Y-structure DNA substrate (7,16), and the oligonucleotide X12-3 TOPL (20) - for the preparation of 93 nt-long ssDNA. The oligonucleotides were ^{32}P-labeled at the 5' terminus with [gamma-^{32}P] ATP and T4 polynucleotide kinase (New England Biolabs) according to manufacturer instructions. Unincorporated nucleotides were removed using MicroSpin G25 columns (GE Healthcare) before annealing of the substrates.

pUC19 dsDNA was linearized with HindIII and purified by phenol-chloroform extraction and ethanol precipitation. Bacteriophage λ dsDNA digested by HindIII was purchased from New England Biolabs. The linearized dsDNA was then 3'-labeled with [alpha-^{32}P] dATP and Klenow fragment of DNA polymerase I (New England Biolabs). Unincorporated nucleotides were removed using MicroSpin G25 columns (GE Healthcare). Circular single-stranded and double-stranded 6.4 kb-long plasmid DNA was derived from bacteriophage M13 and purchase from New England Biolabs.

The randomly labeled 2200 nt-long substrate was prepared by amplification of the yeast DNA Ligase I gene by PCR from yeast genomic DNA using the following primers: forward: 5' ACGCATTAGCTAGCGGATCCCTGGAAGTTCTGTTCCAGGGGCCCATGCG-CAGATTACTGACCGGTTG 3'; reverse: 5' ACGCATTACTCGAGATTTTGCATGTGG-GATTGGT 3'. In addition to the standard dNTP concentration in the PCR reaction (200 nM each), [alpha-^{32}P] dATP (60nM) was added. The PCR reaction was purified using Chroma Spin TE-400 columns (Clontech).

Nuclease and helicase assays

The experiments were performed in a 15-µl volume in 25 mM Tris-acetate (pH 7.5), 2 mM magnesium acetate (if not indicated otherwise), 1 mM ATP, 1 mM dithiothreitol, 0.1 mg/ml BSA (New England Biolabs), 1 mM phosphoenolpyruvate, 16 U/ml pyruvate kinase and 1 nM DNA substrate, unless indicated otherwise. RPA was included into the reactions, where indicated, at a concentration saturating all ssDNA to 300% for oligonucleotide-based substrates and to 150% for longer substrates, assuming a 20 nt-long binding site for RPA. Recombinant proteins were added at indicated concentrations. The reactions were incubated at 30 °C for 30 min, if not indicated otherwise. Reactions were either stopped by adding 5 µl 2% stop solution and

separated on an agarose gels, as described previously (16), or they were stopped by adding 15 µl formamide dye (95% (v/v) formamide, 20 mM EDTA, 0.01% bromophenol blue), heated at 95°C for 4 min and separated on 20 % denaturing polyacrylamide gels (ratio acrylamide:bisacrylamide 19:1, Biorad). After fixing in a solution containing 40% methanol, 10% acetic acid and 5% glycerol for 30 min, the gels were dried on DE81 chromatography paper (Whatman), and exposed to storage phosphor screens (GE Healthcare). The screens were scanned by Typhoon phosphor imager (GE Healthcare).

Acknowledgements

This work has been supported by Swiss National Science Foundation Professorship PP00P3 133636 for P.C. We would like to thank Judith Campbell (Caltech, USA) for the Dna2 expression construct.

Author contribution: P.C. and M.L. conceived the general idea of the study, M.L. and P.C. carried out the experiments and M.L. wrote the manuscript.

Conflict of interest

The authors declare no conflict of interest.

References:

1. Wu, L. and Hickson, I.D. (2006) DNA helicases required for homologous recombination and repair of damaged replication forks. *Annu Rev Genet*, **40**, 279-306.
2. Huang, C., Sloan, E.A. and Boerkoel, C.F. (2003) Chromatin remodeling and human disease. *Curr Opin Genet Dev*, **13**, 246-252.
3. Bae, S.H., Choi, E., Lee, K.H., Park, J.S., Lee, S.H. and Seo, Y.S. (1998) Dna2 of Saccharomyces cerevisiae possesses a single-stranded DNA-specific endonuclease activity that is able to act on double-stranded DNA in the presence of ATP. *J Biol Chem*, **273**, 26880-26890.
4. Budd, M.E., Choe, W. and Campbell, J.L. (2000) The nuclease activity of the yeast DNA2 protein, which is related to the RecB-like nucleases, is essential in vivo. *J Biol Chem*, **275**, 16518-16529.

5. Budd, M.E., Choe, W.C. and Campbell, J.L. (1995) DNA2 encodes a DNA helicase essential for replication of eukaryotic chromosomes. *J Biol Chem*, **270**, 26766-26769.
6. Cejka, P., Cannavo, E., Polaczek, P., Masuda-Sasa, T., Pokharel, S., Campbell, J.L. and Kowalczykowski, S.C. (2010) DNA end resection by Dna2-Sgs1-RPA and its stimulation by Top3-Rmi1 and Mre11-Rad50-Xrs2. *Nature*, **467**, 112-116.
7. Levikova, M., Klaue, D., Seidel, R. and Cejka, P. (2013) Nuclease activity of Saccharomyces cerevisiae Dna2 inhibits its potent DNA helicase activity. *Proc Natl Acad Sci U S A*, **110**, E1992-2001.
8. Budd, M.E. and Campbell, J.L. (2000) The pattern of sensitivity of yeast dna2 mutants to DNA damaging agents suggests a role in DSB and postreplication repair pathways. *Mutat Res*, **459**, 173-186.
9. Formosa, T. and Nittis, T. (1999) Dna2 mutants reveal interactions with Dna polymerase alpha and Ctf4, a Pol alpha accessory factor, and show that full Dna2 helicase activity is not essential for growth. *Genetics*, **151**, 1459-1470.
10. Bennett, R.J., Sharp, J.A. and Wang, J.C. (1998) Purification and characterization of the Sgs1 DNA helicase activity of Saccharomyces cerevisiae. *J Biol Chem*, **273**, 9644-9650.
11. Gangloff, S., McDonald, J.P., Bendixen, C., Arthur, L. and Rothstein, R. (1994) The yeast type I topoisomerase Top3 interacts with Sgs1, a DNA helicase homolog: a potential eukaryotic reverse gyrase. *Mol Cell Biol*, **14**, 8391-8398.
12. Watt, P.M., Louis, E.J., Borts, R.H. and Hickson, I.D. (1995) Sgs1: a eukaryotic homolog of E. coli RecQ that interacts with topoisomerase II in vivo and is required for faithful chromosome segregation. *Cell*, **81**, 253-260.
13. Bennett, R.J., Noirot-Gros, M.F. and Wang, J.C. (2000) Interaction between yeast sgs1 helicase and DNA topoisomerase III. *J Biol Chem*, **275**, 26898-26905.
14. Mullen, J.R., Nallaseth, F.S., Lan, Y.Q., Slagle, C.E. and Brill, S.J. (2005) Yeast Rmi1/Nce4 controls genome stability as a subunit of the Sgs1-Top3 complex. *Mol Cell Biol*, **25**, 4476-4487.
15. Bizard, A.H. and Hickson, I.D. (2014) The dissolution of double Holliday junctions. *Cold Spring Harb Perspect Biol*, **6**, a016477.
16. Cejka, P. and Kowalczykowski, S.C. (2010) The full-length Saccharomyces cerevisiae Sgs1 protein is a vigorous DNA helicase that preferentially unwinds holliday junctions. *J Biol Chem*, **285**, 8290-8301.
17. Cejka, P., Plank, J.L., Dombrowski, C.C. and Kowalczykowski, S.C. (2012) Decatenation of DNA by the S. cerevisiae Sgs1-Top3-Rmi1 and RPA complex: a mechanism for disentangling chromosomes. *Mol Cell*, **47**, 886-896.
18. Zhu, Z., Chung, W.H., Shim, E.Y., Lee, S.E. and Ira, G. (2008) Sgs1 helicase and two nucleases Dna2 and Exo1 resect DNA double-strand break ends. *Cell*, **134**, 981-994.
19. Niu, H., Chung, W.H., Zhu, Z., Kwon, Y., Zhao, W., Chi, P., Prakash, R., Seong, C., Liu, D., Lu, L. *et al.* (2010) Mechanism of the ATP-dependent DNA end-resection machinery from Saccharomyces cerevisiae. *Nature*, **467**, 108-111.
20. Thangavel, S., Berti, M., Levikova, M., Pinto, C., Gomathinayagam, S., Vujanovic, M., Zellweger, R., Moore, H., Lee, E.H., Hendrickson, E.A. *et al.*

(2015) DNA2 drives processing and restart of reversed replication forks in human cells. *J Cell Biol*, **208**, 545-562.
21. Dillingham, M.S. and Kowalczykowski, S.C. (2008) RecBCD enzyme and the repair of double-stranded DNA breaks. *Microbiol Mol Biol Rev*, **72**, 642-671, Table of Contents.
22. Lin, W., Sampathi, S., Dai, H., Liu, C., Zhou, M., Hu, J., Huang, Q., Campbell, J., Shin-Ya, K., Zheng, L. *et al.* (2013) Mammalian DNA2 helicase/nuclease cleaves G-quadruplex DNA and is required for telomere integrity. *Embo J*, **32**, 1425-1439.
23. Kao, H.I., Campbell, J.L. and Bambara, R.A. (2004) Dna2p helicase/nuclease is a tracking protein, like FEN1, for flap cleavage during Okazaki fragment maturation. *J Biol Chem*, **279**, 50840-50849.
24. Bae, K.H., Kim, H.S., Bae, S.H., Kang, H.Y., Brill, S. and Seo, Y.S. (2003) Bimodal interaction between replication-protein A and Dna2 is critical for Dna2 function both in vivo and in vitro. *Nucleic Acids Res*, **31**, 3006-3015.
25. Cannavo, E. and Cejka, P. (2014) Sae2 promotes dsDNA endonuclease activity within Mre11-Rad50-Xrs2 to resect DNA breaks. *Nature*, **514**, 122-125.
26. Bae, S.H., Bae, K.H., Kim, J.A. and Seo, Y.S. (2001) RPA governs endonuclease switching during processing of Okazaki fragments in eukaryotes. *Nature*, **412**, 456-461.
27. Wanrooij, P.H. and Burgers, P.M. (2015) Yet another job for Dna2: Checkpoint activation. *DNA Repair (Amst)*.
28. Toledo, L.I., Altmeyer, M., Rask, M.B., Lukas, C., Larsen, D.H., Povlsen, L.K., Bekker-Jensen, S., Mailand, N., Bartek, J. and Lukas, J. (2013) ATR prohibits replication catastrophe by preventing global exhaustion of RPA. *Cell*, **155**, 1088-1103.
29. Kantake, N., Sugiyama, T., Kolodner, R.D. and Kowalczykowski, S.C. (2003) The recombination-deficient mutant RPA (rfa1-t11) is displaced slowly from single-stranded DNA by Rad51 protein. *J Biol Chem*, **278**, 23410-23417.
30. Levikova, M., and Cejka, P. (2015) The *S. cerevisiae* Dna2 can function as a sole nuclease in the processing of Okazaki fragments in DNA replication. *Nu cleic Acids Res, in press.*

Figure Legends

Figure 1: Helicase activity of Dna2 promotes ssDNA degradation. (**A**) Processing of Y-structure DNA substrate by wild type Dna2, helicase-dead K1080E and nuclease-dead Dna2 E675A variants. The top oligonucleotide was ^{32}P-labelled at the 5' end. The reactions contained RPA (22.5 nM), and various Dna2 concentrations, as indicated, position of the ^{32}P label. Heat, heat-denatured substrate. The panel shows representative 10% polyacrylamide gels. (**B**) Representative agarose gel (1%) showing degradation kinetics of radioactively labeled ssDNA fragments by Dna2 wt and K1080E

(7.5 nM). λ phage DNA was digested with HindIII to produce dsDNA fragments ranging from 125 bp to 23 kbp in length, and ^{32}P-labeled with Klenow fragment of DNA polymerase I. The resulting DNA fragments had 5' ssDNA tails of 3 nt in length at their ends. Dna2 wt or K1080E were incubated for indicated time periods with the heat-denatured restricted DNA (ssDNA fragments) in the presence of RPA (1.08 µM). Heat, heat-denatured substrate. Sizes of dsDNA substrates are indicated on the left.

Figure 2: Dna2 has an endonuclease activity on circular ssDNA only in absence of RPA. (**A**) A representative 1% agarose gel, showing a comparison of the activities of wild type Dna2, helicase-dead K1080E and nuclease-dead E675A variants on circular 6.4 kb-long ssDNA substrate (1.6 nM). Reactions were incubated for 30 min in the presence or absence of RPA (770 nM), as indicated. Reaction buffer contained 2 mM manganese acetate. DNA was visualized by post-staining with GelRed. (**B**) Same experiment as in (**A**), but in 2 mM magnesium acetate. (**C**) Same experiment as in (**A**), but with circular 6.4 kbp-long dsDNA in presence or absence of RPA (1.54 µM), as indicated. Reaction buffer contained 2 mM magnesium acetate.

Figure 3: Efficient ssDNA degradation by Dna2 is promoted by its ATP-dependent ssDNA translocase activity. (**A**) Representative agarose gel (1%) showing degradation kinetics of randomly radioactively labeled PCR product by Dna2 wt and K1080E (3 nM). PCR reaction was conducted in presence of [alpha-^{32}P] dATP, the 2.2 kbp product was PCR purified, heat-denatured and used for the kinetic experiment. Dna2 wt or K1080E were incubated for indicated time periods with the heat-denatured DNA in the presence of RPA (315 nM). Heat, heat-denatured substrate. (**B**) Same as (**A**), the reactions were separated on 20% polyacrylamide denaturing urea gel. Marker: Low molecular weight marker (Affymetrix), 10-100 nt, ^{32}P-labeled at the 5'terminus with [gamma-^{32}P] ATP and T4 polynucleotide kinase. (**C**) Histograms of an experiment such as in Figures 3A, left panel only, showing the optical density analysis of the gel lanes 1-9. Red arrows indicate the 80 nt peak. (**D**), (**E**), Quantitation of experiments such as in Figure 3A. Averages shown, n=3; error bars, s.e.m. In (**E**) only the quantitation of product accumulation with 1 nM Dna2 is shown. (**F**) Degradation kinetics of randomly radioactively labeled PCR product by Dna2 wt and K1080E (3 nM) in absence of ATP. Experiment as shown in (**B**).

Figure 4: RPA stimulates ssDNA degradation by Dna2. (**A**) Experiment as in Figure 2B showing the degradation of PCR substrate by Dna2 wt or K1080E in presence (left panel) or absence of RPA (right panel as indicated). ssDNA substrate was incubated with increasing amounts of Dna2 (1, 3, 10 nM) for 10 min. (**B**), (**C**) Quantitation of experiments such as in (**A**). The data with RPA are the same as in Figure 1DE. Averages shown, n=3; error bars, s.e.m. In (**C**) only the quantitation of product accumulation with 1 nM Dna2 is shown. (**D**) Degradation kinetics of a 93 nt-long oligonucleotide, ^{32}P labeled at the 5' terminus. Dna2 wt was added in presence (left) or absence (right) of RPA. The size of first cleavage product by Dna2 in presence of RPA is between 7-11 nt. (**E**) Same assay as in (**D**), but without ATP. (**F**) Same experiment as in (**D**), but with helicase-dead Dna2 K1080E. (**G**) Model of ssDNA degradation by Dna2 wild type protein. In presence of the helicase activity of Dna2, ATP and RPA the degradation is fast and long DNA fragments are generated first. In absence of either RPA, or ATP, or the helicase activity of Dna2 the ssDNA degradation is slow and short fragments are produced.

Figure 5: Helicase activity of Dna2 wt promotes resection of dsDNA together with Sgs1. (**A**) A representative 1% agarose gel showing a comparison of the activities of wild type Dna2 and helicase-dead K1080E variant on 5' tailed 2.7 kbp dsDNA substrate (7.5 nM) in conjunction with 1nM Sgs1. Reactions were incubated for 30 min in the presence of RPA (1.5 µM). Reaction buffer contained 2 mM ATP. DNA was visualized by staining with ethidium bromide. (**B**) Quantitation of (**A**). Averages shown, n=2; error bars, s.e.m. (**C**) Representative 20% polyacrylamide denaturing urea gels showing the resection kinetics of uniformly radioactively labeled PCR product by Dna2 wt and K1080E (0.2 nM), Sgs1 (0.3 nM), Top3-Rmi1 (10 nM) and Mre11-Rad50-Xrs2 (40 nM). PCR reaction was conducted in presence of [alpha-^{32}P] dATP, the 2.2 kb product was PCR purified and used for the kinetic experiment. Marker: Low molecular weight marker (Affymetrix), 10-100 nt, ^{32}P-labeled at the 5'terminus with [gamma-^{32}P] ATP and T4 polynucleotide kinase.

Figure 1

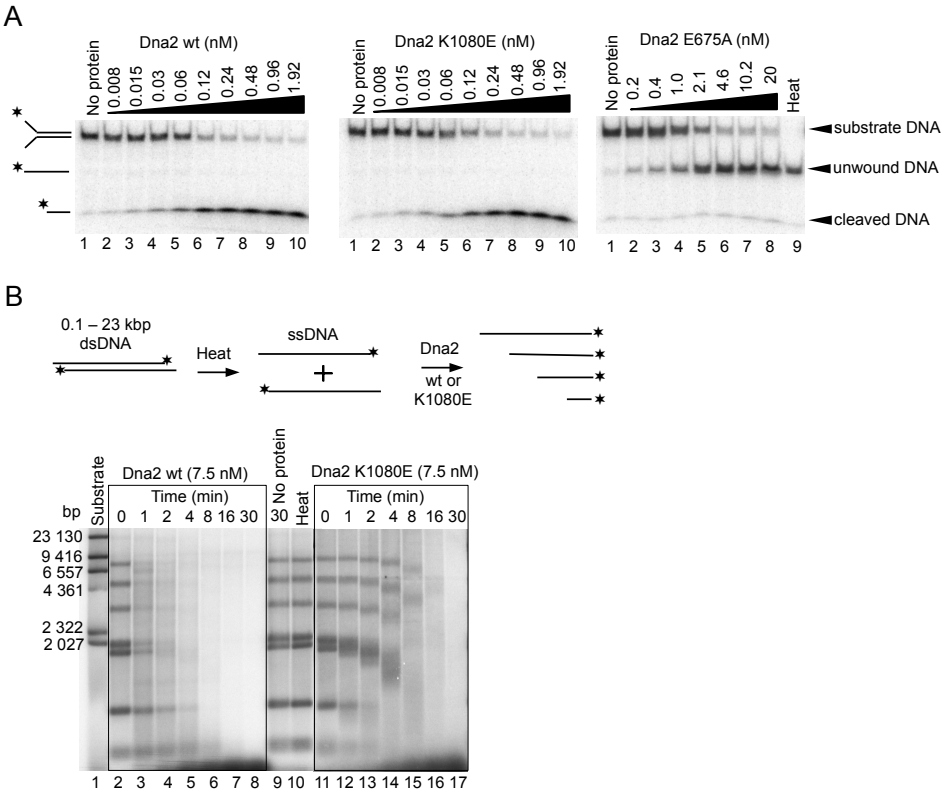

Figure 1: Helicase activity of Dna2 promotes ssDNA degradation
(**A**) Processing of Y-structure DNA substrate by wild type Dna2, helicase-dead K1080E and nuclease-dead Dna2 E675A variants. The top oligonucleotide was ^{32}P-labelled at the 5' end. The reactions contained RPA (22.5 nM), and various Dna2 concentrations, as indicated *, position of the ^{32}P label. Heat, heat-denatured substrate. The panel shows representative 10% polyacrylamide gels. (**B**) Representative agarose gel (1%) showing degradation kinetics of radioactively labeled ssDNA fragments by Dna2 wt and K1080E (7.5 nM). λ phage DNA was digested with *HindIII* to produce dsDNA fragments ranging from 125 bp to 23 kbp in length, and ^{32}P-labeled with Klenow fragment of DNA polymerase I. The resulting DNA fragments had 5' ssDNA tails of 3 nt in length at their ends. Dna2 wt or K1080E were incubated for indicated time periods with the heat-denatured restricted DNA (ssDNA fragments) in the presence of RPA (1.08 μM). Heat, heat-denatured substrate. Sizes of dsDNA substrates are indicated on the left.

Figure 2

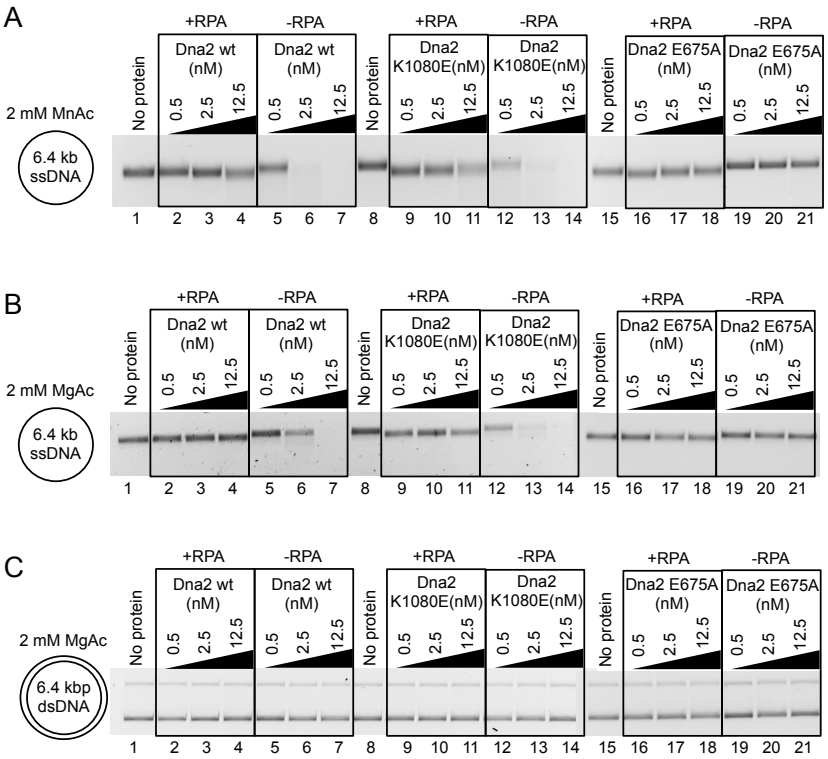

Figure 2: Dna2 has an endonuclease activity on circular ssDNA only in absence of RPA.
(**A**) A representative 1% agarose gel, showing a comparison of the activities of wild type Dna2, helicase-dead K1080E and nuclease-dead E675A variants on circular 6.4 kb-long ssDNA substrate (1.6 nM). Reactions were incubated for 30 min in the presence or absence of RPA (770 nM), as indicated. Reaction buffer contained 2 mM manganese acetate. DNA was visualized by post-staining with GelRed. (**B**) Same experiment as in (**A**), but in 2 mM magnesium acetate. (**C**) Same experiment as in (**A**), but with circular 6.4 kbp-long dsDNA in presence or absence of RPA (1.54 μM), as indicated. Reaction buffer contained 2 mM magnesium acetate.

Figure 3

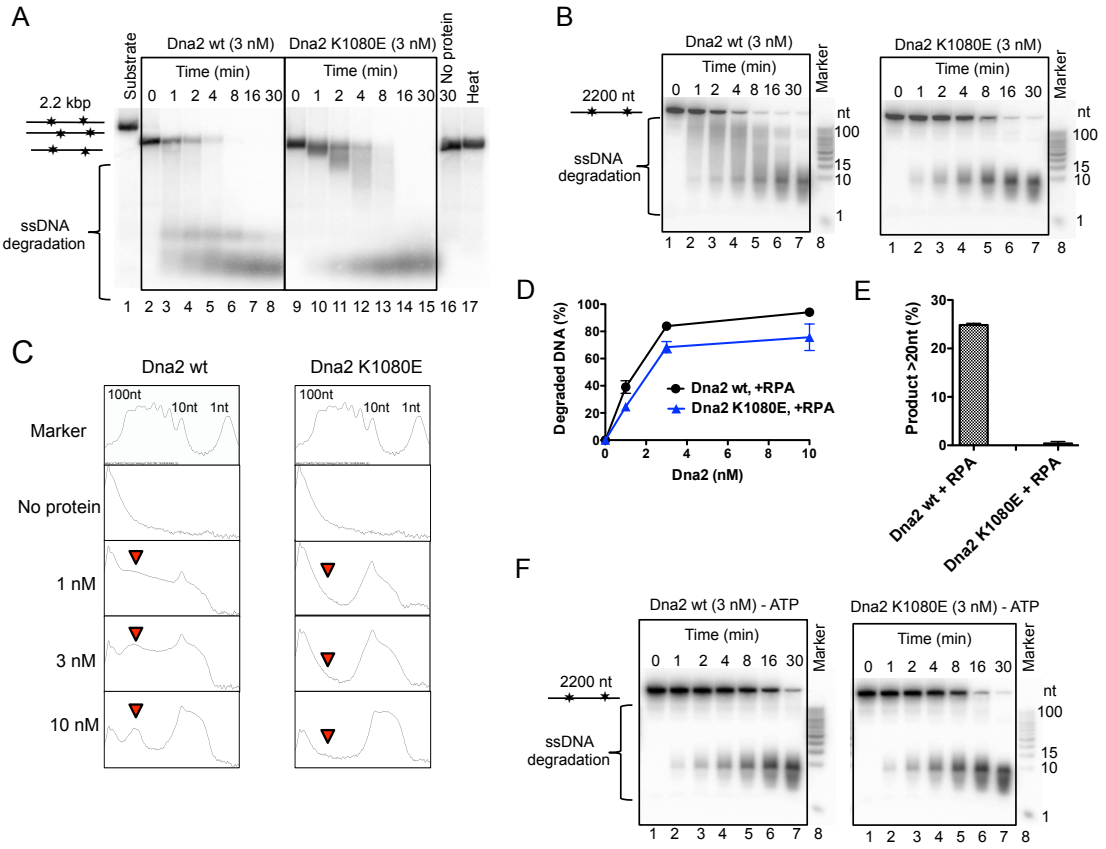

Figure 3: Efficient ssDNA degradation by Dna2 is promoted by its ATP-dependent ssDNA translocase activity

(**A**) Representative agarose gel (1%) showing degradation kinetics of randomly radioactively labeled PCR product by Dna2 wt and K1080E (3 nM). PCR reaction was conducted in presence of [alpha-^{32}P] dATP, the 2.2 kbp product was PCR purified, heat-denatured and used for the kinetic experiment. Dna2 wt or K1080E were incubated for indicated time periods with the heat-denatured DNA in the presence of RPA (315 nM). Heat, heat-denatured substrate. (**B**) Same as (**A**), the reactions were separated on 20% polyacrylamide denaturing urea gel. Marker: low molecular weight marker (Affymetrix), 10-100 nt, ^{32}P-labeled at the 5'terminus with [gamma-^{32}P] ATP and T4 polynucleotide kinase. (**C**) Histograms of an experiment such as in Figures 3A, left panel only, showing the optical density analysis of the gel lanes 1-9. Red arrows indicate the 80 nt peak. (**D**), (**E**), Quantitation of experiments such as in Figure 3A. Averages shown, n=3; error bars, s.e.m. In (**E**) only the quantitation of product accumulation with 1 nM Dna2 is shown. (**F**) Degradation kinetics of randomly radioactively labeled PCR product by Dna2 wt and K1080E (3 nM) in absence of ATP. Experiment as shown in (**B**).

Figure 4

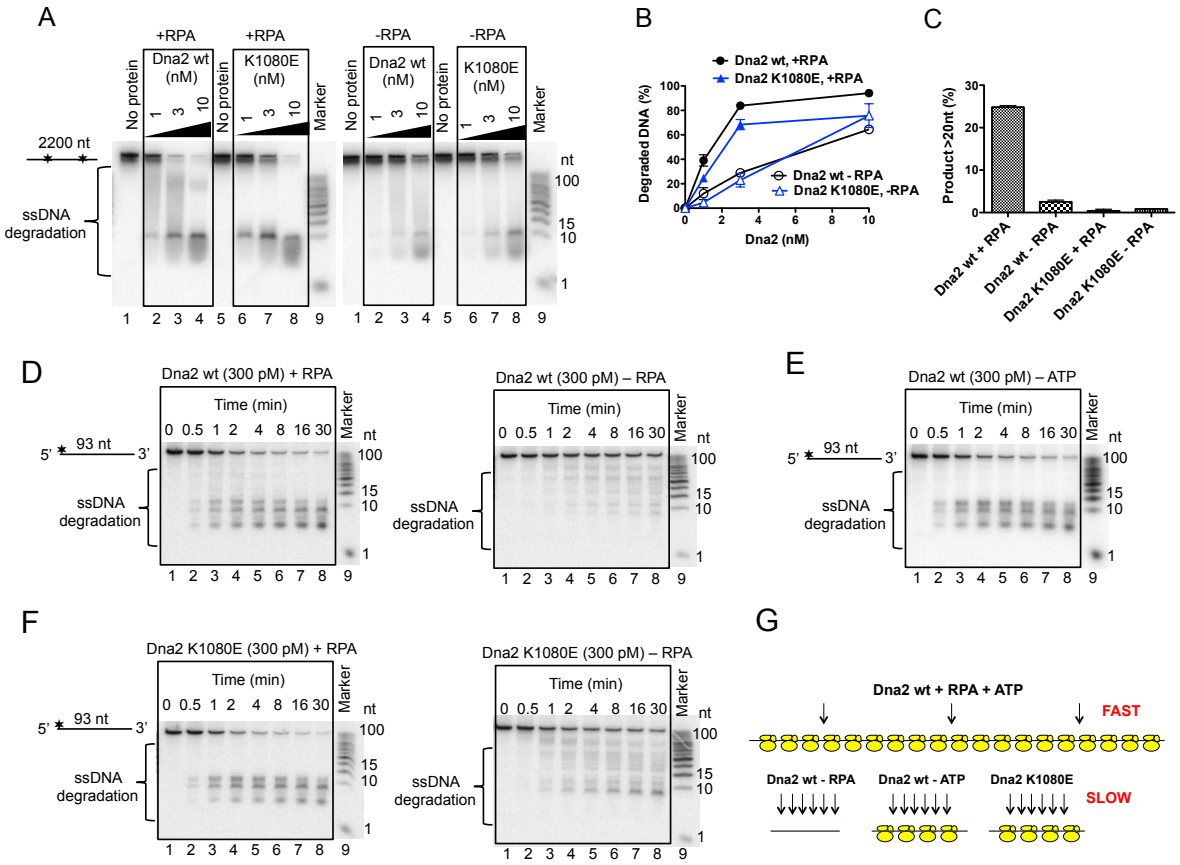

Figure 4: RPA stimulates ssDNA degradation by Dna2
(**A**) Experiment as in Figure 2B showing the degradation of PCR substrate by Dna2 wt or K1080E in presence (left panel) or absence of RPA (right panel as indicated). ssDNA substrate was incubated with increasing amounts of Dna2 (1, 3, 10 nM) for 10 min. (**B**), (**C**) Quantitation of experiments such as in (**A**). The data with RPA are the same as in Figure 1DE. Averages shown, n=3; error bars, s.e.m. In (**C**) only the quantitation of product accumulation with 1 nM Dna2 is shown. (**D**) Degradation kinetics of a 93 nt-long oligonucleotide, ^{32}P labeled at the 5' terminus. Dna2 wt was added in presence (left) or absence (right) of RPA. The size of first cleavage product by Dna2 in presence of RPA is between 7-11 nt. (**E**) Same assay as in (**D**), but without ATP. (**F**) Same experiment as in (**D**), but with helicase-dead Dna2 K1080E. (**G**) Model of ssDNA degradation by Dna2 wild type protein. In presence of the helicase activity of Dna2, ATP and RPA the degradation is fast and long DNA fragments are generated first. In absence of either RPA, or ATP, or the helicase activity of Dna2 the ssDNA degradation is slow and short fragments are produced.

Figure 5

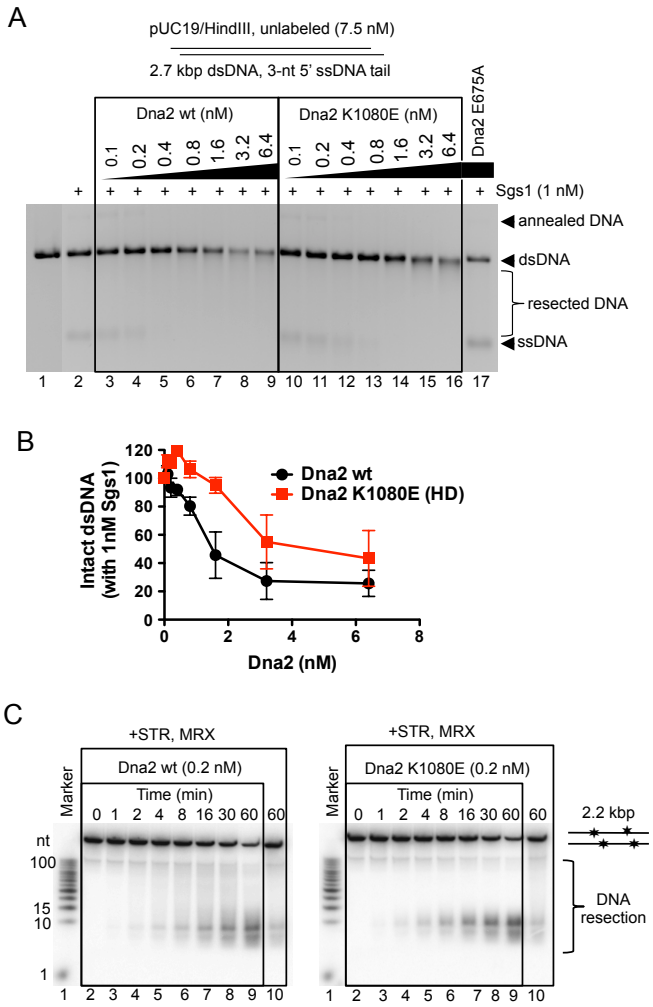

Figure 5: Helicase activity of Dna2 wt promotes resection of dsDNA together with Sgs1.
(**A**) A representative 1% agarose gel showing a comparison of the activities of wild type Dna2 and helicase-dead K1080E variant on 5' tailed 2.7 kbp dsDNA substrate (7.5 nM) in conjunction with 1nM Sgs1. Reactions were incubated for 30 min in the presence of RPA (1.5 μM). Reaction buffer contained 2 mM ATP. DNA was visualized by staining with ethidium bromide. (**B**) Quantitation of (**A**). Averages shown, n=2; error bars, s.e.m. (**C**) Representative 20% polyacrylamide denaturing urea gels showing the resection kinetics of randomly radioactively labeled PCR product by Dna2 wt and K1080E (0.2 nM), Sgs1 (0.3 nM), Top3-Rmi1 (10 nM) and Mre11-Rad50-Xrs2 (40 nM). PCR reaction was conducted in presence of [alpha-^{32}P] dATP, the 2.2 kbp product was PCR purified and used for the kinetic experiment. Marker: low molecular weight marker (Affymetrix), 10-100 nt, ^{32}P-labeled at the 5'terminus with [gamma-^{32}P] ATP and T4 polynucleotide kinase.

2.3 Results from collaborations

2.3.1 DNA2 drives processing and restart of reversed replication forks in human cells

Saravanabhavan Thangavel, Matteo Berti, **Maryna Levikova**, Cosimo Pinto, Shivasankari Gomathinayagham, Marko Vujanovic, Ralph Zellweger, Hayley Moore, Eu Han Lee, Eric A. Hendrickson, Petr Cejka, Sheila Stewart, Massimo Lopes and Alessandro Vindigni.

Article published in Journal of Cell Biology, 2015.

I contributed to this publication by performing biochemical assays shown in Figure 8 A-D, F-G, J, K; Supplementary Figure S4 A-G, J, K; Supplementary Figure S5.

JCB: Article

DNA2 drives processing and restart of reversed replication forks in human cells

Saravanabhavan Thangavel,[1]* Matteo Berti,[1]* Maryna Levikova,[2] Cosimo Pinto,[2] Shivasankari Gomathinayagam,[1] Marko Vujanovic,[2] Ralph Zellweger,[2] Hayley Moore,[3] Eu Han Lee,[4] Eric A. Hendrickson,[4] Petr Cejka,[2] Sheila Stewart,[3] Massimo Lopes,[2] and Alessandro Vindigni[1]

[1]Department of Biochemistry and Molecular Biology, Saint Louis University School of Medicine, St. Louis, MO 63104
[2]Institute of Molecular Cancer Research, University of Zurich, CH-8057 Zurich, Switzerland
[3]Department of Cell Biology and Physiology, Washington University School of Medicine, St. Louis, MO 63110
[4]Department of Biochemistry, Molecular Biology, and Biophysics, University of Minnesota, Minneapolis, MN 55455

Accurate processing of stalled or damaged DNA replication forks is paramount to genomic integrity and recent work points to replication fork reversal and restart as a central mechanism to ensuring high-fidelity DNA replication. Here, we identify a novel DNA2- and WRN-dependent mechanism of reversed replication fork processing and restart after prolonged genotoxic stress. The human DNA2 nuclease and WRN ATPase activities functionally interact to degrade reversed replication forks with a 5′-to-3′ polarity and promote replication restart, thus preventing aberrant processing of unresolved replication intermediates. Unexpectedly, EXO1, MRE11, and CtIP are not involved in the same mechanism of reversed fork processing, whereas human RECQ1 limits DNA2 activity by preventing extensive nascent strand degradation. RAD51 depletion antagonizes this mechanism, presumably by preventing reversed fork formation. These studies define a new mechanism for maintaining genome integrity tightly controlled by specific nucleolytic activities and central homologous recombination factors.

Introduction

The accurate replication of our genome is an essential requirement for the high-fidelity transmission of genetic information to daughter cells. DNA replication forks are constantly challenged and arrested by DNA lesions, induced by endogenous and exogenous agents, and by a diverse range of intrinsic replication fork obstacles, such as transcribing RNA polymerases, unusual DNA structures or tightly bound protein–DNA complexes (Carr and Lambert, 2013). An emerging model of how stalled or damaged forks are processed is that replication forks can reverse to aid repair of the damage (Atkinson and McGlynn, 2009; Ray Chaudhuri et al., 2012; Berti et al., 2013). This model implies significant remodeling of replication fork structures into four-way junctions and the molecular determinants required for reversed fork processing and restart are just beginning to be elucidated. The first evidence that supports the physiological relevance of this DNA transaction during replication stress in human cells arose from studies with DNA topoisomerase I (TOP1) inhibitors (Ray Chaudhuri et al., 2012). Additional studies established that the human RECQ1 helicase promotes the restart of replication forks that have reversed upon TOP1 inhibition by virtue of its ATPase and branch migration activities (Berti et al., 2013). These observations were recently extended to show that the RECQ1 mechanism of reversed fork restart is a more general response to a wide variety of replication challenges (Zellweger et al., 2015). Nonetheless, new lines of evidence point to alternative mechanisms and factors that might mediate either formation or processing of reversed replication forks (Bétous et al., 2012; Gari et al., 2008). These putative mechanisms likely include nucleases that are capable of processing stalled replication intermediates upon genotoxic stress (Cotta-Ramusino et al., 2005; Schlacher et al., 2011; Hu et al., 2012; Ying et al., 2012).

Here, we investigate the contribution of the human DNA2 nuclease/helicase in reversed fork processing. DNA2 is a highly conserved nuclease/helicase initially identified in *Saccharomyces cerevisiae* screening for mutants deficient in DNA replication (Kuo et al., 1983; Budd and Campbell, 1995). Yeast Dna2 plays

*S. Thangavel and M. Berti contributed equally to this paper.

Correspondence to Alessandro Vindigni: avindign@slu.edu

Abbreviations used in this paper: CPT, camptothecin; DSB, double-strand DNA break; EXO1, human exonuclease I; HDR, Homology directed repair; HR, homologous recombination; HU, hydroxyurea; MMC, mitomycin C; MRN, MRE11-RAD50-NBS1; TOP1, DNA topoisomerase I.

The Rockefeller University Press $30.00
J. Cell Biol. Vol. 208 No. 5 545–562
www.jcb.org/cgi/doi/10.1083/jcb.201406100

an essential role in Okazaki fragment maturation during lagging strand DNA replication (Budd and Campbell, 1997; Bae et al., 2001; Ayyagari et al., 2003). However, increasing evidence suggests that DNA2 has important—albeit yet undefined—roles in DNA replication stress response and DNA repair, which go beyond its postulated role in Okazaki fragment processing (Duxin et al., 2012; Karanja et al., 2012; Peng et al., 2012). The notion that DNA2 is important for DNA replication is strengthened by the observation that DNA2 forms a complex with various replication core components, including the replisome protein And-1 (Wawrousek et al., 2010; Duxin et al., 2012). Moreover, human DNA2 seems to play a partially redundant role with human exonuclease I (EXO1) in replication-coupled repair (Karanja et al., 2012), whereas a recent study in *S. pombe* suggested that the nuclease activity of DNA2 is required to prevent stalled forks from reversing upon HU treatment (Hu et al., 2012).

DNA2 also has an independent function in dsDNA break repair. Two distinct pathways act redundantly to mediate processive DSB resection downstream from the MRE11-RAD50-NBS1 (MRN) and CtIP factors in eukaryotic cells: one requires DNA2 and the other EXO1 (Gravel et al., 2008; Mimitou and Symington, 2008; Zhu et al., 2008; Nicolette et al., 2010). Specifically, DNA2 and EXO1 resect the 5′ ends of double-strand DNA breaks (DSBs) to generate 3′ single-stranded overhangs, which are essential to initiate homologous recombination. In yeast, DNA2-dependent dsDNA-end resection reaction requires the Sgs1 helicase to unwind the DNA from the break (Zhu et al., 2008; Cejka et al., 2010; Niu et al., 2010). This mechanism appears to be largely conserved in mammalian cells where DNA2 cooperates with the human BLM helicase to resect dsDNA ends in vitro (Nimonkar et al., 2011). However, mammalian cells possess five human RecQ homologues (RECQ1, RECQ4, RECQ5, BLM, and WRN) and WRN can also assist DNA2-dependent end resection, suggesting that BLM might not be the sole RecQ homologue required for this process (Liao et al., 2008; Sturzenegger et al., 2014). The ability of DNA2 and EXO1 to process dsDNA ends might also be relevant in the context of DNA replication to prevent the accumulation of replication-associated DSBs by promoting homologous recombination (HR) repair (Peng et al., 2012). Alternatively, these nucleases might be involved in the recovery of replication fork blockage by processing specific stalled replication fork structures.

This work uncovers a new DNA2- and WRN-dependent mechanism that mammalian cells use to process replication forks that have reversed as a result of replication inhibition. Importantly, it also shows that this mechanism is tightly regulated by human RECQ1 and the HR factor RAD51. Our observations shed light on a novel pathway for the suppression of chromosomal instability in mammalian cells and provide important new insight into the mechanisms of replication stress response associated with chemotherapeutic drug damage.

Results

DNA2 is required for stalled fork processing and restart

To begin elucidating the role of human DNA2 during replication stress, we monitored replication perturbation by genome-wide single-molecule DNA fiber replication assays. We pulse-labeled human osteosarcoma (U-2 OS) cells with the thymidine analogue CldU for 20 min, followed by a 60-min exposure to a selected genotoxic agent during the CldU labeling period, and by labeling with the second thymidine analogue, IdU, for an additional 40 min after removal of the genotoxic drug. We found that DNA2 plays an important role in restarting replication forks after treatment with the ribonucleotide reductase inhibitor hydroxyurea (HU), the topoisomerase I inhibitor camptothecin (CPT), and the interstrand cross-linking agent mitomycin C (MMC) (Fig. 1 A). In addition, DNA2 depletion increased the percentage of origin firing, but not of fork termination events (Fig. S1 A). Genetic knockdown–rescue experiments confirmed that complementation in DNA2-depleted U-2 OS cells with siRNA-resistant WT DNA2 abrogated the effect of DNA2 depletion on replication fork restart upon HU treatment. Moreover, expression of the nuclease-deficient DNA2 mutant D294A in DNA2-depleted cells revealed that the nuclease activity of DNA2 was essential for its role in replication fork restart (Fig. 1 B and Fig. S1 B).

We next measured whether DNA2 uses its nuclease activity to process stalled replication intermediates by monitoring the integrity of the newly synthesized DNA after HU treatment. To this purpose, we changed the DNA labeling scheme. We first pulsed U-2 OS cells with IdU for 45 min, and then varied the exposure time to HU from 0 to 8 h. The mean length of the IdU tracts progressively decreased during HU treatment from 18.2 µm (0 h) to 12.0 µm (8 h; Fig. 1 C). However, shRNA-mediated DNA2 depletion largely prevented IdU tract shortening, confirming that DNA2 is responsible for the observed nascent strand degradation (Fig. 1 D). Double-labeling experiments confirmed that the observed nascent tract shortening is indeed caused by the DNA2-dependent processing of ongoing replication forks and that this degradation is important to mediate efficient replication fork restart upon prolonged HU treatment (Fig. 1 E). Clonogenic analysis of U-2 OS cells treated with the same HU concentration used for the DNA fiber experiments showed a significantly reduced cell survival upon DNA2 depletion, indicating that the DNA2-dependent processing of stalled replication intermediates is critical for recovery from replication fork blockage (Fig. 2 A). The results obtained with the shRNA DNA2-depleted U-2 OS cells were validated using a new conditional knockout human colorectal carcinoma cell line (HCT116) where addition of tamoxifen to the culture medium led to DNA2-null cells. Analysis of the mean tract lengths confirmed that DNA2 knockout in HCT116 cells abrogates the prominent degradation observed upon HU treatment (Fig. 2 B). Collectively, these results indicate that human DNA2 degrades nascent strands at stalled replication forks to facilitate fork restart and promote viability after genotoxic stress induction.

RECQ1 regulates the fork processing activity of DNA2

On the basis of the recent discovery that RECQ1 is required to restart replication forks that have reversed upon genotoxic stress induction (Berti et al., 2013), we investigated whether RECQ1 regulates the fork processing activity of DNA2. Nascent IdU

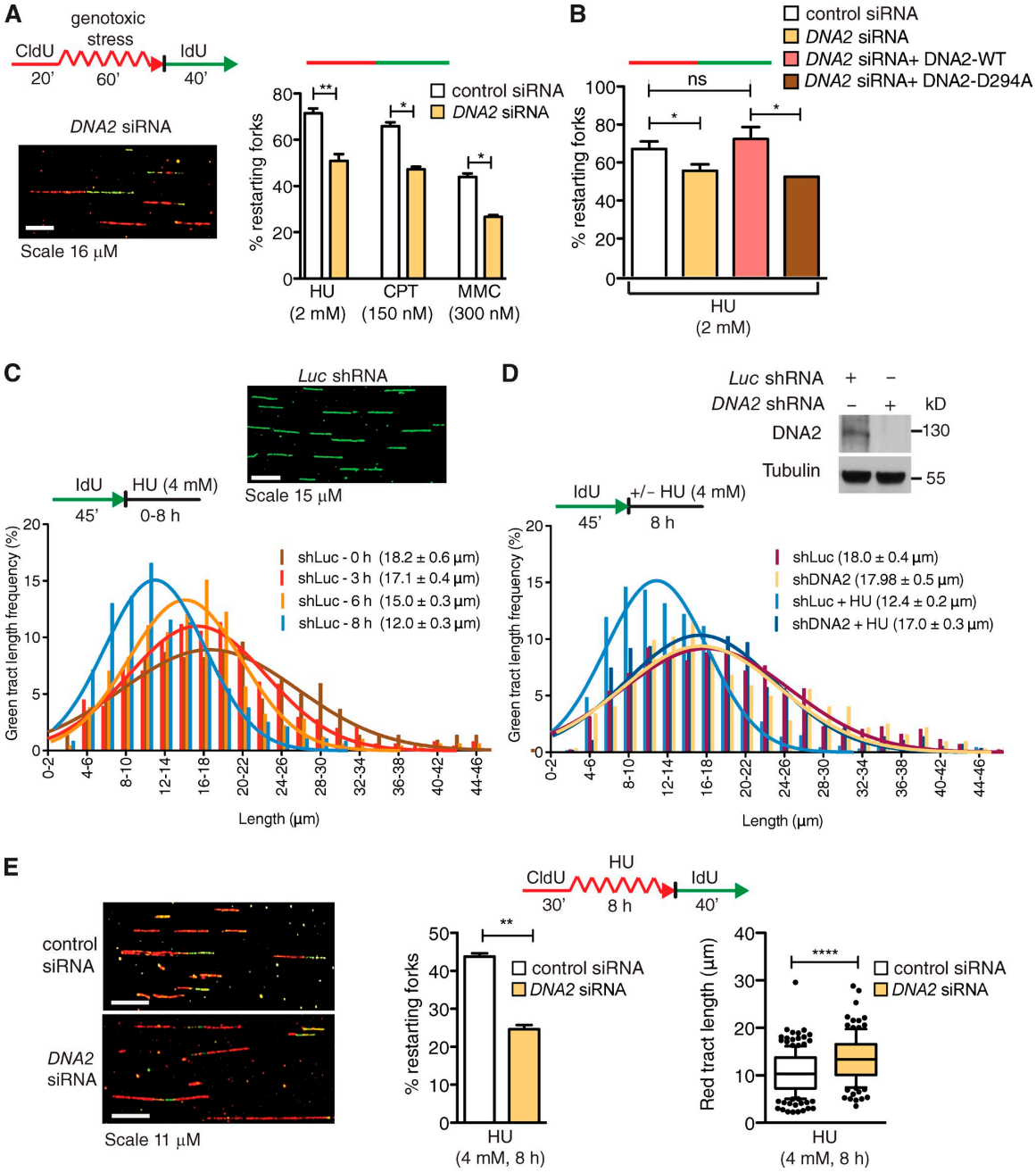

Figure 1. **DNA2 is required for replication fork restart and stalled fork processing upon genotoxic stress.** (A) Schematic of DNA fiber tract analysis. U-2 OS cells were transfected with control siRNA or *DNA2* siRNA before CldU or IdU labeling. Red tracts, CldU; curved red tracts, CldU with genotoxic agents (HU or CPT or MMC); green tracts, IdU. (bottom) Representative DNA fiber image. (right) quantification of red-green contiguous tracts (restarting forks). Mean shown, $n = 3$. Error bars, standard error. ns, not significant; *, $P < 0.05$; **, $P < 0.01$ (paired *t* test). (B) Quantification of restarting forks in DNA2-depleted cells expressing DNA-WT or DNA2-D294A. ns, not significant; *, $P < 0.05$ (paired Student's *t* test). (C, top) Representative DNA fiber image. (bottom) Representative IdU tract length distributions in Luc-depleted cells during different exposure time to HU (out of 3 repeats; $n \geq 300$ tracts scored for each dataset). Mean tract lengths are indicated in parentheses. (D) Top, DNA2 expression after shRNA knockdown. Bottom, representative IdU tracts in DNA2-depleted U-2 OS cells in the presence or absence of HU (out of 2 repeats; $n \geq 700$ scored for each dataset). (E, left) Representative DNA fiber images. (middle) Quantification of red-green contiguous tracts (restarting forks) after 8 h of HU. Mean shown, $n = 3$. Error bars, standard error. **, $P < 0.01$ (paired Student's *t* test). (right) Statistical analysis of CldU tracts detected within contiguous red-green tracts. Whiskers the 10th and 90th percentiles. ****, $P < 0.0001$ (Mann-Whitney test).

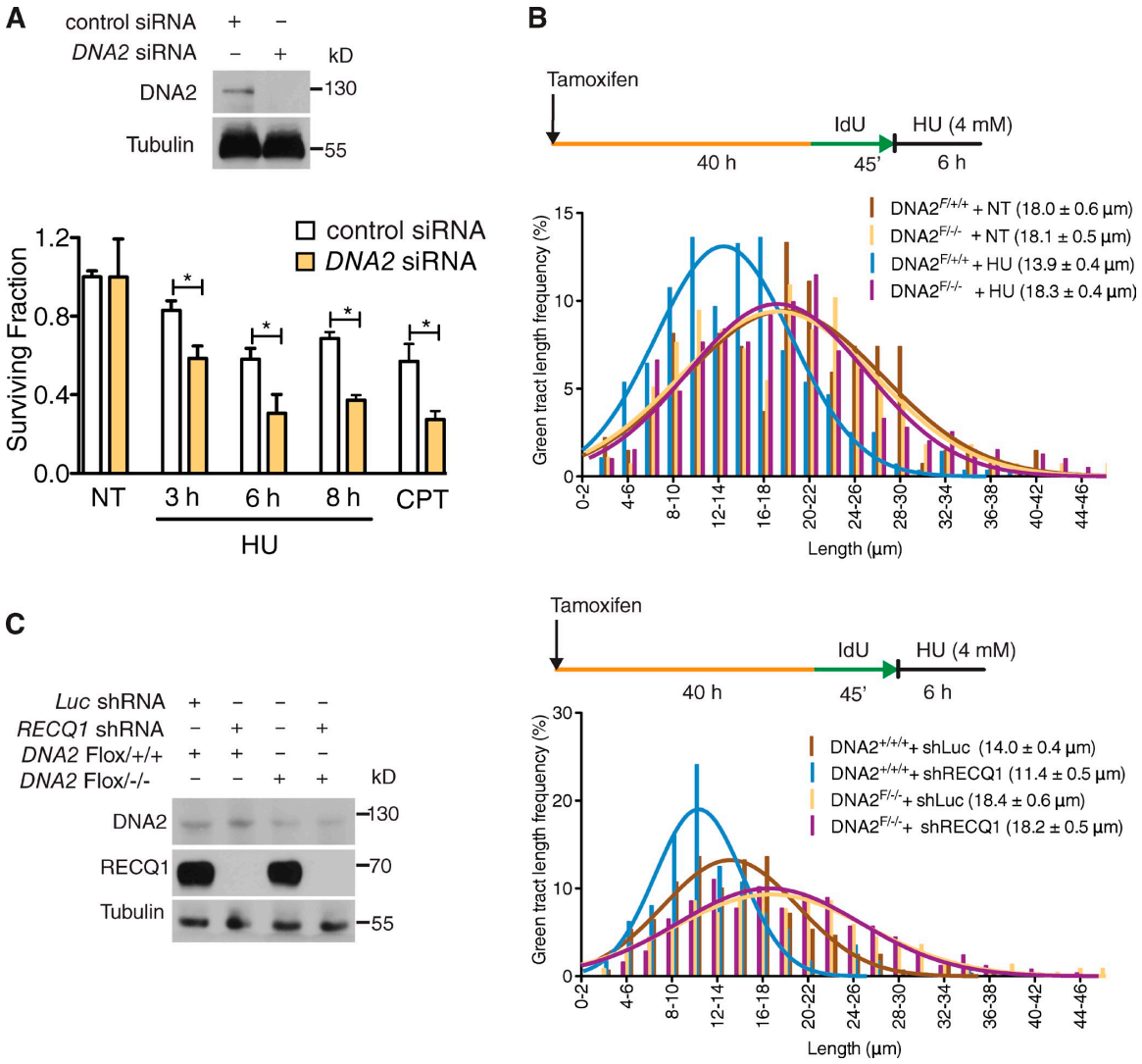

Figure 2. **DNA2 processes stalled replication forks.** (A, top) DNA2 expression after siRNA knockdown. (bottom) Colony-forming assays in control and DNA2-depleted U-2 OS cells treated with 4 mM HU for the indicated time. (B) Representative IdU tracts in DNA2 conditional knockout HCT116 cells (out of two repeats). Tamoxifen was added to generate conditional knockout cells (see Materials and methods). (C, left) Expression of DNA2 and RECQ1 in tamoxifen-treated HCT116 cells. Right, representative IdU tracts in DNA2 conditional knockout HCT116 cells depleted for Luc or RECQ1 (out of three repeats). $n \geq 300$ tracts scored for each dataset shown in B and C.

tracts were substantially shorter in RECQ1-depleted cells compared with control when replication forks were stalled with HU (after 8 h of HU treatment, the mean tract lengths were 7.9 and 12.0 µm, respectively; $P < 0.0001$; Fig. 3, A and B). In agreement with results from luciferase-depleted cells, DNA2 was also responsible for the nascent strand degradation phenotype observed in RECQ1-deficient U-2 OS cells (Fig. 3 C). Analogous results were obtained using the conditional DNA2 knockout HCT116 cell line (Fig. 2 C). In addition, we confirmed that the DNA2-dependent nascent strand degradation observed in the absence of RECQ1 is not limited to a specific replication inhibitor by replacing HU with CPT or MMC (Fig. 3, D and E).

Genetic knockdown–rescue experiments confirmed that complementation in RECQ1-depleted U-2 OS cells with shRNA-resistant WT RECQ1 abrogates the effect of RECQ1 depletion on replication fork processing upon HU treatment (Fig. 3 F). Interestingly, expression of the ATPase-deficient RECQ1 mutant K119R in RECQ1-depleted cells also abrogated the effect of RECQ1 depletion indicating that the ATPase activity of RECQ1 was not required for its role in protecting stalled forks from DNA2-dependent degradation (Fig. 3 F). These results point to an additional role of RECQ1 in protecting replication forks from extensive DNA2-dependent degradation, which is independent of RECQ1 ATPase activity.

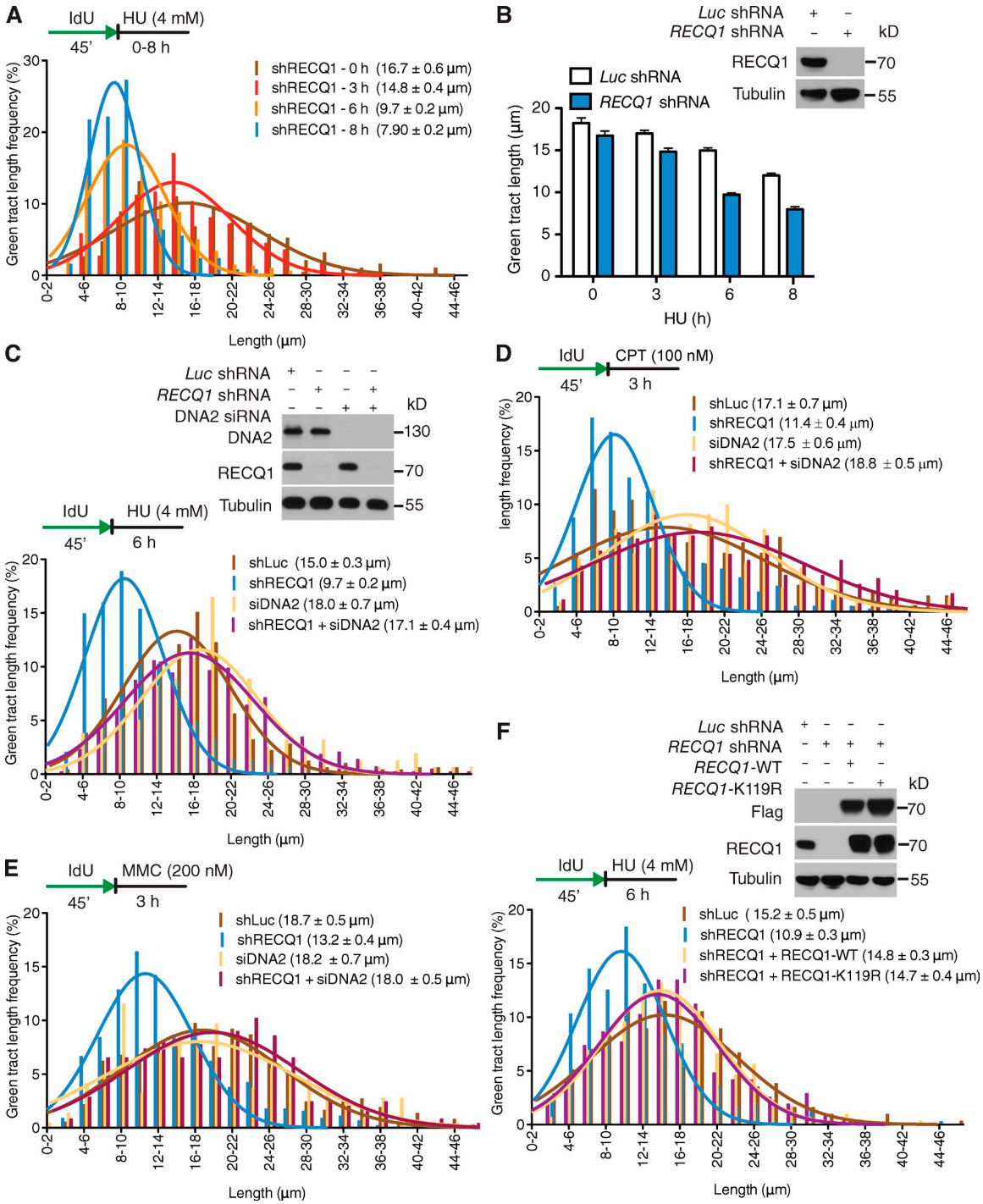

Figure 3. **RECQ1 regulates the DNA2-dependent degradation of stalled forks.** (A) Representative IdU tracts in RECQ1-depleted U-2 OS cells during different exposure time to HU (out of 2 repeats; $n \geq 350$ tracts scored for each dataset). (B) Bar graph represents the mean values of each time point from Figs. 1 C and 2 A. (top) RECQ1 expression after shRNA knockdown. (C, D, and E) Representative IdU tracts in RECQ1-, DNA2-, or RECQ1/DNA2-codepleted U-2 OS cells in the presence of HU (C), CPT (D), and MMC (E; out of 2 repeats; $n \geq 300$ tracts scored for each dataset).(top) RECQ1 and DNA2 expression after shRNA or siRNA knockdown. (F) Representative IdU tracts in RECQ1-depleted U-2 OS cells complemented with shRNA-resistant WT RECQ1 (WT) or ATPase-deficient (K119R) RECQ1 (out of 2 repeats; $n \geq 325$ tracts scored for each dataset). (top) Expression of Flag-tagged RECQ1-WT and RECQ1-K119R in RECQ1-depleted cells.

DNA2 function in stalled fork processing is distinct from EXO1, Mre11, and CtIP

Next, we tested whether other nucleases share a function similar to DNA2 in stalled fork processing. To address this point, we depleted Mre11, EXO1, and CtIP in U-2 OS cells with siRNA-mediated technologies. We found that none of these nucleases share the same phenotype of DNA2 in RECQ1-proficient cells (Fig. 4 A). Furthermore, depletion of these nucleases had only a marginal effect on the rescue of the prominent nascent strand degradation phenotype observed in the absence of RECQ1, indicating that DNA2 has a unique function in reversed fork processing that is not shared by these human nucleases (Fig. 4, B–D). MUS81 is another structure-specific nuclease that plays a critical role in replication fork rescue by converting stalled replication forks into DNA DSBs that can be processed by Homology Directed Repair (HDR) (Hanada et al., 2007; Franchitto et al., 2008). This raised the possibility that the DNA2-dependent degradation originated from the processing of MUS81-dependent DSBs. However, MUS81 depletion did not prevent nascent strand degradation, indicating that DNA2 is not processing stalled replication intermediates that are cleaved by MUS81 (Fig. 4 E).

DNA2 and WRN act together to process stalled replication forks

DNA2-dependent dsDNA-end resection needs the support of a RecQ helicase to unwind the DNA from the break (Cejka et al., 2010; Niu et al., 2010; Nimonkar et al., 2011). To determine the identity of the helicase that acts in conjunction with DNA2 in stalled fork processing, we measured the extent of nascent strand degradation in BLM-, WRN-, and RECQ4-depleted U-2 OS cells. Our DNA fiber analysis showed that WRN depletion mimicked the effect of DNA2-depletion, completely abrogating the prominent nascent strand degradation phenotype observed in RECQ1-depleted U-2 OS cells (Fig. 5 A). The same results were confirmed using WRN and DNA2 codepleted cells, suggesting that DNA2 and WRN are epistatic in nucleolytic processing of stalled forks (Fig. S1 C). The partial nascent strand degradation observed in RECQ1-proficient U-2 OS cells was also abrogated by WRN depletion (Fig. S1 D). Conversely, BLM depletion had only a marginal effect on the nascent strand degradation phenotype observed in RECQ1-depleted cells, whereas RECQ4 depletion had no effect (Fig. S2, A and B). Thus, the WRN helicase plays a prominent role in assisting DNA2-dependent degradation of stalled replication forks.

We next compared the percentage of restarting replication forks in DNA2-depleted, WRN-depleted, and DNA2/WRN-codepleted cells. WRN depletion leads to a decrease in restarting forks (69 to 50%; P = 0.0068). These results are almost identical to those obtained with the DNA2-depleted or DNA2/WRN-codepleted cells, implying that WRN and DNA2 are epistatic also in the restart process (Fig. 5 B). The notion that DNA2 and WRN functionally interact to process stalled replication intermediates is further supported by our observation that the two proteins form a complex both in the presence and absence of replication stress (Fig. 5 C). Of note, RECQ1 is not part of the WRN:DNA2 complex. Collectively, these results suggest that DNA2 cooperates with WRN to promote nascent strand processing and fork restart after HU treatment.

The nuclease activity of DNA2 and the ATPase activity of WRN are essential to process stalled replication forks

DNA2 is characterized by an N-terminal nuclease domain and by a C-terminal helicase domain, but the function of its helicase activity is still debated (Masuda-Sasa et al., 2006). To assess the roles of these two activities in stalled fork processing, we performed genetic knockdown-rescue experiments where we depleted DNA2 and then attempted to rescue fork processing by expressing a Flag-tagged siRNA resistant WT DNA2 control, nuclease-deficient DNA2-D294A, or ATPase-deficient DNA2-K671E. All the experiments were performed in RECQ1-depleted cells, where the effect of DNA2 is more apparent. DNA fiber analysis showed that complementation with nuclease-deficient DNA2 prevents fork processing, whereas complementation with WT or ATPase-deficient DNA2 leads to the same fork processing phenotype observed in DNA2-proficient cells (Fig. 5 D and Fig. S2 C). Therefore, the nuclease, but not the ATPase activity of DNA2, is necessary for fork processing.

Next, we used a Werner Syndrome (WS) fibroblast cell line (AG11395) expressing missense mutant forms of WRN, which inactivate either the exonuclease (WRN-E84A) or the ATPase (K577M) activity of WRN (Pirzio et al., 2008). The ATPase, but not the nuclease activity of WRN, was important for fork processing (Fig. 5 E and Fig. S2 D). These findings were validated by genetic knockdown-rescue experiments where we complemented WRN-depleted U-2 OS cells either with an shRNA resistant WT WRN control or the ATPase-deficient WRN-K577M mutant and found that complementation with the ATPase-deficient mutant prevented fork processing (Fig. S2, E and F). Collectively, these results show that human DNA2 needs the support of the ATPase activity of WRN to promote degradation of the nascent DNA strands.

DNA2 processes reversed replication forks

To gain insight into the actual replication structures processed by DNA2, we inspected the fine architecture of the replication intermediates using a combination of in vivo psoralen cross-linking and EM (Neelsen et al., 2014). Our analysis showed a substantial fraction of reversed replication forks (~24% of molecules analyzed) in control U-2 OS cells treated with 4 mM HU. RECQ1-depletion, and to an even greater extent DNA2-depletion, resulted in a higher frequency of fork reversal events (~30 and 40%, respectively) compared with HU-treated cells. Co-depletion of RECQ1 and DNA2 further increased the frequency of reversed forks (~50%), suggesting that RECQ1 and DNA2 are involved into two distinct mechanisms of reversed fork processing. Interestingly, RECQ1 and/or DNA2 depletion also led to a significant amount of fork reversal events in unperturbed U-2 OS cells (Fig. 6, A and B). WRN-depletion phenocopied DNA2-depletion in terms of reversed fork accumulation, both the presence and in the absence of HU. Moreover, DNA2/

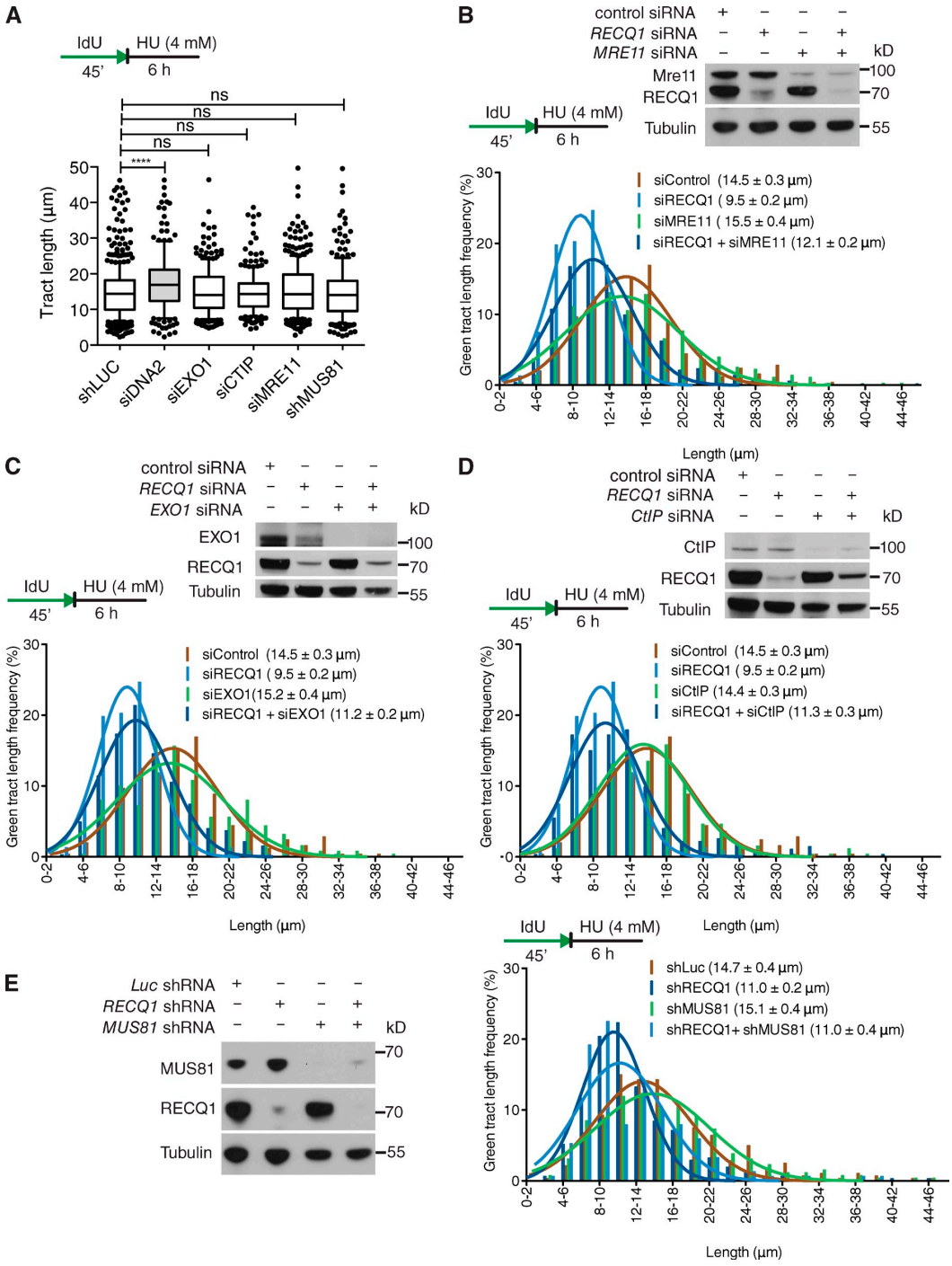

Figure 4. **EXO1, MRE11, CtIP, and MUS81 depletion does not affect stalled fork processing.** (A) Statistical analysis of IdU tracts from U-2 OS cells depleted for the indicated proteins in the presence of 4 mM HU. (B) Representative IdU tracts in control, RECQ1-, MRE11-, or RECQ1/MRE11-codepleted U-2 OS cells (out of 2 repeats). (top) Expression of RECQ1 and MRE11 after siRNA knockdown. (C) Representative IdU tracts in control, RECQ1-, EXO1-, or RECQ1/EXO1-codepleted U-2 OS cells (out of 2 repeats). (top) Expression of RECQ1 and EXO1 after siRNA knockdown. (D) Representative IdU tracts in control, RECQ1-, CtIP-, or RECQ1/CtIP-codepleted U-2 OS cells (out of 2 repeats). (top) Expression of RECQ1 and CtIP after siRNA knockdown. (E) Representative IdU tracts in Luc-, RECQ1-, MUS81-, or RECQ1/MUS81-codepleted U-2 OS cells in the presence of HU (out of 2 repeats). (left) Expression of RECQ1 and MUS81 after shRNA knockdown. $n \geq 300$ tracts scored for each dataset shown in A–E.

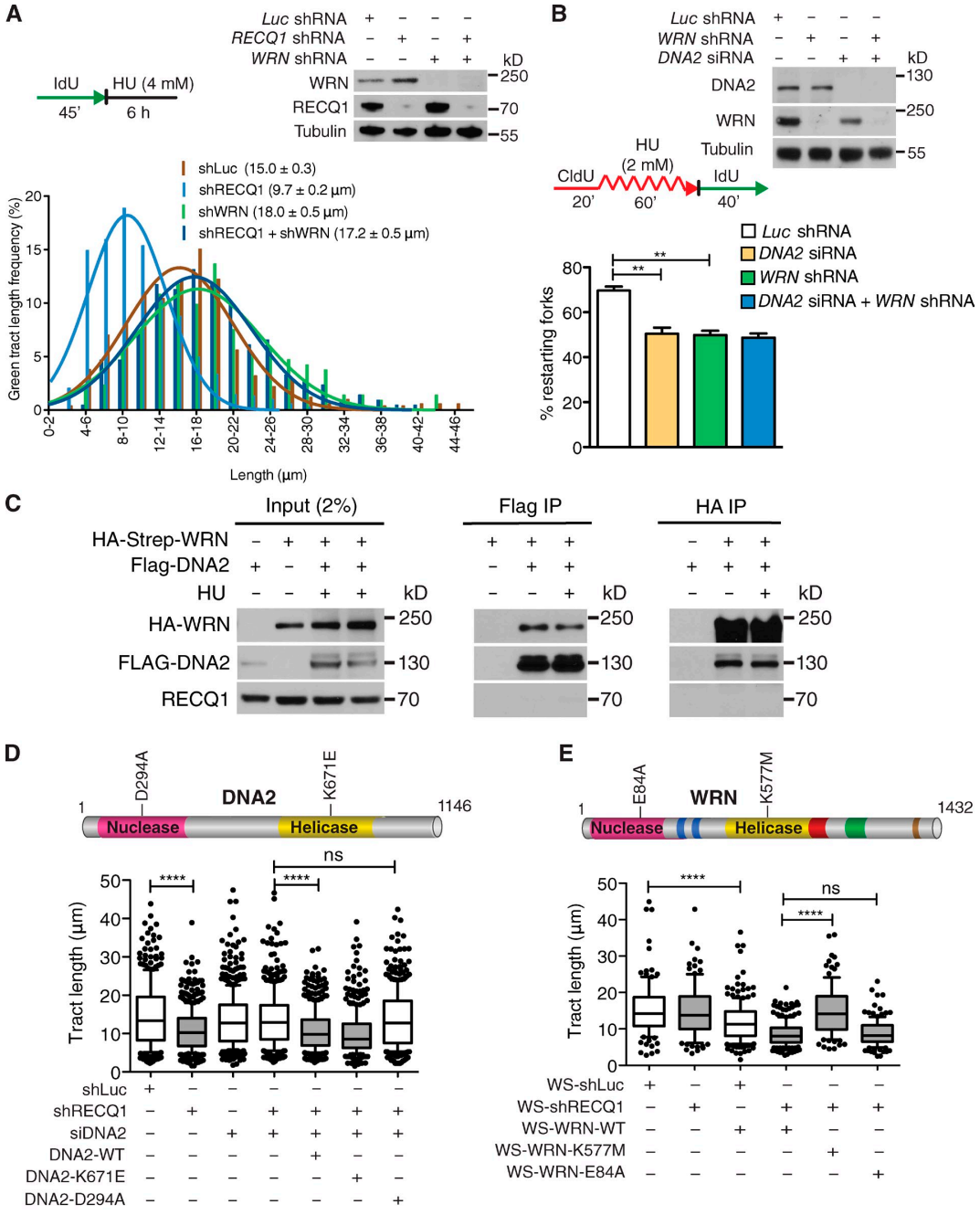

Figure 5. **DNA2 and WRN are epistatic in stalled fork processing and replication restart.** (A) Representative IdU tracts in RECQ1-, WRN-, or RECQ1/WRN-codepleted U-2 OS cells (out of 2 repeats; $n \geq 300$ tracts scored for each dataset). (top) RECQ1 and WRN expression after shRNA knockdown. (B) Quantification of restarting forks in DNA2-, WRN-, or DNA2/WRN-codepleted cells. Mean shown, $n = 3$. Error bars, standard error. *, $P < 0.05$; **, $P < 0.01$ (paired *t* test). (top) Expression of WRN and DNA2 after shRNA knockdown. (C) Co-IP experiments in HEK293T cells transfected with empty vectors, Flag-DNA2, or Strep-HA-WRN. Cells were treated with 4 mM HU (3 h) where indicated. Whole-cell extracts were analyzed before (input) and after IP. (D) Statistical analysis of IdU tracts from RECQ1/DNA2-codepleted U-2 OS cells complemented with WT, ATPase-deficient (K671E), or nuclease-deficient (D294A) DNA2, when indicated. (E) Statistical analysis of IdU tracts from RECQ1-depleted WS cells complemented with WT, ATPase-deficient (K577M), or nuclease-deficient (E84A) WRN. Whiskers in D and E indicate the 10th and 90th percentiles. ns, not significant; ****, $P < 0.0001$ (Mann-Whitney test). $n \geq 300$ tracts scored for each dataset shown in D and E.

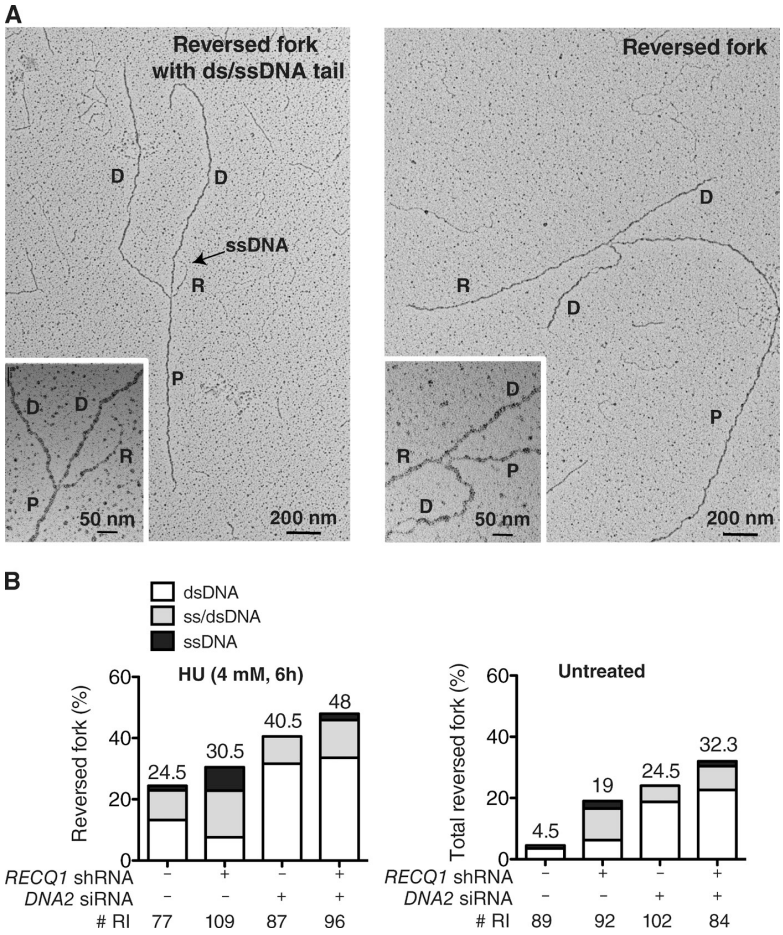

Figure 6. **DNA2 resects reversed replication forks.** (A) Electron micrograph of a partially single-stranded (left) and entirely double-stranded (right) reversed fork observed on genomic DNA upon HU-treatment. The black arrow points to the ssDNA region on the reversed arm. Inset, magnified four-way junction at the reversed replication fork. D, Daughter strand; P, Parental strand; R, Reversed arm. (B) Frequency of fork reversal and ssDNA composition of the reversed arms in RECQ1- or DNA2-depleted U-2 OS cells treated with HU (left) or in unperturbed conditions (right). The percentage values are indicated on the top of the bar. "# RI" indicates the number of analyzed replication intermediates. Data in B are reproduced with very similar results in at least one independent experiment.

WRN-codepletion did not cause a further increase in reversed fork frequency, thus supporting our conclusion that DNA2 and WRN work together in reversed fork processing (Fig. S3 A).

Next, we evaluated the single-strand composition of the regressed arms. To measure ssDNA, we carefully inspected the frequency and length of ssDNA regions on the regressed arms by detecting local difference in filament thickness. DNA2 depletion led to a higher frequency of reversed forks with a dsDNA arm—and a corresponding decrease of partially or entirely single-stranded reversed forks—in both RECQ1-proficient and deficient cells (Fig. 6). Thus, DNA2-mediated resection is directed to completely or partially digest one strand of the reversed arm leading to reversed forks that are either entirely single stranded or have a protruding ssDNA tail. However, prolonged stalling by HU was associated with accumulation of postreplicative ssDNA gaps on replicated duplexes, which was maximal in RECQ1-depleted cells and suppressed by DNA2 depletion (Fig. S3, B and C). Consequently, ssDNA gaps may reflect additional activity of the same nucleolytic apparatus along the postreplicated duplexes or restart of partially resected reversed forks.

As an alternative readout for DNA2-dependent resection, we examined the phosphorylation status of RPA and the checkpoint kinase Chk1 (Zeman and Cimprich, 2014). DNA2 depletion caused a reduction in RPA and Chk1 phosphorylation in both RECQ1-proficient and RECQ1-deficient U-2 OS cells, suggesting that the DNA2-dependent resection of nascent strands might also contribute to checkpoint activation (Fig. S3 D).

RAD51 promotes DNA2-dependent degradation of reversed replication forks

The central recombinase factor RAD51 is directly implicated in reversed fork formation upon genotoxic stress (Zellweger et al., 2015). Thus, we investigated whether RAD51 depletion may affect the reversed fork processing activity of DNA2. We found that RAD51 knockdown largely prevents DNA2 nucleolytic processing both in RECQ1 proficient and RECQ1-deficient cells (Fig. 7 A). Genetic knockdown–rescue experiments confirmed that expression of exogenous RAD51 in RAD51-depleted U-2 OS cells restored the fork processing phenotype (Fig. 7 B). These results indicate that DNA2-dependent nucleolytic

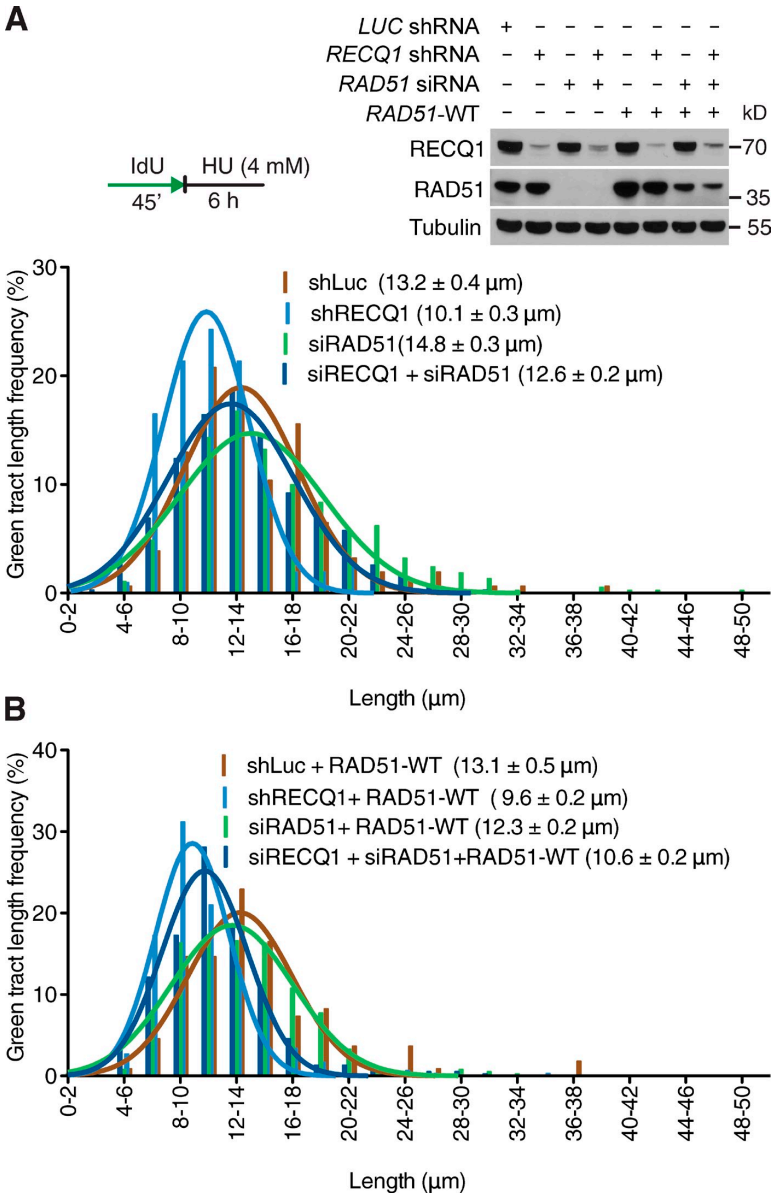

Figure 7. **RAD51 promotes DNA2-depedent degradation of reversed replication forks.** (A) Representative IdU tracts in RECQ1-, RAD51-, or RECQ1/RAD51-codepleted U-2 OS cells (out of 2 repeats). Above, RECQ1 and RAD51 expression after siRNA knockdown RAD51-WT are U-2 OS cells stably expressing siRNA resistant exogenous RAD51. (B) Representative IdU tracts in U-2 OS cells expressing exogenous RAD51 (out of 2 repeats). $n \geq 300$ tracts scored for each dataset shown in A and B.

processing is specifically targeted to reversed fork structures because it is not detected in a genetic background that prevents reversed fork formation—i.e., RAD51 knockdown.

DNA2 preferentially degrades reversed fork structures with a 5′-to-3′ polarity

The notion that DNA2 end resection has a preferential polarity in vivo is consistent with biochemical studies showing that even though DNA2 has the intrinsic capacity to degrade both 5′- and 3′-terminated ssDNA, RPA enforces a primarily 5′-to-3′ end-resection bias (Cejka et al., 2010; Niu et al., 2010; Nimonkar et al., 2011). Thus, we set up new biochemical assays to test whether human DNA2 prefers four-way junction substrates—i.e., reversed replication forks—versus linear DNA duplexes and whether it degrades these substrates with a 5′-to-3′ polarity in the presence of RPA (Fig. 8, A and B). The sequences of the four arms of the four-way junction substrates are mutually heterologous to prevent four-way junction branch migration. DNA2-degraded four-way junction substrates more efficiently than linear dsDNA duplexes, with 20 nM DNA2 required to degrade ∼60% of the four-way junction substrates versus only ∼30% of the linear duplex (Fig. 8 C). Importantly, supplementing the reaction with RPA greatly stimulated the degradation activity of human DNA2 (Fig. 8 D and Fig. S4 A). Additional

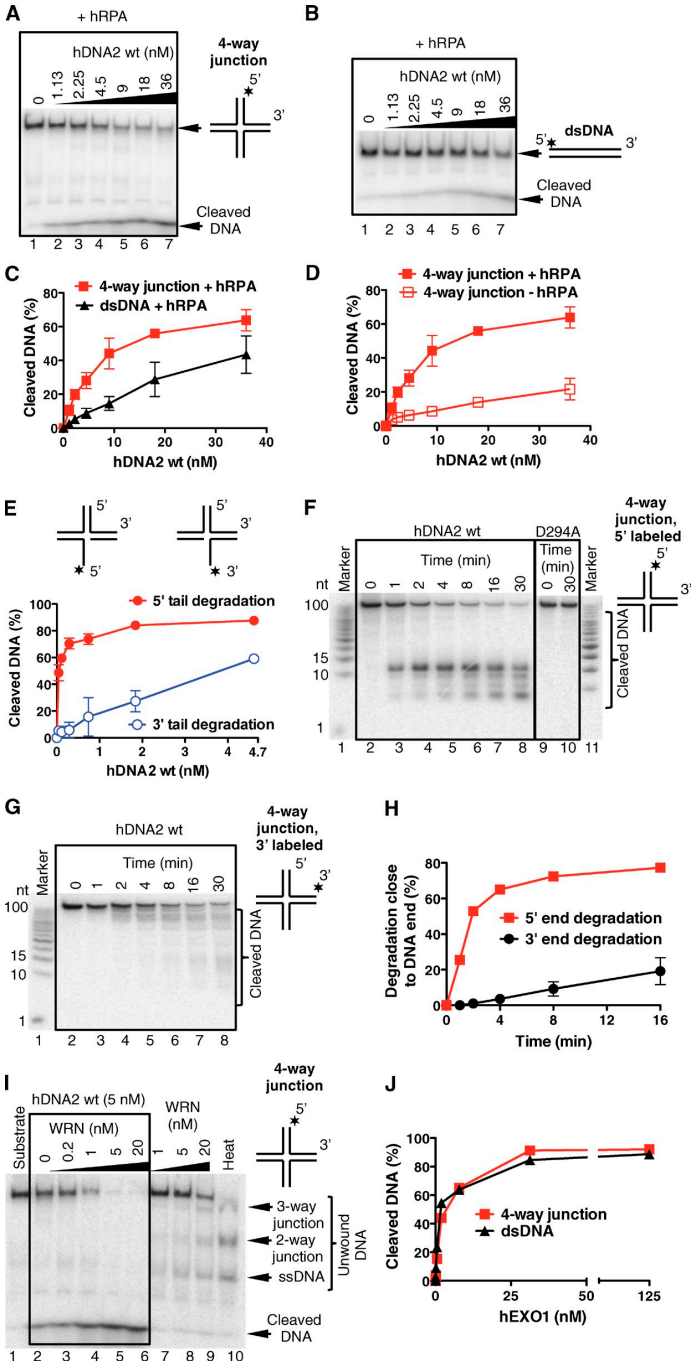

Figure 8. **Human DNA2 preferentially degrades branched DNA in a 5′-3′ direction in reactions stimulated by WRN.** (A) Degradation of a four-way junction by human DNA2 (hDNA2) in the presence of hRPA (native 6% polyacrylamide gel) (B) Experiment as in A, but with dsDNA. (C) Quantitation of data from A and B. Averages shown ± SEM; *n* = 2. (D) DNA degradation is stimulated by hRPA. The data points from +hRPA condition are the same as in C. Averages shown ± SEM; *n* = 2. (E) Quantitation of degradation of a 3′ or 5′ ssDNA-tailed three-way junction by hDNA2. The reactions were performed in 3 mM magnesium acetate and 22.3 nM hRPA. Averages shown ± SEM; *n* = 2. (F) Kinetics of degradation of a four-way junction by hDNA2 (9 nM) in the presence of hRPA (denaturing 20% polyacrylamide gel). The substrate was labeled at the 5′ end (*). D294A, nuclease-dead variant of hDNA2. (G) Experiment as in F, but using a four-way junction labeled at the 3′ end. (H) Quantitation of DNA cleavage near (less than 15 nt) a 5′ or 3′ DNA end from experiments of F and G. Averages shown ± SEM; *n* = 2. (I) WRN and hDNA2 degrade four-way junction DNA in a synergistic manner. Reactions with indicated hDNA2 and/or WRN concentrations and 65 nM hRPA were analyzed on a 6% native polyacrylamide gel. Heat, partially heated DNA substrate indicating the positions of DNA unwinding intermediates. (J) Quantitation of four-way junction and dsDNA degradation by human EXO1 (hEXO1). Averages shown ± SEM; *n* = 2.

experiments using either 5′-end or 3′-end ^{32}P-labeled four-way junctions confirmed that human DNA2 had a strong 5′-to-3′ bias in end resection in the presence of RPA (Fig. 8, E–H; and Fig. S4, B and C). Catalytically dead DNA2 D294A had no capacity to degrade DNA, showing that the nuclease activity is inherent to WT DNA2 (Fig. 8 F). The same results were recapitulated using purified yeast DNA2 (Fig. S5, A–F). Interestingly, addition of the ATPase-deficient RECQ1 mutant (RECQ1-K119R) to the reaction mix significantly inhibited the four-way junction degradation activity of human DNA2 (Fig. S4, D and E). These results suggest that the binding of RECQ1 to stalled replication forks limits the fork processing

activity of DNA2, as inferred by our cellular studies. However, we cannot rule out the possibility that the inhibitory effect observed in the biochemical assays is simply associated with competition for substrate recognition between the two proteins. In agreement with our in vivo data, we show that WRN promoted the degradative capacity of DNA2 on nicked, gapped, or four-way junction substrates (Fig. 8 I and Fig. S4, F and G); similar behavior was observed when yeast Dna2 was coupled with the Sgs1 helicase (Fig. S5, G and H). DNA was degraded by WRN and DNA2 in a remarkably synergistic manner: 5 nM concentration of either WRN or DNA2 alone led only to a minor DNA unwinding/degradation (Fig. 8 I, lanes 2 and 8). When combined, both enzymes completely degraded the four-way junction DNA (Fig. 8 I, lane 5). In contrast, no such synergy was observed when human DNA2 was combined with the noncognate yeast meiotic Mer3 helicase (Fig. S4 H), suggesting that the species-specific interaction between DNA2 and WRN results in a vigorous DNA degradation. Similarly, WT RECQ1 did not promote DNA degradation by DNA2 (Fig. S4 I).

On the basis of our results that DNA2 does not share the same function of EXO1 in reversed fork processing, we decided to compare the end-resection activities of human DNA2 and human EXO1 using the four-way junction substrates. EXO1—unlike DNA2—degraded both four-way junction substrates and linear duplexes with equal efficiency (Fig. 8 J and Fig. S4, J and K). The use of yeast variants of Dna2 and Exo1 yielded analogous results (Fig. S5, I–K). Collectively, these studies further implicate DNA2, and its nuclease activity, in reversed replication fork degradation—that is specifically stimulated by WRN—and point to an important difference in substrate preference between DNA2 and EXO1. Moreover, the polarity of reversed fork degradation by DNA2 measured in the presence of RPA displays the same bias anticipated from the EM analysis of the replication intermediates.

Discussion

The present work uncovers a new mechanism for reversed fork processing and restart that requires the coordinated activities of the human DNA2 nuclease and WRN helicase (Fig. 9). The DNA2-dependent end resection leads to partially single-stranded reversed forks and is required for efficient replication fork restart under conditions of persistent replication blockage. WRN interacts with DNA2 and its ATPase activity is needed for DNA2-dependent degradation, presumably to transiently open the dsDNA arm of the reversed replication forks.

To date, we have identified two mechanisms of reversed replication fork resolution, one dependent on RECQ1 ATPase and branch migration activity (Berti et al., 2013) and the other on DNA2 nuclease and WRN ATPase activity. Moreover, the DNA2/WRN mechanism is tightly regulated by an ATPase-independent function of RECQ1 that might limit DNA2 activity by binding to reversed forks. Of note, our EM experiments show that reversed replication forks accumulate in RECQ1- and DNA2-depleted cells also in unperturbed conditions suggesting that fork reversal is remarkably frequent when DNA replication faces intrinsic replication fork obstacles, and that RECQ1 and DNA2 have a conserved role in restarting reversed forks in unperturbed S-phase.

DNA2 function during DNA replication is vital for maintenance of genome stability (this study; Duxin et al., 2012; Karanja et al., 2012). These findings indicate that the controlled DNA2-dependent degradation of reversed replication forks is a physiologically relevant mechanism to provide resistance to prolonged genotoxic treatments. This mechanism is distinct from the pathological MRE11-dependent degradation of stalled replication intermediates detected in the absence of crucial Fanconi Anemia (FA)/HR factors (Schlacher et al., 2011, 2012; Hashimoto et al., 2012; Ying et al., 2012).

We find that depletion of the central recombinase factor RAD51 prevents nascent strand degradation. This finding, coupled with the recent observation that RAD51 is directly implicated in reversed fork formation (Zellweger et al., 2015), reinforce our conclusion that the DNA2-dependent pathway starts from the reversed arm of stalled replication forks and acts downstream of the RAD51-mediated replication fork reversal. Given that RAD51 is required for reversed fork formation (Zellweger et al., 2015), we speculate that the MRE11-dependent pathway is only uncovered in the absence of fork reversal—i.e., via a perturbation in RAD51 function—and likely attacks unprotected and nonreversed forks upon prolonged stalling. A crucial challenge for future studies will be to investigate why we do not observe a contribution of the MRE11 pathway in nascent strand degradation upon RAD51 depletion. It is tempting to speculate that RAD51 depletion might interfere with MRE11-dependent fork processing, in addition to preventing fork reversal. Conversely, perturbation of RAD51 function—e.g., via BRCA2 depletion (Schlacher et al., 2011)—might be sufficient to prevent fork reversal—hence DNA2-dependent degradation—but still allow residual RAD51 loading to promote MRE11-dependent degradation.

Our DNA fiber analysis suggests that DNA2 degrades stalled replication intermediates beyond the maximum length of the reversed arms measured by EM (up to several kilobases). A possible interpretation of these results is that after the initial DNA2/WRN-mediated regressed arm degradation is complete, other nucleolytic activities or DNA2 itself may codegrade both sides of the replication fork, thus leading to extensive degradation events detectable by DNA fibers. In this scenario, our EM images likely represent snapshots of the "slow steps" of this reaction—i.e., the DNA2/WRN-mediated degradation of the regressed arms—resulting in the drastic increase in reversed fork frequency observed in the absence of DNA2. Once the regressed arm has been resolved, the nucleolytic degradation might quickly proceed to degrade nascent strands behind the junction—as suggested by the DNA2-dependent increase in ssDNA gaps behind the observed forks—finally leading to reannealing of the parental strands and backtracking of the fork (Fig. S3 E). A new reversal event may occur when this extensive degradation leads to asymmetric ssDNA accumulation at the fork (Zellweger et al., 2015), resetting the backtracked fork to the slow step of the process. However, fork backtracking is only one possible model to explain the extensive degradation detected by DNA fibers and further work would be required to uncover additional nucleolytic activities that might be involved in this process.

Biochemical studies suggested that *Schizosaccharomyces pombe* Dna2 cleaves the leading and lagging reversed strands of

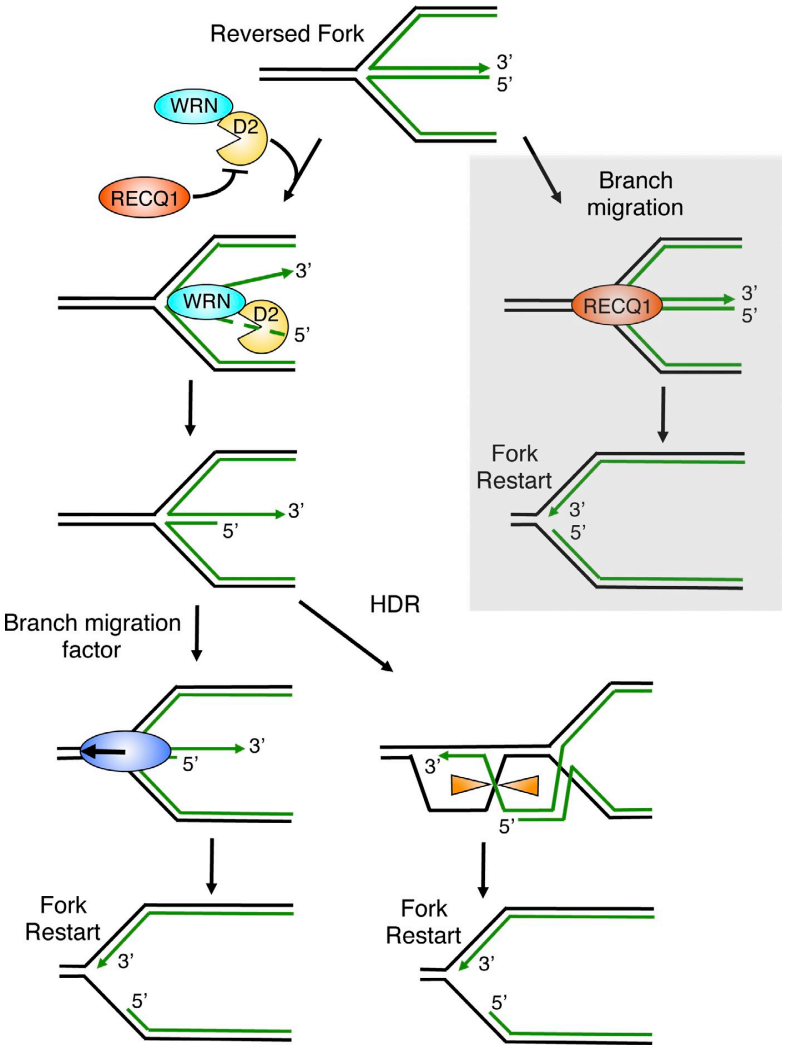

Figure 9. **Schematic model for the combined roles of DNA2 and WRN in reversed fork processing.** DNA2 and WRN functionally interact to process reversed forks. DNA2 degrades reversed forks with a 5′-to-3′ polarity. WRN ATPase activity assists DNA2 degradation possibly by promoting the opening of the reversed arm of the fork. RECQ1 limits DNA2 activity by an ATPase-independent function. Branch migration factors specifically recognize the partially resected reversed forks to promote fork restart. Alternatively, the newly formed 3′ overhang of the reversed fork invades the duplex ahead of the fork, resulting in Holliday junction structures that can be resolved by specific resolvases or dissolvases to promote fork restart. Gray box, RECQ1 can independently restart reversed forks by virtue of its ATPase and branch migration activity.

a model replication fork with similar efficiency in the absence of replication protein A (Hu et al., 2012). However, it is likely that only the 5′-to-3′ directionality is important in vivo, because RPA is known to stimulate the 5′-to-3′ and inhibit the 3′-to-5′ nuclease activity of yeast DNA2 (Cejka et al., 2010; Niu et al., 2010). In agreement with this conclusion, our biochemical data show that DNA2-dependent end resection proceeds with a 5′ to 3′ polarity in the presence of RPA. Moreover, our EM experiments clearly show that DNA2 depletion affects the frequency of reversed forks that are either entirely or partially single-stranded supporting the notion that DNA2-dependent degradation of reversed forks occurs with a preferential polarity in vivo.

The resection activity of human DNA2 was postulated to activate the ATR/Chk1 checkpoint under conditions of replication stress (Karanja et al., 2012). Indeed, we find that DNA2 depletion prevents ATR checkpoint activation after HU treatment. Moreover, the increased origin firing observed upon DNA2 depletion is consistent with observations that the deregulation of checkpoint activity leads to a large increase in the number of newly initiated origins (Couch et al., 2013). However, the extent of ATR activation does not necessarily reflect the amount of ssDNA detected at replication forks, whether at the junction, at ssDNA gaps, or at regressed arms (Zellweger et al., 2015). In light of these findings, we rather suggest that DNA2-dependent ATR activation may reflect DNA2 recruitment to the stalled forks per se, or subtle changes of fork architecture that are associated with its recruitment but possibly escape our EM analysis. This interpretation is supported by the recent discovery that yeast Dna2 has a direct role in Mec1 activation (the ortholog of human ATR), independent from its nuclease or helicase activity (Kumar and Burgers, 2013). Of note, the increased origin firing frequency observed upon DNA2 depletion is not associated to a parallel increase in the frequency of termination events (Fig. S1 A) possibly because the defects in replication fork restart associated

with DNA2 depletion limit the number of termination events even under conditions of increased origin firing.

WRN plays an important—albeit mechanistically ill-defined—role in the recovery from replication blockage, and mutations in the *WRN* gene are linked to the cancer predisposition disorder Werner Syndrome (Sidorova et al., 2008; Murfuni et al., 2012). Our studies infer that the high genomic instability of WRN-deficient cells may result from aberrant processing of reversed replication intermediates. In particular, given the consolidated role of WRN at difficult-to-replicate regions—e.g., telomeres and fragile sites (Crabbe et al., 2004; Murfuni et al., 2012)—we speculate that WRN, in conjunction with DNA2, is required to process reversed forks arising spontaneously at these genomic loci. Biochemical studies pointed to a putative role of WRN in fork reversal and/or restart by showing that WRN efficiently promotes both the formation and restoration of oligonucleotide-based reversed fork substrates (Machwe et al., 2011). We show that WRN ATPase activity is needed for the DNA2-dependent degradation of reversed replication forks. Our interpretation for the role of WRN ATPase activity is that it facilitates DNA2-dependent degradation of the reversed forks by transiently opening the dsDNA arm of the reversed fork. This mechanism is reminiscent to the DNA2-dependent mechanism of DSB resection where the yeast Sgs1 helicase is required to transiently open the DNA duplex to generate a 5′ ssDNA tail that is in turn degraded by DNA2 (Zhu et al., 2008; Cejka et al., 2010; Niu et al., 2010). We suggest that WRN is the functional homologue of Sgs1 in mammalian cells, at least in the context of DNA2-dependent reversed replication fork processing. However, BLM was also shown to interact and cooperate with DNA2 to resect dsDNA ends in vitro opening the possibility that other human RecQ helicases might substitute for WRN, depending on the nature of the DNA lesion being processed or the particular cellular context (Nimonkar et al., 2011; Sturzenegger et al., 2014). This mechanism seems to be well-conserved throughout evolution because it is highly reminiscent of the stalled fork processing pathway described in *E. coli* where the RecJ nuclease cooperates with bacterial RecQ to process blocked replication intermediates (Courcelle et al., 2003). In addition, the prokaryotic RecBCD helicase-nuclease plays an important role in resecting replication forks after reversal (Seigneur et al., 1998) and DNA2 is of the same family of nucleases as RecB. Whether the DNA2/WRN-mediated resection activity can degrade additional stalled replication intermediates other than reversed forks is worth future investigation.

EXO1, MRE11, and CtIP play central roles in DNA repair and are also implicated in the recovery from replication fork blockage (Cotta-Ramusino et al., 2005; Schlacher et al., 2011; Yeo et al., 2014). None of these nucleases, however, participates in the DNA2-dependent processing of reversed replication forks pointing to a specific role of DNA2 that, unlike its function in DSB resection, is not shared by other nucleases. A possible interpretation of these results is that the reversed forks are characterized by a particular structure of the terminal end that does not require the trimming activity of other nucleases to promote DNA2-dependent resection. However, some of these nucleases might still be able to access stalled forks under specific genetic backgrounds. For example, MRE11 degrades stalled replication intermediates only in a BRCA2-deficent background, as already discussed (Schlacher et al., 2011). Moreover, the cleavage of unresolved replicative intermediates by the structure-specific MUS81 endonuclease is a late response to replicative stress, which becomes activated only when other attempts to overcome stalled replication have been exhausted (Hanada et al., 2007; Franchitto et al., 2008). Thus, MUS81 might still resolve reversed replication forks as a back-up system to unlink sister chromatids and facilitate mitotic segregation in the absence of DNA2 or WRN.

Collectively, these studies highlight a new important mechanism for the recovery from replication blockage. This mechanism relies on the DNA2-dependent processing of reversed forks—leading to ssDNA stretches on the regressed arms—which appear to promote efficient fork restart. A possible explanation for the need of partially single-stranded DNA structures to promote fork restart is that they represent a key intermediate to activate an HDR-like mechanism of reversed fork restart, as recently proposed in *S. pombe* (Carr and Lambert, 2013). In particular, the newly formed 3′ overhang of the reversed fork might invade the duplex ahead of the fork resulting in Holliday junction structures that can be resolved by specific resolvases or dissolved by the combined action of the BLM helicase (Sgs1 in yeast) and the type I topoisomerase TOP3 (Fig. 9). Alternatively, resumption of DNA replication might be obtained by reverse branch migration, where the partially resected reversed fork structures might be specifically recognized by a motor protein—e.g., SMARCAL1 (Béous et al., 2013) or a human RecQ helicase—to promote the branch migration-assisted reestablishment of a functional replication fork.

Materials and methods

Cell lines, culture conditions, and reagents

U-2 OS, HEK 293, and Werner Syndrome fibroblast (AG11395) cells were grown in DMEM supplemented with 10% FBS at 37°C in 5% CO_2. HCT116 cells were grown in McCoy's 5A medium supplemented with 10% FBS. CldU, IdU, BrdU, hydroxyurea, mitomycin C, camptothecin, tamoxifen, puromycin, and hygromycin were obtained from Sigma-Aldrich.

DNA2 conditional knockout HCT116 cells

To examine the response of cells to the complete absence of DNA2, we used a DNA2 conditional knockout cell line where exon 2 of the DNA2 gene is deleted (Karanja et al., 2014). The colorectal carcinoma HCT116 cell line carries 3 copies of DNA2 due to a duplication on chromosome 10. Two chromosomal copies were disrupted using rAAV-mediated gene targeting technology and exon 2 of the third allele was replaced with a conditional exon where the exon was flanked by loxP sites (DNA2flox/−/−). To create a conditional cell line these cells were stably transduced with a tamoxifen (4-OHT)-inducible Cre recombinase. Thus, the cell line is viable and can be propagated. The addition of tamoxifen to the culture media leads to excision of the endogenous DNA2 and the generation of a true DNA2-null cell. Complete loss of DNA2 occurs after 72 h of tamoxifen treatment. However, the DNA fiber experiments were performed after 40 h of tamoxifen treatment to have enough S-phase cells for DNA labeling.

Antibodies

Anti-DNA2 rabbit polyclonal (ab96488; 1:1,000), anti-MUS81 mouse monoclonal (ab14387; 1:1,000), and anti-CldU/BrdU rat monoclonal (ab6326; 1:6) antibodies (all from Abcam); anti-CtIP rabbit polyclonal (A300-488A; 1:1,000), anti-EXO1 rabbit polyclonal (A302-639A; 1:1,000), anti-pRPA32 (S4/S8) rabbit polyclonal (A300-245A; 1:1,000), and anti-pRPA32 (S33) rabbit polyclonal (300-246A; 1:2,000; all from

Bethyl); anti-WRN rabbit polyclonal (NB100-471; 1:1,000); and anti-MRE11 rabbit polyclonal (NB100-142; 1:2,000; Novus); anti-RAD51 (H-92) rabbit polyclonal (sc-8349; 1:1,000) and anti-RECQ1 rabbit polyclonal (sc-25547; 1:2,000) from Santa Cruz; anti-rat Alexa (594-A11007; 1:1,000); and anti–mouse Alexa Flour (488-A11001; 1:1,000; Invitrogen); anti-rabbit (31460; 1:10,000; Thermo Fisher Scientific); anti-tubulin mouse monoclonal (T5168; 1:5,000; Sigma-Aldrich); anti-IdU/BrdU mouse monoclonal (347580; 1:6) from BD; anti-Chk1 mouse monoclonal (sc-8408; 1:1,000; Santa Cruz Biotechnology, Inc.); anti-p-Chk1 (S345) rabbit monoclonal (2348; 1:1,000; Cell Signaling Technology); anti-RPA32 mouse monoclonal (NA19L; 1:1,000) from EMD Millipore; anti-RECQ1 rabbit polyclonal, raised against residues 634–649 of human RECQ1, is custom made (Mendoza-Maldonado et al., 2011); anti-BLM rabbit polyclonal, raised against residues 1–449 of human BLM (Wu and Hickson, 2003), was a gift from I. Hickson (University of Copenhagen, Copenhagen, Denmark); and anti-RECQ4 rabbit polyclonal, raised against residues 60–111 of human RECQ4 (Yin et al., 2004), was a gift from W. Wang (National Institute on Aging, Baltimore, MD).

Recombinant proteins

Yeast Dna2 was expressed in yeast WDH668 strain from pGAL:DNA2 vector (Budd et al., 2000) and purified as previously described (Levikova et al., 2013). In brief, the cells were lysed and Dna2 was purified by affinity chromatography on Ni-NTA agarose (QIAGEN) and anti-Flag M2 affinity gel (Sigma-Aldrich). Yeast RPA was expressed in yeast BJ5464 strain containing three plasmids coding for Rfa1, Rfa2, and Rfa3 and purified as previously described (Kantake et al., 2003). In brief, the cells were lysed and yeast RPA was purified by affinity on ssDNA cellulose column (USB corporation) and by ion exchange chromatography using HiTrap Q column (GE Healthcare). Human DNA2 was expressed in Sf9 cells from a pFastBac:hDNA2 vector (polyhedrin promoter) provided by J. Campbell (Masuda-Sasa et al., 2006). The soluble extracts were obtained by salt extraction as previously described for Sgs1 (Cejka and Kowalczykowski, 2010). The subsequent purification of hDNA2 was performed as previously described for yeast Dna2 (Levikova et al., 2013) by affinity chromatography using Ni-NTA agarose (QIAGEN) and Anti-Flag M2 affinity gel (Sigma-Aldrich). Human RPA was expressed from p11d-tRPA vector (Henricksen et al., 1994) in BL21 *E. coli* cells and purified as described (Henricksen et al., 1994). In brief, hRPA was first bound to HiTrap Blue column (GE healthcare) and then to HiTrap Q column. The sequence coding for yeast Mer3 helicase was amplified from yeast genomic DNA (SK1 strain) using primers Mer3FO (5′-GCGCGCGGGCCCATGAAAACAAAGTTTGATCGCCTCGGTACAGGAAAAAGAAGTAGACCCTCTCCAAATAATATTGACTTTAACGACCAG-3′) and Mer3RE (5′-CGCGCGCTCGAGTTCAAACTCTATATCGGAAC-3′). The PCR product was digested with ApaI and XhoI restriction endonucleases (both from New England Biolabs) and cloned into corresponding sites in pFB-MBP-Sgs1-his after the polyhedrin promoter, creating pFB-MBP-Mer3-his vector. Mer3 was then expressed in Sf9 cells and purified using affinity chromatography as previously described for Sgs1 (Cejka and Kowalczykowski, 2010). In brief, MBP-tagged Mer3 was first bound to amylose resin (New England Biolabs), eluted and digested with PreScission protease to cleave the MBP tag. Mer3 was further purified by affinity on Ni-NTA agarose (QIAGEN) exploiting the 10x His-tag at its C-terminus. Sequence information is available on request.

Genetic knock-down-rescue experiments

RECQ1, DNA2, and RAD51 genetic knockdown-rescue experiments were performed using the procedure described (Berti et al., 2013; Yata et al., 2012). In brief, RECQ1 is depleted using the pLKO.1-puro-shRECQ1 (5′-GAGCTTATGTTACCAGTTA-3′) construct and rescue experiments are performed using the shRNA resistant pIRES-RECQ1-WT or K119R (ATPase dead) constructs as described (Berti et al., 2013). DNA2 is depleted using an siRNA targeting the 3′UTR of DNA2 (5′-CAGUAUCUCCUCUAGCUAG-3′). At least one isoform of DNA2 is not targeted by this sequence. DNA2 rescue experiments are performed using the pBabe-hygro-3xFLAG-DNA2 WT, D294A (Nuclease dead), or K671E (helicase dead) constructs. RAD51 is depleted using siRNAs targeting the 3′UTR (5′-GACUGCCAGGAUAAAGCUU-3′ and 5′-GUGCUGCAGCCUAAUGAGA-3′) in U-2 OS stable cell lines expressing WT RAD51 as described (Yata et al., 2012). WRN depletions were achieved using pRS-puro-shWRN (5′-AGGCAGGTGTAGGAATTGAAGGAGATCAG-3′; sequence ID: TI333414) and exogenous expression is done with the shRNA resistant Flag-pCMVTag2B-WRN WT or K577M (helicase dead) constructs. Constructs for WRN depletion and overexpression of WT WRN and ATPase-deficient WRN (WRN-K577M) were kind gifts from Dr. Pietro Pichierri (Insituto Superiore di Sanità, Rome, Italy). All transfections were done with Lipofectamine 2000 (Life technologies Catalog no: 11668027). An shRNA targeting luciferase (5′-ACGCTGAGTACTTCGAAATGT-3′) was used for control shRNA experiments. The silencer select negative control (Life technologies, Catalog no. 4390843) or an siRNA targeting luciferase (5′-CGUACGCGGAAUACUUCGA-3′) were used for control siRNA experiments, as indicated. Lentiviral mediated shRNA depletions were achieved using the following sequences cloned into the pLKO.1 lentiviral shRNA expression vector: BLM (5′-CGAAGGAAGTTGTATGCACTA-3′), WRN (5′-GCTGGCAATTACCAGAACAAT-3′), and MUS81 (5′-CACGCGCTTCGTATTTCAGAA-3′). The procedure for lentiviral generation and transduction has been described (Berti et al., 2013). Transduced U-2 OS cells were selected with 6 µg/ml puromycin. siRNA-mediated depletions were achieved using the following siRNAs from Invitrogen: DNA2 (5′-AUAGCCAGUAGUAUUCGAU-3′), CtIP (5′-CGAAUCUUAGAUGCACAAA-3′), EXO1 (Invitrogen-HSS113557), and RAD51 (Invitrogen-1299001). In brief, siRNAs were transfected using Lipofectamine RNAiMAX (Life Technologies) following the manufacturer's protocol. MRE11 (5′-GAAAGGCUCUAUCGAAUGU-3′) and RECQ4 (SMART pool) siRNAs were from Dharmacon and were transfected as previously described (Thangavel et al., 2010).

Microfluidic-assisted DNA fiber stretching

For DNA replication fork restart analysis, asynchronous cells were pulse-labeled with 50 µM CldU for 20–30 min. 2 mM HU, 300 nM MMC, or 150 nM CPT was added to the CldU containing media and incubated for the indicated times. Cells were washed three times with medium and released with 50 µM IdU for 40 min. For nascent strand degradation analysis, asynchronous cells were pulse-labeled with 50 µM IdU for 45 min, washed three times with medium, incubated with 4 mM HU, 100 nM CPT, 200 nM MMC, or medium for times indicated. The pulse-labeled cells were trypsin collected and lysed in agarose plugs to prevent any mechanical breakage of replication tracts. Microfluidic platform for stretching the high-molecular weight DNA, coverslips, immunostaining and image acquisition of replication tracts were performed as described (Sidorova et al., 2009; Berti et al., 2013). In brief, polydimethylsiloxane (PDMS) stamps with microchannels were Oxygen plasma treated and reversibly sealed to the silanized coverslips. High-molecular weight DNA was loaded and stretched by capillary force into the microchannels. PDMS stamps were peeled-off and coverslips were left drying overnight. For immunostaining, DNA-stretched coverslips were denatured (2.5N HCL for 45 min), neutralized (0.1 M sodium borate and 3 washes with PBS), blocked (5% BSA and 0.5% Tween 20 in PBS for 30 min), incubated with primary antibodies (Anti-IdU/BrdU or both anti-IdU/BrdU and anti-CldU/BrdU for 30 min), washed (1% BSA and 0.1% Tween 20 in PBS, 3 times 5 min each) and incubated with secondary antibodies (anti–mouse Alexa Fluor 488-conjugated, or both anti–mouse Alexa Fluor 488–conjugated and anti–rat Alexa Fluor 594–conjugated for 1 h). Washed slides were mounted in prolong gold anti-fade reagent (Life Technologies) and images were sequentially acquired (for double-label) with LAS AF software using TCS SP5 confocal microscope (Leica). A 63×/1.4 oil immersion objective was used. Images were captured at room temperature. $n \geq 300$ fiber tracts scored for each dataset. The DNA tract lengths were measured using ImageJ and the pixel length values were converted into micrometers using the scale bars created by the microscope. Statistical analysis was done using GraphPad Prism.

Clonogenic survival assay

Colony-forming assays were performed as previously described (Franken et al., 2006). In brief, 1,000 cells were plated per well and treated on the next day with 4 mM HU for 3, 6, and 8 h or 100 nM CPT for 6 h. Colonies were fixed, stained, and quantified 10 d after release from genotoxic stress. The plating efficiency and survival fraction were calculated as previously described (Franken et al., 2006). In brief, colonies were counted using an inverted stereomicroscope and the plating efficiency was calculated using the following formula: Plating Efficiency (PE) = (no. of colonies formed/no. of cells seeded) × 100%. From the plating efficiency, the surviving fraction (SF) was calculated as: SF = (no. of colonies formed after treatment/no. of cells seeded) × PE. The experiments were performed in triplicate and the statistical analysis was performed using GraphPad Prism.

Western blotting

Cells were washed with PBS and lysed either in standard RIPA buffer (PBS, 1% NP-40, 0.5% sodium deoxycholate, 0.1% SDS, 10 µg/ml aprotinin, 10 µg/ml PMSF, 1 mM Na_3VO_4, and 1 mM NaF) or MCL buffer (50 mM Tris, pH 8.0, 5 mM EDTA, 0.5% NP-40, 100 mM NaCl, 2 mM DTT, and freshly added protease and phosphatase inhibitors from Roche (1 tablet/10 ml of buffer). Cell lysates were resolved by SDS-PAGE and transferred to

PVDF membrane (GE Healthcare). Incubation with antibodies was performed overnight at 4°C. Proteins were visualized using ECL (Thermo Fisher Scientific) according to the manufacturer's instructions.

Co-immunoprecipitation experiments

HEK293T cells were transfected with empty vectors, FLAG-DNA2, and Strep-HA-WRN by calcium phosphate. 48 h after transfection, cells were treated with 4 mM HU for 3 h, lysed in benzonase lysis buffer (50 mM Tris-HCl, pH 7.5, 75 mM KCl, 2 mM $MgCl_2$, 20 mM NaF, 10 mM β-glycerophosphate, 0.2 mM Na_3VO_4, and 0.2% Triton X-100) supplemented with protease inhibitors (EDTA-free tablet; Sigma-Aldrich) by passing 10 times through a 26-G syringe needle and incubated 1 h at 4°C with 2 U/µl Benzonase (Sigma-Aldrich) to digest genomic DNA. KCl and EDTA concentrations were adjusted to 120 and 3 mM, respectively, and lysates were centrifuged at 14,000 rpm for 30 min. Immunoprecipitations of clarified lysates were performed with FLAG M2 or HA affinity agarose resin (Sigma-Aldrich) overnight at 4°C. Beads were washed 5 times with wash buffer (50 mM Tris-HCl, pH 7.5, 150 mM KCl, 3 mM EDTA, 2 mM $MgCl_2$, 20 mM NaF, 10 mM β-glycerophosphate, 0.2 mM Na_3VO_4, and 0.2% Triton X-100) and bound proteins were eluted by boiling in SDS-PAGE sample buffer.

EM analysis of genomic DNA in mammalian cells

EM analysis of replication intermediates has been described in detail (Ray Chaudhuri et al., 2012; Neelsen et al., 2014), including a description of the important parameters to consider specifically for the identification and the scoring of reversed forks (Neelsen et al., 2014). In brief, 5–10 × 10^6 U-2 OS cells were harvested and genomic DNA was cross-linked by two rounds of incubation in 10 µg/ml 4,5′,8-trimethylpsoralen (Sigma-Aldrich) and 3 min of irradiation with 366 nm UV light on a precooled metal block. Cells were lysed and genomic DNA was isolated from the nuclei by proteinase K (Roche) digestion and phenol-chloroform extraction. DNA was purified by isopropanol precipitation, digested with PvuII HF in the proper buffer for 3–5 h at 37°C, and replication intermediates were enriched on a benzoylated naphthoylated DEAE–cellulose (Sigma-Aldrich) column. EM samples were prepared by spreading the DNA on carbon-coated grids in the presence of benzyl-dimethyl-alkylammonium chloride and visualized by platinum rotary shadowing. Images were acquired on a transmission electron microscope (JOEL 1200 EX) with side-mounted camera (AMTXR41 supported by AMT software v601) and analyzed with ImageJ (National Institutes of Health).

Preparation of oligonucleotide-based DNA substrates

DNA oligonucleotides were purchased from Microsynth and ^{32}P-labeled either at the 5′ terminus with [γ-^{32}P] ATP and T_4 polynucleotide kinase (New England Biolabs), or at the 3′ end with [α-^{32}P] cordycepin-5′-triphosphate and terminal transferase (New England Biolabs) according to manufacturer's instructions. Unincorporated nucleotides were removed using MicroSpin G25 columns (GE Healthcare). The substrates were prepared by heating the respective oligonucleotides at 95°C and gradually cooling to room temperature. The following oligonucleotides were used for the preparation of the four-way junction (X12-3 TOP L, HJ 1, HJ 2, and HJ 3), three-way junction with 3′ tail (X12-3 TOP L, HJ 1, HJ 2Sb, and HJ 3), three-way junction with 5′ ssDNA tail (X12-3 TOP L, HJ 1S, HJ 2, and HJ 3), nicked four-way junction (X12-3 TOP L, HJ 1, HJ 2Sa, HJ 2Sb, and HJ 3), replication fork (X12-3 TOP L, HJ 1S, HJ 2Sb, and HJ 3), and dsDNA (X12-3 TOP L and Bottom LC), respectively. The sequences of the oligonucleotides were: X12-3 TOP L (93 nt), 5′-GACGTCATAGACGATTACATTGCTAGGACATGCTGTCTAGAGACTATC-GCGACTTACGTTCCATCGCTAGGTTATTTTTTTTTTTTTTTTTT-3′ X12-3 HJ 1 (93 nt), 5′-AAAAAAAAAAAAAAAAAAAATAACCTAGCGATGGAACGTA-AGTCGCGATGGGCTTAACTAGGATGCTACTGGCCCCGAATCAACCGT-ACTTGGG-3′ X12-3 HJ 1S (48 nt), 5′-AAAAAAAAAAAAAAAAAAAT-AACCTAGCGATGGAACGTAAGTCGCGAT-3′ X12-3 HJ 2 (93 nt), 5′-CCCAAGTACGGTTGATTCGGGGCCAGTAGCATCCTAGTTAAGCCCA-TTACGATTCGTTACCCATTCACTGTCAGAAGGCACCAGATAGATCTC-3′ X12-3 HJ 2Sa (45 nt), 5′-CCCAAGTACGGTTGATTCGGGGCCAGTAGCA-TCCTAGTTAAGCCC-3′ X12-3 HJ 2Sb (48 nt), 5′-ATTACGATTCGTTACCC-ATTCACTGTCAGAAGGCACCAGATAGATCTC-3′ X12-3 HJ 3 (93 nt), 5′-GAGATCTATCTGGTGCCTTCTGACAGTGAATGGGTAACGAATCGT-AATAGTCTCTAGACAGCATGTCCTAGCAATGTAATCGTCTATGACGTC-3′ X12-3 BOTTOM LC, 5′-AAAAAAAAAAAAAAAAAAAATAACCTAGCGAT-GGAACGTAAGTCGCGATAGTCTCTAGACAGCATGTCCTAGCAATGTA-ATCGTCTATGACGTC-3′.

Nuclease assays

The experiments were performed in a 15-µl volume in 25 mM Tris-acetate (pH 7.5), 2 mM magnesium acetate, 1 mM ATP, 1 mM dithiothreitol, 0.1 mg/ml BSA (New England Biolabs), 1 mM phosphoenolpyruvate, 80 U/ml pyruvate kinase, 1 nM DNA substrate (molecules), and recombinant proteins, as indicated. The reactions were assembled on ice and incubated for 30 min at 30°C for yeast proteins and at 37°C for human proteins. Unless indicated otherwise, RPA was present in the reactions at saturating concentrations corresponding to a threefold excess over DNA, assuming all DNA was single-stranded and a DNA-binding site size of 25 nt for hRPA and of 20 nt for yRPA. The reactions were terminated by adding 5 µl Stop buffer (150 mM EDTA, 2% SDS, 30% glycerol, and 0.01% bromophenol blue), incubated for 30 min at room temperature and separated on polyacrylamide gels in TBE buffer under native conditions. Alternatively, for denaturing conditions, the reaction were terminated by adding 15 µl Formamide stop buffer (95% (vol/vol) formamide, 20 mM EDTA, 0.01% bromophenol blue), denatured by heating at 95°C for 5 min and separated on 20% denaturing polyacrylamide gels in TBE buffer. Gels were fixed, dried, exposed to a storage phosphor screen, and analyzed on Typhoon phosphor imager (GE Healthcare).

Online supplemental material

Fig. S1 shows quantification of stalled forks, new origins, and termination events in DNA2-depleted cells upon genotoxic stress induction, as well as the statistical analysis of IdU tracts from RECQ1-, DNA2-, WRN-, RECQ1/DNA2-, RECQ1/WRN-, WRN/DNA2-, and RECQ1/WRN/DNA2-depleted U-2 OS cells. Fig. S2 shows the IdU tract length distribution in BLM- and RECQ4-depleted cells, respectively, as well as statistical analysis of IdU tracts from RECQ1/WRN-codepleted cells complemented with WT WRN or with ATPase-deficient WRN. Fig. S3 shows additional EM analysis, as well as the Western blot analysis of ATR-checkpoint activation in RECQ1- and/or DNA2-depleted U-2 OS cells. Fig. S4 shows additional biochemical analysis of substrate specificity of human DNA2 and human EXO1. TFig. S5 shows biochemical assays of substrate specificity of yeast Dna2 and yeast Exo1. Online supplemental material is available at http://www.jcb.org/cgi/content/full/jcb.201406100/DC1.

We are grateful to Pietro Pichierri (Istituto Superiore di Sanità, Rome) for providing the WS cells and WRN constructs, Damian Dalcher for his help with the EM analysis, Stephanie Felscher (University of Zurich) for kindly providing human EXO1 protein, Marc Wold (University of Iowa) for human RPA expression construct, Lepakshi Ranjha (University of Zurich) for Mer3 protein, Fumiko Esashi (University of Oxford) for the Rad51 siRNAs and the U-2 OS cells stably expressing exogenous RAD51, and Judith Campbell (California Institute of Technology) for human and yeast DNA2/Dna2 expression constructs. We thank the Research Microscopy Core Facility of Saint Louis University for technical support.

This work was supported by National Institutes of Health grant R01GM108648 to A. Vindigni, by startup funding from the Doisy Department of Biochemistry and Molecular Biology and from the Saint Louis University Cancer Center to A. Vindigni, by grants from the President's Research Fund of Saint Louis University and by the GLIOMA-Interreg (Slovenian-Italian Cooperation 2007-2013) project to A. Vindigni, by the Swiss National Science Foundation grants 31003A_146924 to M. Levikova and PP00P3 133636 to P. Cejka, by National Institutes of Health grant GM0088351 and CA15446 to E.A. Hendrickson, and by a research contract from Horizon Discovery, Ltd to E.A. Hendrickson. M. Berti was supported by an EMBO short-term fellowship to perform EM experiments in M. Levikova laboratory.

The authors declare no competing financial interests.

Submitted: 24 June 2014
Accepted: 14 January 2015

References

Atkinson, J., and P. McGlynn. 2009. Replication fork reversal and the maintenance of genome stability. *Nucleic Acids Res.* 37:3475–3492. http://dx.doi.org/10.1093/nar/gkp244

Ayyagari, R., X.V. Gomes, D.A. Gordenin, and P.M. Burgers. 2003. Okazaki fragment maturation in yeast. I. Distribution of functions between FEN1 AND DNA2. *J. Biol. Chem.* 278:1618–1625. http://dx.doi.org/10.1074/jbc.M209801200

Bae, S.H., K.H. Bae, J.A. Kim, and Y.S. Seo. 2001. RPA governs endonuclease switching during processing of Okazaki fragments in eukaryotes. *Nature.* 412:456–461. http://dx.doi.org/10.1038/35086609

Berti, M., A. Ray Chaudhuri, S. Thangavel, S. Gomathinayagam, S. Kenig, M. Vujanovic, F. Odreman, T. Glatter, S. Graziano, R. Mendoza-Maldonado, et al. 2013. Human RECQ1 promotes restart of replication forks reversed by DNA topoisomerase I inhibition. *Nat. Struct. Mol. Biol.* 20:347–354. http://dx.doi.org/10.1038/nsmb.2501

Bétous, R., A.C. Mason, R.P. Rambo, C.E. Bansbach, A. Badu-Nkansah, B.M. Sirbu, B.F. Eichman, and D. Cortez. 2012. SMARCAL1 catalyzes fork regression and Holliday junction migration to maintain genome stability during DNA replication. *Genes Dev.* 26:151–162. http://dx.doi.org/10.1101/gad.178459.111

Bétous, R., F.B. Couch, A.C. Mason, B.F. Eichman, M. Manosas, and D. Cortez. 2013. Substrate-selective repair and restart of replication forks by DNA translocases. *Cell Reports*. 3:1958–1969. http://dx.doi.org/10.1016/j.celrep.2013.05.002

Budd, M.E., and J.L. Campbell. 1995. A yeast gene required for DNA replication encodes a protein with homology to DNA helicases. *Proc. Natl. Acad. Sci. USA*. 92:7642–7646. http://dx.doi.org/10.1073/pnas.92.17.7642

Budd, M.E., and J.L. Campbell. 1997. A yeast replicative helicase, Dna2 helicase, interacts with yeast FEN-1 nuclease in carrying out its essential function. *Mol. Cell. Biol.* 17:2136–2142.

Budd, M.E., W. Choe, and J.L. Campbell. 2000. The nuclease activity of the yeast DNA2 protein, which is related to the RecB-like nucleases, is essential in vivo. *J. Biol. Chem.* 275:16518–16529. http://dx.doi.org/10.1074/jbc.M909511199

Carr, A.M., and S. Lambert. 2013. Replication stress-induced genome instability: the dark side of replication maintenance by homologous recombination. *J. Mol. Biol.* 425:4733–4744. http://dx.doi.org/10.1016/j.jmb.2013.04.023

Cejka, P., and S.C. Kowalczykowski. 2010. The full-length *Saccharomyces cerevisiae* Sgs1 protein is a vigorous DNA helicase that preferentially unwinds holliday junctions. *J. Biol. Chem.* 285:8290–8301. http://dx.doi.org/10.1074/jbc.M109.083196

Cejka, P., E. Cannavo, P. Polaczek, T. Masuda-Sasa, S. Pokharel, J.L. Campbell, and S.C. Kowalczykowski. 2010. DNA end resection by Dna2-Sgs1-RPA and its stimulation by Top3-Rmi1 and Mre11-Rad50-Xrs2. *Nature*. 467:112–116. http://dx.doi.org/10.1038/nature09355

Cotta-Ramusino, C., D. Fachinetti, C. Lucca, Y. Doksani, M. Lopes, J. Sogo, and M. Foiani. 2005. Exo1 processes stalled replication forks and counteracts fork reversal in checkpoint-defective cells. *Mol. Cell*. 17:153–159. http://dx.doi.org/10.1016/j.molcel.2004.11.032

Couch, F.B., C.E. Bansbach, R. Driscoll, J.W. Luzwick, G.G. Glick, R. Bétous, C.M. Carroll, S.Y. Jung, J. Qin, K.A. Cimprich, and D. Cortez. 2013. ATR phosphorylates SMARCAL1 to prevent replication fork collapse. *Genes Dev.* 27:1610–1623. http://dx.doi.org/10.1101/gad.214080.113

Courcelle, J., J.R. Donaldson, K.H. Chow, and C.T. Courcelle. 2003. DNA damage-induced replication fork regression and processing in Escherichia coli. *Science*. 299:1064–1067. http://dx.doi.org/10.1126/science.1081328

Crabbe, L., R.E. Verdun, C.I. Haggblom, and J. Karlseder. 2004. Defective telomere lagging strand synthesis in cells lacking WRN helicase activity. *Science*. 306:1951–1953. http://dx.doi.org/10.1126/science.1103619

Duxin, J.P., H.R. Moore, J. Sidorova, K. Karanja, Y. Honaker, B. Dao, H. Piwnica-Worms, J.L. Campbell, R.J. Monnat Jr., and S.A. Stewart. 2012. Okazaki fragment processing-independent role for human Dna2 enzyme during DNA replication. *J. Biol. Chem.* 287:21980–21991. http://dx.doi.org/10.1074/jbc.M112.359018

Franchitto, A., L.M. Pirzio, E. Prosperi, O. Sapora, M. Bignami, and P. Pichierri. 2008. Replication fork stalling in WRN-deficient cells is overcome by prompt activation of a MUS81-dependent pathway. *J. Cell Biol.* 183:241–252. http://dx.doi.org/10.1083/jcb.200803173

Franken, N.A., H.M. Rodermond, J. Stap, J. Haveman, and C. van Bree. 2006. Clonogenic assay of cells in vitro. *Nat. Protoc.* 1:2315–2319. http://dx.doi.org/10.1038/nprot.2006.339

Gari, K., C. Décaillet, M. Delannoy, L. Wu, and A. Constantinou. 2008. Remodeling of DNA replication structures by the branch point translocase FANCM. *Proc. Natl. Acad. Sci. USA*. 105:16107–16112. http://dx.doi.org/10.1073/pnas.0804777105

Gravel, S., J.R. Chapman, C. Magill, and S.P. Jackson. 2008. DNA helicases Sgs1 and BLM promote DNA double-strand break resection. *Genes Dev.* 22:2767–2772. http://dx.doi.org/10.1101/gad.503108

Hanada, K., M. Budzowska, S.L. Davies, E. van Drunen, H. Onizawa, H.B. Beverloo, A. Maas, J. Essers, I.D. Hickson, and R. Kanaar. 2007. The structure-specific endonuclease Mus81 contributes to replication restart by generating double-strand DNA breaks. *Nat. Struct. Mol. Biol.* 14:1096–1104. http://dx.doi.org/10.1038/nsmb1313

Hashimoto, Y., F. Puddu, and V. Costanzo. 2012. RAD51- and MRE11-dependent reassembly of uncoupled CMG helicase complex at collapsed replication forks. *Nat. Struct. Mol. Biol.* 19:17–24. http://dx.doi.org/10.1038/nsmb.2177

Henricksen, L.A., C.B. Umbricht, and M.S. Wold. 1994. Recombinant replication protein A: expression, complex formation, and functional characterization. *J. Biol. Chem.* 269:11121–11132.

Hu, J., L. Sun, F. Shen, Y. Chen, Y. Hua, Y. Liu, M. Zhang, Y. Hu, Q. Wang, W. Xu, et al. 2012. The intra-S phase checkpoint targets Dna2 to prevent stalled replication forks from reversing. *Cell*. 149:1221–1232. http://dx.doi.org/10.1016/j.cell.2012.04.030

Kantake, N., T. Sugiyama, R.D. Kolodner, and S.C. Kowalczykowski. 2003. The recombination-deficient mutant RPA (rfa1-t11) is displaced slowly from single-stranded DNA by Rad51 protein. *J. Biol. Chem.* 278:23410–23417. http://dx.doi.org/10.1074/jbc.M302995200

Karanja, K.K., S.W. Cox, J.P. Duxin, S.A. Stewart, and J.L. Campbell. 2012. DNA2 and EXO1 in replication-coupled, homology-directed repair and in the interplay between HDR and the FA/BRCA network. *Cell Cycle*. 11:3983–3996. http://dx.doi.org/10.4161/cc.22215

Karanja, K.K., E.H. Lee, E.A. Hendrickson, and J.L. Campbell. 2014. Preventing over-resection by DNA2 helicase/nuclease suppresses repair defects in Fanconi anemia cells. *Cell Cycle*. 13:1540–1550. http://dx.doi.org/10.4161/cc.28476

Kumar, S., and P.M. Burgers. 2013. Lagging strand maturation factor Dna2 is a component of the replication checkpoint initiation machinery. *Genes Dev.* 27:313–321. http://dx.doi.org/10.1101/gad.204750.112

Kuo, C., H. Nuang, and J.L. Campbell. 1983. Isolation of yeast DNA replication mutants in permeabilized cells. *Proc. Natl. Acad. Sci. USA*. 80:6465–6469. http://dx.doi.org/10.1073/pnas.80.21.6465

Levikova, M., D. Klaue, R. Seidel, and P. Cejka. 2013. Nuclease activity of *Saccharomyces cerevisiae* Dna2 inhibits its potent DNA helicase activity. *Proc. Natl. Acad. Sci. USA*. 110:E1992–E2001. http://dx.doi.org/10.1073/pnas.1300390110

Liao, S., T. Toczylowski, and H. Yan. 2008. Identification of the Xenopus DNA2 protein as a major nuclease for the 5′->3′ strand-specific processing of DNA ends. *Nucleic Acids Res.* 36:6091–6100. http://dx.doi.org/10.1093/nar/gkn616

Machwe, A., R. Karale, X. Xu, Y. Liu, and D.K. Orren. 2011. The Werner and Bloom syndrome proteins help resolve replication blockage by converting (regressed) holliday junctions to functional replication forks. *Biochemistry*. 50:6774–6788. http://dx.doi.org/10.1021/bi2001054

Masuda-Sasa, T., O. Imamura, and J.L. Campbell. 2006. Biochemical analysis of human Dna2. *Nucleic Acids Res.* 34:1865–1875. http://dx.doi.org/10.1093/nar/gkl070

Mendoza-Maldonado, R., V. Faoro, S. Bajpai, M. Berti, F. Odreman, M. Vindigni, T. Ius, A. Ghasemian, S. Bonin, M. Skrap, et al. 2011. The human RECQ1 helicase is highly expressed in glioblastoma and plays an important role in tumor cell proliferation. *Mol. Cancer*. 10:83. http://dx.doi.org/10.1186/1476-4598-10-83

Mimitou, E.P., and L.S. Symington. 2008. Sae2, Exo1 and Sgs1 collaborate in DNA double-strand break processing. *Nature*. 455:770–774. http://dx.doi.org/10.1038/nature07312

Murfuni, I., A. De Santis, M. Federico, M. Bignami, P. Pichierri, and A. Franchitto. 2012. Perturbed replication induced genome wide or at common fragile sites is differently managed in the absence of WRN. *Carcinogenesis*. 33:1655–1663. http://dx.doi.org/10.1093/carcin/bgs206

Neelsen, K.J., A.R. Chaudhuri, C. Follonier, R. Herrador, and M. Lopes. 2014. Visualization and interpretation of eukaryotic DNA replication intermediates in vivo by electron microscopy. *Methods Mol. Biol.* 1094:177–208. http://dx.doi.org/10.1007/978-1-62703-706-8_15

Nicolette, M.L., K. Lee, Z. Guo, M. Rani, J.M. Chow, S.E. Lee, and T.T. Paull. 2010. Mre11-Rad50-Xrs2 and Sae2 promote 5′ strand resection of DNA double-strand breaks. *Nat. Struct. Mol. Biol.* 17:1478–1485. http://dx.doi.org/10.1038/nsmb.1957

Nimonkar, A.V., J. Genschel, E. Kinoshita, P. Polaczek, J.L. Campbell, C. Wyman, P. Modrich, and S.C. Kowalczykowski. 2011. BLM-DNA2-RPA-MRN and EXO1-BLM-RPA-MRN constitute two DNA end resection machineries for human DNA break repair. *Genes Dev.* 25:350–362. http://dx.doi.org/10.1101/gad.2003811

Niu, H., W.H. Chung, Z. Zhu, Y. Kwon, W. Zhao, P. Chi, R. Prakash, C. Seong, D. Liu, L. Lu, et al. 2010. Mechanism of the ATP-dependent DNA end-resection machinery from *Saccharomyces cerevisiae*. *Nature*. 467:108–111. http://dx.doi.org/10.1038/nature09318

Peng, G., H. Dai, W. Zhang, H.J. Hsieh, M.R. Pan, Y.Y. Park, R.Y. Tsai, I. Bedrosian, J.S. Lee, G. Ira, and S.Y. Lin. 2012. Human nuclease/helicase DNA2 alleviates replication stress by promoting DNA end resection. *Cancer Res.* 72:2802–2813. http://dx.doi.org/10.1158/0008-5472.CAN-11-3152

Pirzio, L.M., P. Pichierri, M. Bignami, and A. Franchitto. 2008. Werner syndrome helicase activity is essential in maintaining fragile site stability. *J. Cell Biol.* 180:305–314. http://dx.doi.org/10.1083/jcb.200705126

Ray Chaudhuri, A., Y. Hashimoto, R. Herrador, K.J. Neelsen, D. Fachinetti, R. Bermejo, A. Cocito, V. Costanzo, and M. Lopes. 2012. Topoisomerase I poisoning results in PARP-mediated replication fork reversal. *Nat. Struct. Mol. Biol.* 19:417–423. http://dx.doi.org/10.1038/nsmb.2258

Schlacher, K., N. Christ, N. Siaud, A. Egashira, H. Wu, and M. Jasin. 2011. Double-strand break repair-independent role for BRCA2 in blocking stalled replication fork degradation by MRE11. *Cell*. 145:529–542. http://dx.doi.org/10.1016/j.cell.2011.03.041

Schlacher, K., H. Wu, and M. Jasin. 2012. A distinct replication fork protection pathway connects Fanconi anemia tumor suppressors to RAD51-BRCA1/2. *Cancer Cell*. 22:106–116. http://dx.doi.org/10.1016/j.ccr.2012.05.015

Seigneur, M., V. Bidnenko, S.D. Ehrlich, and B. Michel. 1998. RuvAB acts at arrested replication forks. *Cell*. 95:419–430. http://dx.doi.org/10.1016/S0092-8674(00)81772-9

Sidorova, J.M., N. Li, A. Folch, and R.J. Monnat Jr. 2008. The RecQ helicase WRN is required for normal replication fork progression after DNA damage or replication fork arrest. *Cell Cycle*. 7:796–807. http://dx.doi.org/10.4161/cc.7.6.5566

Sidorova, J.M., N. Li, D.C. Schwartz, A. Folch, and R.J. Monnat Jr. 2009. Microfluidic-assisted analysis of replicating DNA molecules. *Nat. Protoc.* 4:849–861. http://dx.doi.org/10.1038/nprot.2009.54

Sturzenegger, A., K. Burdova, R. Kanagaraj, M. Levikova, C. Pinto, P. Cejka, and P. Janscak. 2014. DNA2 cooperates with the WRN and BLM RecQ helicases to mediate long-range DNA end resection in human cells. *J. Biol. Chem.* 289:27314–27326. http://dx.doi.org/10.1074/jbc.M114.578823

Thangavel, S., R. Mendoza-Maldonado, E. Tissino, J.M. Sidorova, J. Yin, W. Wang, R.J. Monnat Jr., A. Falaschi, and A. Vindigni. 2010. Human RECQ1 and RECQ4 helicases play distinct roles in DNA replication initiation. *Mol. Cell. Biol.* 30:1382–1396. http://dx.doi.org/10.1128/MCB.01290-09

Wawrousek, K.E., B.K. Fortini, P. Polaczek, L. Chen, Q. Liu, W.G. Dunphy, and J.L. Campbell. 2010. Xenopus DNA2 is a helicase/nuclease that is found in complexes with replication proteins And-1/Ctf4 and Mcm10 and DSB response proteins Nbs1 and ATM. *Cell Cycle*. 9:1156–1166. http://dx.doi.org/10.4161/cc.9.6.11049

Wu, L., and I.D. Hickson. 2003. The Bloom's syndrome helicase suppresses crossing over during homologous recombination. *Nature*. 426:870–874. http://dx.doi.org/10.1038/nature02253

Yata, K., J. Lloyd, S. Maslen, J.Y. Bleuyard, M. Skehel, S.J. Smerdon, and F. Esashi. 2012. Plk1 and CK2 act in concert to regulate Rad51 during DNA double strand break repair. *Mol. Cell*. 45:371–383. http://dx.doi.org/10.1016/j.molcel.2011.12.028

Yeo, J.E., E.H. Lee, E.A. Hendrickson, and A. Sobeck. 2014. CtIP mediates replication fork recovery in a FANCD2-regulated manner. *Hum. Mol. Genet.* 23:3695–3705. http://dx.doi.org/10.1093/hmg/ddu078

Yin, J., Y.T. Kwon, A. Varshavsky, and W. Wang. 2004. RECQL4, mutated in the Rothmund-Thomson and RAPADILINO syndromes, interacts with ubiquitin ligases UBR1 and UBR2 of the N-end rule pathway. *Hum. Mol. Genet.* 13:2421–2430. http://dx.doi.org/10.1093/hmg/ddh269

Ying, S., F.C. Hamdy, and T. Helleday. 2012. Mre11-dependent degradation of stalled DNA replication forks is prevented by BRCA2 and PARP1. *Cancer Res.* 72:2814–2821. http://dx.doi.org/10.1158/0008-5472.CAN-11-3417

Zellweger, R., D. Dalcher, K. Mutreja, R. Herrador, M. Berti, A. Vindigni, and M. Lopes. 2015. Rad51-mediated replication fork reversal is a global response to genotoxic treatments in human cells. *J. Cell Biol.* 208:563–579.

Zeman, M.K., and K.A. Cimprich. 2014. Causes and consequences of replication stress. *Nat. Cell Biol.* 16:2–9. http://dx.doi.org/10.1038/ncb2897

Zhu, Z., W.H. Chung, E.Y. Shim, S.E. Lee, and G. Ira. 2008. Sgs1 helicase and two nucleases Dna2 and Exo1 resect DNA double-strand break ends. *Cell*. 134:981–994. http://dx.doi.org/10.1016/j.cell.2008.08.037

SUPPLEMENTAL MATERIAL JCB

Thangalev et al., http://www.jcb.org/cgi/content/full/jcb.201406100/DC1

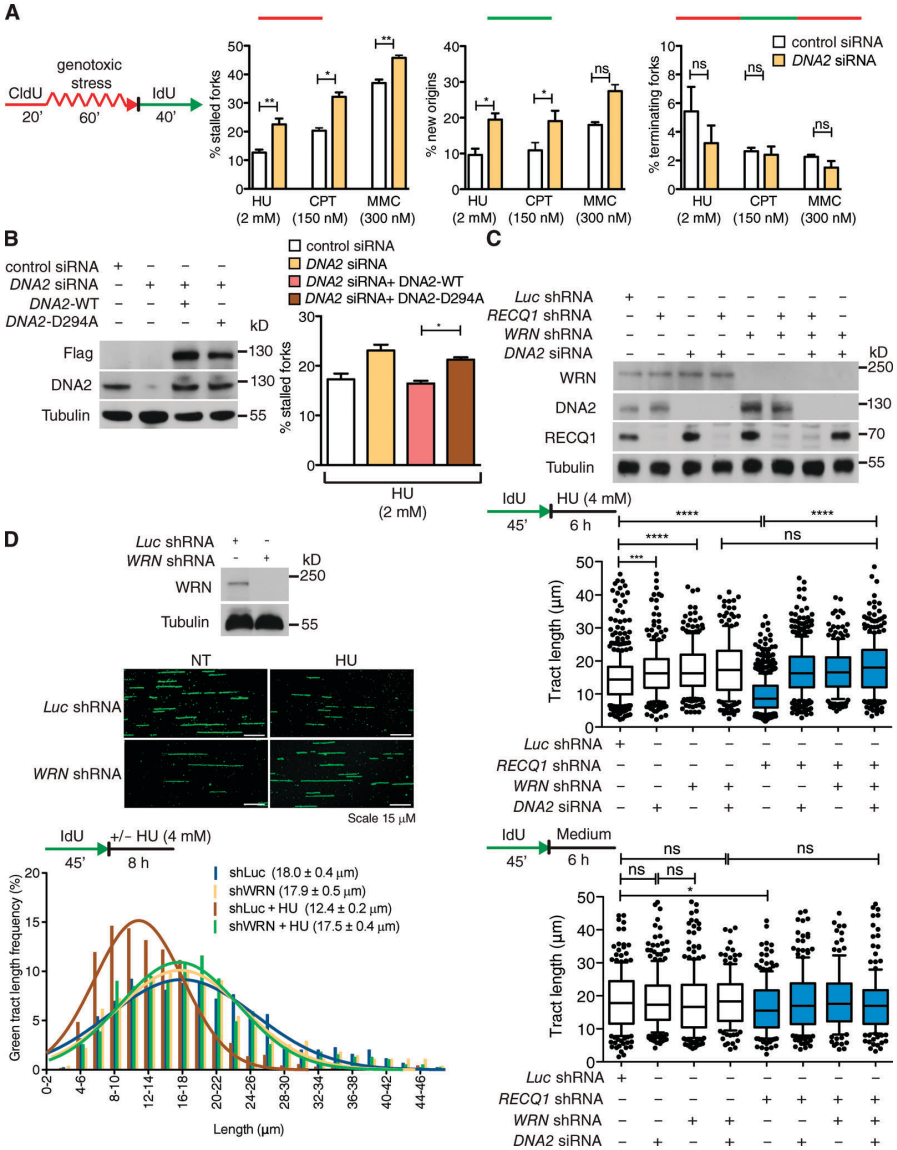

Figure S1. **DNA2 and WRN function in stalled fork processing.** (A, left) Schematic of DNA fiber tract analysis. (right) Quantification of red tracts (stalled forks), green tracts (new origins), and contiguous red–green–red tracts (termination events). Proper quantification of stalled forks is complicated by the fact that termination events might also lead to red tracts if termination occurs before the addition of the second label. Mean shown, $n = 3$. Error bars, standard error. ns, not significant; *, $P < 0.05$; **, $P < 0.01$; ***, $P < 0.001$ (paired Student's *t* test). (B, left) Expression of Flag-tagged WT (DNA2-WT) or nuclease-dead (DNA2-D294A) DNA2 in DNA2-depleted U-2 OS cells. (right) Quantification of stalled forks in DNA2-depleted cells expressing DNA-WT or DNA2-D294A. Mean shown, $n = 3$. Error bars, standard error. ns, not significant; *, $P < 0.05$ (paired *t* test). (C, top) Expression of RECQ1, WRN, DNA2, and tubulin in U-2 OS cells transfected with the indicated shRNA or siRNA. (middle) Statistical analysis of IdU tracts from U-2 OS cells depleted for the indicated proteins in the presence of 4 mM HU. (bottom) Statistical analysis of IdU tracts from U-2 OS cells depleted for the indicated proteins in the absence of drug treatment. Whiskers indicate the 10th and 90th percentiles. ns, not significant (Mann-Whitney test). $n \geq 300$ scored for each dataset. (D, top) Expression of WRN after WRN knockdown and representative fiber tract images in Luc- and WRN-depleted U-2 OS cells. Bar, 15 µm. Representative IdU tracts in WRN-depleted U-2 OS cells in the presence or absence of HU (out of 2 repeats; $n \geq 700$ scored for each dataset).

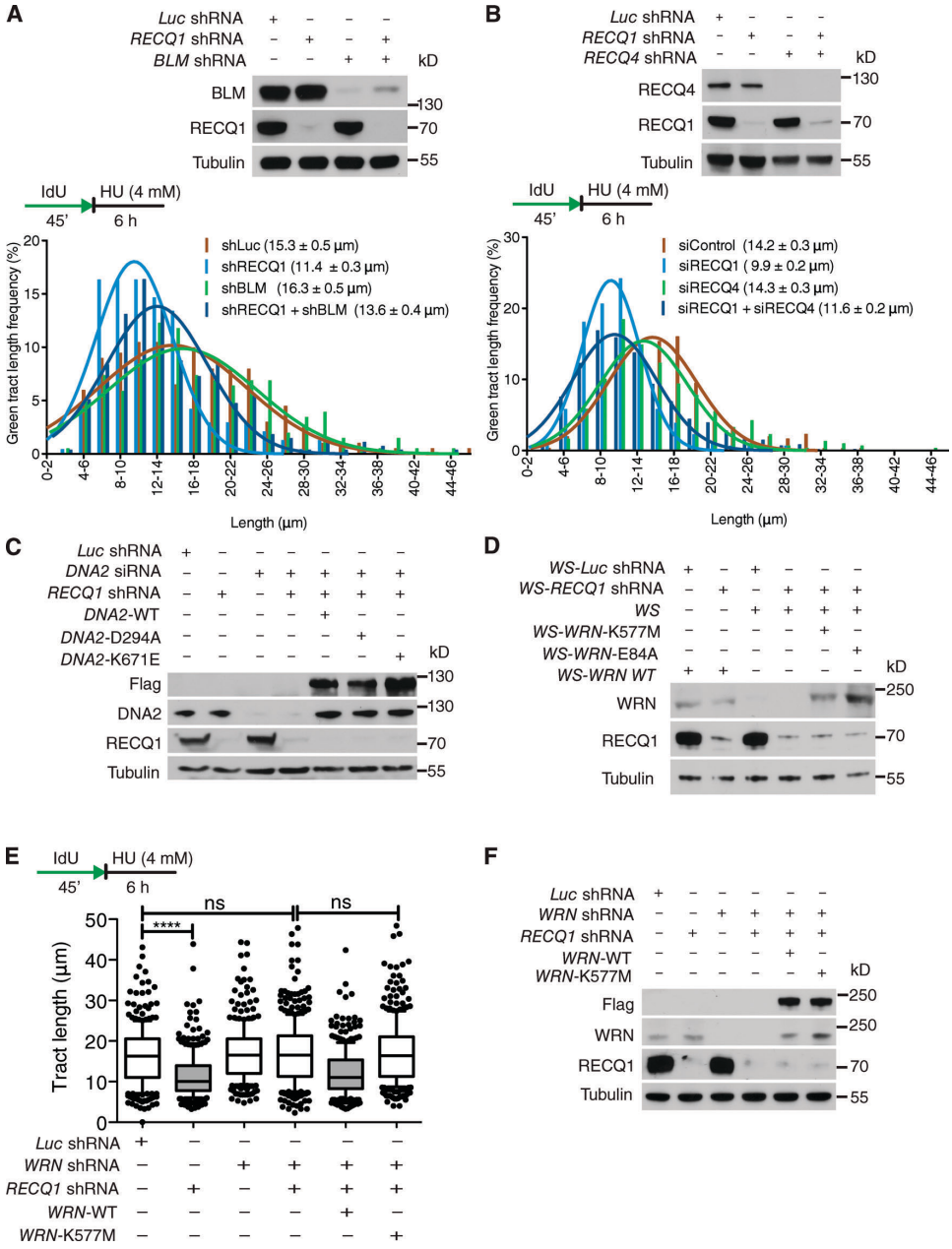

Figure S2. **BLM or RECQ4 depletion does not have a significant effect on stalled fork processing.** (A) Representative IdU tracts in Luc-, RECQ1-, BLM-, or RECQ1/BLM-codepleted U-2 OS cells in the presence of HU (out of 2 repeats; $n \geq 300$ scored for each dataset). (top) Expression of RECQ1, BLM and tubulin in U-2 OS cells transfected with indicated shRNA. (B) Representative IdU tracts in control, RECQ1-, RECQ4-, or RECQ1/RECQ4-codepleted U-2 OS cells in the presence of HU (out of 2 repeats; $n \geq 350$ scored for each dataset). (top) Expression of RECQ1, RECQ4 and tubulin in U-2 OS cells transfected with indicated shRNA. (C) Expression of RECQ1, DNA2-WT, DNA2-K671E, and DNA2-D294A in U-2 OS cells transfected with the indicated shRNA or siRNA. (D) Expression of RECQ1, WRN-WT, WRN-K577M, and WRN-E84A in WS cells. (E) Statistical analysis of IdU tracts from RECQ1-, WRN-, or RECQ1/WRN-codepleted U-2 OS cells. The RECQ1/WRN-codepleted cells were complemented with WT or ATPase-deficient (K577M) WRN, where indicated. Whiskers indicate the 10th and 90th percentiles. ns, not significant; ****, $P < 0.0001$ (Mann-Whitney test). (F) Expression of RECQ1, WRN-WT, and WRN-K577M in U-2 OS cells transfected with the indicated shRNA.

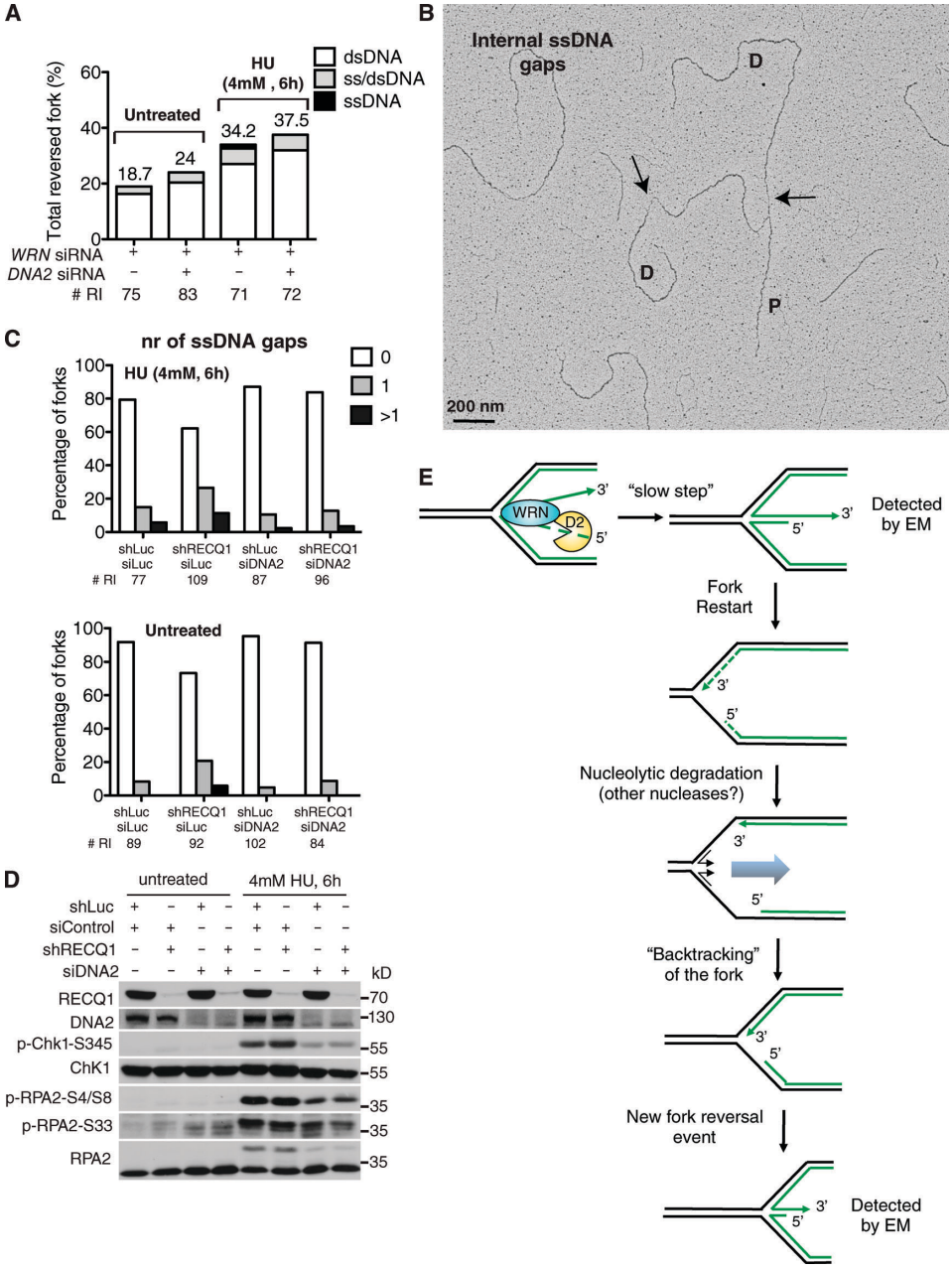

Figure S3. **DNA2 promotes ssDNA gap accumulation on replicated duplexes and the ATR-mediated checkpoint activation.** (A) Frequency of fork reversal and ssDNA composition of the reversed arms in WRN- and/or DNA2-depleted U-2 OS cells in the presence and absence of HU. The percentage values are indicated on the top of the bar. "# RI" indicates the number of analyzed replication intermediates. (B) Representative electron micrographs of replication forks displaying ssDNA gaps on the replicated duplexes or at the replication fork junction observed on genomic DNA in shRECQ1 U-2 OS cells upon HU-treatment. The black arrows point to ssDNA gaps. D, Daughter strand; P, Parental strand. (C) Statistical distribution of ssDNA gaps on newly replicated duplexes in RECQ1- and/or DNA2-depleted U-2 OS cells treated with HU (top) or in unperturbed conditions (bottom). "# RI" is the number of analyzed replication intermediates. (D) Western blot analysis of ATR-checkpoint activation (pChk1 and pRPA) in RECQ1- and/or DNA2-depleted U-2 OS cells with or without HU treatment. Total Chk1 and RPA level are displayed and used as loading control. (E) Schematic of the different structures detected by EM and DNA fibers. EM is a static method, which enriches for snapshots of the "slow steps" of a reaction (i.e., partially resected reversed forks). After fork restart, the nucleolytic degradation quickly proceeds to degrade nascent strands behind the junction. Reannealing of the parental strands leads to "backtracking" of the fork. A new reversal event arises as a consequence of asymmetric degradation, and thus ssDNA accumulation in proximity to the fork. Backtracking is easily detected by DNA fiber, but not by EM because a reversed fork formed after degradation and backtracking is indistinguishable from the original reversed fork present before initial degradation.

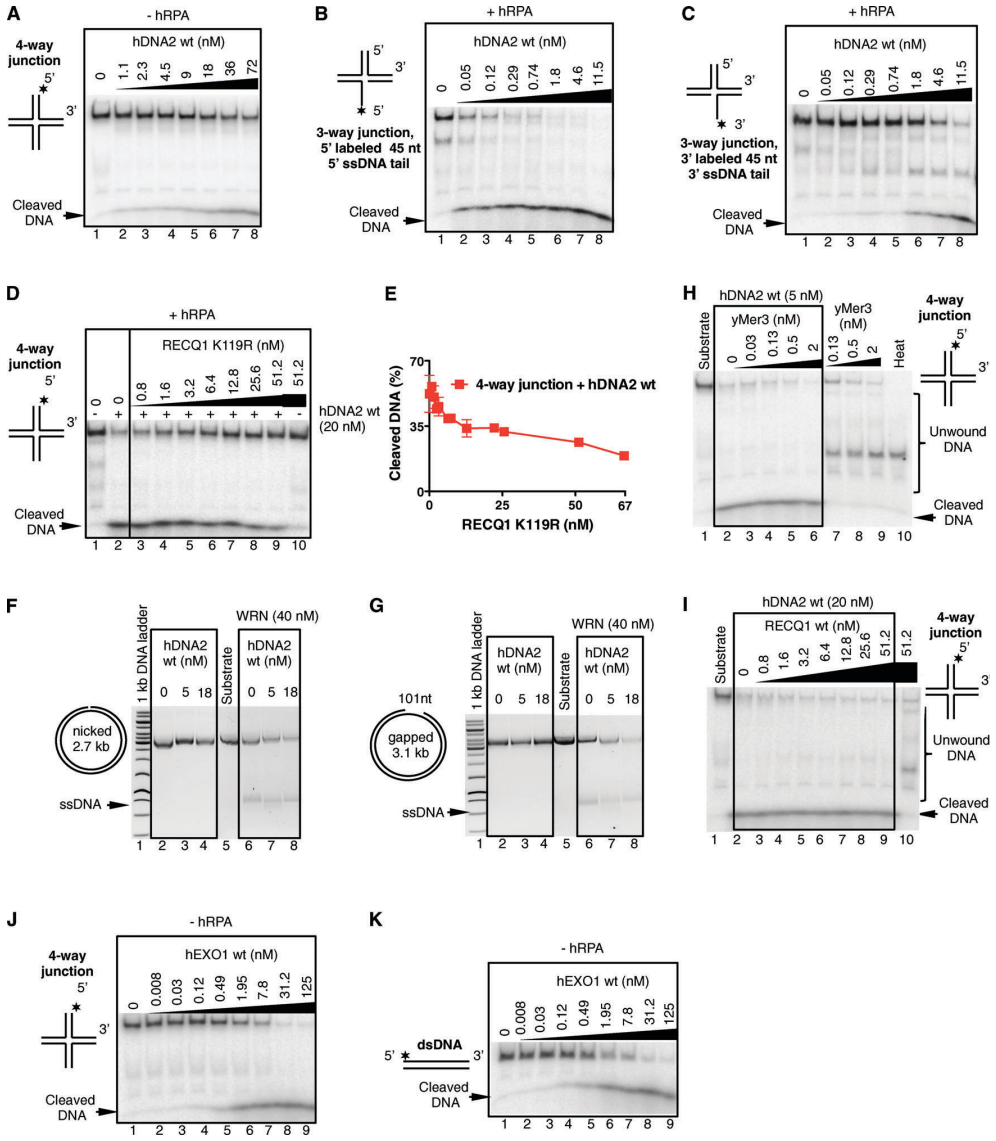

Figure S4. **Human DNA2 but not EXO1 preferentially degrades branched DNA.** (A) Degradation of a four-way junction by hDNA2 without human RPA (hRPA). Reaction products were separated on a native polyacrylamide gel (6%); *, position of the ^{32}P label. (B) Degradation of a three-way junction with a 5′ ssDNA tail by hDNA2 in the presence of hRPA (22.3 nM). Reaction products were separated on a native polyacrylamide gel (6%); *, position of the ^{32}P label. (C) Same experiment as in B, but with a junction containing a 3′ ssDNA tail. (D) RECQ1 K119R (ATPase-dead) inhibits four-way junction degradation by hDNA2. Increasing concentrations of RECQ1 (K119R) were preincubated with the substrate, and then hDNA2 (20 nM) was added to the reaction mixture. All reactions contained hRPA (65 nM). Reaction products were separated on a native polyacrylamide gel (6%); *, position of the ^{32}P label. (E) Quantitation of data from D. Averages shown ± SEM, $n = 2$. (F) Synergistic action of hDNA2 and WRN on a nicked plasmid based DNA substrate. The reactions contained 614 nM hRPA and were incubated at 37°C for 60 min. Products were separated on a 1% agarose gel and stained with GelRed. WRN helicase promotes degradation of nicked DNA by hDNA2. (G) Same experiment as in F, but with a gapped DNA substrate. (H) Degradation of a four-way junction by hDNA2 and *S. cerevisiae* Mer3. hDNA2 only degrades ssDNA unwound by Mer3, no synergy in DNA degradation was observed. All reactions contained hRPA, and were analyzed on a native polyacrylamide gel (6%). (I) Degradation of four-way junction by hDNA2 is not stimulated by WT hRECQ1. All reactions contained hRPA (65 nM). Reaction products were separated on a native polyacrylamide gel (6%). (J) Degradation of a four-way junction by hEXO1. Reaction products were separated on a native polyacrylamide gel (6%); *, position of the ^{32}P label. (K) Same experiment as in J, but with dsDNA.

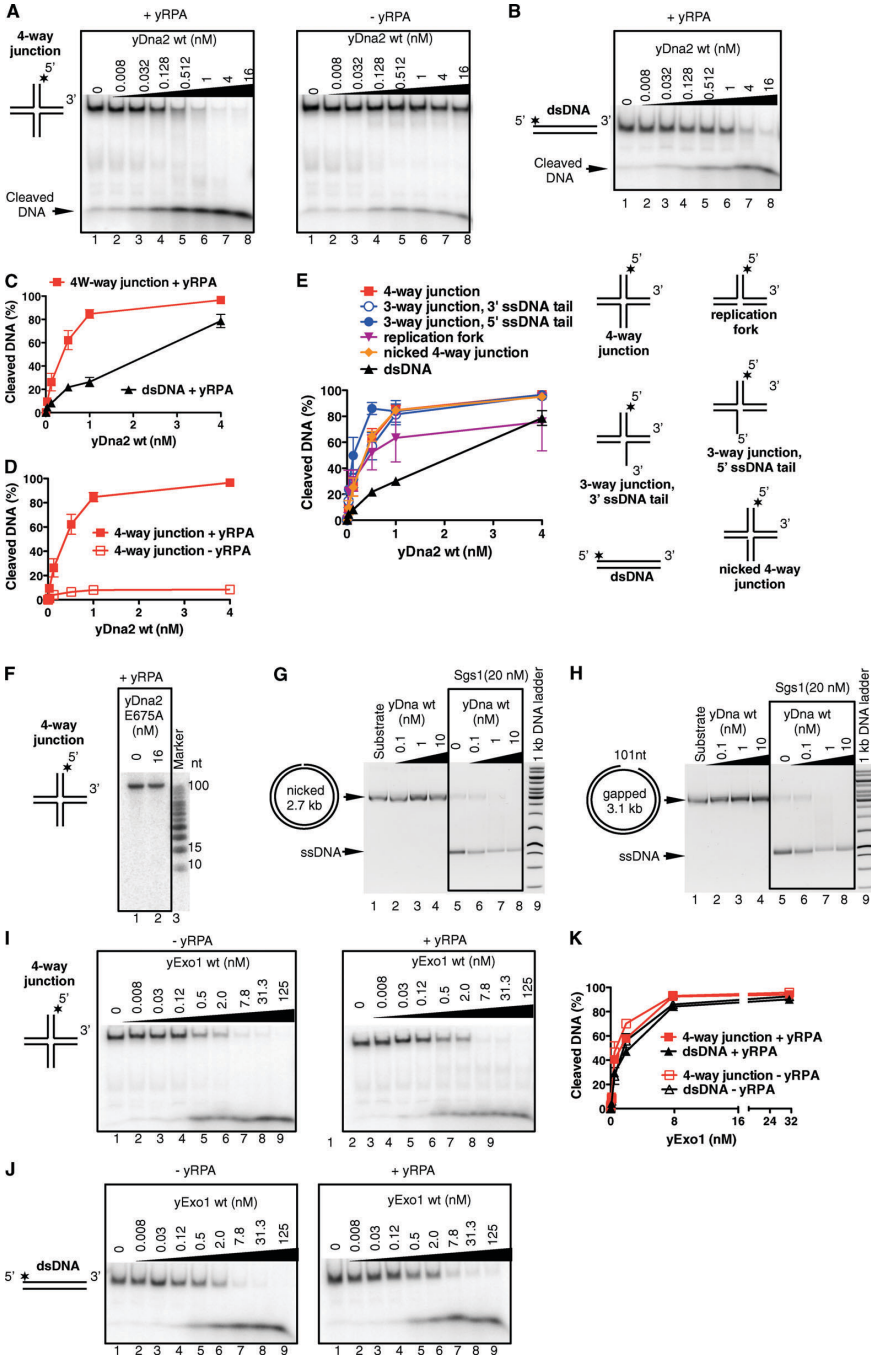

Figure S5. **Yeast Dna2 but not Exo1 preferentially degrades branched DNA.** (A) Degradation of a four-way junction by yDna2 in presence (left) or absence (right) of yeast RPA (yRPA). Reactions were separated on a native polyacrylamide gel (6%), *, position of the ^{32}P label. (B) Experiment as in A, but with dsDNA and yRPA. (C) Yeast Dna2 preferentially degrades four-way junctions in the presence of yRPA. Quantitation of data from A and B. Averages shown ± SEM; $n = 2$. (D) yRPA promotes DNA degradation by yDna2. Quantitation of data from A. The data points representing the degradation of a four-way junction in the presence of yRPA are identical to those from C. Mean shown ± SEM, $n = 2$. (E) Yeast Dna2 preferentially degrades branched structures over dsDNA. Quantitation of degradation of various DNA substrates as indicated (cartoons on the right) by yDna2 WT in presence of yRPA. Averages shown ± SEM; $n = 2$. (F) Denaturing 20% polyacrylamide gel showing that nuclease-dead yDna2 E675A variant does not degrade the four-way junction substrate. (G) Synergistic action of yDna2 and Sgs1 helicase on a nicked dsDNA plasmid based substrates. The reactions contained 770 nM yRPA and were incubated at 30°C for 60 min before being separated on a 1% agarose gel containing GelRed. (H) Experiment as in G, but with gapped DNA substrate. (I) Degradation of a four-way junction by yExo1 in the presence (right) or absence (left) of yRPA. (J) Same experiment as in I, but with dsDNA. (K) Quantitation of data from I and J. Averages shown ± SEM, $n = 2$.

2.3.2 Dna2 nuclease-helicase and Holliday junction resolvase Yen1 provide a two-tiered response to replication stress

Gizem Ölmezer, **Maryna Levikova**, Dominique Klein, Gabriele Fontana, Petr Cejka and Ulrich Rass.

Article under revision in Nature Communications.

I contributed to this manuscript by performing biochemical assays with helicase-dead Dna2 R1253Q variant.

Dna2 nuclease-helicase and Holliday junction resolvase Yen1 provide a two-tiered response to replication stress

Gizem Ölmezer[1], Maryna Levikova[2,*], Dominique Klein[1,*], Gabriele Fontana[1], Petr Cejka[2] & Ulrich Rass[1,§]

[1] Friedrich Miescher Institute for Biomedical Research, Maulbeerstrasse 66, CH-4058 Basel, Switzerland.

[2] Institute of Molecular Cancer Research, Winterthurerstrasse 190, CH-8057 Zürich, Switzerland.

[*] Both authors contributed equally to this work.

[§] To whom correspondence should be addressed: ulrich.rass@fmi.ch.

Key words: chromosome stability, replication fork reversal, replication fork regression, DNA repair, Holliday junction resolution, structure-specific nucleases

Abstract

Transmission of a stable genome from mother cell to daughter cell requires each chromosome to be fully replicated. To avoid underreplication, cells have evolved mechanisms to protect, restart, and repair perturbed replication forks. Using budding yeast as a model, we find that the helicase activity of the conserved nuclease-helicase Dna2 is required for the completion of DNA replication. Dna2 helicase-defective cells accumulate post-replicative inter-sister chromatid DNA links. Yen1, but not the other Holliday junction (HJ) resolvases Slx1-Slx4 and Mus81-Mms4, targets these DNA structures to safeguard chromosome segregation along a pathway distinct from canonical HJ resolution. Because Yen1 activation requires entry into mitosis, Dna2 helicase-defective cells are susceptible to terminal DNA damage checkpoint arrest at the G2/M transition. These findings explain the exquisite sensitivity of Dna2 helicase-defective cells to replication stress and suggest molecular mechanisms of genome instability and cell death that may underlie human pathologies associated with *DNA2* such as cancer and Seckel syndrome.

2.3.3 DNA2 cooperates with WRN and BLM RecQ helicases to mediate long-range DNA end resection in human cells

Andreas Sturzenegger, Kamila Burdova, Radhakrishnan Kanagaraj, **Maryna Levikova**, Cosimo Pinto, Petr Cejka and Pavel Janscak.

Article published in Journal of Biological Chemistry, 2014.

I contributed to this publication by performing protein expression and purification of human DNA2 protein together with C.P. and P.C.

THE JOURNAL OF BIOLOGICAL CHEMISTRY VOL. 289, NO. 39, pp. 27314–27326, September 26, 2014

DNA2 Cooperates with the WRN and BLM RecQ Helicases to Mediate Long-range DNA End Resection in Human Cells*

Received for publication, May 3, 2014, and in revised form, August 12, 2014 Published, JBC Papers in Press, August 13, 2014, DOI 10.1074/jbc.M114.578823

Andreas Sturzenegger[‡1], **Kamila Burdova**[§1], **Radhakrishnan Kanagaraj**[‡2], **Maryna Levikova**[‡], **Cosimo Pinto**[‡], **Petr Cejka**[‡], **and Pavel Janscak**[‡§3]

From the [‡]*Institute of Molecular Cancer Research, University of Zurich, 8057 Zurich, Switzerland and the* [§]*Institute of Molecular Genetics, Academy of Sciences of the Czech Republic, 14300 Prague, Czech Republic*

Background: DNA end resection is a critical step in the homology-directed repair of DNA double strand breaks (DSBs).
Results: Human WRN helicase stimulates the DNA2-catalyzed resection of DNA ends and acts in concert with DNA2 to promote DSB repair by single strand annealing.
Conclusion: DNA2 cooperates with WRN or BLM to mediate the resection of DSBs in mammalian cells.
Significance: Defects in DNA end resection might, in part, account for the genomic instability phenotype of Werner syndrome.

The 5′-3′ resection of DNA ends is a prerequisite for the repair of DNA double strand breaks by homologous recombination, microhomology-mediated end joining, and single strand annealing. Recent studies in yeast have shown that, following initial DNA end processing by the Mre11-Rad50-Xrs2 complex and Sae2, the extension of resection tracts is mediated either by exonuclease 1 or by combined activities of the RecQ family DNA helicase Sgs1 and the helicase/endonuclease Dna2. Although human DNA2 has been shown to cooperate with the BLM helicase to catalyze the resection of DNA ends, it remains a matter of debate whether another human RecQ helicase, WRN, can substitute for BLM in DNA2-catalyzed resection. Here we present evidence that WRN and BLM act epistatically with DNA2 to promote the long-range resection of double strand break ends in human cells. Our biochemical experiments show that WRN and DNA2 interact physically and coordinate their enzymatic activities to mediate 5′-3′ DNA end resection in a reaction dependent on RPA. In addition, we present *in vitro* and *in vivo* data suggesting that BLM promotes DNA end resection as part of the BLM-TOPOIIIα-RMI1-RMI2 complex. Our study provides new mechanistic insights into the process of DNA end resection in mammalian cells.

DNA double strand breaks (DSBs)[4] are a very dangerous form of DNA damage because they can cause cell death or chromosomal rearrangements, a hallmark of cancer (1). DSBs can occur accidentally during normal cellular metabolism or upon exposure of cells to exogenous agents such as ionizing radiation and radiomimetic drugs (2). There are also programmed DSBs that drive recombination events essential for physiological processes, such as meiosis and lymphocyte development (3, 4). In eukaryotic cells, DSBs are repaired by one of two major pathways: non-homologous end joining (NHEJ) and homologous recombination (HR). NHEJ involves religation of the broken DNA ends and is frequently associated with a short deletion or insertion of DNA at the break site (5). In contrast, HR restores the DNA integrity accurately because it uses sister chromatids or homologous chromosomes as a template for repair (6, 7). HR is initiated by resection of the broken DNA ends to generate 3′ single-stranded (ss) DNA tails that are utilized by the RAD51 recombinase for a homology search on the donor DNA molecule (6, 7). Genetic and biochemical studies in budding yeast have shown that broken DNA ends are resected in a two-step process (8–10). DNA end resection in yeast is initiated by the Mre11-Rad50-Xrs2 complex in conjunction with Sae2 (8, 9, 11). These proteins may initiate resection of the 5′ strand of the broken DNA to remove a stretch of about 100–200 nucleotides from the DNA end (8, 9, 11). The Mre11-Rad50-Xrs2 complex also recruits the components of the long-range resection pathways Exo1 or Dna2-Sgs1 (8–10, 12, 13). Exo1 is a dsDNA-dependent 5′-3′ exonuclease that preferentially degrades DNA substrates with a 3′ ssDNA tail in a reaction stimulated by the ssDNA-binding protein RPA (13). Dna2 is a ssDNA-specific nuclease and a DNA helicase that functions in conjunction with the RecQ family DNA helicase Sgs1 and RPA to catalyze long-range DNA end resection (10, 14). In this reaction, RPA stimulates DNA unwinding by Sgs1 and promotes degradation of the 5′-terminated strand by Dna2 while protecting the growing 3′ ssDNA tail (10). DNA end resection is also the initial step in two other DSB repair pathways, single strand annealing (SSA) and microhomology-mediated end joining (8, 15).

The molecular machinery of DNA end resection appears to be largely conserved between yeast and man (15–19). However, it remains a matter of debate which DNA helicase mediates DNA2-catalyzed resection in mammalian cells. Mammals pos-

* This work was supported by Swiss National Science Foundation Grants 31003A-129747 and 31003A_146206, by Czech Science Foundation Grant GAP305/10/0281, and by the Stiftung zur Krebsbekämpfung. This work was also supported by Swiss National Science Foundation Grant PP00P3 133636 (to P.C.) and by Forschungskredit of the University of Zurich Grant FK-13-098 (to A. S.).
[1] Both authors contributed equally to this work.
[2] Present address: London Research Institute, Cancer Research UK, Clare Hall Laboratories, South Mimms, Herts, EN6 3LD, UK.
[3] To whom correspondence should be addressed: Institute of Molecular Cancer Research, University of Zurich, Winterthurerstr. 190, 8057 Zurich, Switzerland. Tel.: 41-44-6353470; Fax: 41-44-6353484; E-mail: pjanscak@imcr.uzh.ch.
[4] The abbreviations used are: DSB, double strand break; NHEJ, non-homologous end joining; HR, homologous recombination; ssDNA, single-stranded DNA; SSA, single strand annealing; BTRR, BLM-TOPOIIIα-RMI1-RMI2; nt, nucleotide(s); CPT, camptothecin.

sess five RecQ homologues: RECQ1, BLM, WRN, RECQ4, and RECQ5 (20). Biochemical studies have shown that human DNA2 can act in conjunction with the BLM helicase and RPA to mediate 5′-3′ resection of DNA ends *in vitro* (17). In agreement with these findings, it has been observed that cells depleted of both BLM and EXO1 show a reduction in the formation of RPA foci in response to DSBs and are defective in DSB repair by HR (16, 19). However, studies using *Xenopus* egg extracts and purified proteins have shown that Dna2 mediates DNA end resection together with WRN rather than BLM (21–23). This discrepancy prompted us to investigate the role of WRN in DNA end resection in human cells. Here we demonstrate that WRN helicase is capable of acting in concert with DNA2 and RPA to resect 5′-recessed DNA ends *in vitro* with a catalytic efficiency even higher than that of BLM. Moreover, our results show that human cells may employ either BLM or WRN to assist DNA2 in long-range DNA end resection. Finally, we present data suggesting that BLM acts in DNA end resection as part of the BLM-TOPOIIIα-RMI1-RMI2 (BTRR) complex.

EXPERIMENTAL PROCEDURES

Antibodies and siRNA—Primary antibodies used for immunoblotting were as follows: mouse monoclonal anti-WRN (BD Biosciences, catalog no. 611169), rabbit polyclonal anti-DNA2 (Abcam, catalog no. ab96488), rabbit polyclonal anti-BLM (Abcam, catalog no. ab476), rabbit polyclonal anti-TFIIH (Santa Cruz Biotechnology, catalog no. sc293), mouse monoclonal anti-FLAG (Sigma, catalog no. F1804), and rabbit polyclonal anti-RMI1 (Proteintech, catalog no. 14630-1-AP). Anti-FLAG M2 magnetic beads (Sigma) were used for immunoprecipitation. Primary antibodies used for immunofluorescence staining were as follows: mouse monoclonal anti-RPA2 (Abcam, catalog no. ab2175) and rabbit monoclonal anti-γ-H2AX (Cell Signaling Technology, catalog no. 9718S). Rabbit polyclonal anti-WRN antibody used for immunoprecipitation has been described previously (24).

All siRNA oligoduplexes used in this study were purchased from Microsynth. The sequences of the sense strands of these duplexes were as follows: siLuc, 5′-CGUACGCGGAAUACUUCGAdTdT-3′; siWRN, 5′-UAGAGGGAAACUUGGCAAAdTdT-3′; siBLM, 5′-CCGAAUCUCAAUGUACAUAGAdTdT-3′; siDNA2, 5′-UACCGCUUAAAUCUAAGUCAAdTdT-3′; siEXO1, 5′-CAGCCAUUCUUACUACGCUAAdTdT-3′; siMRE11, 5′-GAGCAUAACUCCAUAAGUAdTdT-3′ (25); siCtIP, 5′-UCCACAACAUAAUCCUAAUdTdT-3′ (26); and siRMI1, 5′-AGCCUUCACGAAUGUUGAUdTdT-3′ (27).

Plasmid Constructions—The human DNA2 (hDNA2) ORF was amplified by PCR without the initiation and stop codons to generate a fragment including ggatcc-hDNA2-ctcgag. After digestion with BamHI and XhoI, the hDNA2 fragment was cloned into pFLAG-CMV2 (Sigma) digested with BglII/SalI (pFLAG-CMV2-hDNA2). The human WRN (hWRN) ORF was inserted into pcDNA3.1/Hygro(−) (Invitrogen) via the NheI and DraI sites (pcDNA3.1-hWRN). The siRNA-resistant form of this construct was generated by changing four nucleotides in the siWRN-targeting region (T270C, A273G, G276C, and A279G) using the QuikChange site-directed mutagenesis kit (Stratagene).

Protein Purifications—Wild-type and mutant forms of WRN, BLM, EXO1, and RPA were produced and purified as described previously (28–31). The TOPOIIIα-RMI1-RMI2 (TRR) complex was a gift from Drs. Kata Sarlos and Ian Hickson (University of Copenhagen, Denmark). DNA2 was produced as a fusion with a His_6 tag (N terminus) and a FLAG tag (C terminus) in Sf9 cells using the Bac-to-Bac baculovirus expression system (Invitrogen). The transfer vector for bacmid preparation was a gift from Dr. Judith L. Campbell (32). The transfer vectors for nuclease-deficient (D227A) and helicase-deficient (K654R) mutants of DNA2 were generated using the QuikChange site-directed mutagenesis kit (Stratagene). Sf9 cells expressing DNA2 fusion proteins were harvested 52 h after infection (typically a 800-ml culture) and washed with PBS. All subsequent steps were carried out at 4 °C. Pelleted cells were resuspended in lysis buffer (25 mM Tris-HCl (pH 7.5), 2 mM β-mercaptoethanol, 1× complete EDTA-free protease inhibitor (Roche), 1 mM phenylmethylsulfonyl fluoride, 30 μg/ml leupeptin, and 15 mM imidazole) and incubated for 20 min under continuous stirring. Subsequently, glycerol and 5 M NaCl were added slowly to final concentrations of 15% (v/v) and 300 mM, respectively, while mixing the sample. The cell suspension was then incubated for an additional 30 min under continuous stirring. The cell lysate was centrifuged at 55,000 × *g* for 30 min to obtain soluble extract, which was then incubated with 5 ml of nickel-nitrilotriacetic acid-agarose beads (Qiagen) for 1 h batchwise. The resin was washed extensively with lysis buffer containing 10% (v/v) glycerol and 1 M NaCl. The protein was eluted with lysis buffer supplemented with 10% (v/v) glycerol, 100 mM NaCl, and 250 mM imidazole. Fractions containing detectable amounts of protein, as measured by Bradford assay, were pooled, diluted 1:1 with TBS buffer (50 mM Tris-HCl (pH 7.5) and 150 mM NaCl) and incubated batchwise with 1 ml of anti-FLAG M2 affinity resin (Sigma) for 30 min. The resin was then transferred to a gravity flow column and washed with TBS-PI buffer (TBS buffer containing 1 mM β-mercaptoethanol and 5 μg/ml leupeptin). Elution of the protein was achieved by adding TBS-PI buffer supplemented with 200 μg/ml 3× FLAG peptide (Sigma). Fractions containing DNA2 were pooled, diluted with 0.5 volumes of water and 1 volume of AQ buffer (25 mM Tris-HCl (pH 7.5), 100 mM NaCl, 10% (v/v) glycerol, and 5 mM β-mercaptoethanol) and loaded onto a 1-ml HiTrap Q column (GE Healthcare) pre-equilibrated with AQ buffer. The column was washed with AQ buffer and DNA2 was eluted by AQ buffer supplemented with 600 mM NaCl. Fractions containing DNA2 were identified by SDS-PAGE, pooled, and stored at −80 °C. The activity of purified recombinant DNA2 proteins was tested using a Y structure oligonucleotide duplex with single-stranded arms (10). In agreement with previous reports, wild-type DNA2 was found to be capable of degrading both ssDNA arms of this structure (data not shown) (10, 17). In the presence of RPA, the cleavage of the 3′ ssDNA arm by DNA2 was inhibited, and DNA2 degraded preferentially the 5′ ssDNA arm (data not shown) (10, 17). The DNA2-D227A mutant did not contain any nuclease activity, which indicated that the nuclease activity of our wild-type DNA2 preparation was inherent to DNA2 (data not shown).

The Role of WRN and BLM in DNA End Resection

Nuclease and Helicase Assays—To test the activity of purified DNA2, we used a 31-bp forked duplex with 19-nt ssDNA arms, as described previously (10). The helicase activity of WRN and BLM was tested using a 29-bp forked duplex generated by annealing of the following oligonucleotides: f-9 (5′-ACTATCATTC AGTCATGTAA CCTAGTCAAT CTGCGAGCTC GAATTCACTG GAGTGACCT-3′) and f-10 (5′-GAGGTCACTC CAGTGAATTC GAGCTCGCAG TCAATGTCGA CATACCTAGT ACTTTACTCC-3′). Both DNA substrates were radiolabeled at the end of the 5′ ssDNA arm.

Nuclease and helicase assays were performed in buffer containing 25 mM Tris acetate (pH 7.5), 2 mM magnesium acetate, 1 mM dithiothreitol, 0.1 mg/ml BSA, 10.7 mM phosphocreatine, and 0.02 mg/ml creatine phosphokinase. Reactions (15 μl) contained 1 nM ^{32}P-labeled forked DNA substrate and the indicated concentrations of DNA2 or WRN/BLM. Where indicated, RPA was present at a concentration of 6 nM. Reactions were assembled on ice and started by addition of ATP to a concentration of 1 mM. Reactions were incubated for 30 min at 37 °C. Termination of the reactions was achieved by adding 1/3 volume of stop solution (150 mM EDTA, 2% (w/v) SDS, 30% (v/v) glycerol, and 0.1% (w/v) bromphenol blue) and 1/15 volume of Proteinase K (10 mg/ml), followed by incubation at 37 °C for 15 min. The reaction products were separated by electrophoresis in a 10% Tris borate-EDTA polyacrylamide gel. Gels were dried on Whatman MM3 paper and analyzed by phosphorimaging using a Typhoon 9400 scanner (GE Healthcare). Images were quantified using ImageQuantTL software.

Construction of DNA Substrates for Resection Assays—The DNA substrates used in resection assays were derived from the plasmid pUC19 (2686 bp). The self-complementary oligonucleotide, 5′-AGCT GCTGAGG GCTGAGG GCTGAGG GCTGAGG AGGCCT CCTCAGC CCTCAGC CCTCAGC CCTCAGC-3′, was annealed to form a duplex that was cloned into the HindIII site of pUC19. This destroyed the HindIII site and inserted a single recognition sequence for StuI (AGGCCT) flanked on each side by four recognition sequences for the nickase Nt.BbvCI (CC*TCAGC; the cleavage position is indicated by the asterisk) that are oriented as an inverted repeat with respect to the StuI site. The resulting pOH-S plasmid allowed us to prepare a linear DNA substrate with 3′ overhangs of 26 nucleotides (nt) in length. A blunt-ended substrate was generated by digestion of pOH-S with StuI (New England Biolabs), followed by DNA purification using a Macherey Nagel NucleoSpin® gel and PCR cleanup kit. The substrate with 26-nt 3′ overhangs was generated as follows. After digestion of pOH-S with StuI and its heat inactivation, Nt.BbvCI (New England Biolabs) was added, and the reaction was incubated further for 2 h at 37 °C. Subsequently, the reaction mixture was diluted six times with water and incubated at 85 °C for 15 min. DNA purification was performed as described above. DNA concentration was determined using a NanoDrop ND-1000 spectrophotometer (Witec AG).

DNA End Resection Assays—DNA end resection reactions were carried out in a buffer containing 25 mM Tris acetate (pH 7.5), 2 mM magnesium acetate, 1 mM dithiothreitol, 0.1 mg/ml BSA, 10.7 mM phosphocreatine, 0.02 mg/ml creatine phosphokinase, and 1 mM ATP. Reactions contained 2 nM DNA substrate (molecules), 8 nM DNA2, 350 nM RPA (100% DNA strand coverage, assuming all DNA was single-stranded), and various concentrations of WRN or BLM as indicated. EXO1 was present at a concentration of 20 nM. The reactions were assembled on ice and initiated by the addition of ATP. Reaction mixtures (15 μl) were incubated at 37 °C for 60 min in the case of protein titration experiments. In time course experiments, 15-μl reaction aliquots were withdrawn at defined time points as indicated. Reactions were terminated as described for the helicase assays. The samples were subjected to electrophoresis in a 1% agarose gel run in 1× TAE buffer. Gels were post-stained with SYBR Gold (Invitrogen) and analyzed using MultiImage Light Cabinet (Alpha Innotech). To monitor resection by hybridization of radiolabeled oligonucleotide probes, terminated reactions (21 μl) were divided equally into two tubes. 5′ end-labeled oligonucleotide probes were then added to a final concentration of 5 nM. This mixture was heated in an oven to 75 °C for 5 min and then slowly cooled down to room temperature over 2.5 h. Reaction products were separated by electrophoresis in a 1% agarose gel. Gels were dried on DE81 anion exchange paper (Whatman) and subjected to phosphorimaging analysis using a Typhoon 9400 scanner (GE Healthcare). Images were quantified using ImageQuantTL software. The relative concentration of the resection products generated in WRN-DNA2 or BLM-DNA2 reactions was calculated as a percentage of the product generated in a reaction containing 20 nM EXO1 at the 2-min time point, which led to 100% resection within the region probed with radiolabeled oligonucleotides. Usually, the EXO1 reaction was loaded on each gel in triplicates. The following oligonucleotides were used for the preparation of the hybridization probes: oligo#224, 5′-GGCCGTCGTTTTACAACGTCGT-3′ (it anneals to the 3′-terminated strand; annealing position, 112–133 nt upstream of the StuI cleavage site; the complementary sequence is underlined); oligo#227, 5′-GGCATAGTTAAGCCAGCCCCGA-3′ (it anneals to the 3′-terminated strand; annealing position, 353–374 nt upstream of the StuI cleavage site); and oligo#237, 5′-GGTCGGGGCTGGCTTAACTATG-3′ (it anneals to the 5′-terminated strand; annealing position, 122–133 nt upstream of the StuI cleavage site). Oligonucleotides were 5′ end-labeled using [γ-^{32}P]ATP and T4 polynucleotide kinase (New England Biolabs). The two noncomplementary dG residues at the 5′ end of the oligonucleotides were added to ensure equal labeling efficiency.

Cell Culture and Transfection—U2OS and HEK293 cells were grown in DMEM (Sigma) supplemented with 10% fetal calf serum (Invitrogen) and streptomycin/penicillin (100 units/ml). Plasmid DNA was transfected using standard linear polyethyleneimine method. Lipofectamine RNAiMAX (Invitrogen) was used for siRNA transfection. To generate HEK293 clones stably expressing FLAG-DNA2, cells were cotransfected with pFLAG-CMV2-hDNA2 and pBABE-puro (Addgene) and subjected to puromycin 1 (μg/ml) selection. Puromycin-resistant clones were tested for expression of FLAG-DNA2 by Western blotting.

Immunoprecipitation—HEK293 cells were transfected with the pcDNA3.1-hWRN and/or pFLAG-CMV2-hDNA2 vectors. Cells were harvested to lysis buffer (50 mM Tris-HCl (pH 8.0), 120 mM NaCl, 20 mM NaF, 15 mM sodium pyrophosphate, and

0.5% (v/v) Nonidet P-40) supplemented before use with protease (Complete EDTA-free, Roche) and phosphatase (PhosSTOP, Roche) inhibitors, 2 mM $MgCl_2$ and benzonase (50 units/ml). Cells were sonicated briefly, and lysates were clarified by centrifugation at 16,000 × *g* for 30 min. Cell extracts (1 mg of protein) were subjected to immunoprecipitation using anti-FLAG M2 magnetic beads (10 μl) or Protein A/G Plus UltraLink Resin (10 μl, Thermo Scientific) coated with rabbit polyclonal anti-WRN antibody (10 μg), which was carried out overnight at 4 °C. Immunoprecipitates were washed four times with lysis buffer. Bound proteins were eluted by Laemmli sample buffer and analyzed by SDS-PAGE and Western blotting. To test the interaction between purified WRN and DNA2 proteins, 500 ng of each protein was mixed in 200 μl of NET-N100 buffer (10 mM Tris-HCl (pH 8.0), 1 mM EDTA, 100 mM NaCl, and 0.5% (v/v) Nonidet P-40) and incubated at 4 °C for 4 h. As a control, DNA2 was incubated in the absence of WRN. The protein mixtures were subsequently subjected to immunoprecipitation using anti-WRN antibody (4 μg), which was carried out at 4 °C for 2 h. Immunoprecipitates were washed four times with NET-N100 buffer. Bound proteins were eluted by Laemmli sample buffer and analyzed by SDS-PAGE and Western blotting.

GST Pulldown Assay—GST-tagged fragments of WRN were produced in the *Escherichia coli* BL21-CodonPlus(DE3)-RIL strain (Stratagene) and bound to GSH Sepharose 4B (GE Healthcare) as described previously (24). As a control, beads were coated with GST protein only. The beads were incubated with 500 ng of purified His_6-DNA2-FLAG protein in 400 μl of NET-N100 buffer at 4 °C for 2 h. After extensive washing with NET-N100 buffer, proteins bound to the beads were analyzed by Western blotting. Blots were first stained in Ponceau S solution (0.1% (w/v) Ponceau S and 5% (v/v) acetic acid) to visualize WRN fragments and subsequently probed with anti-FLAG antibody.

Reverse Transcription and Quantitative Real-time PCR—Total RNA was isolated from cells using the RNeasy mini kit (Qiagen). 200 ng of RNA was used for cDNA synthesis using a high-capacity cDNA reverse transcription kit (Applied Biosystems). The target gene expression level was determined by quantitative real-time PCR that was performed on a ABI Prism 7300 (Applied Biosystems) using SYBR Select Master Mix (Applied Biosystems). The following primer pairs were used to determine EXO1 mRNA levels: 5′-ACCTCTAAGG AACAAGGTTC-3′ (forward) and 5′-AGGAGGAAGC TTTTC-AGAATC-3′ (reverse). The housekeeping gene RPLPO, used as a control, was amplified with the following primers: 5′-CCAG-TCTGGA GAAACTGCTG-3′ (forward) and 5′-CAGCAG-CTGG CACCTTATTGG-3′ (reverse). The Pfaffl equation was used for normalization and calculation of relative EXO1 expression levels in comparison with the control gene (33).

SA-GFP Reporter Assay—SA-GFP reporter assays were performed as described previously (34, 35). HEK293/SA-GFP cells were seeded in poly-L-lysine-coated 6-well plates at a density of 0.5 million cells/well. U2OS/SA-GFP cells were seeded in 6-well plates at a density of 0.25 million cells/well. The next day, cells were transfected with appropriate siRNA (40 nM) using Lipofectamine RNAiMAX (Invitrogen). After 24 h, siRNA-transfected cells were transferred into a 12-well plate, with 200,000 cells/well for HEK293/SA-GFP and 100,000 cells/well for U2OS/SA-GFP. 44 h after siRNA transfection, cells were transfected with 0.6 μg of the I-SceI expression vector pCBASce (36) using linear polyethyleneimine and, 6 h later, with appropriate siRNA (20 nM) using the standard calcium phosphate method. 52 h after I-SceI transfection, cells were harvested and subjected to flow cytometry analysis using LSRII (BD Biosciences) and FlowJo software to determine the percentage of GFP-positive cells. The mean values obtained with control siRNA (siLuc) samples were 0.9% for HEK293/SA-GFP cells and 2.0% for U2OS/SA-GFP cells. To test the effect of ectopic expression of WRN on SSA repair efficiency of WRN-depleted HEK293/SA-GFP cells, the mutant form of the pcDNA3.1-hWRN construct harboring silent mutations in the siWRN-targeting region (0.6 μg) was cotransfected with pCBASce (0.6 μg). The plasmid pcDNA3.1 was used as a control vector in these experiments. Cells were subjected to flow cytometry analysis at 52 h after plasmid transfection.

Immunofluorescence Assays—U2OS cells transfected with the indicated siRNAs were cultured on glass coverslips. 48 h after siRNA transfection, cells were treated with 1 μM camptothecin (CPT) for 1 h. After pre-extraction for 5 min on ice in 25 mM HEPES (pH 7.4) buffer containing 0.5% (v/v) Triton X-100, 50 mM NaCl, 1 mM EDTA, 3 mM $MgCl_2$ and 0.3 M sucrose, cells were fixed with 4% (v/v) formaldehyde for 15 min at room temperature. Subsequently, cells were permeabilized by soaking in 0.2% (v/v) Triton X-100 for 5 min at room temperature. After blocking in PBS containing 10 mg/ml BSA for 30 min at room temperature, fixed cells were incubated for 2 h at room temperature with the indicated primary antibodies. The slides were washed with PBS and incubated for 1 h at room temperature with secondary antibodies diluted in blocking solution (Alexa Fluor 568-conjugated goat anti-rabbit IgG and Alexa Fluor 488-conjugated goat anti-mouse IgG (Invitrogen)). After washing with PBS, coverslips were mounted using Vectashield containing DAPI (Vector Laboratories). Automated image acquisition was performed using an Olympus IX70 microscope equipped with the Scan^R imaging platform. A ×40/1.3 numerical aperture objective was used. 10 z stacks at a spacing of 0.3 μm were taken, and 100 images were acquired for each sample. Analysis was performed using Scan^R analysis software. Nuclei were identified on the basis of the DAPI signal, and RPA foci were identified on the basis of edge-based subobject counts. At least 1000 cells were analyzed for each condition.

RESULTS

DNA2 Can Mediate DNA End Resection in Conjunction with WRN Helicase—To test whether the human WRN helicase can mediate resection of broken DNA ends in concert with DNA2, we purified these proteins to homogeneity and analyzed their activities *in vitro* (Fig. 1*A*). WRN and BLM unwind DNA in the 3′-5′ direction and require a 3′ ssDNA tail for loading onto the DNA substrate (37, 38). Therefore, we generated a derivative of the pUC19 plasmid in which a StuI site was flanked on each side by four recognition sites for the nicking endonuclease Nt. BbvCI. Cleavage of this pUC19 derivative with StuI and Nt.BbvCI resulted in a 2.7-kb-long linear DNA molecule ending with 3′

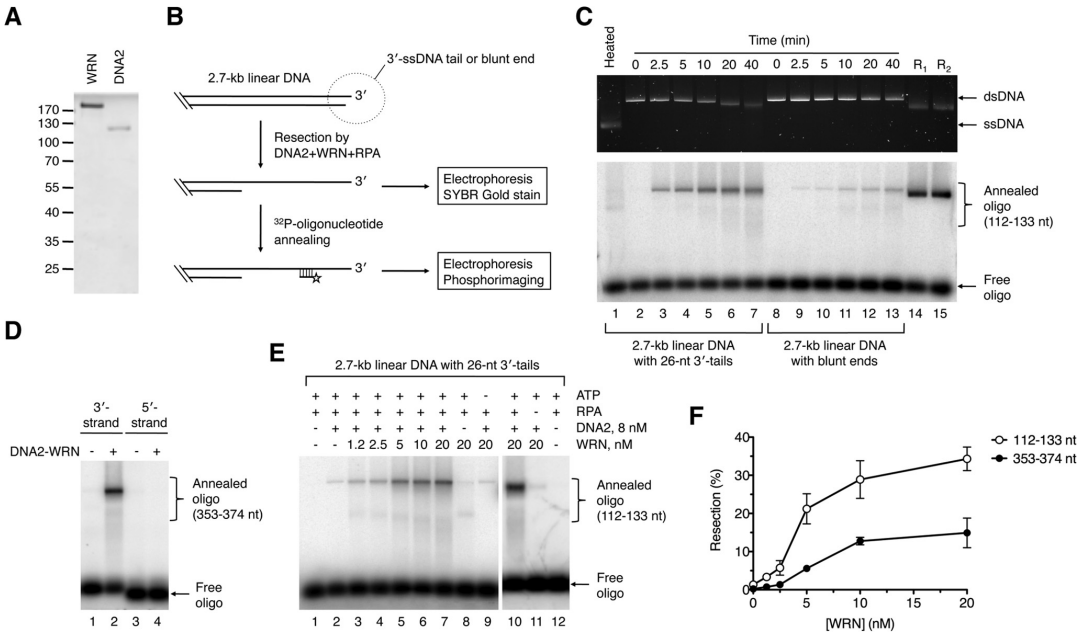

FIGURE 1. **DNA end resection by DNA2 and WRN.** *A*, SDS-PAGE analysis of purified WRN (0.7 μg) and DNA2 (0.4 μg) proteins. Gel was stained with Coomassie Brilliant Blue R-250. The molecular weights of protein standards are indicated on the *left*. *B*, schematic of the DNA end resection assay. The resection products were either left untreated or hybridized with synthetic ^{32}P-labeled oligonucleotides complementary to the 3′-terminated strand. DNA species were separated by electrophoresis in a 1% agarose gel and visualized by SYBR gold staining and phosphorimaging, respectively. Probes complementary to the regions spanning nt positions 112–133 and 353–374 (relative to the 3′ end) were used in this study. Only a part of the DNA substrate is shown. *C*, time course of resection of 3′-tailed (26 nt) and blunt-ended DNA substrates by DNA2 and WRN. Reactions were carried out at 37 °C and contained 2 nM DNA, 350 nM RPA, 10 nM WRN, and 8 nM DNA2. Reaction products at the indicated time points were analyzed as outlined in *B*. The 112- to 133-nt probe was used in this analysis. *Lane 1*, heat-denatured substrate; *lane 14*, 3′-tailed substrate incubated with 20 nM EXO1 and 350 nM RPA for 2 min (R1); *lane 15*, blunt-ended substrate incubated with 20 nM EXO1 and 350 nM RPA for 2 min (R2). *D*, directionality of DNA end resection by WRN-DNA2. Reactions were carried out at 37 °C for 60 min and contained 2 nM 3′-tailed DNA substrate, 350 nM RPA, 8 nM DNA2, and 10 nM WRN. Resection products were annealed with radiolabeled oligonucleotide probes complementary to either 3′-terminated (position 353–374 nt relative to the 3′ end) or 5′-terminated (position 353–374 nt relative to 3′ end) strand and analyzed as in *C*. *E*, 5′ end resection of 3′-tailed DNA substrate by WRN-DNA2 is dependent on WRN concentration and the presence of ATP and RPA. Reactions were carried out at 37 °C for 60 min and contained, as indicated, 2 nM DNA, 350 nM RPA, 1 mM ATP, 8 nM DNA2, and different WRN concentrations. Resection products were detected using the 112–133-nt probe. *F*, dependence of WRN-DNA2-catalyzed resection of 3′-tailed substrate on WRN concentration. Resection at the positions of 112–133 nt and 353–374 nt from the 3′ end of the DNA substrate was monitored. Reactions were carried out as in *E*. Relative concentration of the resection product generated by WRN-DNA2 at each WRN concentration was calculated as a percentage of the product generated by 20 nM EXO1 after 2 min. Data are mean ± S.D. ($n = 3$).

overhangs of 26 nt in length, whereas its cleavage by StuI alone gave rise to a linear DNA molecule with blunt ends. Processing of the DNA substrates was monitored by agarose gel electrophoresis followed by SYBR gold staining (Fig. 1*B*). In addition, ^{32}P-labeled synthetic oligonucleotides complementary to the 3′-terminated strand were used as hybridization probes to detect ssDNA generated by resection at specific positions (Fig. 1*B*) (10). We found that WRN, together with DNA2 and RPA, could catalyze efficient 5′ end resection on the 3′-tailed substrate but not the blunt-ended substrate (Fig. 1*C*). As expected, no reaction products were detected with an oligonucleotide probe complementary to the 5′-terminated strand, indicating that the observed DNA resection activity is limited to the 5′ strand (Fig. 1*D*). Of note, the end product of the resection reaction on the 3′-tailed DNA substrate appeared as a discrete band on SYBR gold-stained gel that was clearly shifted with respect to the unprocessed dsDNA substrate, indicating extensive resection (Fig. 1*C*, *top panel*, compare *lanes 2* and *7*). In contrast, no gradual shift in the electrophoretic mobility of the resection product was apparent after annealing of the radioactive probes. This is most likely due to the fact that DNA2 nuclease generates short oligonucleotides that can reanneal to the resected DNA along with the radioactive probe, leading to a DNA molecule with an electrophoretic mobility similar to that of the DNA substrate. Together, these results clearly demonstrate that DNA2, in conjunction with WRN and RPA, can catalyze extensive 5′ end resection, providing that the DNA substrate contains a 3′ ssDNA overhang.

To further characterize the DNA end resection reaction mediated by WRN-DNA2, reactions with the 3′-tailed substrate were carried out at various WRN concentrations, whereas DNA2 was kept at a concentration of 8 nM. We observed that the amount of resection product increased gradually with WRN concentration, reaching a plateau at about 10 nM (Fig. 1*E*, *lanes 2–7*, and Fig. 1*F*). Quantitative analysis of gel images revealed that about 35% of the DNA substrate was resected to the position of 133 nt from the 3′ end and that about 15% of the DNA substrate was resected to the position of 374 nt

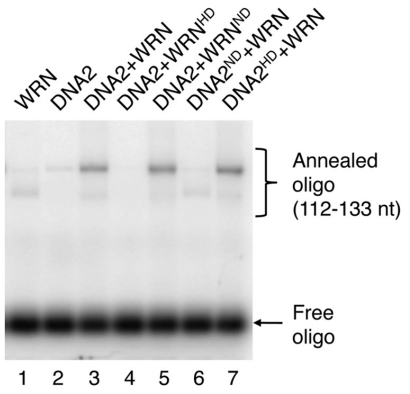

FIGURE 2. **5′ end resection of 3′-tailed DNA substrate by WRN-DNA2 depends on the helicase activity of WRN and the nuclease activity of DNA2.** Reactions were carried out at 37 °C for 60 min and contained 2 nM DNA, 350 nM RPA, 1 mM ATP, 8 nM DNA2, and 10 nM WRN. Resection products were detected using the 112–133 nt probe. *WRN^{HD}*, helicase-deficient mutant of WRN (K567M); *WRNND*, nuclease-deficient mutant of WRN (E84A); *DNA2^{HD}*, helicase-deficient mutant of DNA2 (K654R); *DNA2ND*, nuclease-deficient mutant of DNA2 (D277A).

within 1 h of incubation (Fig. 1*F*). Interestingly, a small amount of resected product (1–2%) could also be detected in the absence of WRN, suggesting that DNA2 itself could slowly resect dsDNA ends, likely following RPA-mediated stabilization of ssDNA ends generated by thermal fraying (Fig. 1*E*, *lane 2*). In the absence of DNA2, WRN was only capable of DNA unwinding, as evident from the appearance of a fast-migrating band (Fig. 1*E*, *lane 8*). The resection process catalyzed by WRN and DNA2 was found to be dependent on the presence of ATP and RPA, as expected for a helicase-driven reaction (Fig. 1*E*, compare *lanes 9–12*).

WRN acts not only as a 3′-5′ DNA helicase, but it also possesses a dsDNA-dependent 3′-5′ exonuclease activity residing in a separate domain located in the N-terminal portion of the protein (39, 40). DNA2 functions as a 5′-3′ helicase and a ssDNA-specific endonuclease (32, 41). To define the functions of the enzymatic activities of WRN and DNA2 in DNA end resection, we carried out a set of resection reactions with the 3′-tailed pUC19 substrate where either WRN or DNA2 were substituted with catalytically inactive mutants. We found that the helicase-deficient mutant of WRN (K567M) failed to stimulate DNA resection by DNA2, whereas the nuclease-deficient mutant of WRN (E84A) behaved similarly as the wild-type WRN in this reaction (Fig. 2, *lanes 2–4*). Substitution of DNA2 with its nuclease-deficient mutant (D277A) completely abolished resection and stimulated unwinding of the plasmid substrate (Fig. 2, *lane 6*). In contrast, the helicase-deficient mutant of DNA2 (K654E) could resect the DNA substrate to the same degree as the wild-type protein (Fig. 2, compare *lanes 3* and *7*). These results indicate that DNA end resection mediated by DNA2, WRN, and RPA is dependent on the helicase activity of WRN and the endonuclease activity of DNA2.

DNA2 and WRN Interact Physically—Yeast Dna2 has been shown to interact physically with Sgs1 (10). Likewise, BLM forms a complex with human DNA2 (17). Therefore, we investigated whether human DNA2 interacts physically with WRN. To this end, HEK293 cells were transfected with plasmids expressing WRN and FLAG-tagged DNA2, respectively, and complex formation between these proteins was tested by immunoprecipitation using beads conjugated with anti-FLAG M2 antibody. We found that WRN coimmunoprecipitated with FLAG-DNA2, indicating that these proteins form a complex *in vivo* (Fig. 3*A*, *lane 3*). This interaction was specific because anti-FLAG beads did not immunoprecipitate WRN from an extract lacking FLAG-DNA2 (Fig. 3*A*, *lane 1*). To further investigate complex formation between WRN and DNA2, we generated a stable HEK293 cell line expressing FLAG-DNA2. By immunoprecipitation using anti-FLAG M2 beads or anti-WRN antibody, we found that FLAG-DNA2 formed a complex with endogenous WRN in these cells (Fig. 3, *B* and *C*). Western blot analysis indicated that the level of FLAG-DNA2 in these cells was only slightly higher than that of endogenous DNA2, suggesting that WRN and DNA2 form a complex under physiological conditions (Fig. 3*B*, *top panel*). Interaction between FLAG-DNA2 and endogenous BLM was also detected as expected (Fig. 3*B*) (17). The cellular concentration of these protein complexes was not altered when cells were subjected to treatment with CPT, which causes breakage of DNA replication forks (Fig. 3*B*, *lanes 2–5*) (42). This suggests that the interaction of DNA2 with WRN and BLM in the cell is not dependent on DNA damage.

To test whether WRN and DNA2 interact directly, purified proteins were mixed and incubated at 4 °C for 4 h. Complex formation between WRN and DNA2 was tested by immunoprecipitation using anti-WRN antibody. We found that DNA2 coimmunoprecipitated with WRN. DNA2 was not present in the immunoprecipitated material whether WRN was omitted, confirming a direct protein-protein interaction (Fig. 3*D*). To map the interaction site of DNA2 on WRN, we tested binding of purified His_6-DNA2-FLAG protein to various WRN fragments covering the entire WRN polypeptide (Fig. 3*E*). The WRN fragments were produced in *E. coli* as fusions with a GST tag and isolated on GSH-Sepharose beads. Using a GST pulldown assay, we found that DNA2 bound specifically to a WRN fragment including the core helicase domain (helicase/Zn^{2+}-binding domains) and the winged helix domain (Fig. 3*F*, compare *lanes 1* and *4*) a binding site of a number of other proteins shown to interact with WRN (43, 44). DNA2 was also bound to a fragment containing only the helicase core or to the C-terminal portion of WRN starting at the beginning of the winged helix domain (Fig. 3*F*, compare *lanes 1*, *3*, *4*, and *5*). In contrast, DNA2 did not bind the N-terminal portion of WRN containing the exonuclease domain (Fig. 3*F*, *lane 2*). Collectively, these results suggest that there are at least two DNA2-interaction sites on WRN: one located in the central helicase domain and the other in the C-terminal region of WRN.

WRN-DNA2 Resects DNA Ends More Efficiently Than BLM-DNA2—Next, we set out to compare WRN and BLM with respect to their abilities to resect DNA ends in concert with DNA2 and RPA *in vitro*. Using a Y structure oligonucleotide duplex (29 bp) with single-stranded arms (30 nt each), we found that our preparations of WRN and BLM exhibited similar levels of specific helicase activity (Fig. 4*A*). For resection reactions, we used the 3′-tailed DNA substrate that was readily processed by

The Role of WRN and BLM in DNA End Resection

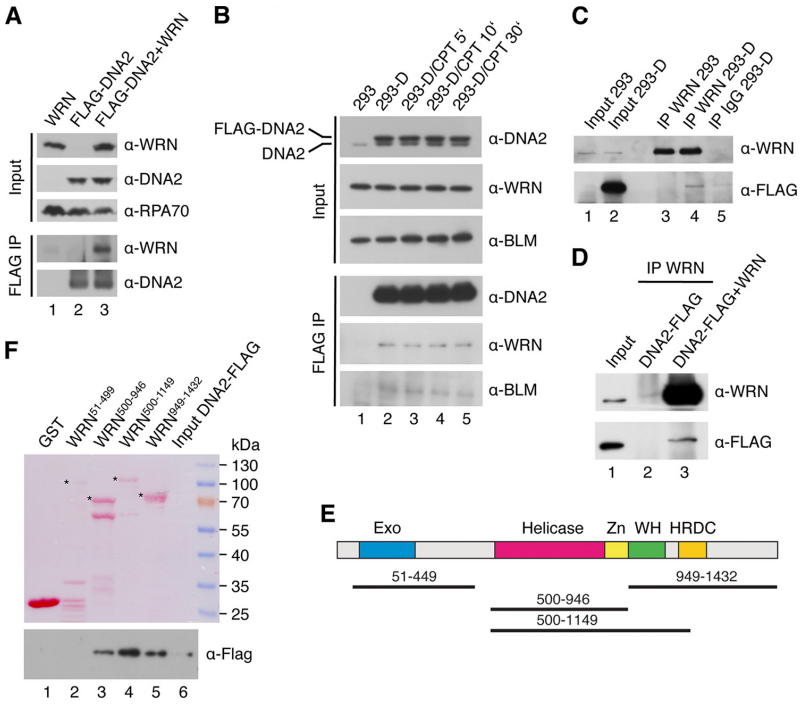

FIGURE 3. **Physical interaction between DNA2 and WRN *in vitro* and *in vivo*.** *A*, coimmunoprecipitation of WRN with DNA2 from human cells. HEK293 cells were transfected with vectors expressing FLAG-DNA2 and WRN as indicated. Cell extracts were immunoprecipitated (*IP*) with anti-FLAG antibody as described under "Experimental Procedures." Blots were probed with the indicated antibodies. 5% of input material was loaded. *B*, effect of DNA damage on the formation of DNA2-WRN and DNA2-BLM complexes in human cells. HEK293 cells stably transfected with the FLAG-DNA2 construct (*HEK293-D*) were treated with 1 μM CPT. At the indicated time points, complex formation between FLAG-DNA2 and endogenous WRN and BLM, respectively, was tested by immunoprecipitation using anti-FLAG antibody. *C*, coimmunoprecipitation of DNA2 with WRN from human cells. Extracts from HEK293-D cells were subjected to immunoprecipitation with anti-WRN antibody or control IgG. The immunoprecipitates were tested for the presence of FLAG-DNA2 and WRN by Western blotting. As a control, a WRN immunoprecipitate from HEK293 cells was also analyzed (*lane 3*). *D*, coimmunoprecipitation of DNA2 with WRN from a mixture of purified proteins. DNA2 (500 ng) was incubated with or without WRN (500 ng) at 4 °C for 4 h. The mixtures were subjected to immunoprecipitation with anti-WRN antibody. *E*, domain organization of WRN. *Exo*, exonuclease domain; *Zn*, zinc-binding domain; *WH*, winged-helix domain; *HRDC*, helicase and RNaseD C-terminal domain. *Black lines* indicate WRN fragments used for mapping the DNA2-interaction site on WRN. *F*, GST pulldown assay. Glutathione beads coated with the indicated GST-tagged fragments of WRN were incubated with purified His_6-DNA2-FLAG protein at 4 °C for 2 h, and bound proteins were analyzed by Western blotting as described under "Experimental Procedures." 1% of input was loaded in *B* and *C*, whereas 10% of input was loaded in *D* and *F*.

WRN-DNA2 in the presence of RPA (Fig. 1*C*). The extent of DNA resection at various reaction time points was monitored by annealing of radiolabeled oligonucleotide probes. These experiments clearly showed that WRN-DNA2 resected the DNA substrate at a much higher rate compared with BLM-DNA2 (Fig. 4, *B* and *C*). Notably, WRN-DNA2-catalyzed resection to the position of 374 nt away from the 3′ end was faster than BLM-DNA2-catalyzed resection to the position of 133 nt (Fig. 4, *B* and *C*). We also compared the activities of WRN-DNA2 and BLM-DNA2 on blunt-ended DNA substrate in the presence of RPA. We found that this DNA substrate was largely refractory not only to processing by WRN-DNA2 but also to processing by BLM-DNA2 (Fig. 4*D*, compare *lanes 4* and *5* to *lanes 10* and *11*). Taken together, we show that WRN-DNA2 resects DNA ends more efficiently than BLM-DNA2 *in vitro*.

Dissection of Pathways Involved in DNA End Resection in Human Cells—To assess whether WRN is involved in DNA end resection *in vivo*, we investigated the effect of its depletion on the efficiency of SSA-mediated repair of endonuclease-induced DSBs in cells that were either proficient or deficient for EXO1 and DNA2, respectively. For this epistasis analysis, we initially used the human embryonic kidney cell line HEK293 stably transfected with the SA-GFP reporter cassette consisting of two truncated *GFP* gene alleles (*5′GFP* and *Sce3′GFP*) that form a direct sequence repeat (280 bp) separated by a region of about 2.4 kb (Fig. 5*A*) (34, 45). SSA-mediated recombination between these homologous sequences triggered by a DSB generated in the distal GFP allele by the I-SceI endonuclease results in the formation of a functional *GFP* gene (Fig. 5*A*). This requires extensive DNA end resection to expose the complementary ssDNA regions for annealing. The proteins of interest were depleted from HEK293/SA-GFP cells by RNA interference. Cells were subsequently transfected with an I-SceI expression vector to create a DSB in the reporter cassette, and the percentage of GFP positive cells arising upon SSA-mediated repair was determined by flow cytometry 2 days after plasmid transfection. We found that cells depleted of either EXO1, WRN, or DNA2 exhibited a marked reduction in the frequency of SSA repair events (55, 65, and 75%, respectively) compared with mock-depleted cells (Fig. 5, *B* and *C*). In contrast, knockdown of

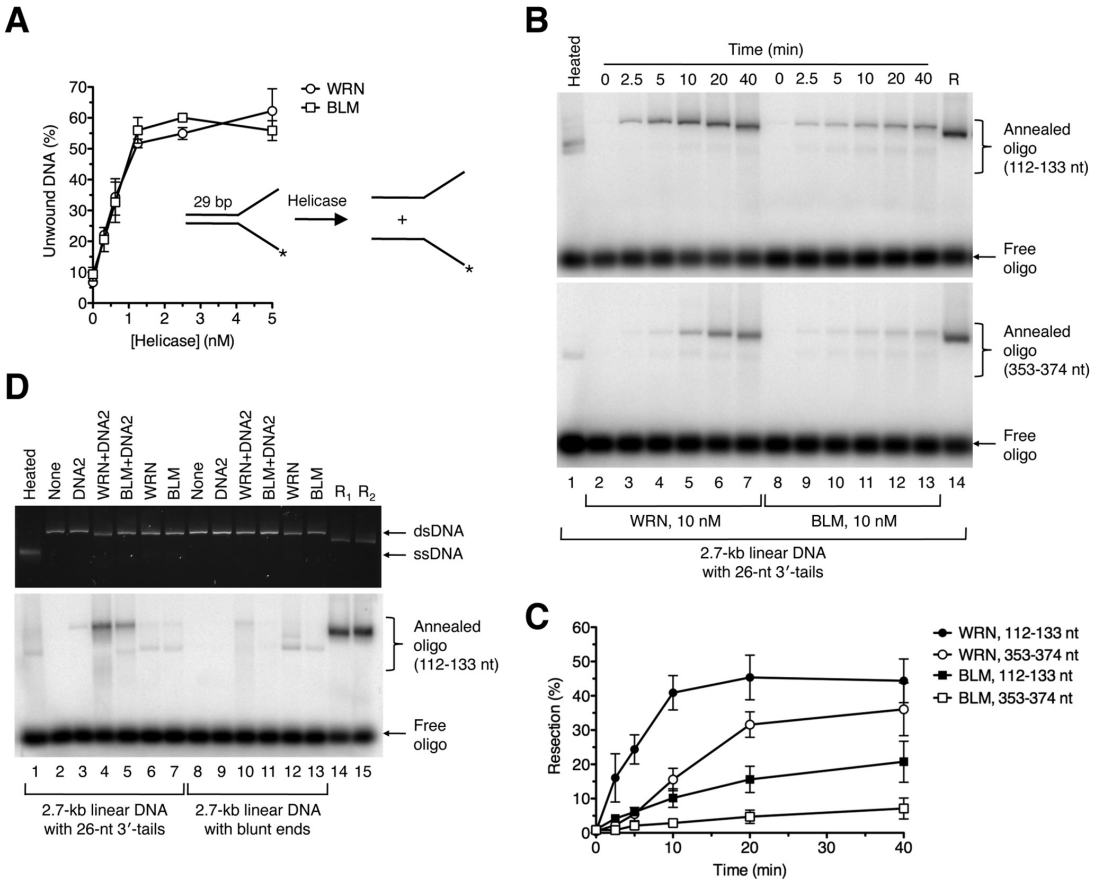

FIGURE 4. **Comparison of DNA end resection activities of WRN-DNA2 and BLM-DNA2.** *A*, comparison of helicase activities of WRN and BLM. Reactions contained 1 nM ^{32}P-labeled forked DNA duplex (*inset*) and different concentrations of WRN or BLM. Reactions were incubated at 37 °C for 30 min, and reaction products were quantified as described under "Experimental Procedures." Data are mean ± S.D. ($n = 3$). *B*, time course of resection of 3′-tailed DNA substrate catalyzed by WRN-DNA2 and BLM-DNA2, respectively. Reactions contained 2 nM DNA, 350 nM RPA, 8 nM DNA2, and 10 nM WRN/BLM. Reaction aliquots withdrawn at the indicated time points were subjected to electrophoresis on a 1% agarose gel after hybridization of radiolabeled probes complementary to 3′-terminated strand at the indicated positions. Radiolabeled DNA species were visualized by phosphorimaging. *C*, quantification of the reactions in *B*. Relative concentration of resection products generated at each time point was calculated as a percentage of the product generated by 20 nM EXO1 after 2 min. Data are mean ± S.D. ($n = 3$). *D*, processing of 3′-tailed (26 nt) and blunt-ended DNA substrates in reactions with indicated composition. Reactions were carried out at 37 °C for 60 min and contained 2 nM DNA, 350 nM RPA, and, where indicated, 8 nM DNA2, 20 nM WRN, and 20 nM BLM. Reaction products were analyzed as in Fig. 1*C*. *Lane 1*, heat-denatured substrate; *lane 14*, 3′-tailed substrate incubated with 20 nM EXO1 for 2 min (R1); *lane 15*, blunt-ended substrate incubated with 20 nM EXO1 for 2 min (R2).

BLM was found to be associated with a significant increase in SSA repair efficiency (140%) compared with control cells (Fig. 5, *B* and *C*). Of note, the SSA repair defect of WRN-depleted cells could be rescued by ectopic expression of the siRNA-resistant form of WRN, excluding an off-target effect of the WRN siRNA used in this study (Fig. 5*D*). Combined depletion of EXO1 and WRN or EXO1 and DNA2 further decreased the repair efficiency compared with the respective single depletions, whereas codepletion of DNA2 and WRN did not (Fig. 5, *B* and *C*). In addition, combined depletion of EXO1 and BLM had nearly the same effect on the SSA repair efficiency as EXO1 depletion (Fig. 5, *B* and *C*). Therefore, these findings suggest that HEK293 cells have at least two pathways for long-range resection of DSB ends: one mediated by EXO1 and the other dependent upon DNA2 and WRN.

To substantiate these findings, we performed a similar set of experiments using U2OS/SA-GFP cells (35). This analysis indicated that combined depletion of EXO1 and DNA2 almost completely abolished (reduced by 91%) SSA-mediated DSB repair in U2OS/SA-GFP cells, as did depletion of MRE11 (by 89%) or CtIP (by 82%), suggesting that long-range DNA end resection in U2OS cells is largely dependent on EXO1 and DNA2 (Fig. 5, *E–G*). However, in contrast to the results obtained with HEK293/SA-GFP cells, we observed a significant reduction in SSA repair efficiency not only after depletion of WRN (by 57%) but also after depletion of BLM (by 59%) (Fig. 5, *E* and *F*). Codepletion of BLM and WRN further decreased the repair efficiency to a level comparable with that in DNA2-depleted (by 73%) cells (Fig. 5, *E* and *F*). Moreover, combined depletion of DNA2 with either BLM or WRN had nearly the

The Role of WRN and BLM in DNA End Resection

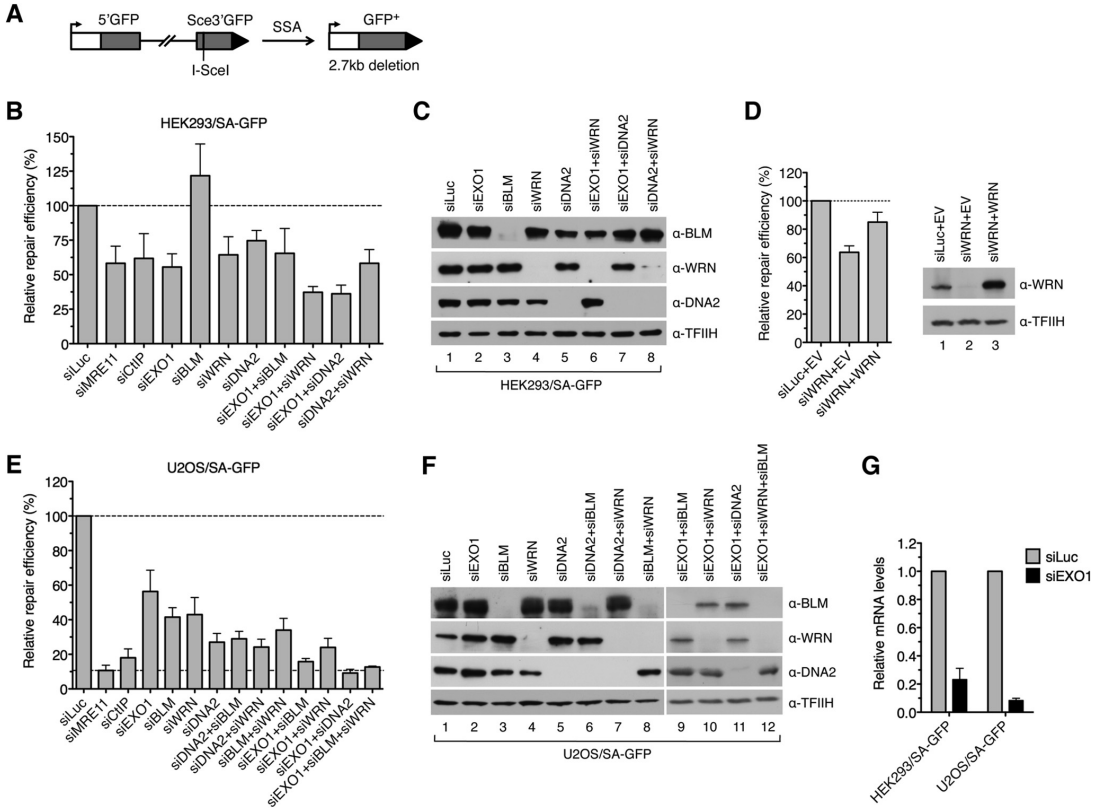

FIGURE 5. **WRN and BLM interact epistatically with DNA2 to promote DSB repair by SSA in human cells.** *A*, schematic of the SA-GFP reporter cassette. SSA-mediated repair of a DSB at the I-SceI-cutting site results in the formation of a functional GFP allele. *B*, efficiency of SSA-mediated repair of I-SceI-induced DSB in HEK293/SA-GFP cells treated with the indicated siRNAs. Cells were transfected with the appropriate siRNAs (40 nM) 2 days prior to transfection of the I-SceI-expressing plasmid. The percentage of GFP-positive cells in each sample was measured by flow cytometry 2 days after I-SceI plasmid transfection and taken as a measure of DSB repair efficiency. The plotted values represent the relative repair efficiency calculated as a percentage of repair efficiency measured in cells transfected with control siRNA (*siLuc*, 100%). Data are mean ± S.D. (n ≥ 3). *C*, Western blot analysis of extracts from HEK293/SA-GFP cells transfected with indicated siRNAs under the same conditions as for SA-GFP reporter assays. Blots were probed with the indicated antibodies. *D*, rescue of the SSA-repair defect of WRN-depleted HEK293/SA-GFP cells by expression of the siRNA-resistant variant of WRN. An SA-GFP reporter assay was performed as in *B*. The WRN plasmid (*WRN*) or empty vector (*EV*) were cotransfected with the I-SceI plasmid. *E*, efficiency of SSA-mediated repair of I-SceI-induced DSB in U2OS/SA-GFP cells treated with the indicated siRNAs. Experiments were performed as in *B*. *F*, Western blot analysis of extracts from U2OS/SA-GFP cells transfected with the indicated siRNAs. Blots were probed with the indicated antibodies. *G*, quantitative real-time PCR showing that EXO1 mRNA levels are down-regulated by specific siRNA. Data are mean ± S.D. ($n = 3$).

same inhibitory effect on SSA repair as DNA2 depletion (Fig. 5, *E* and *F*). On the contrary, codepletion of EXO1 with either WRN or BLM caused a much higher reduction in repair efficiency than depletion of DNA2 alone, and triple depletion of EXO1, BLM, and WRN brought repair efficiency down to the level measured in cells depleted of EXO1 and DNA2 (Fig. 5, *E* and *F*). Collectively, these data suggest that, in U2OS cells, both WRN and BLM assist DNA2 to mediate long-range resection of broken DNA ends.

To bolster our conclusion that DNA2, WRN, and BLM have an epistatic relationship in DSB end resection, we extended our analysis to measurement of RPA focus formation in U2OS cells treated with CPT. As expected, 1 h after addition of CPT, RPA formed numerous foci in γ-H2AX-positive cells, which were dependent on the presence of CtIP (Fig. 6). Depletion of DNA2 resulted in a marked reduction in the number of RPA foci per cell compared with mock-depleted cells (Fig. 6). Cells depleted of BLM or WRN displayed a mild decrease in RPA focus frequency compared with mock-depleted cells (Fig. 6). In contrast, combined depletion of BLM and WRN caused approximately the same reduction in RPA focus frequency as depletion of DNA2 alone. Moreover, cells depleted of DNA2 and BLM or DNA2 and WRN displayed an RPA foci frequency comparable with that of DNA2-depleted cells (Fig. 6). These data further support the conclusion that DNA2, WRN, and BLM operate in the same DNA end resection pathway.

Role of the BLM-TOPOIIIα-RMI1-RMI2 Complex in DNA End Resection—In human cells, BLM exists in a complex with TOPOIIIα, RMI1, and RMI2, which is known to catalyze double Holliday junction dissolution during HR (46–49). Studies in yeast have shown that Top3α and Rmi1 are also required for DNA-end resection *in vivo* and stimulate DNA end resection by

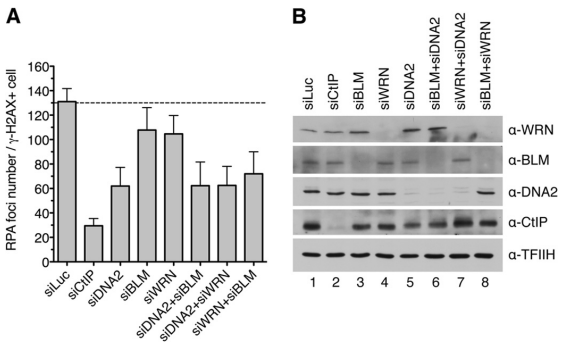

FIGURE 6. **DNA2, WRN, and BLM act in the same pathway of DSB end resection.** *A*, frequency of camptothecin-induced RPA foci in nuclei of U2OS cells depleted of the indicated proteins. Cells were transfected with appropriate siRNAs and, 48 h later, treated with 1 μM camptothecin for 1 h. Cells were then detergent-extracted and fixed with formaldehyde. RPA and γ-H2AX (a marker of DNA damage) were visualized by indirect immunofluorescence. DAPI was used to stain nuclei. The average number of RPA foci per γ-H2AX-positive cell was determined for each sample using an Olympus Scan^R screening station. The data points are mean ± S.D. ($n = 3$). *B*, Western blot analysis of extracts from U2OS cells transfected with indicated siRNAs. Blots were probed with the antibodies indicated on the *right*.

Sgs1-Dna2 *in vitro* by promoting the helicase activity of Sgs1 (9, 10, 14). Our study revealed that BLM-DNA2 resects DNA ends less efficiently than WRN-DNA2 *in vitro*, whereas *in vivo*, at least in U2OS cells, BLM and WRN appeared to contribute equally to promote DNA end resection (Fig. 5*E*). Therefore, we investigated whether BLM requires TOPOIIIα, RMI1, and RMI2 (TRR) to efficiently support DNA end resection by DNA2. To this end, we first investigated the effect of a purified TRR complex on DNA end resection by BLM-DNA2 *in vitro* (Fig. 7*A*). We found that TRR enhanced resection of the 3′-tailed pUC19 substrate by BLM-DNA2 (Fig. 7, *B* and *C*, *lanes 3–6*). On the contrary, the TRR complex had no effect on DNA end resection by WRN-DNA2 (data not shown). Moreover, it could not enhance DNA end resection by DNA2 in the absence of BLM (Fig. 7, *B* and *C*, compare *lanes 2* and *7*).

Next we tested the effect of depletion of RMI1 on the efficiency of SSA-mediated repair of I-SceI-induced DSBs in U2OS/SA-GFP cells. We found that RMI1 depletion reduced the repair efficiency to the level displayed by BLM- or DNA2-depleted cells (Fig. 7, *D* and *E*). Importantly, codepletion of RMI1 with BLM or DNA2 did not further reduce the repair efficiency compared with single depletions of these proteins, suggesting that RMI1, BLM, and DNA2 act in the same pathway (Fig. 7, *D* and *E*). Collectively, these results suggest that, in human cells, BLM promotes long-range DNA end resection as part of the BTRR complex.

DISCUSSION

Here we present evidence suggesting that human DNA2 acts in conjunction with either WRN or BLM to mediate long-range resection of broken DNA ends *in vivo*. Moreover, we show that WRN helicase can cooperate with DNA2 and RPA to catalyze resection of DNA ends *in vitro*, generating long 3′-terminated ssDNA tails. Our study also reveals that both WRN-DNA2 and BLM-DNA2 require a 3′ ssDNA overhang to efficiently initiate DNA end resection *in vitro*, which is in agreement with the "two-step" resection model in which the initial 5′ end trimming is carried out by the MRE11-RAD50-NBS1/Xrs2 complex in conjunction with CtIP/Sae2 (8, 9, 11, 19). In addition, we present evidence that BLM and DNA2 interact epistatically with RMI1 to mediate DNA end resection *in vivo*. Moreover, we show that the TRR complex stimulates DNA end resection by BLM-DNA2 *in vitro*. These data suggest that, in cells, BLM mediates DNA end resection as part of the BTRR complex.

Our discovery of the involvement of WRN in DNA end resection is consistent with the findings that WRN interacts physically with the MRN complex and accumulates at sites of DSBs in human cells (50, 51). Moreover, it has been demonstrated that WRN depletion leads to a marked reduction in the frequency of RPA and BrdU/ssDNA foci formed in response to ionizing radiation, indicative of a resection defect (52). A similar phenotype has been observed in DNA2-depleted cells (18). Although the previous studies did not address the relationship between WRN and DNA2, they demonstrated that these enzymes act synergistically with EXO1 to promote DNA end resection in human cells (18, 52). A role for WRN as a critical DNA end resection factor is also consistent with the cellular phenotype of Werner syndrome, a severe premature aging disorder caused by inherited mutations in the *WRN* gene (53). Cells derived from Werner syndrome patients are characterized by non-homologous chromosome exchanges, termed variegated translocation mosaicism, and large chromosomal deletions that may result from aberrant DSB repair by NHEJ as a consequence of a defect in DNA end resection (54–56). Indeed, it is becoming clear that NHEJ accounts for most chromosomal translocations in humans (57). Moreover, a role for DNA end resection as the critical determinant of DSB repair pathway choice is well established (58). Accumulating evidence suggests that defects in homology-directed repair pathways, which are dependent on DNA end resection, result in overuse of NHEJ for repair, leading to accumulation of chromosomal rearrangements (57). However, it should be noted that WRN is also known to promote DSB repair by the classical Ku-dependent NHEJ (C-NHEJ) pathway to suppress microhomology-mediated end joining (59, 60). This alternative end joining pathway is capable of producing chromosomal translocations, particularly when Ku-dependent NHEJ is deficient (57). Moreover, WRN has been shown to be involved in the resolution HR intermediates (61, 62). Therefore, it seems that the genomic instability in Werner syndrome is a consequence of multiple defects in DNA repair pathways.

Our finding that the TRR complex stimulates DNA end resection by BLM-DNA2 *in vitro* is consistent with previous reports showing that the association of BLM with TOPOIIIα and RMI1 enhances its DNA unwinding activity, which drives the BLM-DNA2-catalyzed resection reaction (17, 63). Similarly, RMI1 and RMI2 have been shown to enhance the efficiency of the BLM-TOPOIIIα-mediated double Holliday junction dissolution reaction (48, 49, 64). It has also been shown that RMI1 forms a complex with RPA and that this interaction is essential for the stimulatory effect of RPA on double Holliday junction dissolution by the BTRR complex (65). Therefore, it is possible that a physical interaction between RMI1 and RPA

The Role of WRN and BLM in DNA End Resection

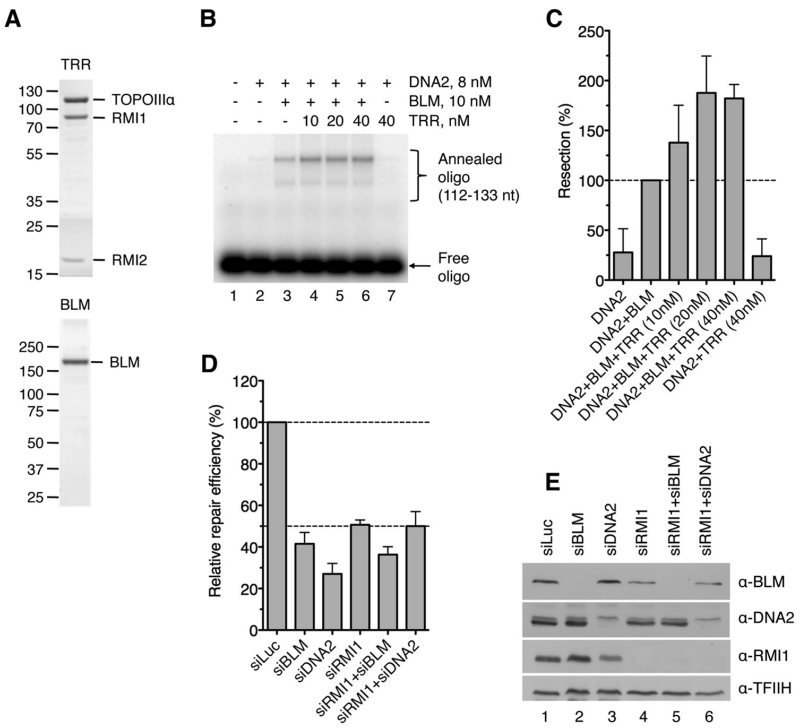

FIGURE 7. **Involvement of TOPOIIIα, RMI1, and RMI2 in DNA end resection.** *A*, SDS-PAGE analysis of purified TRR complex (1.5 μg) and BLM (0.5 μg). The gel was stained with Coomassie Brilliant Blue R-250. The molecular weights of protein standards are indicated on the *left*. *B*, stimulation of BLM-DNA2-catalyzed DNA end resection by the TRR complex. Reactions contained 2 nM 3′-tailed pUC19 substrate, 8 nM DNA2, 10 nM BLM, 350 nM RPA, and varying concentrations of TRR. BLM and TRR were preincubated for 5 min on ice prior to addition to the reaction. Reaction products were analyzed as in Fig. 1*C* using the 112–133-nt probe. *C*, quantification of the product of reactions in *B*. Data are mean ± S.D. ($n = 3$). The data are normalized to the amount of product in the reaction containing only BLM and DNA2 (100%). *D*, RMI1 acts epistatically with BLM and DNA2 to promote DSB repair by SSA in human cells. Efficiency of SSA-mediated repair of I-SceI-induced DSB in U2OS/SA-GFP cells transfected with indicated siRNAs was measured as in Fig. 5*E*. *E*, Western blot analysis of extracts from U2OS/SA-GFP cells transfected with indicated siRNAs under the same conditions as for SA-GFP reporter assays. Blots were probed with the indicated antibodies.

loaded on the 3′-terminated DNA strand during DNA2-catalyzed resection might enhance the DNA unwinding processivity of the BTRR complex and, hence, increase the efficiency of the resection reaction. However, it should be noted that the stimulatory effect of the TRR complex on DNA end resection by BLM-DNA2 *in vitro* was rather modest under our experimental conditions. On the contrary, RMI1 depletion in U2OS/SA-GFP cells reduced the efficiency of SSA-mediated DSB repair to levels displayed by BLM- or DNA2-deficient cells, suggesting that BLM requires RMI1 to promote DNA end resection *in vivo*. Of note, it has been shown that silencing of RMI1 or RMI2 expression by RNA interference destabilizes both BLM and TOPOIIIα (47, 49). Therefore, it is evident that, in addition to being important for the functional attributes of the BTRR complex, RMI1 and RMI2 are indispensable for the structural integrity of its components *in vivo*.

Although BLM depletion compromised SSA-mediated DSB repair in U2OS/SA-GFP cells, it had an opposite effect on SSA in HEK293/SA-GFP cells. Similarly, the efficiency of SSA-mediated DSB repair in HEK293/SA-GFP cells was elevated significantly upon depletion of RMI1 (data not shown). These findings suggest that, in HEK293 cells, the BTRR complex might act as an SSA suppressor, most likely through unwinding of the annealed intermediate formed following DNA end resection. Strikingly, we found that BLM concentration in HEK293 cells was much higher than in U2OS cells (data not shown). Therefore, it appears that the BTRR complex exerts an inhibitory effect on SSA when its concentration in the cell exceeds certain threshold.

Acknowledgments—We thank Kata Sarlos and Ian D. Hickson for the purified TRR complex, Judith L. Campbell for the transfer vector for preparation of the bacmid expressing His$_6$-hDNA2-FLAG, Jeremy M. Stark for the HEK293/SA-GFP and U2OS/SA-GFP cell lines, Stefano Ferrari and Stephanie Bregenhorn for help with protein purification, and Christiane Koenig for technical assistance.

REFERENCES

1. Jackson, S. P., and Bartek, J. (2009) The DNA-damage response in human biology and disease. *Nature* **461,** 1071–1078
2. Khanna, K. K., and Jackson, S. P. (2001) DNA double-strand breaks: signaling, repair and the cancer connection. *Nat. Genet.* **27,** 247–254
3. Longhese, M. P., Bonetti, D., Guerini, I., Manfrini, N., and Clerici, M. (2009) DNA double-strand breaks in meiosis: checking their formation,

processing and repair. *DNA Repair* **8,** 1127–1138
4. Soulas-Sprauel, P., Rivera-Munoz, P., Malivert, L., Le Guyader, G., Abramowski, V., Revy, P., and de Villartay, J. P. (2007) V(D)J and immunoglobulin class switch recombinations: a paradigm to study the regulation of DNA end-joining. *Oncogene* **26,** 7780–7791
5. Lieber, M. R. (2010) The mechanism of double-strand DNA break repair by the nonhomologous DNA end-joining pathway. *Annu. Rev. Biochem.* **79,** 181–211
6. San Filippo, J., Sung, P., and Klein, H. (2008) Mechanism of eukaryotic homologous recombination. *Annu. Rev. Biochem.* **77,** 229–257
7. Heyer, W. D., Ehmsen, K. T., and Liu, J. (2010) Regulation of homologous recombination in eukaryotes. *Annu. Rev. Genet.* **44,** 113–139
8. Mimitou, E. P., and Symington, L. S. (2008) Sae2, Exo1 and Sgs1 collaborate in DNA double-strand break processing. *Nature* **455,** 770–774
9. Zhu, Z., Chung, W. H., Shim, E. Y., Lee, S. E., and Ira, G. (2008) Sgs1 helicase and two nucleases Dna2 and Exo1 resect DNA double-strand break ends. *Cell* **134,** 981–994
10. Cejka, P., Cannavo, E., Polaczek, P., Masuda-Sasa, T., Pokharel, S., Campbell, J. L., and Kowalczykowski, S. C. (2010) DNA end resection by Dna2-Sgs1-RPA and its stimulation by Top3-Rmi1 and Mre11-Rad50-Xrs2. *Nature* **467,** 112–116
11. Nicolette, M. L., Lee, K., Guo, Z., Rani, M., Chow, J. M., Lee, S. E., and Paull, T. T. (2010) Mre11-Rad50-Xrs2 and Sae2 promote 5′ strand resection of DNA double-strand breaks. *Nat. Struct. Mol. Biol.* **17,** 1478–1485
12. Shim, E. Y., Chung, W. H., Nicolette, M. L., Zhang, Y., Davis, M., Zhu, Z., Paull, T. T., Ira, G., and Lee, S. E. (2010) *Saccharomyces cerevisiae* Mre11/Rad50/Xrs2 and Ku proteins regulate association of Exo1 and Dna2 with DNA breaks. *EMBO J.* **29,** 3370–3380
13. Cannavo, E., Cejka, P., and Kowalczykowski, S. C. (2013) Relationship of DNA degradation by *Saccharomyces cerevisiae* exonuclease 1 and its stimulation by RPA and Mre11-Rad50-Xrs2 to DNA end resection. *Proc. Natl. Acad. Sci. U.S.A.* **110,** E1661–E1668
14. Niu, H., Chung, W. H., Zhu, Z., Kwon, Y., Zhao, W., Chi, P., Prakash, R., Seong, C., Liu, D., Lu, L., Ira, G., and Sung, P. (2010) Mechanism of the ATP-dependent DNA end-resection machinery from *Saccharomyces cerevisiae*. *Nature* **467,** 108–111
15. Truong, L. N., Li, Y., Shi, L. Z., Hwang, P. Y., He, J., Wang, H., Razavian, N., Berns, M. W., and Wu, X. (2013) Microhomology-mediated end joining and homologous recombination share the initial end resection step to repair DNA double-strand breaks in mammalian cells. *Proc. Natl. Acad. Sci. U.S.A.* **110,** 7720–7725
16. Gravel, S., Chapman, J. R., Magill, C., and Jackson, S. P. (2008) DNA helicases Sgs1 and BLM promote DNA double-strand break resection. *Genes Dev.* **22,** 2767–2772
17. Nimonkar, A. V., Genschel, J., Kinoshita, E., Polaczek, P., Campbell, J. L., Wyman, C., Modrich, P., and Kowalczykowski, S. C. (2011) BLM-DNA2-RPA-MRN and EXO1-BLM-RPA-MRN constitute two DNA end resection machineries for human DNA break repair. *Genes Dev.* **25,** 350–362
18. Karanja, K. K., Cox, S. W., Duxin, J. P., Stewart, S. A., and Campbell, J. L. (2012) DNA2 and EXO1 in replication-coupled, homology-directed repair and in the interplay between HDR and the FA/BRCA network. *Cell Cycle* **11,** 3983–3996
19. Shibata, A., Moiani, D., Arvai, A. S., Perry, J., Harding, S. M., Genois, M. M., Maity, R., van Rossum-Fikkert, S., Kertokalio, A., Romoli, F., Ismail, A., Ismalaj, E., Petricci, E., Neale, M. J., Bristow, R. G., Masson, J. Y., Wyman, C., Jeggo, P. A., and Tainer, J. A. (2014) DNA double-strand break repair pathway choice is directed by distinct MRE11 nuclease activities. *Mol. Cell* **53,** 7–18
20. Bernstein, K. A., Gangloff, S., and Rothstein, R. (2010) The RecQ DNA helicases in DNA repair. *Annu. Rev. Genet.* **44,** 393–417
21. Yan, H., McCane, J., Toczylowski, T., and Chen, C. (2005) Analysis of the *Xenopus* Werner syndrome protein in DNA double-strand break repair. *J. Cell Biol.* **171,** 217–227
22. Liao, S., Toczylowski, T., and Yan, H. (2008) Identification of the Xenopus DNA2 protein as a major nuclease for the 5′→3′ strand-specific processing of DNA ends. *Nucleic Acids Res.* **36,** 6091–6100
23. Liao, S., Guay, C., Toczylowski, T., and Yan, H. (2012) Analysis of MRE11's function in the 5′→3′ processing of DNA double-strand breaks. *Nucleic Acids Res.* **40,** 4496–4506
24. Saydam, N., Kanagaraj, R., Dietschy, T., Garcia, P. L., Peña-Diaz, J., Shevelev, I., Stagljar, I., and Janscak, P. (2007) Physical and functional interactions between Werner syndrome helicase and mismatch-repair initiation factors. *Nucleic Acids Res.* **35,** 5706–5716
25. Adams, K. E., Medhurst, A. L., Dart, D. A., and Lakin, N. D. (2006) Recruitment of ATR to sites of ionising radiation-induced DNA damage requires ATM and components of the MRN protein complex. *Oncogene* **25,** 3894–3904
26. Sartori, A. A., Lukas, C., Coates, J., Mistrik, M., Fu, S., Bartek, J., Baer, R., Lukas, J., and Jackson, S. P. (2007) Human CtIP promotes DNA end resection. *Nature* **450,** 509–514
27. Yang, J., O'Donnell, L., Durocher, D., and Brown, G. W. (2012) RMI1 promotes DNA replication fork progression and recovery from replication fork stress. *Mol. Cell Biol.* **32,** 3054–3064
28. Orren, D. K., Brosh, R. M., Jr., Nehlin, J. O., Machwe, A., Gray, M. D., and Bohr, V. A. (1999) Enzymatic and DNA binding properties of purified WRN protein: high affinity binding to single-stranded DNA but not to DNA damage induced by 4NQO. *Nucleic Acids Res.* **27,** 3557–3566
29. Kanagaraj, R., Saydam, N., Garcia, P. L., Zheng, L., and Janscak, P. (2006) Human RECQ5β helicase promotes strand exchange on synthetic DNA structures resembling a stalled replication fork. *Nucleic Acids Res.* **34,** 5217–5231
30. El-Shemerly, M., Janscak, P., Hess, D., Jiricny, J., and Ferrari, S. (2005) Degradation of human exonuclease 1b upon DNA synthesis inhibition. *Cancer Res.* **65,** 3604–3609
31. Henricksen, L. A., Umbricht, C. B., and Wold, M. S. (1994) Recombinant replication protein A: expression, complex formation, and functional characterization. *J. Biol. Chem.* **269,** 11121–11132
32. Masuda-Sasa, T., Imamura, O., and Campbell, J. L. (2006) Biochemical analysis of human Dna2. *Nucleic Acids Res.* **34,** 1865–1875
33. Pfaffl, M. W. (2001) A new mathematical model for relative quantification in real-time RT-PCR. *Nucleic Acids Res.* **29,** e45
34. Bennardo, N., Cheng, A., Huang, N., and Stark, J. M. (2008) Alternative-NHEJ is a mechanistically distinct pathway of mammalian chromosome break repair. *PLoS Genet.* **4,** e1000110
35. Gunn, A., and Stark, J. M. (2012) I-SceI-based assays to examine distinct repair outcomes of mammalian chromosomal double strand breaks. *Methods Mol. Biol.* **920,** 379–391
36. Richardson, C., Moynahan, M. E., and Jasin, M. (1998) Double-strand break repair by interchromosomal recombination: suppression of chromosomal translocations. *Genes Dev.* **12,** 3831–3842
37. Karow, J. K., Chakraverty, R. K., and Hickson, I. D. (1997) The Bloom's syndrome gene product is a 3′-5′ DNA helicase. *J. Biol. Chem.* **272,** 30611–30614
38. Brosh, R. M., Jr., Waheed, J., and Sommers, J. A. (2002) Biochemical characterization of the DNA substrate specificity of Werner syndrome helicase. *J. Biol. Chem.* **277,** 23236–23245
39. Shen, J. C., Gray, M. D., Oshima, J., Kamath-Loeb, A. S., Fry, M., and Loeb, L. A. (1998) Werner syndrome protein: I: DNA helicase and DNA exonuclease reside on the same polypeptide. *J. Biol. Chem.* **273,** 34139–34144
40. Kamath-Loeb, A. S., Shen, J. C., Loeb, L. A., and Fry, M. (1998) Werner syndrome protein: II: characterization of the integral 3′ → 5′ DNA exonuclease. *J. Biol. Chem.* **273,** 34145–34150
41. Kim, J. H., Kim, H. D., Ryu, G. H., Kim, D. H., Hurwitz, J., and Seo, Y. S. (2006) Isolation of human DNA2 endonuclease and characterization of its enzymatic properties. *Nucleic Acids Res.* **34,** 1854–1864
42. Avemann, K., Knippers, R., Koller, T., and Sogo, J. M. (1988) Camptothecin, a specific inhibitor of type I DNA topoisomerase, induces DNA breakage at replication forks. *Mol. Cell Biol.* **8,** 3026–3034
43. Lee, J. W., Harrigan, J., Opresko, P. L., and Bohr, V. A. (2005) Pathways and functions of the Werner syndrome protein. *Mech. Ageing Dev.* **126,** 79–86
44. Kanagaraj, R., Parasuraman, P., Mihaljevic, B., van Loon, B., Burdova, K., König, C., Furrer, A., Bohr, V. A., Hübscher, U., and Janscak, P. (2012) Involvement of Werner syndrome protein in MUTYH-mediated repair of oxidative DNA damage. *Nucleic Acids Res.* **40,** 8449–8459
45. Stark, J. M., Pierce, A. J., Oh, J., Pastink, A., and Jasin, M. (2004) Genetic steps of mammalian homologous repair with distinct mutagenic conse-

quences. *Mol. Cell Biol.* **24,** 9305–9316
46. Wu, L., and Hickson, I. D. (2003) The Bloom's syndrome helicase suppresses crossing over during homologous recombination. *Nature* **426,** 870–874
47. Yin, J., Sobeck, A., Xu, C., Meetei, A. R., Hoatlin, M., Li, L., and Wang, W. (2005) BLAP75, an essential component of Bloom's syndrome protein complexes that maintain genome integrity. *EMBO J.* **24,** 1465–1476
48. Wu, L., Bachrati, C. Z., Ou, J., Xu, C., Yin, J., Chang, M., Wang, W., Li, L., Brown, G. W., and Hickson, I. D. (2006) BLAP75/RMI1 promotes the BLM-dependent dissolution of homologous recombination intermediates. *Proc. Natl. Acad. Sci. U.S.A.* **103,** 4068–4073
49. Xu, D., Guo, R., Sobeck, A., Bachrati, C. Z., Yang, J., Enomoto, T., Brown, G. W., Hoatlin, M. E., Hickson, I. D., and Wang, W. (2008) RMI, a new OB-fold complex essential for Bloom syndrome protein to maintain genome stability. *Genes Dev.* **22,** 2843–2855
50. Cheng, W. H., von Kobbe, C., Opresko, P. L., Arthur, L. M., Komatsu, K., Seidman, M. M., Carney, J. P., and Bohr, V. A. (2004) Linkage between Werner syndrome protein and the Mre11 complex via Nbs1. *J. Biol. Chem.* **279,** 21169–21176
51. Lan, L., Nakajima, S., Komatsu, K., Nussenzweig, A., Shimamoto, A., Oshima, J., and Yasui, A. (2005) Accumulation of Werner protein at DNA double-strand breaks in human cells. *J. Cell Sci.* **118,** 4153–4162
52. Tomimatsu, N., Mukherjee, B., Deland, K., Kurimasa, A., Bolderson, E., Khanna, K. K., and Burma, S. (2012) Exo1 plays a major role in DNA end resection in humans and influences double-strand break repair and damage signaling decisions. *DNA Repair* **11,** 441–448
53. Yu, C. E., Oshima, J., Fu, Y. H., Wijsman, E. M., Hisama, F., Alisch, R., Matthews, S., Nakura, J., Miki, T., Ouais, S., Martin, G. M., Mulligan, J., and Schellenberg, G. D. (1996) Positional cloning of the Werner's syndrome gene. *Science* **272,** 258–262
54. Salk, D., Au, K., Hoehn, H., and Martin, G. M. (1981) Cytogenetics of Werner's syndrome cultured skin fibroblasts: variegated translocation mosaicism. *Cytogenet. Cell Genet.* **30,** 92–107
55. Fukuchi, K., Martin, G. M., and Monnat, R. J., Jr. (1989) Mutator phenotype of Werner syndrome is characterized by extensive deletions. *Proc. Natl. Acad. Sci. U.S.A.* **86,** 5893–5897
56. Melcher, R., von Golitschek, R., Steinlein, C., Schindler, D., Neitzel, H., Kainer, K., Schmid, M., and Hoehn, H. (2000) Spectral karyotyping of Werner syndrome fibroblast cultures. *Cytogenet. Cell Genet.* **91,** 180–185
57. Bunting, S. F., and Nussenzweig, A. (2013) End-joining, translocations and cancer. *Nat. Rev. Cancer* **13,** 443–454
58. Symington, L. S., and Gautier, J. (2011) Double-strand break end resection and repair pathway choice. *Annu. Rev. Genet.* **45,** 247–271
59. Chen, L., Huang, S., Lee, L., Davalos, A., Schiestl, R. H., Campisi, J., and Oshima, J. (2003) WRN, the protein deficient in Werner syndrome, plays a critical structural role in optimizing DNA repair. *Aging Cell* **2,** 191–199
60. Perry, J. J., Yannone, S. M., Holden, L. G., Hitomi, C., Asaithamby, A., Han, S., Cooper, P. K., Chen, D. J., and Tainer, J. A. (2006) WRN exonuclease structure and molecular mechanism imply an editing role in DNA end processing. *Nat. Struct. Mol. Biol.* **13,** 414–422
61. Saintigny, Y., Makienko, K., Swanson, C., Emond, M. J., and Monnat, R. J., Jr. (2002) Homologous recombination resolution defect in Werner syndrome. *Mol. Cell Biol.* **22,** 6971–6978
62. Swanson, C., Saintigny, Y., Emond, M. J., and Monnat, R. J., Jr. (2004) The Werner syndrome protein has separable recombination and survival functions. *DNA Repair* **3,** 475–482
63. Bussen, W., Raynard, S., Busygina, V., Singh, A. K., and Sung, P. (2007) Holliday junction processing activity of the BLM-Topo IIIα-BLAP75 complex. *J. Biol. Chem.* **282,** 31484–31492
64. Raynard, S., Bussen, W., and Sung, P. (2006) A double Holliday junction dissolvasome comprising BLM, topoisomerase IIIα, and BLAP75. *J. Biol. Chem.* **281,** 13861–13864
65. Xue, X., Raynard, S., Busygina, V., Singh, A. K., and Sung, P. (2013) Role of replication protein A in double Holliday junction dissolution mediated by the BLM-Topo IIIα-RMI1-RMI2 protein complex. *J. Biol. Chem.* **288,** 14221–14227

2.3.4 Force regulated dynamics of RPA on a DNA fork

Felix E. Kemmerich, Peter Daldrop, **Maryna Levikova,** Cosimo Pinto, Petr Cejka and Ralf Seidel.

Manuscript.

I contributed to this manuscript by performing expression and purification of yeast and human RPA proteins together with C.P. and P.C.

Published online XX month year

Nucleic Acids Research, 2014, Vol. XX, No. XX ***1–10***
doi:10.1093/nar/gkn000

Force regulated dynamics of RPA on a DNA fork

Felix E. Kemmerich [†,1,2], Peter Daldrop [†,2], Maryna Levikova [3], Cosimo Pinto [3], Petr Cejka [3] and Ralf Seidel [1,2*]

[†]Equal contribution

[1]Molecular Biophysics group, Institute of Experimental Physics I, Universität Leipzig, Linnéstr. 5, 04103 Leipzig, Germany,
[1]Institute for Molecular Cell Biology, University of Münster, Schlossplatz 5, 48149 Münster, Germany,
[3]Institute of Molecular Cancer Research, University of Zurich, Winterthurerstr. 190, CH-8057 Zürich, Switzerland.

Received January 1, 2014; Revised February 1, 2014; Accepted March 1, 2014

ABSTRACT

Replication protein A (RPA) is a single-stranded DNA binding protein, involved in most aspects of eukaryotic DNA metabolism. The strong binding of RPA to single-stranded DNA is well established. However, at boundaries between single- and double-stranded DNA (ssDNA and dsDNA) the binding and release of RPA must be carefully tuned such that the DNA can be made accessible to the DNA processing machinery without interfering with its function. Here we study the dynamics of RPA for such a situation using a replication fork mimic that is subjected to force by magnetic tweezers. We show that both yeast and human RPA can open the forked DNA in a step-wise manner when sufficient tension is applied. In contrast, when the force is reduced, RPA becomes rapidly displaced by the rehybridization of the progressively closing DNA fork. A simple theoretical model can explain the observed dynamics of DNA opening and closing, which is driven by passive binding of RPA to the ssDNA fork arms rather than active DNA duplex destabilization. Rate limiting step for both processes is only the binding or the release of a few bp-long RPA microdomain (toehold). This provides an extremely rapid exchange dynamics of RPA at the fork. Fork rezipping rates reach up to hundreds of base pairs per second, being orders of magnitudes faster than RPA dissociation from ssDNA alone. Additionally, we show that RPA undergoes diffusive motion on ssDNA, such that it can be pushed over long distances by a rezipping fork. Generally the behavior of both RPA types is generally very similar. However, the dissociation of human RPA from ssDNA is greatly reduced at low Mg^{2+} concentrations, such that it can melt DNA in absence of force. In contrast the behavior of yeast RPA is rather invariant against changes of the Mg^{2+} level.

INTRODUCTION

Replication protein A (RPA) is a highly ubiquitous (1), heterotrimeric (2), protein essential in virtually all aspects of eukaryotic DNA processing involving single-stranded DNA (ssDNA) intermediates (3). Due to the strong binding of RPA to ssDNA (2, 4, 5, 6) RPA was originally thought to solely prevent the formation of secondary structures and confer protection from nucleolytic degradation. However, strong evidence for direct interactions with specific protein partners has been reported (7, 8, 9, 10), and a new paradigm emerged. In there RPA additionally acts as a scaffold for the recruitment of other DNA processing enzymes on ssDNA intermediates, in order to channel the processing along specific pathways (11, 12). Of particular interest are hereby boundaries between ssDNA and double-stranded DNA (dsDNA), where many DNA processing factors are acting. There, in particular in the cellular context, the binding and release of RPA must be highly dynamic, and organized in such a way that the DNA can be rapidly made accessible to the subsequent processing machinery.

The importance of ssDNA-dsDNA boundaries is also highlighted by the fact, that despite the low affinity towards dsDNA (13), RPA binds appreciably to damaged dsDNA (14, 15), is able to disrupt partially double-stranded DNA structures such as triplexes (16), tetraplexes (17, 18), and suppresses formation of secondary structures such as hairpins (11). Under certain circumstances, the ATP-independent melting of dsDNA by RPA has also been shown, (19, 20, 21) where it was proposed that the observed duplex destabilization proceeds by trapping fluctuations of the helix (21).

Several recent studies have advanced our understanding of the molecular mechanisms that may control the coordination of RPA by employing single-molecule analysis techniques: (i) Using single-molecule DNA supercoiling experiments in magnetic tweezers it was shown that RPA can bind to transiently forming bubbles in the DNA duplex in a torque-dependent manner (22). (ii) Single-molecule imaging of fluorescent RPA has shown that RPA bound ssDNA may undergo more rapid exchange in presence of free RPA in solution (23). (iii) Using

*To whom correspondence should be addressed. Tel: +49 341 97 32501; Fax: +49 341 97 32599; Email: ralf.seidel@physik.uni-leipzig.de

a combination of single-molecule fluorescence techniques it was found that under certain conditions RPA may diffuse/slide along ssDNA (24), transpiring the intriguing possibility that this way it provides access of other enzymes to the DNA. Recently Chen and Wold (12) pointed out that, central to all of these single-molecule studies is the emerging view that RPA binding is highly dynamic and that microscopic rearrangements of the RPA DNA binding domains (DBDs) are underlying the observed dynamics. However, it was also emphasized that more work is required to fully understand the rich dynamics RPA in compex with various DNA structures.

Here, we investigate in detail the dynamics of RPA at the boundary of ssDNA and dsDNA such as arising at a replication fork. For this we utilize magnetic tweezers that allow precise manipulation and length determination of immobilized DNA substrates via an attached magnetic microsphere (25). At the single-molecule level they support the study of fast dynamic processes while preserving intrinsic molecular variation with spatial resolution on the scale of one base-pair (25).

By these means, we have characterized the force-dependent binding dynamics of RPA from human and budding yeast (*Saccharomyces cerevisiae*) on a DNA fork down to single protein association events. The interplay between RPA, fork and force tightly regulates the opening and closing of the fork. Our results indicate that RPA uses a 'toehold'-like mechanism to trap small transient openings of the DNA helix with a microdomain that then get expanded by binding of the full protein. Similarly RPA displacement by the rezipping fork first occurs through an initial rate-limiting displacement of a toehold. This gives rise to a very rapid helix rezipping upon which RPA dissociates much faster then on ssDNA. Thus, while RPA protects ssDNA rather firmly and statically, it is extremely dynamic at DNA processing sites. This is additionally supported by the observation that a DNA fork can slide/push RPA upon rezipping.

MATERIALS AND METHODS

DNA and proteins

The hairpin substrate containing a 488 bp long hairpin was prepared as described (26). The 5' end the of the hairpin carried a single biotin modification, while the 3' end was linked through a 40 nt ssDNA spacer to a ∼600 bp ds DNA spacer folled by a ∼600 bp digoxigenin-modified attachment handle.

The nicked dsDNA substrate was prepared as described (27). Central part is a 6.1 kbp unmodified dsDNA with a nick being located at 700 bp from its proximal DNA end. ∼600 bp attachment handles carrying multiple digoxigenins and biotins were attached to the 6.1 kbp fragment at its nick-proximal and distal ends, respectively.

yRPA (28) and hRPA were recombinantly expressed and purified as described.

Magnetic tweezers experiments

For the single molecule experiments a home-built magnetic tweezers setup was applied (25, 29). Magnetic tweezers experiments were conducted at room temperature using flow cells assembled from two coverslips that were separated by a layer of Parafilm into which a sample chamber was cut out. The bottom coverslip was coated with polystyrene. 3 μm carboxyl-modified latex beads (Invitrogen) that served as reference were attached to the bottom slide of the mounted flow cell by incubation in 1 M NaCl for 1 h. Subsequently, anti-digoxigenin (Roche) was allowed to unspecifically bind to the coated surface of the flow cell, by incubation with 50 μg/mL for 1 h at room temperature. Subsequently, the flow cell was passivated by over-night incubation with 10 mg/mL bovine serum albumin (BSA) (NEB). DNA constructs were bound to streptavidin-coated M280 magnetic beads (Invitrogen) and then flushed into the flow cell. After allowing them to bind for approximately 5 min, excess beads were washed out with PBS rendering the sample chamber ready for experiments. The positions of reference and DNA-attached beads were tracked in all three dimensions at 300 Hz using videomicroscopy and real-time GPU-accelerated image analysis (25). Typically multiple beads were evaluated in parallel. Forces were calibrated using a recent methodology that supports the usage of short molecules and high forces (30). Experiments were conducted in 50 mM Tris acetate pH 7.5 supplemented with magnesium acetate in concentrations as described in the results. Data were analyzed in Labview (National Instruments), Origin 9.1 (OriginLab) and Matlab (MathWorks). Length changes measured in nm for opening of the hairpin or melting of the nicked DNA construct were converted into the number of opened base pairs as detailed in Supplementary Methods.

RESULTS

RPA association and dissociation at a DNA fork

We measured the association and dissociation of RPA on a 488 bp long DNA hairpin substrate using magnetic tweezers. One end of the hairpin is immobilized via a dsDNA spacer at the bottom surface of a fluidic-cell. The other end is tethered to a 2.8 μm magnetic bead (Figure 1a). A set of permanent magnets is mounted on a movable stage above the fluidic-cell, such that the magnetic force acting on the bead can be controlled by lowering or raising the magnets (see Materials & Methods for details).

The DNA hairpin substrate can be opened mechanically by applying sufficient force on the bead. At forces above a critical force, further called unzipping curve, a series of sudden, well-defined transitions in DNA extension occurs, amounting to about 475 nm from the fully-closed to the fully-open state over the course of about 1 s (see Supplementary Figure S1).

In contrast, when adding 20 nM yRPA a gradual opening of the hairpin at forces well below the unzipping force was observed. Also the opening process extended over a much longer time-scale and continued until the hairpin was extended to the fully opened state (Figure 1b). Upon force reduction , a gradual reversion to the closed state took place. We interpret these gradual transitions as the result of RPA binding to the fork of the hairpin. The sequential association of more RPA opened the hairpin and generated RPA-covered ssDNA. Upon lowering the force, RPA is displaced by the rezipping DNA (Figure 1a). The slopes of both association and dissociation are approximately constant throughout the complete hairpin opening or closing process, irrespective of the amount of double stranded substrate remaining, suggesting that binding

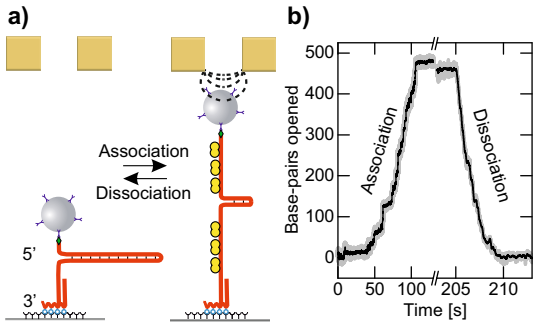

Figure 1. Force-controlled association and dissociation of RPA on a DNA fork substrate. **(a)** Schematic of the experiment: A 488 base-pair long DNA hairpin substrate (red), is immobilized onto a glass-surface and tethered to a magnetic bead. When sufficient force is applied to the bead, RPA (yellow) can bind to the ssDNA/dsDNA interface at the fork. As a result, the hairpin is opened to accommodate the entire RPA heterotrimer. Further association proceeds by the contiguous binding of RPA to the fork until the hairpin is fully opened. Upon lowering the magnetic force the DNA helix refolds reversibly and RPA dissociates from the ssDNA. **(b)** Example time-trace of force-controlled RPA association and dissociation in presence of 3 mM Mg^{2+}. At a force of 13.2 pN, sequential binding of RPA opens the hairpin with a rate of 4.7 bp/s, until it is fully opened and completely covered with RPA. Lowering the force to 4.5 pN causes dissociation of RPA evident in rapid refolding of the hairpin with a rate of 107 bp/s.

occurs only at the fork in a contiguous manner with respect the previously bound RPA. We emphasize that the process is fully reversible and the same molecule can be opened and closed multiple times without systematic alteration of the resulting curves.

Force-dependence of RPA binding at the fork

Next, we investigated the influence of the applied force on the association and dissociation rates of RPA on the DNA hairpin substrate. These rates showed a strong dependence on the applied force. Above 11 pN we observed a gradual opening of the hairpin and the rate of opening increased with stronger force (Figure 2a). When the force acting on such an RPA covered, open hairpin, was reduced below 11 pN, we observed a gradual closing of the hairpin and the rate of closing was the faster, the lower the applied force was (Figure 2b).

Plotting the rates of hairpin opening and closing against the applied force, it became apparent, that both the association and dissociation rates varied exponentially with force as shown in Figure 2c. We devised a model in which the net rate of RPA binding to the DNA is the rate difference between force-dependent RPA association and RPA dissociation at the fork. Each rate is is expressed by an exponential Arrhenius terms as obtained from transition-state theory in which the applied force F effects the height of the transition barrier:

$$v_{net} = k_{on} \cdot exp\left(\frac{Fc\Delta z_{on}}{k_B T}\right) - k_{off} \cdot exp\left(\frac{-Fc\Delta z_{off}}{k_B T}\right) \quad (1)$$

Hereby the pre-exponential factors k_{on} and k_{off} describe the expected rates for association and dissociation at zero force. The second pair of fit parameters (Δz_{on} and Δz_{off}) corresponds to the distance of the initial state (before association/dissoctiation of a new RPA) from the transition state along the relevant reaction coordinate, in this case the number of base-pairs along the DNA hairpin. For association (Δz_{on}) it is thus the number of base pairs that need to spontaneously open to allow a sufficiently long part of an RPA complex to bind to allow full complex binding. For dissociation Δz_{off} it is the number of base pairs that need to rezip and displace part of the RPA complex to allow full complex dissociation. The factor c converts the number of base-pairs into a DNA extension change, i.e. a length. c is itself a function of the force and was determined as described in the Supplementary Information. The model well describes the force-dependent rates, as evident in a fit to the data (Figure 2c). This provided at 20 nM yRPA and 3 mM Mg^{2+} a hairpin closure rate at zero force of $k_{off} = 308.9$ bp s^{-1}. Furthermore, $\Delta z_{on} = 3.5$ bp and $\Delta z_{off} = 2.5$ bp was obtained, i.e. that spontaneous helix opening or partial RPA displacement amounting to only few base pairs is required to overcome the transitions state for RPA association or dissociation, respectively. This is reminiscent to the toehold mechanism in DNA nanotechnology, where an association of a small protein microdomain (toehold) is the rate limiting step for full protein binding and further helix opening. Vice versa disengagement of a terminal microdomain is rate limiting for helix rezipping. The fit also provides the hairpin opening rate at zero force of $k_{on} = 9.8 \times 10^{-4}$ bp s^{-1} (see Table 1 for full set of fit parameters). This implies that in the absence of force, dissociation dominates and equilibrium favors the unbound state. The equilibrium force at which the two processes balance out resulting in a net rate of zero is 11.2 pN.

For the distance of the initial reactant state from the transition state we find values of $\Delta z_{on} = 3.5$ bp for the association reaction and $\Delta z_{off} = 2.5$ bp for dissociation.

RPA binding on a nicked DNA duplex substrate

Next, we probed whether the observed RPA binding behavior is unique to the DNA hairpin geometry, or if it could be observed on a nicked DNA duplex as well. The DNA substrate utilized in this case consists of a 6.1 kbp stretch of dsDNA with a nicked strand (see Materials and Methods), as illustrated in Figure 3a. This DNA construct undergoes a rapid disruption of the base-pairing in the dsDNA when the applied force exceeds 65 pN, as indicated by a marked increase in the DNA length. This corresponds to the DNA overstretching transition (31, 32).

In the presence of 20 nM of yRPA, again a gradual increase in DNA length for forces well below the overstretching transition can be observed, which proceeds for several thousand base-pairs, see Figure 3b. This is in agreement with the association of RPA at the junction of ssDNA and dsDNA of the substrate, generating RPA-coated ssDNA as illustrated in Figure 3a. As observed previously for the DNA hairpin geometry, the process is again fully reversible. Upon reduction of the applied force the DNA extension gradually decreases until the duplex is fully restored, corresponding to the sequential refolding of the helix when RPA dissociates.

Examining the association and dissociation rates as function of the applied force, again an exponential dependence is revealed. Applying our previous model yields an excellent

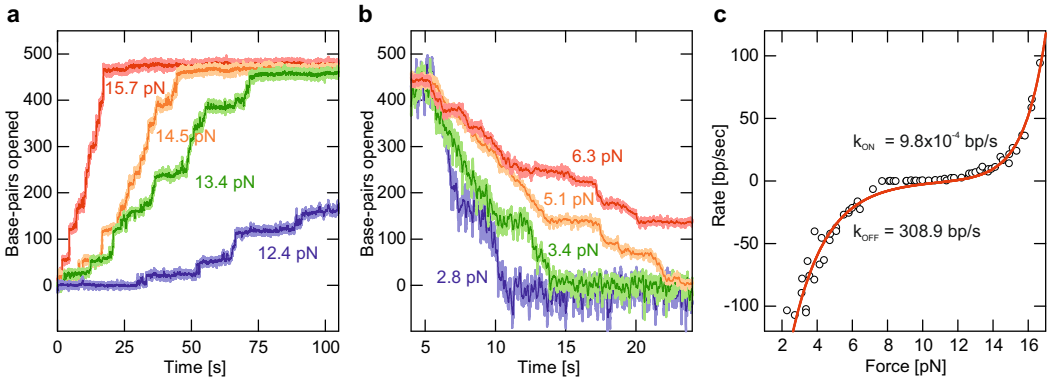

Figure 2. Force dependence of the RPA association/dissociation kinetics at the fork in presence of 3 mM Mg^{2+}. **(a)** Example time-traces of RPA association on the DNA hairpin at different forces. The DNA hairpin sequentially opened due to successive association events of RPA. With increasing forces the overall association rate becomes faster, ranging from 2.8 bp s^{-1} at 12.4 pN (blue) to 36.6 bp s^{-1} at 15.7 pN (red). **(b)** RPA dissociation time-traces for varying force. Following a complete coverage of RPA on the DNA hairpin substrate, the force was lowered to the indicated values causing the hairpin to close and RPA to dissociate. The rate of dissociation is much faster than association and ranges from 107 bp s^{-1} at 2.8 pN (blue) to 16.2 bp s^{-1} at 6.3 pN (red). **(c)** Association and dissociation rates as function of force obtained by tracking multiple DNA substrates with magnetic beads in parallel (open circles). A fit to the data with Equation **1** (red line) zero-force rates of 9.8×10^{-4} bp s^{-1} for association and 308.9 bp s^{-1} for dissociation.

fit to the data (Figure 3c). The zero force association and dissociation rate parameters from the fit are comparable with the hairpin geometry, with $k_{on}=5.9\times10^{-3}$ bp/s and $k_{off}=564.0$ bp/s. Because of the altered geometry of this DNA substrate, an elevated force of 43 pN is required to bring these competing processes to equilibrium. The distances to the transition state, $\Delta z_{on}=2.9$ bp and $\Delta z_{off}=1.6$ bp, are also in good agreement to the values obtained for the DNA hairpin geometry (see Table 1).

Magnesium dependence of RPA binding

The ionic strength in general and magnesium in particular are of vital importance for DNA-protein interactions due to both a general screening of charges and also the specific mediation of important contacts by Mg^{2+}(33, 34). Our bulk experiments, confirm earlier work reporting that hRPA is capable of melting dsDNA even in the absence of force under conditions of low magnesium concentration (19, 20, 21), see Supplementary Figure S2. Therefore, we probed RPA-mediated opening / closing of DNA hairpins as a function of the magnesium concentration also at the single-molecule level.

To this end, the behavior of hRPA binding to the DNA hairpin under comparable conditions as for yRPA was investigated. Generally speaking, hRPA behaves comparably to yRPA. Again the force dependent opening and closing of the DNA hairpin is observed, which can be attributed to the association and dissociation of hRPA on the DNA at the fork (data not shown). Also in terms of the absolute force-dependent rates the two paralogs are comparable as shown in Figure 4a. Our model (Equation **1**) also fits the hRPA data well, yielding fit parameters that closely resemble those of yRPA as summarized in Table 1.

Varying the concentration of Mg^{2+} in the range of 1 to 10 mM shows no considerable effect for yRPA in terms of the force-dependent kinetics, as shown in Figure 4a. Within the margins of experimental uncertainty and stochastic error, the fit parameters remain practically unchanged over the examined concentration range as tabulated in Table 1. For hRPA however, there is a pronounced effect on the

	yRPA			hRPA		
	1 mM Mg^{2+}	*3 mM Mg^{2+}*	*10 mM Mg^{2+}*	*3 mM Mg^{2+}*	*5 mM Mg^{2+}*	*10 mM Mg^{2+}*
k_{on} [bp/s]	3.6×10^{-7}	9.8×10^{-5}	3.3×10^{-3}	9.2×10^{-5}	1.2×10^{-2}	1.4×10^{-2}
k_{off} [bp/s]	310	300	400	40	120	200
dz_{on} [bp]	5.3	3.5	2.5	3.2	2.1	2.5
dz_{off} [bp]	2.3	2.0	2.0	0.9	1.0	0.8

Table 1. Fit parameters for yRPA and hRPA association and dissociation kinetics. k_{on} and k_{off} are the apparent rates of association and dissociation at zero force, dz_{on} and dz_{off} are the transition state distances for binding or dissociation of an RPA heterotrimer in base-pairs. The parameters were obtained by fitting the force-dependent association and dissociation rates of yRPA and hRPA on the 488 base-pair DNA hairpin, to a model comprised of two Arrhenius terms (see Equation 1).

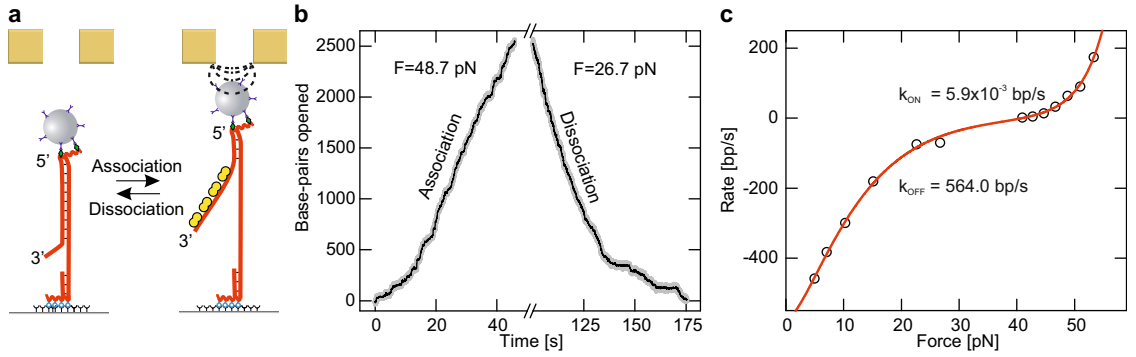

Figure 3. Association and dissociation can be measured also on a DNA duplex substrate. **(a)** RPA also associates reversibly onto a 6.1 kbp long DNA duplex with a 40 nt long 5'-end flap subject to force. **(b)** Example time-trace of RPA association and dissociation. The duplex is seen to open continuously over several thousand base-pairs, caused by association of RPA. In this geometry, association proceeds at a rate of 63.8 bp/s, when a magnetic force of 48.7 pN is exerted. Complete opening is avoided, to prevent detachment of the magnetic bead, by lowering the force. At 26.7 pN force, the helix refolds rapidly with a rate of 70 bp/s as RPA dissociates. **(c)** Association and dissociation rates are plotted against the applied force (open circles). Again both the association and dissociation rates vary exponentially with the applied force. A double exponential (see main text) fits the data well (red line), and reveals zero-force rates of 5.9×10^{-3} bp/s for association and 564.0 bp/s for dissociation.

dissociation rates, which drop from 200 bp/s in 10 mM Mg^{2+} down to 120 bp/s at 5 mM Mg^{2+} and 40 bp/s at 3 mM Mg^{2+}. Below 3 mM Mg^{2+} dissociation is no longer measurable. This is demonstrated by the exemplary time traces recorded at 2 pN force shown in Figure 4b. The DNA hairpin remains open under conditions where yRPA dissociates with the same rate as at higher levels of Mg^{2+}.

In fact, even in the absence of force the DNA hairpin is completely opened after introducing hRPA in buffer containing $<$3 mM Mg^{2+}. This is in agreement to the melting of the duplex DNA under similar conditions evident from our bulk experiments (Supplementary Figure S2). Furthermore, extrapolation of the dissociation rates from the single-molecule assay shows that the rate is expected to reach zero below 2.5 mM Mg^{2+}. This is consistent with the onset of melting activity observed in bulk.

Finally, the measurement of the RPA binding kinetics were repeated in the absence of salt, and find that the entire curve is shifted towards lower forces while its shape is preserved, and the shift is consistent with the shift of 2 pN that we see for the

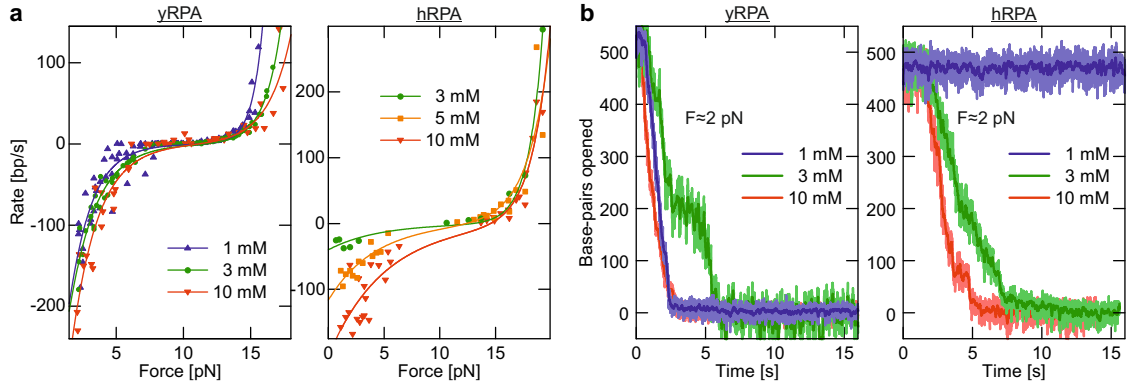

Figure 4. Comparison of human and yeast RPA association/dissociation on the DNA hairpin substrate, and the effect of varying the magnesium concentration. **(a)** The association and dissociation behavior of yeast RPA (left panel) and human RPA (right panel) is generally quite similar. Individual association/dissociation rates measured over a range of forces are indicated by markers, and are on the same order of magnitude for human and yeast RPA. For both paralogs the rates exhibit exponential force dependence, which is well described by a double exponential model (solid lines, see main text). Force-dependent association and dissociation rates of yRPA are not affected significantly by changing the concentration of Mg^{2+} in the range of 1 to 10 mM, our model fits the data well and parameters obtained are comparable (see Table 1). For hRPA our model describes the force-dependence equally well, however, lowering the concentration of Mg^{2+} results in significantly reduced dissociation rates in the range of 3 to 10 mM. **(b)** Example time-traces of dissociation are shown for both yRPA and hRPA at forces close to 2 pN for different magnesium concentrations. For yRPA, changing Mg^{2+} concentration from 1 to 10 mM has no marked effect as indicated by the hairpin opening distance decreasing with comparable slope in all cases. In contrast, the dissociation rate of hRPA becomes reduced at lower Mg^{2+} concentrations until no dissociation is observable at all below 3 mM, as shown by the hairpin remaining fully open (right panel, blue curve).

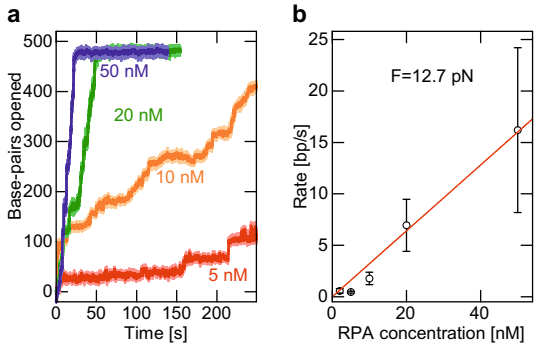

Figure 5. Concentration dependent association of yRPA on the DNA hairpin substrate. **(a)** Example time-traces of association at a force of 12.7 pN are shown. The rate of association is increased from 0.4 bp/s at 5 nM RPA (red curve), to 16.2 bp/s at 50 nM (blue curve). **(b)** Observed association rates (open-circles) vary linearly with the concentration of RPA as indicated by the linear fit (red line). Points shown correspond to mean values of triplicate measurements with error bars representing one standard deviation.

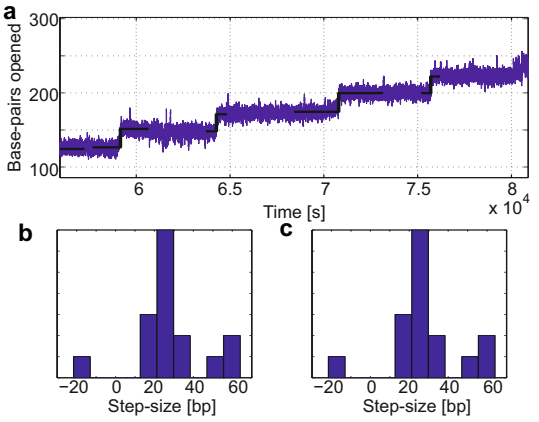

Figure 6. Binding-site size of RPA. **(a)** Exemplary time trace for yRPA association on the hairpin substrate showing clearly resolved steps. **(a)** Step-size distribution for yRPA (from multiple traces collected under the same conditions), calculated using a step-finding algorithm. The step-size of 25 bp occurs most frequently in the data), co **(c)** The step-size distribution for hRPA is similar, with the most common size being 28 bp.

difference in unzipping force in salt-free buffer and containing 1 mM Mg^{2+} (see Supplementary Information).

Concentration effect on RPA association kinetics

We also examined the influence of the concentration of yRPA on the rate of association on the DNA hairpin substrate. Time traces recorded at concentrations ranging from 2 to 50 nM are shown in Figure 5a for a given force. It can be seen that the rate of association is increased from 0.6 bp/s at 5 nM to 16 bp/s at 50 nM, and as expected, the association rate follows a linear dependence on the RPA concentration (Figure 5b).

Binding-site size determination

We carefully examined our data to investigate whether we could identify consistently sized steps in the opening of the DNA hairpin resulting from RPA binding. In conditions favoring very slow association (moderate force and low RPA concentration) steps become well resolved and discernible as shown in Figure 6a.

Constructing dwell-state histograms reveals that the DNA hairpin opening occurs via discrete well-populated states which are separated by sharp transitions (steps). Examining the separation of adjacent dwell states provides some estimate of the step-size. The value of ∼20 nt is consistent the binding-site size of RPA reported in literature (24, 35).

We interpret these steps as the consequence of single binding events, and thus analyzed our data using an in-house developed step-finding algorithm (see Supplementary Methods). Using this analysis, an average step-size of 24 for yRPA and 26 for hRPA is most prominent, see Figure 6b. Steps of this size are persistent throughout the length of the hairpin opening and this step-size is independent of the applied force. In conditions where dissociation occurs at appreciable rates, backward steps of similar size were observed.

Sliding of hRPA along ssDNA

Finally, it was investigated whether a single hRPA heterotrimer could be pushed along the ssDNA by the hairpin refolding behind it. To achieve this, the hairpin was repetitively opened and closed by alternating between forces above and below the characteristic unzipping force (22.5 and 15.5 pN, respectively) in about 0.5 s intervals. In the absence of hRPA the hairpin reproducibly closes in a single fast transition. At very low concentrations of hRPA (150 pM), the hairpin closing is in some instances perturbed, such that a continuous slower refolding takes place (Figure 7a). This slow closing takes place only about once in 10 force cycles, and at a force for which our previous experiments indicate that association is favored over dissociation. Furthermore, the closing observed in this case takes place in a smooth fashion, whereas dissociation data at higher hRPA concentration (down to 5 nM) takes place in a more discontinuous almost step-wise manner, as one hRPA heterotrimer is sheared off after the other.

Therefore, we believe that the events observed here correspond to the binding of a single hRPA to the ssDNA while the hairpin is open, and a pushing of the refolding hairpin against the friction of the single hRPA heterotrimer sliding along the ssDNA (see Figure 7b). The fact that this sliding can be interrupted by again increasing the force to open the hairpin, and then resumes upon re-lowering the force (see Figure 7a, second highlighted portion) substantiates this explanation.

Systematically varying the closing force (defined as the difference between the applied force and the characteristic unzipping force of 17.8 pN under these conditions), reveals that the average velocity depends linearly on the force. Figure 7c shows the mean velocities as function of the closing force. A linear fit describes the observed trend well (R^2=0.86), with the intersection of the velocity axis at -18.23 nt/s for zero force. Furthermore, the slope of this fit can be used to calculate a friction coefficient, as the velocity is expected to vary with

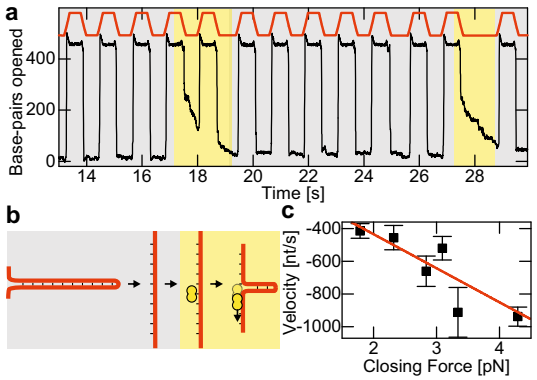

Figure 7. hRPA can slide along ssDNA. **(a)** Repetitively opening and closing the hairpin by alternating the applied force between 22.5 and 15.5 pN (as indicated in red) in conditions of very low (150 pM) hRPA concentration reveals sliding of hRPA. For the majority of these cycles (gray background) the closing of the hairpin is unperturbed, however approximately once in ten cycles, a continuous slower closing is observed (pale yellow background). **(b)** Cartoon illustrating the observed behavior. After opening the hairpin, a single hRPA heterotrimer may bind to the exposed ssDNA. When the force is reduced, the closing hairpin pushes the hRPA along the ssDNA. **(c)** Estimation of the friction coefficient. The mean sliding velocity (black markers, error bars indicate standard errors) is shown to vary linearly with the closing force (defined as the difference between the applied force and characteristic unzipping force). The slope of the linear fit to the data (shown in red) provides an estimate for the friction coefficient, for which a value of ζ=0.005 pN·nt^{-1}·s.

the force as given by $F=\zeta\cdot v$, for which we find a value of ζ=0.005 $\pm$ 0.0009 pN·nt^{-1}·s.

DISCUSSION

We have shown that both human and yeast RPA destabilize forked dsDNA. The fact that both yeast and human RPA exhibit comparable behavior underlines the relevance of our findings. In both the DNA hairpin and duplex geometries a gradual opening is observed, at forces far below the characteristic forces for unzipping or the overstretching transition, respectively. We attribute this gradual opening to the binding of RPA to short stretches of single-stranded DNA exposed by intermittent openings of the DNA helix. As a result of the strong binding of RPA to ssDNA, these transient openings are trapped and the hairpin is opened further to accommodate the entire unit of RPA. The sequential opening of the dsDNA then proceeds by successive binding events of RPA to the interface of ssDNA and dsDNA.

This interpretation of our data is consistent with previous work investigating the association and dissociation of yRPA on super-coiled dsDNA (22), where RPA was found to bind to transient bubbles that occur on the DNA, destabilized by the applied torque. The forked geometry is of advantage because it is more well-defined and much better resolved. On super-coiled substrates bubbles that are trapped by RPA may occur in multiple sites, as dsDNA overstretching experiments, using fluorescently-modified RPA as probe for single-stranded regions, show that melting initiates throughout the DNA molecule by localized base-pair breaking, leading to melting bubbles (36, 37). In our forked substrates the unzipping most likely initiates only from the fork, albeit binding can occur to either strand. Especially for the hairpin substrate, in which the opening of a single base-pair causes an extension of two nucleotides single-stranded DNA, our fork geometry provides a much improved signal as compared to super-coiled substrates. Consistently with these super-coiling experiments, however, our measurement of the RPA dynamics on forked DNA also suggests a passive mechanism for the observed helix opening, as had already been proposed previously (21).

The strong force dependence of the kinetics of RPA association supports this passive view, as the breathing of the DNA helix required for initial RPA binding becomes enhanced by stronger forces in both its length scale and duration. Our model for this force-dependence consists of an Arrhenius exponential. Using the association rate extrapolated to zero force k_{on} from this model, together with the linear concentration dependence (that one may expect for simple first-order binding kinetics), and the determined footprint of yRPA, one can estimate the absolute rate (for 2 mM Mg^{2+}) as $k_{on}^{\ominus}=\frac{9.8\times10^{-5}\ \mathrm{bp/s}}{20\ \mathrm{nM}\cdot 25\ \mathrm{bp}}=2\times10^{-7}\ \mathrm{nM^{-1}s^{-1}}$. The rate of association on a DNA fork is thus 7 orders of magnitude slower than the association rate on pure single-stranded DNA of 2 nM^{-1}·s^{-1} (also at 2 mM Mg^{2+})(38), consistent with view that binding to the fork is rate-limited by the fluctuations of the DNA helix. Similarly, an absolute dissociation rate can be estimated: $k_{off}=\frac{300\ \mathrm{bp/s}}{25\ \mathrm{bp}}=60\ \mathrm{s^{-1}}$, which is 4 orders of magnitude faster than the rate of 0.006 s^{-1} (measured in 5mM Mg^{2+}) for dissociation from ssDNA (39). Again this is consistent with the interpretation that the rapid rehybridization of the helix is the driving force for dissociation on forked DNA. This provides further support for the fact that a passive helix destabilization mechanism underlies the opening and closing of forked DNA mediated by RPA, and the dynamics are governed by simple mechanics.

By comparison of equilibrium forces (at which the rates of association and dissociation balance out to yield a net rate of zero) with the force required to mechanically unzip the DNA (the unzipping force or the overstretching force for the two respective geometries), the energetic contribution of RPA towards destabilization of the DNA helix can be calculated. For yRPA and the DNA hairpin configuration, using the values of 17.2 pN for mechanical unzipping in buffer containing 2 mM magnesium and the equilibrium force of 11.2 pN, this corresponds to an energetic contribution of 35 %. Intriguingly, the relative fraction is the same also for yRPA on the nicked duplex DNA, for which we find 34 % using 65 pN for the DNA overstretching transition and an equilibrium force of 43 pN. This implies that RPA supplies a contribution of one-third of the total energy required to fully destabilize dsDNA in a fork. Using these equilibrium force values together with the size of the RPA binding site determined by our analysis, it is furthermore possible to estimate the binding energy of RPA: $\Delta G_{bind}=F_{eq}^{RPA}\cdot z_{RPA}=138$ pN·nm, which corresponds to the binding energy of a single RPA heterotrimer to the stretch of DNA corresponding to its binding site size and is equal to a standard free-energy change of $\Delta G_{bind}^{\ominus}$=83 kJ mol^{-1}. This energy, however, cannot be converted into a binding constant

in a straightforward manner. RPA can bind on both strands of the DNA duplex and additionally neighboring RPAs might be bound with some gaps in between the individual heterotrimers. However, our simple model (Equation **1**) for the force-dependent net rate, which sufficiently describes the observed kinetics as the superposition of two Arrhenius exponentials for the association and dissociation rate, respectively, allows an estimation of an apparent dissociation constant. Comparing the parameters k_{on} and k_{off}, $K_d \approx k_{on}/k_{off} \approx 20$ nM. It becomes clear, that in the absence of force dissociation strongly dominates and the RPA unbound state is favored.

This observation holds over a wide range of ionic strength conditions, with the exception of hRPA dissociation (discussed below), such that no considerable changes to the kinetics are instigated in the range of 1 to 10 mM Mg^{2+}. We examined how the unzipping force of our DNA hairpin construct varies under the same conditions in the absence of RPA, and found that these vary only slightly between 1 and 2.5 mM, and do not vary at all in excess of 2.5 mM. The predominant effect of increasing the ionic strength is the stabilization of the DNA helix by screening the negative charges in the phosphodiester backbone, however the largest part of this effect takes place already below 1 mM Mg^{2+}. Our data recorded in the absence of salt indicates that yRPA - DNA interactions are unchanged and the observed shift in the equilibrium point is caused by the reduced helix stability under these conditions. The fact that apart from DNA stabilization, the ionic strength has insignificant effect on our measured kinetics, is in agreement with our passive model of the destabilization of the helix mediated by RPA.

The magnesium dependence of the dissociation rate we observed is specific to hRPA, yRPA did not exhibit this behavior. The ionic strength in general and magnesium in particular are of vital importance for DNA-protein interactions. Beyond the effect of charge screening on the DNA, the mutual approach of negatively charged RPA and the DNA is also affected. Together these factors may account for a minute increase we see in the apparent association rates. However, the much more significant influence on the hRPA dissociation rates seems to involve a highly specific effect of magnesium on the binding of RPA to the DNA. It is conceivable that yRPA may have conserved a salt-independence evolutionarily, in order to allow for variable magnesium concentrations in the cell. Yeast cells are expected to have greater variability of their intracellular ion composition due to the diversity of environments in which they grow. Indeed intracellular magnesium concentrations strongly depend on the magnesium concentration outside of the cell (40). Alternatively the possibility exists that the hRPA binding equilibrium could be regulated by cell-cycle dependent regulation of intra-nuclear magnesium levels. Moderate magnesium concentrations are essential for the activity of a whole host of DNA repair proteins (41) and the distribution of intracellular magnesium is both variable, (40, 42, 43), and tightly regulated throughout the cell-cycle progression (41).

Our model describing the force-dependence of kinetics is based on transition-state theory. In this view the parameters Δz_{on} and Δz_{off} correspond to the distance between the initial reactant state and the transition state along the relevant reaction coordinate, in this case the number of base-pairs along the DNA hairpin. An analogous formalism was previously used, where the corresponding parameter descibes the step-size for a helicase (44). The values we find for RPA are on the order of only a few base-pairs throughout the experimental conditions we examined (Table 1). Compared to the binding-site size of RPA this is quite small, indicating that it is sufficient for only a small portion of RPA to engage contact with the DNA, in order for the rest of the RPA heterotrimer to then wedge in, and open the DNA hairpin by length necessary to accommodate the entire RPA heterotrimer. Similarly, in the context of dissociation, where the corresponding parameter is consistently slightly lower than for the reverse reaction, this means that it is sufficient for the helix to refold by only one-two base-pairs in order to destabilize the binding of RPA sufficiently and shear it off. Such a toe-hold model has been proposed previously, in order to explain the observed binding properties of RPA (12, 22, 23). Furthermore, recent studies suggest that these binding properties can be understood in terms of the structural information available for RPA binding to the DNA. RPA has multiple DNA binding domains (DBDs) flexibly-linked together that interact with the DNA in a defined orientation. Interestingly the toe-hold size we observe for the association compares well with the length of DNA that interacts with a single DBD as determined crystallographically (45, 46).

Despite the strong binding reported for each of the DBD subdomains (3), diffusion of hRPA on ssDNA as reported in (24). We investigated this possibility in terms of single hRPA heterotrimers sliding along the ssDNA, pushed by the closing hairpin. Since the capability to diffuse is a prerequisite to the sliding behavior, that we indeed observe, we can confirm that hRPA is capable of diffusion on ssDNA. Furthermore, from our data of the mean sliding velocities as function of the closing force, a friction coefficient of ζ=0.005 pN·nt^{-1}·s can be calculated. This can in turn be used to estimate the diffusion coefficient via the Einstein relation: $D = \frac{k_B T}{\zeta}$. From this data a one-dimensional diffusion coefficient of $D = 960 \pm 350$nt^2/s on ssDNA can be estimated, which is surprisingly well comparable to the published value of $D = 2800 \pm 200$ nt^2/s (24), particularly given the high salt concentration of 0.5 M NaCl used in that study. The possibility of RPA to diffuse along allows for the possibility of bound hRPA to rearrange itself on the ssDNA, in order to free-up access to other processing factors.

To recapitulate, we find that RPA dynamics on forked DNA are governed by a passive mechanism in which a RPA binds to short stretches of ssDNA that are intermittently exposed from the dsDNA helix, using a small toe-hold. As the binding energy is only sufficient to overcome one-third of the base-pairing energy of the DNA, and given the predominance of the dissociation rate in the absence of force, we conjecture that it is unlikely that RPA disrupts dsDNA on its own in a cellular context. It seems more likely that RPA strongly binds and protects ssDNA generated in other DNA processing steps, such as DNA repair, stalled-replication, and homologous recombination, and for the case of a DNA fork, DNA processing helicases or other enzymes bound to the fork, will prevent RPA from dissociation due to the refolding of the helix. In such a context it could then provide a scaffold for the recruitment of further DNA processing machinery, and the capability to diffuse suggests a mechanism in which access to

the DNA can be freed-up. Then, the possibility exists that the degree of RPA binding could be controlled by small changes in force or torque exerted by downstream enzymes. Remarkably however, the refolding of the helix is sufficient to rapidly expel RPA by shearing it off the ssDNA with speeds of several hundred base-pairs per second corresponding to a removal of tens of RPA heterotrimers per second. Thus RPA may not be sufficient to maintain a stretch of DNA as single-stranded by impeding the helix rehybridization, eg. once a helicase uncouples its activity, as has recently been postulated for SSBs in general (47), as the refolding helix could very rapidly drive the removal of RPA. Furthermore, this also implies that no further processing enzymes are absolutely necessary to remove RPA, as could be expected and would be a plausible role for helicases that preferentially rewind the helix (26) as has also previously been speculated (48). Instead the helix refolding can be sufficient to return the dsDNA to its native RPA-unbound state, once processing has been completed and the processing machinery has dissociated from the DNA.

CONCLUSION

We have shown that RPA destabilizes the double helix protruding from a DNA fork by binding to intermittently exposed stretches of ssDNA using a microscopic toe-hold. These findings hold for both yRPA as well as hRPA. This destabilization can be understood as passive trapping of fluctuations on the helix, and with the aid of additional force, it is sufficient to disrupt DNA double helix. Our results indicate that RPA binding to forked DNA is highly dynamic, as it is governed by competition with the hybridization of the DNA helix. As the binding energy is only sufficient to overcome one-third of the base-pairing energy of the DNA, we conjecture that it is unlikely that RPA disrupts dsDNA on its own in a cellular context. For yRPA, we found the process to be independent of the magnesium concentration. For hRPA in contrast, the dissociation of RPA from the single strand is highly dependent on magnesium, such that under certain circumstances, equilibrium may favor DNA melting in the absence of force. Furthermore, we confirm a previous report that revealed that hRPA is capable of diffusion on ssDNA, and this capability may allow RPA to free-up access to the ssDNA for other processing factors. In summary, our single-molecule measurements characterize the binding kinetics of RPA on forked DNA and provide insight into the underlying molecular mechanisms. The mechanistic details we draw from our results fit in well with the emerging view, RPA binding is highly dynamic, and governed by microscopic domains, that are compete for ssDNA with the hybridization of the helix. Regarding its function *in vivo*, we believe that RPA does not melt dsDNA on its own, but rather coats ssDNA intermediates to protect them, while providing a scaffold for the recruitment of further effector proteins. These may then dislodge RPA by rearrangement of RPAs microscopic domains DNA binding and furthermore RPA may slide along the ssDNA to permit access. Ultimately, for the release of RPA from a fork after DNA processing, we believe that rehybridization of the double helix after removal of the processing machinery, is sufficient as the driving force.

ACKNOWLEDGMENTS

We thank Dominik Kauert, Jasmina Dikic, Christophe Rouillon and Marius Rutkauskas for discussion and advice. Furthermore, we thank Ina Kowsky and Gerda Scheidtgen-Kleyboldt for general laboratory support.

Conflict of interest statement. None declared.

REFERENCES

1. Seroussi,E. and Lavi,S. (1993) Replication protein A is the major single-stranded DNA binding protein detected in mammalian cell extracts by gel retardation assays and UV cross-linking of long and short single-stranded DNA molecules. *J. Biol. Chem.*, **268**, 7147–7154.
2. Wold,M.S. and Kelly,T. (1988) Purification and characterization of replication protein A, a cellular protein required for in vitro replication of simian virus 40 DNA. *Proc. Natl. Acad. Sci. U. S. A.*, **85**, 2523–2527.
3. Wold,M.S. (1997) REPLICATION PROTEIN A:A Heterotrimeric, Single-Stranded DNA-Binding Protein Required for Eukaryotic DNA Metabolism. *Annu. Rev. Biochem.*, **66**, 61–92.
4. Wobbe,C.R., Weissbach,L., Borowiec,J.A., Dean,F.B., Murakami,Y., Bullock,P., and Hurwitz,J. (1987) Replication of simian virus 40 origin-containing DNA in vitro with purified proteins. *Proc. Natl. Acad. Sci. U. S. A.*, **84**, 1834–1838.
5. Kim,C., Paulus,B.F., and Wold,M.S. (1994) Interactions of human replication protein A with oligonucleotides. *Biochemistry*, **33**, 14197–14206.
6. Brill,S.J. and Stillman,B. (1989) Yeast replication factor-A functions in the unwinding of the SV40 origin of DNA replication. *Nature*, **342**, 92–95.
7. Cejka,P., Cannavo,E., Polaczek,P., Masuda-Sasa,T., Pokharel,S., Campbell,J.L., and Kowalczykowski,S.C. (2010) DNA end resection by Dna2-Sgs1-RPA and its stimulation by Top3-Rmi1 and Mre11-Rad50-Xrs2. *Nature*, **467**, 112–116.
8. Namiki,Y. and Zou,L. (2006) ATRIP associates with replication protein A-coated ssDNA through multiple interactions. *Proc. Natl. Acad. Sci. U. S. A.*, **103**, 580–585.
9. Oakley,G.G., Tillison,K., Opiyo,S.A., Glanzer,J.G., Horn,J.M., and Patrick,S.M. (2009) Physical Interaction between Replication Protein A (RPA) and MRN: Involvement of RPA2 Phosphorylation and the N-Terminus of RPA1. *Biochemistry*, **48**, 7473–7481.
10. Feldkamp,M.D., Mason,A.C., Eichman,B.F., and Chazin,W.J. (2014) Structural Analysis of Replication Protein A Recruitment of the DNA Damage Response Protein SMARCAL1. *Biochemistry*, **53**, 3052–3061.
11. Chen,H., Lisby,M., and Symington,L. (2013) RPA Coordinates DNA End Resection and Prevents Formation of DNA Hairpins. *Mol. Cell*, **50**, 589–600.
12. Chen,R. and Wold,M.S. (2014) Replication protein A: Single-stranded DNA's first responder. *Bioessays*, n/a–n/a.
13. Kim,C., Snyder,R.O., and Wold,M.S. (1992) Binding properties of replication protein A from human and yeast cells. *Mol. Cell. Biol.*, **12**, 3050–3059.
14. Patrick,S.M. and Turchi,J.J. (1999) Replication Protein A (RPA) Binding to Duplex Cisplatin-damaged DNA Is Mediated through the Generation of Single-stranded DNA. *J. Biol. Chem.*, **274**, 14972–14978.
15. Lao,Y., Gomes,X.V., Ren,Y., Taylor,J.S., and Wold,M.S. (2000) Replication Protein A Interactions with DNA. III. Molecular Basis of Recognition of Damaged DNA. *Biochemistry*, **39**, 850–859.
16. Wu,Y., Rawtani,N., Thazhathveetil,A.K., Kenny,M.K., Seidman,M.M., and Brosh,R.M. (2008) Human Replication Protein A Melts a DNA Triple Helix Structure in a Potent and Specific Manner. *Biochemistry*, **47**, 5068–5077.
17. Salas,T.R., Petruseva,I., Lavrik,O., Bourdoncle,A., Mergny,J.L., Favre,A., and Saintom,C. (2006) Human replication protein A unfolds telomeric G-quadruplexes. *Nucleic Acids Res.*, **34**, 4857–4865.
18. Prakash,A., Natarajan,A., Marky,L.A., Ouellette,M.M., and Borgstahl,G.E.O. (2011) Identification of the DNA-Binding Domains of Human Replication Protein A That Recognize G-Quadruplex DNA. *J. Nucleic Acids*, **2011**, 14.
19. Georgaki,A., Strack,B., Podust,V., and Hbscher,U. (1992) DNA unwinding activity of replication protein A. *FEBS Lett.*, **308**, 240–244.

20. Treuner,K., Ramsperger,U., and Knippers,R. (1996) Replication Protein A Induces the Unwinding of Long Double-stranded DNA Regions. *J. Mol. Biol.*, **259**, 104–112.
21. Lao,Y., Lee,C.G., and Wold,M.S. (1999) Replication Protein A Interactions with DNA. 2. Characterization of Double-Stranded DNA-Binding/Helix-Destabilization Activities and the Role of the Zinc-Finger Domain in DNA Interactions. *Biochemistry*, **38**, 3974–3984.
22. De Vlaminck,I., Vidic,I., van Loenhout,M.T.J., Kanaar,R., Lebbink,J.H.G., and Dekker,C. (2010) Torsional regulation of hRPA-induced unwinding of double-stranded DNA. *Nucleic Acids Res.*, **38**, 4133–4142.
23. Gibb,B., Ye,L.F., Gergoudis,S.C., Kwon,Y., Niu,H., Sung,P., and Greene,E.C. (2014) Concentration-Dependent Exchange of Replication Protein A on Single-Stranded DNA Revealed by Single-Molecule Imaging. *PLoS ONE*, **9**, e87922–.
24. Nguyen,B., Sokoloski,J., Galletto,R., Elson,E.L., Wold,M.S., and Lohman,T.M. (2014) Diffusion of Human Replication Protein A along Single-Stranded DNA. *J. Mol. Biol.*, **426**, 3246–3261.
25. Huhle,A., Klaue,D., Brutzer,H., Daldrop,P., Joo,S., Otto,O., Keyser,U., and Seidel,R. (2014) Camera-based real-time 3D particle tracking at kHz rates and ngstrm accuracy. *Nat. Commun.*
26. Klaue,D., Kobbe,D., Kemmerich,F., Kozikowska,A., Puchta,H., and Seidel,R. (2013) Fork sensing and strand switching control antagonistic activities of RecQ helicases. *Nat. Commun.*, **4**, 2024.
27. Levikova,M., Klaue,D., Seidel,R., and Cejka,P. (2013) Nuclease activity of Saccharomyces cerevisiae Dna2 inhibits its potent DNA helicase activity. *Proc. Natl. Acad. Sci. U. S. A.*, **110**, E1992–E2001.
28. Kantake,N., Sugiyama,T., Kolodner,R.D., and Kowalczykowski,S.C. (2003) The recombination-deficient mutant RPA (rfa1-t11) is displaced slowly from single-stranded DNA by Rad51 protein. *J. Biol. Chem.*, **278**, 23410–23417.
29. Klaue,D. and Seidel,R. (2009) Torsional stiffness of single superparamagnetic microspheres in an external magnetic field. *Phys. Rev. Lett.*, **102**, 028302.
30. Daldrop,P., Brutzer,H., Huhle,A., Kauert,D.J., and Seidel,R. (2015) Extending the range for force calibration in magnetic tweezers. *Biophys. J.*, **108**, 2550–2561.
31. Smith,S.B., Cui,Y., and Bustamante,C. (1996) Overstretching B-DNA: The Elastic Response of Individual Double-Stranded and Single-Stranded DNA Molecules. *Science*, **271**, 795–799.
32. Cluzel,P., Lebrun,A., Heller,C., Lavery,R., Viovy,J.L., Chatenay,D., and Caron,F. (1996) DNA: An Extensible Molecule. *Science*, **271**, 792–794.
33. Anderson,C.F. and Record,Jr,M. (1995) Salt-nucleic acid interactions. *Annu. Rev. Phys. Chem.*, **46**, 657–700.
34. Guéroult,M., Boittin,O., Mauffret,O., Etchebest,C., and Hartmann,B. (2012) Mg2+ in the major groove modulates B-DNA structure and dynamics. *PLoS One*, **7**, e41704.
35. Kumaran,S., Kozlov,A.G., and Lohman,T.M. (2006) Saccharomyces cerevisiae Replication Protein A Binds to Single-Stranded DNA in Multiple Salt-Dependent Modes. *Biochemistry*, **45**, 11958–11973.
36. van Mameren,J., Gross,P., Farge,G., Hooijman,P., Modesti,M., Falkenberg,M., Wuite,G.J.L., and Peterman,E.J.G. (2009) Unraveling the structure of DNA during overstretching by using multicolor, single-molecule fluorescence imaging. *Proc. Natl. Acad. Sci. U. S. A.*, **106**, 18231–18236.
37. King,G.A., Gross,P., Bockelmann,U., Modesti,M., Wuite,G.J.L., and Peterman,E.J.G. (2013) Revealing the competition between peeled ssDNA, melting bubbles, and S-DNA during DNA overstretching using fluorescence microscopy. *Proc. Natl. Acad. Sci. U. S. A.*, **110**, 3859–3864.
38. Patrick,S.M. and Turchi,J.J. (2001) Stopped-flow Kinetic Analysis of Replication Protein A-binding DNA: DAMAGE RECOGNITION AND AFFINITY FOR SINGLE-STRANDED DNA REVEAL DIFFERENTIAL CONTRIBUTIONS OF k on ANDk off RATE CONSTANTS. *J. Biol. Chem.*, **276**, 22630–22637.
39. Deng,S.K., Gibb,B., de Almeida,M.J., Greene,E.C., and Symington,L.S. (2014) RPA antagonizes microhomology-mediated repair of DNA double-strand breaks. *Nat. Struct. Mol. Biol.*, **21**, 405–412.
40. Kroeger,H. and Trösch,W. (1974) Influence of the explantation milieu on intranuclear [Na], [K] and [Mg] of Chironomus thummi salivary gland cells. *J. Cell. Physiol.*, **83**, 19–25.
41. Hartwig,A. (2001) Role of magnesium in genomic stability. *Mutat. Res.*, –.
42. Cohen SM FAU Burt,C.T. and CT,B. (1977) 31P nuclear magnetic relaxation studies of phosphocreatine in intact muscle: determination of intracellular free magnesium. *Proc. Natl. Acad. Sci. U. S. A.*, **74**, –.
43. Adhikari,S., Karmahapatra,S., Karve,T., Bandyopadhyay,S., Woodrick,J., Manthena,P., Glasgow,E., Byers,S., Saha,T., and Uren,A. (2012) Characterization of magnesium requirement of human 5'-tyrosyl DNA phosphodiesterase mediated reaction. *BMC Research Notes*, **5**, 134–.
44. Lionnet,T., Spiering,M.M., Benkovic,S.J., Bensimon,D., and Croquette,V. (2007) Real-time observation of bacteriophage T4 gp41 helicase reveals an unwinding mechanism. *Proc. Natl. Acad. Sci. U. S. A.*, **104**, 19790–19795.
45. Bochkarev,A., Pfuetzner,R.A., Edwards,A.M., and Frappier,L. (1997) Structure of the single-stranded-DNA-binding domain of replication protein A bound to DNA. *Nature*, **385**, 176–181.
46. Cai,L., Roginskaya,M., Qu,Y., Yang,Z., Xu,Y., and Zou,Y. (2007) Structural Characterization of Human RPA Sequential Binding to Single-Stranded DNA Using ssDNA as a Molecular Ruler. *Biochemistry*, **46**, 8226–8233.
47. Yeeles,J., vanAelst,K., Dillingham,M., and Moreno-Herrero,F. (2011) Recombination Hotspots and Single-Stranded DNA Binding Proteins Couple DNA Translocation to DNA Unwinding by the AddAB Helicase-Nuclease. *Mol. Cell*, **42**, 806–816.
48. Yusufzai,T. and Kadonaga,J.T. (2008) HARP Is an ATP-Driven Annealing Helicase. *Science*, **322**, 748–750.

3. DISCUSSION

3.1 Biochemical activities of Dna2 and its regulation

S. cerevisiae Dna2 protein has a tripartite structure as it contains a C-terminal superfamily I helicase domain, a central RecB family nuclease domain and an unstructured N-terminal tail (35). The nuclease activity has a 5' to 3' polarity in the presence of RPA and is essential for cell survival (25,27,28). The ATP-dependent helicase activity of Dna2 has been considered as weak, although helicase-dead mutants exhibited increased sensitivity to alkylating agents and ionizing radiation (17,30,31). The N-terminal domain has been proposed to mediate DNA binding to secondary structure DNA, to be involved in the interaction with RPA as well as to be a Mec1 activator (36,37,39).

We were able to show that Dna2 has a vigorous, but cryptic helicase activity that is comparable to that of Sgs1 ((125); see 2.2.1). However, in the wild type Dna2 the nuclease activity masks the helicase, so the question arised whether there is an additional regulatory mechanism attenuating Dna2 nuclease activity. Indeed, we demonstrate that Dna2 is sumoylated *in vitro* and *in vivo* (Levikova *et al*., manuscript in preparation, see 2.2.2). *In vitro*, we show that six lysines within the N-terminal domain are modified by SUMO and that the sumoylation selectively attenuates the nuclease activity of Dna2, without affecting its helicase or ATPase. We hypothesize that the sumoylated N-terminal tail of Dna2 might interact with the SUMO-interaction motifs (SIMs) within the nuclease domain of Dna2, thus partially inhibiting its activity. *In vivo,* we found Dna2 to be sumoylated primarily in the late S/G2 phases of the cell cycle. Furthermore, sumoylation appeared to protect Dna2 from reduction of protein levels induced by the alkylating agent MMS and radiomimetic drug Bleomycin. It appears that sumoylation is not only modulating the balance between the nuclease and helicase within Dna2, but also has a protective function. The attenuation of the nuclease induced by sumoylation brings possibly the helicase into play, which seems to be important in late S/G2 phases of the cell cycle

and upon genotoxic stress. Interestingly, we detected sumoylated Dna2 upon treatment with alkylating and radiomimetic drugs; both treatments to which helicase-dead mutants displayed increased sensitivity (17,31). Taken together, these results would infer that in late replication and upon genotoxic stress Dna2 nuclease is attenuated by sumoylation so the potent helicase can come into play and possibly contribute to more efficient "screening" of DNA for specific structures/lesions like flaps, DNA breaks and G4 quadruplexes. Moreover, sumoylation hubs were described to occur at sites of DNA damage as well as at telomeres (126), suggesting that Dna2 might be part of those events.

3.2 Role of Dna2 in replication and replication stress response

Dna2 was described to be essential for replication (16). It has an established role in Okazaki fragment processing where it acts together with Fen1 to remove flaps arising form strand displacement activity of pol δ that are refractory to subsequent ligation (53,54). However, this sequential model was based on the biochemical observation that Dna2 can cleave the DNA flap structures only up to 5-8 nucleotides away from the base, thus providing the requirement for a second nuclease activity (54). Moreover, *dna2Δ* mutation is lethal, while *rad27Δ* cells are viable (16,56,57), which stands in contrast to the notion of Dna2 acting upstream of Fen1.

We show that our Dna2 protein preparation is able to cleave the flaps at or near their base and the products can be ligated by DNA ligase I (Levikova and Cejka, NAR 2015, in press; see 2.2.3). In conjunction with replication Dna2 was highly efficient in Okazaki fragment processing as a sole nuclease. Addition of Fen1 had only a very moderate additive effect on the overall processing efficiency, suggesting that Dna2 is able to process long RPA-bound DNA flaps alone, which fits with genetic data. These observations raise the question about the redundancy of the Okazaki fragment processing pathways. We propose that Fen1 and Dna2 act in different time frames during the cell cycle. Several lines of evidence suggest that Fen1 is acting primarily in the S phase of the cell cycle as human FEN1 is degraded in late S/G2 and *fen1* yeast cells arrest already in S phase (127,128). In contrast, *dna2* mutants are proficient in

DNA bulk synthesis, but arrest in G2/M (129). Also human cell depleted from DNA2 arrest in late S/G2 (41). So, we think that Fen1 is still responsible for the processing of the majority of flaps in S phase, while Dna2 takes care of those that became long enough to bind RPA, which is refractory to Fen1 cleavage. It is also possible that Dna2 is additionally involved in the cleavage of flaps that arised during post-replicative repair in late S/G2 phases. Furthermore, Dna2 might function in telomere replication as well, as it was shown to localize to telomeres in late S/G2 and to cleave/unwind telomeric G4 structures (109,110,113).

Additionally, we show that Dna2 is also involved in replication under perturbed conditions. In a collaborative work we demonstrate that Dna2 is able to process reversed forks, thus driving their restart ((130); see 2.3.1). Furthermore, we demonstrate that the helicase activity of Dna2 is required for completion of replication and helicase-deficient cells depend on Yen1 upon replication stress (Ölmezer *et al*., under revision in Nat. Com., see 2.3.2). Hence, these findings support the idea of Dna2 involvement in error-free DNA damage tolerance pathway at multiple levels.

Taken together, our results posit Dna2 as a safeguard of replication and its checkpoint function (37) stresses even more the importance of Dna2 for genome stability.

3.3 Dna2 and DNA end resection

Dna2 has a well-established role in long-range DNA end resection where it acts together with Sgs1 (28,92,93). So far, the contribution of Dna2 helicase activity to this process was negligible (93).

Using biochemical assays we show now that the motor activity of Dna2 acts as a ssDNA translocase especially in presence of RPA and greatly promotes degradation of long stretches of ssDNA (Levikova and Cejka, manuscript in preparation, see 2.2.4). RPA stimulates the recruitment of Dna2 and its translocase as well as its nuclease activities. We think that in resection Sgs1 is the lead helicase, translocating with 3' to 5' polarity, while Dna2 translocase activity allows it to keep up with Sgs1

on the 5'-terminated strand. These findings provide a further proof for analogy between Dna2-Sgs1 and the RecBCD complex. Nevertheless, additional research is needed to show the contribution of Dna2 helicase activity to DNA end resection *in vivo*.

Another collaborative work provided further evidence for human DNA2 acting in conjunction with BLM or WRN in long-range DNA resection ((131); see 2.3.3). This work underlines the evolutionary conservation of DNA2 enzymatic functions. It would be interesting to know whether human DNA2 helicase plays a similar role here as in the yeast protein.

We and others demonstrated the importance of RPA in DNA end resection and its stimulatory activity on Dna2 (28,54,92,125). However, the molecular basis of RPA polymerization on ssDNA and depolymerization was still outstanding. The single-molecule analysis of RPA behavior was conducted by the laboratory of Prof. Ralf Seidel (Kemmerich *et al.*, manuscript in preparation, see 2.2.4). Their results infer that RPA is not capable of disrupting dsDNA on its own, but rather it binds and protects ssDNA. This is in agreement with the role of RPA in resection where it promotes Dna2-mediated degradation of the 5'-terminated strand, while protecting the 3'-terminated tail (28,92). Furthermore, the study confirms the previously reported diffusion of human RPA along ssDNA (132), thus leading to "melting" of dsDNA and possibly allowing access to ssDNA to other proteins.

4. PERSPECTIVES

This work underlines the multifunctionality of the essential Dna2 enzyme and its importance for maintaining genome integrity. It provides possible explanations for the complex role of Dna2 in cancer development where its involvement is ambiguous. Dna2 is a caretaker gene, thus loss of its activity might be one of the initial events in cancer development and the driving force of genome instability, while during cancer progression overexpression of Dna2 provides cancer cells with additional fitness and helps to survive higher levels of replication stress induced by increased proliferation. Thus, targeting Dna2 in cancer therapy is a considerable option, especially in combination with other treatments. However, thorough analysis of tumor genome and gene expression profile as well as proper staging is pivotal before such treatment. In collaboration with the laboratory of Prof. Lumir Krejci (Masaryk University, Brno, Czech Republic) we are currently conducting a high-throughput screening of a small molecule library in order to obtain a selective inhibitor of both yeast and human Dna2. In case of success, first biochemical and cell biological validation would be required, with a possible long-term perspective of testing it in mouse models.

Cancer is a very complex disease and we are now only starting to see the big picture. The idea of finding THE cancer-inducing mutation and targeting the mutated protein turned out to be utopic, as cancers display a large variety of mutational landscapes that even differ within one tumor entity (133). Further, the concept of oncogene addiction and targeting the oncogene within the corresponding pathway appears to be difficult (134), as cancers develop multiple escape mechanisms and drug resistance. It appears that personalized combinational therapies, targeting multiple hallmarks, are the future of cancer therapy. To develop these therapies we need to collaborate on an interdisciplinary level and above all the teamwork between clinicians and basic scientists is of an essential importance.

5. REFERENCES

1. Hanahan, D. and Weinberg, R.A. (2000) The hallmarks of cancer. *Cell*, **100**, 57-70.
2. Hanahan, D. and Weinberg, R.A. (2011) Hallmarks of cancer: the next generation. *Cell*, **144**, 646-674.
3. De Bont, R. and van Larebeke, N. (2004) Endogenous DNA damage in humans: a review of quantitative data. *Mutagenesis*, **19**, 169-185.
4. Schar, P. (2001) Spontaneous DNA damage, genome instability, and cancer--when DNA replication escapes control. *Cell*, **104**, 329-332.
5. Hoeijmakers, J.H. (2001) Genome maintenance mechanisms for preventing cancer. *Nature*, **411**, 366-374.
6. Hoeijmakers, J.H. (2009) DNA damage, aging, and cancer. *N Engl J Med*, **361**, 1475-1485.
7. Robertson, A.B., Klungland, A., Rognes, T. and Leiros, I. (2009) DNA repair in mammalian cells: Base excision repair: the long and short of it. *Cell Mol Life Sci*, **66**, 981-993.
8. Scharer, O.D. (2013) Nucleotide excision repair in eukaryotes. *Cold Spring Harb Perspect Biol*, **5**, a012609.
9. Jiricny, J. (2006) The multifaceted mismatch-repair system. *Nat Rev Mol Cell Biol*, **7**, 335-346.
10. Chapman, J.R., Taylor, M.R. and Boulton, S.J. (2012) Playing the end game: DNA double-strand break repair pathway choice. *Mol Cell*, **47**, 497-510.
11. Prakash, S., Johnson, R.E. and Prakash, L. (2005) Eukaryotic translesion synthesis DNA polymerases: specificity of structure and function. *Annu Rev Biochem*, **74**, 317-353.
12. Kim, H. and D'Andrea, A.D. (2012) Regulation of DNA cross-link repair by the Fanconi anemia/BRCA pathway. *Genes Dev*, **26**, 1393-1408.
13. Negrini, S., Gorgoulis, V.G. and Halazonetis, T.D. (2010) Genomic instability--an evolving hallmark of cancer. *Nat Rev Mol Cell Biol*, **11**, 220-228.
14. Loeb, L.A. (1991) Mutator phenotype may be required for multistage carcinogenesis. *Cancer Res*, **51**, 3075-3079.
15. Halazonetis, T.D., Gorgoulis, V.G. and Bartek, J. (2008) An oncogene-induced DNA damage model for cancer development. *Science*, **319**, 1352-1355.
16. Budd, M.E., Choe, W.C. and Campbell, J.L. (1995) DNA2 encodes a DNA helicase essential for replication of eukaryotic chromosomes. *J Biol Chem*, **270**, 26766-26769.
17. Formosa, T. and Nittis, T. (1999) Dna2 mutants reveal interactions with Dna polymerase alpha and Ctf4, a Pol alpha accessory factor, and show that full Dna2 helicase activity is not essential for growth. *Genetics*, **151**, 1459-1470.
18. Kuo, C.L. and Campbell, J.L. (1983) Cloning of Saccharomyces cerevisiae DNA replication genes: isolation of the CDC8 gene and two genes that compensate for the cdc8-1 mutation. *Mol Cell Biol*, **3**, 1730-1737.

19. Pokharel, S. and Campbell, J.L. (2012) Cross talk between the nuclease and helicase activities of Dna2: role of an essential iron-sulfur cluster domain. *Nucleic Acids Res*, **40**, 7821-7830.
20. Yeeles, J.T., Cammack, R. and Dillingham, M.S. (2009) An iron-sulfur cluster is essential for the binding of broken DNA by AddAB-type helicase-nucleases. *J Biol Chem*, **284**, 7746-7755.
21. Eki, T., Okumura, K., Shiratori, A., Abe, M., Nogami, M., Taguchi, H., Shibata, T., Murakami, Y. and Hanaoka, F. (1996) Assignment of the closest human homologue (DNA2L:KIAA0083) of the yeast Dna2 helicase gene to chromosome band 10q21.3-q22.1. *Genomics*, **37**, 408-410.
22. Gould, K.L., Burns, C.G., Feoktistova, A., Hu, C.P., Pasion, S.G. and Forsburg, S.L. (1998) Fission yeast cdc24(+) encodes a novel replication factor required for chromosome integrity. *Genetics*, **149**, 1221-1233.
23. Liu, Q., Choe, W. and Campbell, J.L. (2000) Identification of the Xenopus laevis homolog of Saccharomyces cerevisiae DNA2 and its role in DNA replication. *J Biol Chem*, **275**, 1615-1624.
24. Wanrooij, P.H. and Burgers, P.M. (2015) Yet another job for Dna2: Checkpoint activation. *DNA Repair (Amst)*.
25. Bae, S.H., Choi, E., Lee, K.H., Park, J.S., Lee, S.H. and Seo, Y.S. (1998) Dna2 of Saccharomyces cerevisiae possesses a single-stranded DNA-specific endonuclease activity that is able to act on double-stranded DNA in the presence of ATP. *J Biol Chem*, **273**, 26880-26890.
26. Bae, S.H. and Seo, Y.S. (2000) Characterization of the enzymatic properties of the yeast dna2 Helicase/endonuclease suggests a new model for Okazaki fragment processing. *J Biol Chem*, **275**, 38022-38031.
27. Budd, M.E., Choe, W. and Campbell, J.L. (2000) The nuclease activity of the yeast DNA2 protein, which is related to the RecB-like nucleases, is essential in vivo. *J Biol Chem*, **275**, 16518-16529.
28. Cejka, P., Cannavo, E., Polaczek, P., Masuda-Sasa, T., Pokharel, S., Campbell, J.L. and Kowalczykowski, S.C. (2010) DNA end resection by Dna2-Sgs1-RPA and its stimulation by Top3-Rmi1 and Mre11-Rad50-Xrs2. *Nature*, **467**, 112-116.
29. Lee, K.H., Kim, D.W., Bae, S.H., Kim, J.A., Ryu, G.H., Kwon, Y.N., Kim, K.A., Koo, H.S. and Seo, Y.S. (2000) The endonuclease activity of the yeast Dna2 enzyme is essential in vivo. *Nucleic Acids Res*, **28**, 2873-2881.
30. Balakrishnan, L., Polaczek, P., Pokharel, S., Campbell, J.L. and Bambara, R.A. (2010) Dna2 exhibits a unique strand end-dependent helicase function. *J Biol Chem*, **285**, 38861-38868.
31. Budd, M.E. and Campbell, J.L. (2000) The pattern of sensitivity of yeast dna2 mutants to DNA damaging agents suggests a role in DSB and postreplication repair pathways. *Mutat Res*, **459**, 173-186.
32. Kim, J.H., Kim, H.D., Ryu, G.H., Kim, D.H., Hurwitz, J. and Seo, Y.S. (2006) Isolation of human Dna2 endonuclease and characterization of its enzymatic properties. *Nucleic Acids Res*, **34**, 1854-1864.
33. Masuda-Sasa, T., Imamura, O. and Campbell, J.L. (2006) Biochemical analysis of human Dna2. *Nucleic Acids Res*, **34**, 1865-1875.

34. Masuda-Sasa, T., Polaczek, P. and Campbell, J.L. (2006) Single strand annealing and ATP-independent strand exchange activities of yeast and human DNA2: possible role in Okazaki fragment maturation. *J Biol Chem*, **281**, 38555-38564.
35. Bae, S.H., Kim, J.A., Choi, E., Lee, K.H., Kang, H.Y., Kim, H.D., Kim, J.H., Bae, K.H., Cho, Y., Park, C. *et al.* (2001) Tripartite structure of Saccharomyces cerevisiae Dna2 helicase/endonuclease. *Nucleic Acids Res*, **29**, 3069-3079.
36. Lee, C.H., Lee, M., Kang, H.J., Kim, D.H., Kang, Y.H., Bae, S.H. and Seo, Y.S. (2013) The N-terminal 45-kDa domain of Dna2 endonuclease/helicase targets the enzyme to secondary structure DNA. *J Biol Chem*, **288**, 9468-9481.
37. Kumar, S. and Burgers, P.M. (2013) Lagging strand maturation factor Dna2 is a component of the replication checkpoint initiation machinery. *Genes Dev*, **27**, 313-321.
38. Kosugi, S., Hasebe, M., Matsumura, N., Takashima, H., Miyamoto-Sato, E., Tomita, M. and Yanagawa, H. (2009) Six classes of nuclear localization signals specific to different binding grooves of importin alpha. *J Biol Chem*, **284**, 478-485.
39. Bae, K.H., Kim, H.S., Bae, S.H., Kang, H.Y., Brill, S. and Seo, Y.S. (2003) Bimodal interaction between replication-protein A and Dna2 is critical for Dna2 function both in vivo and in vitro. *Nucleic Acids Res*, **31**, 3006-3015.
40. Zheng, L., Zhou, M., Guo, Z., Lu, H., Qian, L., Dai, H., Qiu, J., Yakubovskaya, E., Bogenhagen, D.F., Demple, B. *et al.* (2008) Human DNA2 is a mitochondrial nuclease/helicase for efficient processing of DNA replication and repair intermediates. *Mol Cell*, **32**, 325-336.
41. Duxin, J.P., Dao, B., Martinsson, P., Rajala, N., Guittat, L., Campbell, J.L., Spelbrink, J.N. and Stewart, S.A. (2009) Human Dna2 is a nuclear and mitochondrial DNA maintenance protein. *Mol Cell Biol*, **29**, 4274-4282.
42. DePamphilis, M.L., Blow, J.J., Ghosh, S., Saha, T., Noguchi, K. and Vassilev, A. (2006) Regulating the licensing of DNA replication origins in metazoa. *Curr Opin Cell Biol*, **18**, 231-239.
43. Kelly, T.J. and Brown, G.W. (2000) Regulation of chromosome replication. *Annu Rev Biochem*, **69**, 829-880.
44. Tanaka, S. and Araki, H. (2013) Helicase activation and establishment of replication forks at chromosomal origins of replication. *Cold Spring Harb Perspect Biol*, **5**, a010371.
45. Wang, J.C. (2002) Cellular roles of DNA topoisomerases: a molecular perspective. *Nat Rev Mol Cell Biol*, **3**, 430-440.
46. Hubscher, U. and Seo, Y.S. (2001) Replication of the lagging strand: a concert of at least 23 polypeptides. *Mol Cells*, **12**, 149-157.
47. Kang, Y.H., Lee, C.H. and Seo, Y.S. (2010) Dna2 on the road to Okazaki fragment processing and genome stability in eukaryotes. *Crit Rev Biochem Mol Biol*, **45**, 71-96.
48. Huang, L., Kim, Y., Turchi, J.J. and Bambara, R.A. (1994) Structure-specific cleavage of the RNA primer from Okazaki fragments by calf thymus RNase HI. *J Biol Chem*, **269**, 25922-25927.

49. Murante, R.S., Rumbaugh, J.A., Barnes, C.J., Norton, J.R. and Bambara, R.A. (1996) Calf RTH-1 nuclease can remove the initiator RNAs of Okazaki fragments by endonuclease activity. *J Biol Chem*, **271**, 25888-25897.
50. Turchi, J.J., Huang, L., Murante, R.S., Kim, Y. and Bambara, R.A. (1994) Enzymatic completion of mammalian lagging-strand DNA replication. *Proc Natl Acad Sci U S A*, **91**, 9803-9807.
51. Burgers, P.M. (1998) Eukaryotic DNA polymerases in DNA replication and DNA repair. *Chromosoma*, **107**, 218-227.
52. Burgers, P.M. (2009) Polymerase dynamics at the eukaryotic DNA replication fork. *J Biol Chem*, **284**, 4041-4045.
53. Ayyagari, R., Gomes, X.V., Gordenin, D.A. and Burgers, P.M. (2003) Okazaki fragment maturation in yeast. I. Distribution of functions between FEN1 AND DNA2. *J Biol Chem*, **278**, 1618-1625.
54. Bae, S.H., Bae, K.H., Kim, J.A. and Seo, Y.S. (2001) RPA governs endonuclease switching during processing of Okazaki fragments in eukaryotes. *Nature*, **412**, 456-461.
55. Kao, H.I., Campbell, J.L. and Bambara, R.A. (2004) Dna2p helicase/nuclease is a tracking protein, like FEN1, for flap cleavage during Okazaki fragment maturation. *J Biol Chem*, **279**, 50840-50849.
56. Gary, R., Park, M.S., Nolan, J.P., Cornelius, H.L., Kozyreva, O.G., Tran, H.T., Lobachev, K.S., Resnick, M.A. and Gordenin, D.A. (1999) A novel role in DNA metabolism for the binding of Fen1/Rad27 to PCNA and implications for genetic risk. *Mol Cell Biol*, **19**, 5373-5382.
57. Symington, L.S. (1998) Homologous recombination is required for the viability of rad27 mutants. *Nucleic Acids Res*, **26**, 5589-5595.
58. Budd, M.E., Reis, C.C., Smith, S., Myung, K. and Campbell, J.L. (2006) Evidence suggesting that Pif1 helicase functions in DNA replication with the Dna2 helicase/nuclease and DNA polymerase delta. *Mol Cell Biol*, **26**, 2490-2500.
59. Budd, M.E., Tong, A.H., Polaczek, P., Peng, X., Boone, C. and Campbell, J.L. (2005) A network of multi-tasking proteins at the DNA replication fork preserves genome stability. *PLoS Genet*, **1**, e61.
60. Pike, J.E., Burgers, P.M., Campbell, J.L. and Bambara, R.A. (2009) Pif1 helicase lengthens some Okazaki fragment flaps necessitating Dna2 nuclease/helicase action in the two-nuclease processing pathway. *J Biol Chem*, **284**, 25170-25180.
61. Stith, C.M., Sterling, J., Resnick, M.A., Gordenin, D.A. and Burgers, P.M. (2008) Flexibility of eukaryotic Okazaki fragment maturation through regulated strand displacement synthesis. *J Biol Chem*, **283**, 34129-34140.
62. Duxin, J.P., Moore, H.R., Sidorova, J., Karanja, K., Honaker, Y., Dao, B., Piwnica-Worms, H., Campbell, J.L., Monnat, R.J., Jr. and Stewart, S.A. (2012) Okazaki fragment processing-independent role for human Dna2 enzyme during DNA replication. *J Biol Chem*, **287**, 21980-21991.
63. Follonier, C., Oehler, J., Herrador, R. and Lopes, M. (2013) Friedreich's ataxia-associated GAA repeats induce replication-fork reversal and unusual molecular junctions. *Nat Struct Mol Biol*, **20**, 486-494.

64. Neelsen, K.J. and Lopes, M. (2015) Replication fork reversal in eukaryotes: from dead end to dynamic response. *Nat Rev Mol Cell Biol*, **16**, 207-220.
65. Zellweger, R., Dalcher, D., Mutreja, K., Berti, M., Schmid, J.A., Herrador, R., Vindigni, A. and Lopes, M. (2015) Rad51-mediated replication fork reversal is a global response to genotoxic treatments in human cells. *J Cell Biol*, **208**, 563-579.
66. Higgins, N.P., Kato, K. and Strauss, B. (1976) A model for replication repair in mammalian cells. *J Mol Biol*, **101**, 417-425.
67. Fugger, K., Mistrik, M., Neelsen, K.J., Yao, Q., Zellweger, R., Kousholt, A.N., Haahr, P., Chu, W.K., Bartek, J., Lopes, M. *et al.* (2015) FBH1 Catalyzes Regression of Stalled Replication Forks. *Cell Rep*.
68. Berti, M., Ray Chaudhuri, A., Thangavel, S., Gomathinayagam, S., Kenig, S., Vujanovic, M., Odreman, F., Glatter, T., Graziano, S., Mendoza-Maldonado, R. *et al.* (2013) Human RECQ1 promotes restart of replication forks reversed by DNA topoisomerase I inhibition. *Nat Struct Mol Biol*, **20**, 347-354.
69. Hanada, K., Budzowska, M., Davies, S.L., van Drunen, E., Onizawa, H., Beverloo, H.B., Maas, A., Essers, J., Hickson, I.D. and Kanaar, R. (2007) The structure-specific endonuclease Mus81 contributes to replication restart by generating double-strand DNA breaks. *Nat Struct Mol Biol*, **14**, 1096-1104.
70. Neelsen, K.J., Zanini, I.M., Herrador, R. and Lopes, M. (2013) Oncogenes induce genotoxic stress by mitotic processing of unusual replication intermediates. *J Cell Biol*, **200**, 699-708.
71. Murfuni, I., De Santis, A., Federico, M., Bignami, M., Pichierri, P. and Franchitto, A. (2012) Perturbed replication induced genome wide or at common fragile sites is differently managed in the absence of WRN. *Carcinogenesis*, **33**, 1655-1663.
72. Hu, J., Sun, L., Shen, F., Chen, Y., Hua, Y., Liu, Y., Zhang, M., Hu, Y., Wang, Q., Xu, W. *et al.* (2012) The intra-S phase checkpoint targets Dna2 to prevent stalled replication forks from reversing. *Cell*, **149**, 1221-1232.
73. Ray Chaudhuri, A., Ahuja, A.K., Herrador, R. and Lopes, M. (2015) Poly(ADP-ribosyl) glycohydrolase prevents the accumulation of unusual replication structures during unperturbed S phase. *Mol Cell Biol*, **35**, 856-865.
74. McMurray, C.T. (2010) Mechanisms of trinucleotide repeat instability during human development. *Nat Rev Genet*, **11**, 786-799.
75. Mladenov, E. and Iliakis, G. (2011) Induction and repair of DNA double strand breaks: the increasing spectrum of non-homologous end joining pathways. *Mutat Res*, **711**, 61-72.
76. Soulas-Sprauel, P., Le Guyader, G., Rivera-Munoz, P., Abramowski, V., Olivier-Martin, C., Goujet-Zalc, C., Charneau, P. and de Villartay, J.P. (2007) Role for DNA repair factor XRCC4 in immunoglobulin class switch recombination. *J Exp Med*, **204**, 1717-1727.
77. Jasin, M. and Rothstein, R. (2013) Repair of strand breaks by homologous recombination. *Cold Spring Harb Perspect Biol*, **5**, a012740.
78. Bennardo, N., Cheng, A., Huang, N. and Stark, J.M. (2008) Alternative-NHEJ is a mechanistically distinct pathway of mammalian chromosome break repair. *PLoS Genet*, **4**, e1000110.

79. Heyer, W.D., Ehmsen, K.T. and Liu, J. (2010) Regulation of homologous recombination in eukaryotes. *Annu Rev Genet*, **44**, 113-139.
80. Malkova, A. and Haber, J.E. (2012) Mutations arising during repair of chromosome breaks. *Annu Rev Genet*, **46**, 455-473.
81. Mehta, A. and Haber, J.E. (2014) Sources of DNA double-strand breaks and models of recombinational DNA repair. *Cold Spring Harb Perspect Biol*, **6**, a016428.
82. Keeney, S. and Neale, M.J. (2006) Initiation of meiotic recombination by formation of DNA double-strand breaks: mechanism and regulation. *Biochem Soc Trans*, **34**, 523-525.
83. Andersen, P.L., Xu, F. and Xiao, W. (2008) Eukaryotic DNA damage tolerance and translesion synthesis through covalent modifications of PCNA. *Cell Res*, **18**, 162-173.
84. Hoege, C., Pfander, B., Moldovan, G.L., Pyrowolakis, G. and Jentsch, S. (2002) RAD6-dependent DNA repair is linked to modification of PCNA by ubiquitin and SUMO. *Nature*, **419**, 135-141.
85. Bizard, A.H. and Hickson, I.D. (2014) The dissolution of double Holliday junctions. *Cold Spring Harb Perspect Biol*, **6**, a016477.
86. Cejka, P., Plank, J.L., Dombrowski, C.C. and Kowalczykowski, S.C. (2012) Decatenation of DNA by the S. cerevisiae Sgs1-Top3-Rmi1 and RPA complex: a mechanism for disentangling chromosomes. *Mol Cell*, **47**, 886-896.
87. Sarbajna, S. and West, S.C. (2014) Holliday junction processing enzymes as guardians of genome stability. *Trends Biochem Sci*, **39**, 409-419.
88. Cannavo, E. and Cejka, P. (2014) Sae2 promotes dsDNA endonuclease activity within Mre11-Rad50-Xrs2 to resect DNA breaks. *Nature*, **514**, 122-125.
89. Daley, J.M., Niu, H., Miller, A.S. and Sung, P. (2015) Biochemical mechanism of DSB end resection and its regulation. *DNA Repair (Amst)*.
90. Symington, L.S. (2014) End resection at double-strand breaks: mechanism and regulation. *Cold Spring Harb Perspect Biol*, **6**.
91. Bernstein, K.A., Gangloff, S. and Rothstein, R. (2010) The RecQ DNA helicases in DNA repair. *Annu Rev Genet*, **44**, 393-417.
92. Niu, H., Chung, W.H., Zhu, Z., Kwon, Y., Zhao, W., Chi, P., Prakash, R., Seong, C., Liu, D., Lu, L. *et al.* (2010) Mechanism of the ATP-dependent DNA end-resection machinery from Saccharomyces cerevisiae. *Nature*, **467**, 108-111.
93. Zhu, Z., Chung, W.H., Shim, E.Y., Lee, S.E. and Ira, G. (2008) Sgs1 helicase and two nucleases Dna2 and Exo1 resect DNA double-strand break ends. *Cell*, **134**, 981-994.
94. Symington, L.S. and Gautier, J. (2011) Double-strand break end resection and repair pathway choice. *Annu Rev Genet*, **45**, 247-271.
95. Karanja, K.K., Cox, S.W., Duxin, J.P., Stewart, S.A. and Campbell, J.L. (2012) DNA2 and EXO1 in replication-coupled, homology-directed repair and in the interplay between HDR and the FA/BRCA network. *Cell Cycle*, **11**, 3983-3996.
96. Harrison, J.C. and Haber, J.E. (2006) Surviving the breakup: the DNA damage checkpoint. *Annu Rev Genet*, **40**, 209-235.
97. Shiotani, B. and Zou, L. (2009) ATR signaling at a glance. *J Cell Sci*, **122**, 301-304.

98. Paciotti, V., Clerici, M., Lucchini, G. and Longhese, M.P. (2000) The checkpoint protein Ddc2, functionally related to S. pombe Rad26, interacts with Mec1 and is regulated by Mec1-dependent phosphorylation in budding yeast. *Genes Dev*, **14**, 2046-2059.
99. Ball, H.L., Ehrhardt, M.R., Mordes, D.A., Glick, G.G., Chazin, W.J. and Cortez, D. (2007) Function of a conserved checkpoint recruitment domain in ATRIP proteins. *Mol Cell Biol*, **27**, 3367-3377.
100. Zou, L. and Elledge, S.J. (2003) Sensing DNA damage through ATRIP recognition of RPA-ssDNA complexes. *Science*, **300**, 1542-1548.
101. Majka, J., Niedziela-Majka, A. and Burgers, P.M. (2006) The checkpoint clamp activates Mec1 kinase during initiation of the DNA damage checkpoint. *Mol Cell*, **24**, 891-901.
102. Navadgi-Patil, V.M. and Burgers, P.M. (2009) A tale of two tails: activation of DNA damage checkpoint kinase Mec1/ATR by the 9-1-1 clamp and by Dpb11/TopBP1. *DNA Repair (Amst)*, **8**, 996-1003.
103. Delacroix, S., Wagner, J.M., Kobayashi, M., Yamamoto, K. and Karnitz, L.M. (2007) The Rad9-Hus1-Rad1 (9-1-1) clamp activates checkpoint signaling via TopBP1. *Genes Dev*, **21**, 1472-1477.
104. De Lange, T. (2005) Telomere-related genome instability in cancer. *Cold Spring Harb Symp Quant Biol*, **70**, 197-204.
105. Palm, W. and de Lange, T. (2008) How shelterin protects mammalian telomeres. *Annu Rev Genet*, **42**, 301-334.
106. Wellinger, R.J. and Zakian, V.A. (2012) Everything you ever wanted to know about Saccharomyces cerevisiae telomeres: beginning to end. *Genetics*, **191**, 1073-1105.
107. Bonetti, D., Martina, M., Clerici, M., Lucchini, G. and Longhese, M.P. (2009) Multiple pathways regulate 3' overhang generation at S. cerevisiae telomeres. *Mol Cell*, **35**, 70-81.
108. Gravel, S., Larrivee, M., Labrecque, P. and Wellinger, R.J. (1998) Yeast Ku as a regulator of chromosomal DNA end structure. *Science*, **280**, 741-744.
109. Choe, W., Budd, M., Imamura, O., Hoopes, L. and Campbell, J.L. (2002) Dynamic localization of an Okazaki fragment processing protein suggests a novel role in telomere replication. *Mol Cell Biol*, **22**, 4202-4217.
110. Lin, W., Sampathi, S., Dai, H., Liu, C., Zhou, M., Hu, J., Huang, Q., Campbell, J., Shin-Ya, K., Zheng, L. *et al.* (2013) Mammalian DNA2 helicase/nuclease cleaves G-quadruplex DNA and is required for telomere integrity. *Embo J*, **32**, 1425-1439.
111. Paeschke, K., Capra, J.A. and Zakian, V.A. (2011) DNA replication through G-quadruplex motifs is promoted by the Saccharomyces cerevisiae Pif1 DNA helicase. *Cell*, **145**, 678-691.
112. Paeschke, K., Simonsson, T., Postberg, J., Rhodes, D. and Lipps, H.J. (2005) Telomere end-binding proteins control the formation of G-quadruplex DNA structures in vivo. *Nat Struct Mol Biol*, **12**, 847-854.

113. Masuda-Sasa, T., Polaczek, P., Peng, X.P., Chen, L. and Campbell, J.L. (2008) Processing of G4 DNA by Dna2 helicase/nuclease and replication protein A (RPA) provides insights into the mechanism of Dna2/RPA substrate recognition. *J Biol Chem*, **283**, 24359-24373.
114. Ronchi, D., Di Fonzo, A., Lin, W., Bordoni, A., Liu, C., Fassone, E., Pagliarani, S., Rizzuti, M., Zheng, L., Filosto, M. *et al.* (2013) Mutations in DNA2 link progressive myopathy to mitochondrial DNA instability. *Am J Hum Genet*, **92**, 293-300.
115. Tangutoori, S., Baldwin, P. and Sridhar, S. (2015) PARP inhibitors: A new era of targeted therapy. *Maturitas*, **81**, 5-9.
116. Rouleau, M., Patel, A., Hendzel, M.J., Kaufmann, S.H. and Poirier, G.G. (2010) PARP inhibition: PARP1 and beyond. *Nat Rev Cancer*, **10**, 293-301.
117. Peng, G., Dai, H., Zhang, W., Hsieh, H.J., Pan, M.R., Park, Y.Y., Tsai, R.Y., Bedrosian, I., Lee, J.S., Ira, G. *et al.* (2012) Human nuclease/helicase DNA2 alleviates replication stress by promoting DNA end resection. *Cancer Res*, **72**, 2802-2813.
118. Strauss, C., Kornowski, M., Benvenisty, A., Shahar, A., Masury, H., Ben-Porath, I., Ravid, T., Arbel-Eden, A. and Goldberg, M. (2014) The DNA2 nuclease/helicase is an estrogen-dependent gene mutated in breast and ovarian cancers. *Oncotarget*, **5**, 9396-9409.
119. Torgovnick, A. and Schumacher, B. (2015) DNA repair mechanisms in cancer development and therapy. *Front Genet*, **6**, 157.
120. Kawahara, M., Takahashi, Y., Takazawa, K., Tsuchiya, H., Tomita, K., Yokogawa, K. and Miyamoto, K. (2008) Caffeine dose-dependently potentiates the antitumor effect of cisplatin on osteosarcomas. *Anticancer Res*, **28**, 1681-1685.
121. Sinn, B., Tallen, G., Schroeder, G., Grassl, B., Schulze, J., Budach, V. and Tinhofer, I. (2010) Caffeine confers radiosensitization of PTEN-deficient malignant glioma cells by enhancing ionizing radiation-induced G1 arrest and negatively regulating Akt phosphorylation. *Mol Cancer Ther*, **9**, 480-488.
122. Powell, S.N., DeFrank, J.S., Connell, P., Eogan, M., Preffer, F., Dombkowski, D., Tang, W. and Friend, S. (1995) Differential sensitivity of p53(-) and p53(+) cells to caffeine-induced radiosensitization and override of G2 delay. *Cancer Res*, **55**, 1643-1648.
123. Wang, H., Wang, X., Iliakis, G. and Wang, Y. (2003) Caffeine could not efficiently sensitize homologous recombination repair-deficient cells to ionizing radiation-induced killing. *Radiat Res*, **159**, 420-425.
124. Tsabar, M., Eapen, V.V., Mason, J.M., Memisoglu, G., Waterman, D.P., Long, M.J., Bishop, D.K. and Haber, J.E. (2015) Caffeine impairs resection during DNA break repair by reducing the levels of nucleases Sae2 and Dna2. *Nucleic Acids Res*.
125. Levikova, M., Klaue, D., Seidel, R. and Cejka, P. (2013) Nuclease activity of Saccharomyces cerevisiae Dna2 inhibits its potent DNA helicase activity. *Proc Natl Acad Sci U S A*, **110**, E1992-2001.
126. Jentsch, S. and Psakhye, I. (2013) Control of nuclear activities by substrate-selective and protein-group SUMOylation. *Annu Rev Genet*, **47**, 167-186.

127. Guo, Z., Kanjanapangka, J., Liu, N., Liu, S., Liu, C., Wu, Z., Wang, Y., Loh, T., Kowolik, C., Jamsen, J. *et al.* (2012) Sequential posttranslational modifications program FEN1 degradation during cell-cycle progression. *Mol Cell*, **47**, 444-456.
128. Vallen, E.A. and Cross, F.R. (1995) Mutations in RAD27 define a potential link between G1 cyclins and DNA replication. *Mol Cell Biol*, **15**, 4291-4302.
129. Fiorentino, D.F. and Crabtree, G.R. (1997) Characterization of Saccharomyces cerevisiae dna2 mutants suggests a role for the helicase late in S phase. *Mol Biol Cell*, **8**, 2519-2537.
130. Thangavel, S., Berti, M., Levikova, M., Pinto, C., Gomathinayagam, S., Vujanovic, M., Zellweger, R., Moore, H., Lee, E.H., Hendrickson, E.A. *et al.* (2015) DNA2 drives processing and restart of reversed replication forks in human cells. *J Cell Biol*, **208**, 545-562.
131. Sturzenegger, A., Burdova, K., Kanagaraj, R., Levikova, M., Pinto, C., Cejka, P. and Janscak, P. (2014) DNA2 cooperates with the WRN and BLM RecQ helicases to mediate long-range DNA end resection in human cells. *J Biol Chem*, **289**, 27314-27326.
132. Nguyen, B., Sokoloski, J., Galletto, R., Elson, E.L., Wold, M.S. and Lohman, T.M. (2014) Diffusion of human replication protein A along single-stranded DNA. *J Mol Biol*, **426**, 3246-3261.
133. Burrell, R.A., McGranahan, N., Bartek, J. and Swanton, C. (2013) The causes and consequences of genetic heterogeneity in cancer evolution. *Nature*, **501**, 338-345.
134. Torti, D. and Trusolino, L. (2011) Oncogene addiction as a foundational rationale for targeted anti-cancer therapy: promises and perils. *EMBO Mol Med*, **3**, 623-636.

6. ACKNOWLEDGEMENTS

First of all I would like to thank Prof. Petr Cejka for great supervision, always helpful advice and very productive ideas.

A special thanks goes to all Cejka lab members for making working in the lab easy and enjoyable. I would like to thank Elda and Lepakshi for valuable discussions. Many thanks to Cosimo for his help and support, and also for uncomplicated and effective collaboration on multiple projects.

I would like to thank my PhD Committee members Prof. Massimo Lopes, Prof. Ralf Seidel and Dr. Pavel Janscak for their scientific advice and fruitful discussions during my PhD.

Huge thanks to IMCR for very interactive working atmosphere, and of course to Joe Jiricny for sustaining such a great institute. Special thanks to Marko for always being there for me.

I thank Cancer Biology PhD program where I found many friends.

Last but not least I would like to thank my family and friends, especially my parents and my grandmother who always supported me.

7. CURRICULUM VITAE

Surname	**LEVIKOVA**
Name	**Maryna**
Date of birth	12.12.1986
Place of birth	Charkiw, Ukraine
Nationality	German

Education

01/2012 - present **PhD** studies, Cancer Biology PhD program, Group of Prof. Dr. Petr Cejka, Institute of Molecular Cancer Research, University of Zurich, Switzerland. Title of PhD thesis: Biochemical analysis and *in vivo* role of Dna2 nuclease-helicase.

10/2009 - 11/2011 **Master of Science in Biotechnology** (with distinction), Aachen University of Technology, Germany. Master thesis in the laboratory of Prof. Dr. Bernhard Lüscher, Institute of Biochemistry and Molecular Biology, University Hospital of Aachen University of Technology. Title: Mechanism of endotoxin tolerance in mast cells.

09/2006 - 09/2009 **Bachelor of Science in Biotechnology**, Aachen University of Technology, Germany. Bachelor thesis at Fraunhofer Center for Molecular Biotechnology, Newark, Delaware, USA. Title: Antibody production in clonal cultures.

08/2001 - 06/2006 **Certificate of secondary education (Abitur)**, Hugo-Junkers Gymnasium, Mönchengladbach, Germany.

Professional experience

02/2010 - 10/2010 Student research assistant at Fraunhofer Institute of Molecular Biology and Applied Ecology, Department of Plant Biotechnology, Aachen, Germany.

Teaching experience

03/2013 - 03/2014	Supervision of a master student, laboratory of Prof. Petr Cejka.
04/2012, 04/2015	Teaching assistant, practical block course "Genome instability and Molecular Cancer Research", University of Zurich.
11/2013 - 12/2013	Teaching assistant, basic practical block course in biology for bachelor students, University of Zurich.
05/2011 - 06/2011	Teaching assistant, practical block course in biochemistry and molecular biology for medical students, Aachen University of Technology.

Awards and Scholarships

- Poster prize at the 6th Cancer Network Zurich retreat, 04/2015. Poster: Role of Dna2 in eukaryotic DNA replication.
- Poster prize at the Fusion Conference "DNA replication as a source of DNA damage", Morocco, 09/2014. Poster: Fen1-independent role for Dna2 in flap processing.
- "Springorum Denkmünze" for passing the master examination in biotechnology with distinction.
- Schoeneborn award for excellent performance during Bachelor of Science studies in biotechnology.
- Scholarship for bachelor and master studies by Studienstiftung des Deutschen Volkes e. V. (03/2007 - 12/2011).

Scientific Conferences and Workshops

- StratCan Interactive Summer School in Cancer 2015 "Targeting DNA Repair in Cancer", Stockholm, Sweden, 22-25 June 2015. Talk: Function of Dna2 in eukaryotic DNA replication.
- Abcam conference "Maintenance of Genome Stability", St. Kitts, St Kitts and Nevis, 3-6 March 2014. Poster: Nuclease activity of *Saccharomyces cerevisiae* Dna2 inhibits its potent helicase activity.
- EMBO workshop "Structure-Specific Nucleases in Replication", Côte d'Azur, France, 16-20 September 2012.

Publications

Kemmerich FE, Daldrop P, **Levikova M**, Pinto C, Cejka P, Seidel R. Force regulated dynamics of RPA on a DNA fork. Manuscript in preparation.

Ölmezer G, **Levikova M,** Klein D, Fontana G, Cejka P, Rass U. Dna2 nuclease-helicase and Holliday junction resolvase Yen1 provide a two-tiered response to replication stress. Under revision in Nat Com.

Levikova M, Cejka P. The *S. cerevisiae* Dna2 can function as a sole nuclease in the processing of Okazaki fragments in DNA replication. Nucleic Acids Res 2015. In press.

Thangavel S, Berti M, **Levikova M**, Pinto C, Gomathinayagham S, Vujanovic M, Zellweger R, Moore H, Lee EH, Hendrickson EA, Cejka P, Stewart S, Lopes M, Vindigni A. DNA2 drives processing and restart of reversed replication forks in human cells. J Cell Biol. 2015 Mar 2;208(5):545-62.

Sturzenegger A, Burdova K, Kanagaraj R, **Levikova M**, Pinto C, Cejka P, Janscak P. DNA2 cooperates with the WRN and BLM RecQ helicases to mediate long-range DNA end resection in human cells. J Biol Chem. 2014 Sep 26;289(39):27314-26.

Levikova M, Klaue D, Seidel R, Cejka P. Nuclease activity of *Saccharomyces cerevisiae* Dna2 inhibits its potent helicase activity. Proc Natl Acad Sci U S A. 2013 May 28;110(22):E1992-2001.